Palaeomagnetism of late Archaean flood basalt terrains:

implications for early Earth geodynamics and geomagnetism

Geert H.M.A. Strik

Palaeomagnetism of late Archaean flood basalt terrains:

implications for early Earth geodynamics and geomagnetism

Paleomagnetisme van laat Archaïsche plateaubasaltterreinen:

implicaties voor de geodynamica en het geomagnetisme van de vroege Aarde

(met een samenvatting in het Nederlands)

PROEFSCHRIFT

ter verkrijging van de graad van doctor aan de Universiteit Utrecht
op gezag van de Rector Magnificus, Prof. Dr. W.H. Gispen,
ingevolge het besluit van het College voor Promoties
in het openbaar te verdedigen op
donderdag 6 oktober 2004 des middags te 12.45 uur

door

Gerardus Henricus Martina Anna Strik

geboren op 11 december 1973,
te Oss

PROMOTOR   Prof. Dr. C.G. Langereis
         Faculty of Geosciences, Utrecht University
         Utrecht, The Netherlands

MEMBERS OF THE DISSERTATION COMMITTEE

Prof. Dr. Lisa Tauxe
Scripps Institution of Oceanography, University of California San Diego
La Jolla, United States of America

Prof. Dr. Chris J. Spiers
Faculty of Geosciences, Utrecht University
Utrecht, The Netherlands

Prof. Dr. Maarten J. de Wit
CIGCES, Department of Geological Sciences, University of Cape Town
Rondebosch, South Africa

Dr. Conall Mac Niocaill
Department of Earth Sciences, University of Oxford
Oxford, United Kingdom

Dr. Jan R. Wijbrans
Faculty of Earth Sciences, Vrije University Amsterdam
Amsterdam, The Netherlands

Bibliography

The following chapters are published in or (to be) submitted to scientific journals:

Chapter 1
G. Strik, T.S. Blake, T.E. Zegers, S.H. White and C.G. Langereis (2003). Palaeomagnetism of flood basalts in the Pilbara Craton, Western Australia: late Archaean continental drift and the oldest known reversal of the geomagnetic field, J. Geophys. Res., 108(B12), 2551, doi:10.1029/2003JB002475.

Chapter 4
G. Strik, M.J. de Wit and C.G. Langereis (submitted). Palaeomagnetism of the Neoarchaean Pongola and Ventersdorp Supergroups and an appraisal of the 3.0-1.9 Ga apparent polar wander path of the Kaapvaal Craton, Southern Africa, Precamb. Res.

Chapter 5
G. Strik, L. Tauxe and C.G. Langereis (to be submitted). Similarity between the late Archaean and current geodynamo: secular variation and palaeointensity analysis of 2.8-2.7 Ga flood basalts from the Pilbara Craton, Australia, Earth Planet. Sci. Let.

Contents

Prologue

The Man from Marble Bar

Satan sat by the fires of Hell
As from endless time he's sat,
And he sniffed great draughts of the brimstone's smell
That came as the tongue-flames spat;

Then all at once the devil looked stern
For there in the depths of Hell
Was a fellow whom never a flame could burn
Or goad to an anguished yell;

So Satan stalked to the lonely scene
And growled with a stormy brow,
'Now, stranger, tell me what does this mean?
You should be well scorched by now.'

But the chappie replied with a laugh quite new;
'This place is too cold by far
Just chuck on an extra log or two
I'VE COME IN FROM MARBLE BAR!'

Victor Courtney

Prologue

The study that is reported here focuses on the palaeomagnetism of late Archaean flood basalts and the implications for geodynamic and geomagnetic processes during a part of this interval of early Earth history. The late Archaean is the geological time period that covers 500 million years between 3.0 and 2.5 billion years before present and is the youngest part of the Archaean Era, which spans 1500 million years between 4.0 and 2.5 billion years before present. The world looked totally different from today, and can be imagined as vast areas of bare rock and oceans, high volcanic activity, an atmosphere without oxygen and no signs of life, apart perhaps from some microbiological activity. Ever since the birth of our Earth, it has tried to lose its heat to the surrounding universe, obeying the laws of physics. Most probably, the Earth was hotter in the Archaean than it is today and as a consequence many geological and geophysical processes may have worked in a different way. If and how some of these processes worked differently in the late Archaean are general questions that I have tried to address in this thesis, besides from some more specific, area dependent questions. I will now briefly introduce the background to the main research questions, the fieldwork areas and finally, I will give a summary of the contents of this thesis. I could not have completed this thesis without significant contributions of the people who co-author the (to be submitted) papers that constitute the chapters of my thesis, so whenever I write 'we', I am referring to the relevant co-workers and myself.

Geodynamics: Plate tectonics in the late Archaean?
Nowadays, the Earth loses most of its heat by continuous recycling of the lithosphere in a convection related process called plate tectonics, which is a very effective way of heat loss. A major driving force of plate tectonics is considered to be the so-called slab-pull, which is a force acting on the subducting part of a plate at the convergent margin. This part of the plate has cooled down since it was created at the ridge and has thus become denser, which eventually results in the lithosphere getting pulled down into the less dense asthenosphere. This density-driven process, however, may not have occurred in the Archaean, with higher crust and mantle temperatures (e.g. Hamilton, 1998). Instead, pressure-release melting of diapirs would cause a thick and stable compositional boundary layer, deficient in mechanical coherency and thus inhibiting modern-style plate tectonics (e.g. Vlaar et al., 1994). In the absence of plate tectonics, heat loss of the Earth could still be efficient enough, but vertical rather than horizontal tectonics would then be dominant. So far, however, no consensus has been reached whether or not plate tectonics occurred in the Archaean. One of the most important aims of my study is to investigate whether tectonics were dominantly horizontal or vertical in the (late) Archaean.

Tectonic reconstructions highly depend on palaeomagnetic studies, because only with palaeomagnetism can we give minimum estimates of displacement and can we, in conjunction with geochronology, determine plate velocities. A prerequisite for reliable displacement estimates is that the studied sequence has preserved its original natural remanent magnetisation (NRM), i.e. the magnetic direction preserved in the rocks is still indicating where the magnetic north was when the rock was formed. This is by no means trivial, especially for rocks of Archaean age. Remagnetisation, caused by for example metamorphism or hydrothermal activity, is the rule rather than the exception in rocks of such old age. This study therefore commenced with having to select terrains that could still have preserved the original NRM.

Geomagnetism: Validity of the geocentric axial dipole (GAD) hypothesis

The NRM preserved in a rock, if of primary origin, gives us information about the latitude at which the rock was formed. The angle that the magnetic direction makes with the horizontal is called magnetic inclination. The magnetic inclination can be expressed as a (palaeo)latitude according to the dipole formula:

$$\tan I = 2 \tan \lambda$$

where I is the magnetic inclination and λ the palaeolatitude. This relation is true under the assumption that the Earth's magnetic field is that of a geocentric axial dipole (GAD). Currently, the dipole contribution to the magnetic field is ca. 90 %. The remaining 10 % constitutes of quadrupole, octupole and higher order pole contributions, which change with time and cause the position of the magnetic pole to vary independent of plate motions. This is called secular variation. However, when taken over a sufficient time interval, the multipole contributions are believed to average out, with only the dipole contribution remaining. This hypothesis is known as the GAD hypothesis. For Archaean tectonic reconstructions based on palaeomagnetic measurements, it is fundamental that the Earth also had a GAD in those times.

The occurrence of geomagnetic field reversals, during which the magnetic north pole becomes the magnetic south pole and vice versa, can be used to verify the GAD hypothesis. If the field in fact was on average dipolar, the magnetic directions preserved in a rock sequence before and after a field reversal should be exactly antipodal. This can be tested with the so-called reversal test, which is also a powerful test to check the probability that the original NRM has been preserved. During this study, we hoped for the occurrence of field reversals within the studied sections, and it was fortunate that these did indeed occur.

Convection currents in the liquid (outer) core generate the Earth's magnetic field. I intentionally put 'outer' between brackets, because whether or not the Earth's core had segregated into a solid inner core and a liquid outer core in the Archaean, or at least by the end of the Archaean, is a topic of debate (e.g. Labrosse et al., 2001; Smirnov et al., 2003) and so far, physical evidence is absent. The inner core is thought to have a stabilising function on the geodynamo (e.g. Gubbins, 1993) so without a solid inner core, it is imaginable that the magnetic field behaves much more chaotic than it does today, and perhaps it would have a different magnetic intensity. Because there is such a paucity of palaeomagnetic data for the Archaean, the behaviour of the Archaean field is very poorly constrained. Therefore, another important goal of this thesis is to analyse the large database of newly acquired data to study secular variation in the late Archaean, and to provide measurements that will give an estimate of the intensity of the late Archaean magnetic field.

Fieldwork areas

Many Archaean terrains have a complex tectonic and metamorphic history and are not ideal for palaeomagnetic studies, since chances are high that the original NRM has been overprinted or remagnetised. The Pilbara Craton of northwestern Australia and the Kaapvaal Craton of southern Africa are the two best-preserved Archaean terrains in the world. They contain large areas of late Archaean successions that formed in extensional settings and encompass large volumes of flood basalts, which are usually good recorders of the geomagnetic field. These successions are generally only gently folded and display only low metamorphic grades, in no case higher than lower-greenschist facies, which means

that temperatures generally stayed below 350 °C. Therefore, these areas have been the focus of my research.

The Pilbara Craton

The Pilbara Craton, Western Australia constitutes mid to late Archaean granite-greenstone terrains, unconformably overlain by a late Archaean subaerial flood basalt dominated succession (Fig. 1). Most of the fieldwork for this thesis was carried out in the latter succession, which is divided in the ca. 2775-2715 Ma Nullagine and Mount Jope Supersequences. The geology of these sequences has been studied extensively (e.g. Blake, 1993; Blake, 2001; Thorne and Trendall, 2001) and has recently been dated with high precision geochronology (e.g. Arndt et al., 1991; Blake et al., 2004; Wingate, 1999).

The Pilbara Craton lies some 1300 km north of Perth, Western Australia's only big city. The Pilbara itself constitutes only a handful of settlements, of which the larger ones lie along the coast. Fieldwork was done in three separate basins, and accordingly a base camp was chosen either in the towns of Nullagine, Marble Bar or Karratha. Access to the fieldwork areas is only possible with four-wheel drive vehicles. Some trips have taken a full day just to get to the target area, so usually camps were set up for 4 to 5 days or longer, depending on how remote the area was and how difficult to reach. During the course of this project, I have spent more than half a year in the field in the Pilbara. The Pilbara has an arid-tropical, semi desert climate and borders with Australia's Great Sandy Desert. The fieldworks took place between June and September, during the Australian winter. Despite an average temperature between a pleasant 25 and 30 °C, temperatures could still occasionally rise to high thirties and I have the deepest respect for those who are out there in the field in December when temperatures are above 37 °C almost continuously. Marble Bar has been called Australia's hottest town, since for 161 consecutive days during the summer of 1923-1924 the temperature in the town never dropped below 100 °F (37.8 °C).

Target fieldwork areas were usually selected with the aid of 1:100 000 scale geological maps (Blake, 1990) and aerial photographs. Pilot palaeomagnetic studies by Ton van Hoof (1996) showed that sites in somewhat deeper incised valleys gave better results than sites in open spaces, because the latter were almost always struck by lightning, which has a destructive effect on the palaeomagnetic signal. The aerial photographs were therefore used to select sites protected from lightning, generally in creek beds. The additional advantage of sampling in creek beds is that exposure is commonly very fresh, with weathering layers of only some millimetres. Samples were taken with a hand-held, petrol driven, diamond bitted drill, and were oriented, collected and shipped home, where they were prepared and analysed in the laboratory.

The Kaapvaal Craton

The Kaapvaal Craton, localised in southern Africa, constitutes mid to late Archaean granite-greenstone terrains, overlain by various sediment dominated and basalt dominated successions (Fig. 1). The aim was to follow the same sampling approach as for the Pilbara Craton; hence the focus was on two successions encompassing extensive basaltic sequences. The first studied succession is the ca. 2.95-2.85 Ga Pongola Supergroup. The geology of the Pongola Supergroup has recently been described by e.g. Beukes and Cairncross (1991) and Gold and von Veh (1995). Secondly, the ca. 2.71-2.70 Ga Ventersdorp Supergroup was targeted. Many of the type sections here are based on drill-cores, because exposure is limited. The geology has been described in detail by e.g. Winter (1976) and in a more recent review
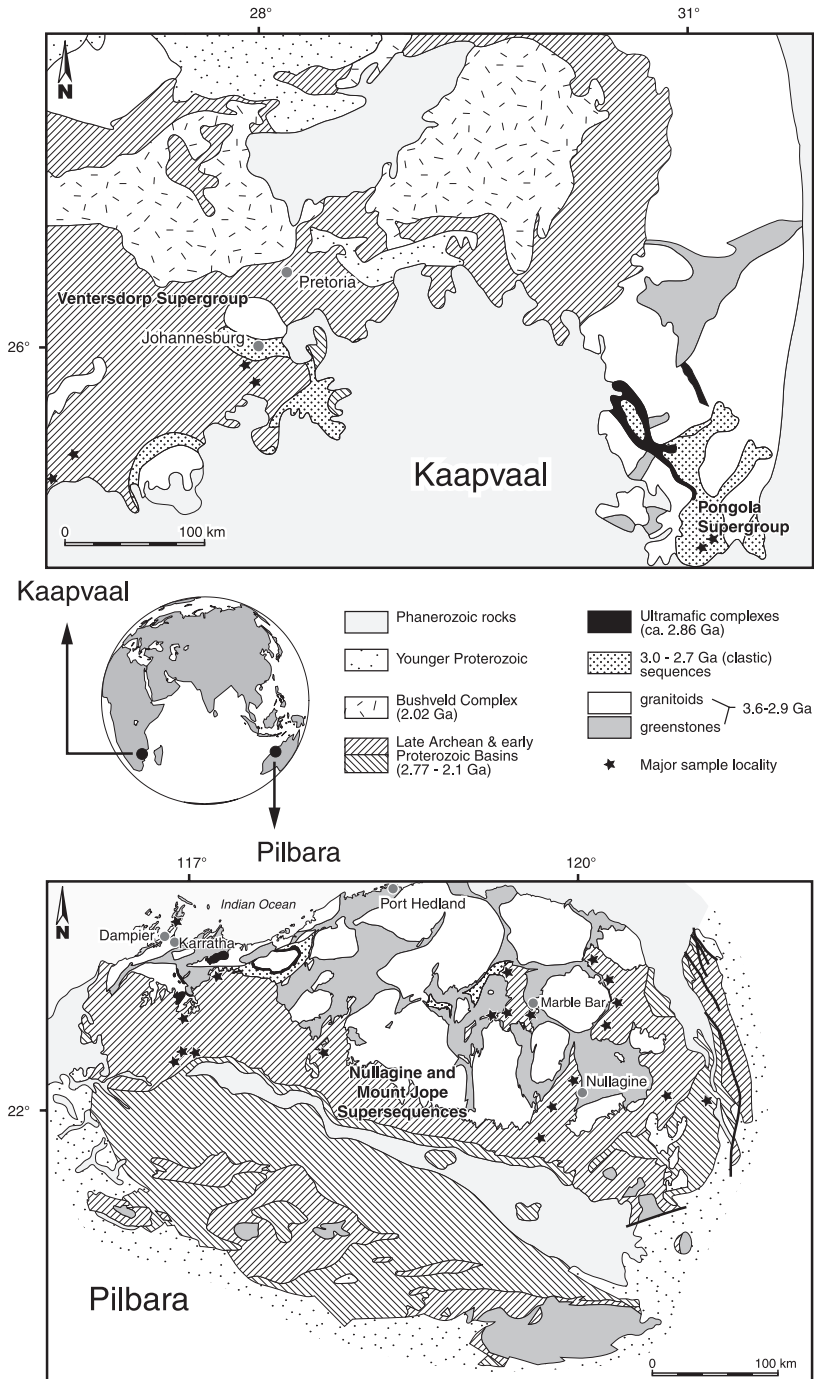
Figure 1
Simplified geology of the Kaapvaal and Pilbara Cratons, indicating major sample localities.

by van der Westhuizen et al. (1991). The geochronology of both the Pongola and the Ventersdorp Supergroups is less detailed than the section studied on the Pilbara Craton, primarily because hardly any rocks suitable for high precision dating within these successions have been encountered so far.

Fieldwork on the Kaapvaal Craton is in many ways different from fieldwork in Australia. Access to exposure is easy and logistics are no problem at all. The Pongola Supergroup area has high relief, which makes finding suitable exposure relatively easy. Most of the Ventersdorp Supergroup outcrop, however, is on flat lying farmland, which complicates the search for decent exposures. All I have seen of the Rietgat basalt, for example, are the endless wheat fields on top of it. Besides an excellent section along the Vaal River, fieldwork was mostly confined to quarries and even underground mines. The advantage of this is that the sampled rocks are fresh and not struck by lightning. Although, the disadvantage of underground mines is that sampling is confined to new development only and that compass readings are possibly affected by the great quantities of steel equipment around.

Summary

Palaeomagnetism of the Pilbara Craton

A palaeomagnetic interest in the Pilbara Craton dates back to 1967 with results from the Early Proterozoic banded iron formations at Mount Tom Price and Mount Newman (Porath, 1967). Since then, on average less than two studies per decade have contributed to the Precambrian apparent polar wander path (APWP) of the Pilbara, resulting in large time gaps between subsequent pole positions, which complicates tectonic interpretations. Various remagnetisations have been identified (e.g. Li et al., 2000; Schmidt and Embleton, 1985), which have been contributed to burial metamorphism and Proterozoic orogenic phases, but for which solid proof is still lacking.

The ca. 2775-2715 Ma Nullagine and Mount Jope Supersequences are almost unmetamorphosed, relatively undeformed and are recognised throughout the Pilbara Craton. They have been interpreted as the rock record of a two-phase continental breakup in the late Archaean (e.g. Blake, 1993; Blake and Barley, 1992). For this reason, this succession is an ideal target for a palaeomagnetic study, and particularly for one with the question of which tectonic style (dominantly horizontal versus vertical tectonics) operated in the late Archaean.

Chapter 1 focuses on the Nullagine Synclinorium, an area within the East Pilbara Basin. Here, the Nullagine and Mount Jope Supersequences have been subdivided into 12 packages (named Package 1 to Package 12) separated by unconformities (Blake, 2001). The most important aim of this chapter for my study was to convincingly demonstrate that the original NRM is still preserved in the succession. Without this, any tectonic interpretation is meaningless. Packages 1 to 10 were sampled and by means of positive conglomerate, fold and reversal tests, the primary nature of the NRM could indeed be demonstrated for a high temperature component that could be isolated for 7 out of 10 packages. A pervasive medium temperature component was also identified, with a direction that slightly differs from earlier reported remagnetisations, and this points to a younger and major thermal event. In Package 2, the magnetisation appeared to be reversed with respect to the dominant polarity present in the rocks. With the positive reversal test, there is a good indication that the GAD hypothesis holds for the late Archaean.

The palaeomagnetic data reveal a major shift in pole position across the Package 7/ 8 boundary. We argue that it is not likely that this shift is the result of a geophysical process like true polar wander of the magnetic pole, or that it is caused by a systematic quadrupole or octupole contribution. Rather, we think that this shift actually represents horizontal movement of the Pilbara at ca. 2.72 Ga, at greater speeds than observed in Phanerozoic successions.

Further, there are four generations of mafic dykes in the Nullagine Synclinorium area that were proposed to correlate to some of the flood basalt packages of the Nullagine and Mount Jope Supersequences (Blake, 2001). These correlations are palaeomagnetically supported and we confirm that the dykes likely were the feeders to the flood basalts. Finally, four new pole positions could be added to the Archaean APWP of the Pilbara. From these new results, we could demonstrate that the arguments to reject a possible Archaean connection between the Pilbara and Kaapvaal Cratons at ca 2.8 Ga (Wingate, 1998) are no longer valid.

The stratigraphic subdivision of the ca. 2775-2715 Ma succession of the Nullagine Synclinorium into 12 packages was expanded to the entire northern Pilbara (Blake, 2004). Since the number of sites and the covered area in Chapter 1 are still relatively limited for the interpretation of tectonic style and geomagnetic implications, in **Chapter 2** the research area is expanded to the whole East Pilbara Basin and the Marble Bar Basin. One of the major aims of this chapter was to test the package subdivision of Blake (2004). The subdivision could indeed be confirmed with the palaeomagnetic data, although we had to make some adjustments to the correlation with the Marble Bar Basin. Here, the palaeomagnetic data revealed that the lowermost flood basalt package does not correlate with Package 1 in the East Pilbara Basin, as was thought originally, but is in fact (significantly) older than Package 1 because it has a distinctly different palaeomagnetic pole position. We therefore named it Package 0. Flood basalts of the second flood basalt package in the Marble Bar Basin have an identical pole position as the basalts of Package 1 in the East Pilbara Basin, which we now interpreted to be of the same age. The pole position of Package 0 is very different to the other pole positions, which probably implies that the Pilbara Craton rotated almost 180 degrees between the extrusion of Package 0 and Package 1 basalts. This solution may be controversial, but is the most conservative approach and more acceptable than solutions involving large amounts of true polar wander, complex excursions of the field or major non-dipole behaviour.

A further aim of Chapter 2 was to constrain the palaeomagnetic shift across the Package 7/8 boundary. The combined data of all areas within the East Pilbara Basin result in an average estimated minimum drift rate of ca. 50 cm/yr, which is 10 to 20 cm per year faster than the fastest drift rates reported for the Phanerozoic (e.g. Meert, 1999; Meert et al., 1993). Finally, the reversed direction of Package 2 has been recorded in the entire East Pilbara Basin, and an additional reversed polarity was found in a basalt flow of Package 7. With the combined data of Chapters 1 and 2, the APWP of the Pilbara is well determined between ca. 2775 and 2715 Ma, especially for Archaean standards.

Chapter 3 focuses on the palaeomagnetism of the West Pilbara Basin. The correlation to the packages as defined for the Nullagine Synclinorium is more complex (Blake, 2004), with missing packages and additional lithologies such as mafic sills. The aims of Chapter 3 are to further expand the palaeomagnetic test of the proposed stratigraphic correlation to the Nullagine Synclinorium (Blake, 2004) and to apply the entire northern Pilbara palaeomagnetic data set for the development of a new model of tectonic evolution for the

Pilbara between 2775 and 2715 Ma, integrated with an existing model that is based on geological evidence (Blake, 1993; Blake and Barley, 1992). The number of meaningful palaeomagnetic data from the West Pilbara Basin appeared to be lower than for the East Pilbara and Marble Bar Basins, which may indicate a slightly higher metamorphic grade in the West Pilbara Basin. Indications for a Package 7 age reversal from a basalt flow in the East Pilbara Basin are confirmed by the reversed polarity found West Pilbara Basin mafic sills that are correlated to Package 7. These have a positive reversal test and once more demonstrate the primary nature of NRM. The palaeomagnetic data support the proposed stratigraphic correlations of Blake et al. (2004).

The tectonic evolution of the (northern) Pilbara Craton between 2775 and 2715 Ma, based on the palaeomagnetic data of Chapters 1 to 3 and combined with geological evidence, can be summarised as follows: during the first phase of tectonic breakup, from the formation of Package 1 to that of Package 7, the Pilbara Craton extended in a WNW-ESE direction with a possible minimum horizontal velocity of 2.5 cm/yr and rotated approximately 30 degrees counter-clockwise. During the second phase of breakup, between ca. 2721 and 2718 Ma, the Pilbara rifted approximately 1600 km northwards, with an average minimum drift rate of 50 cm/yr, which demonstrates the occurrence of rapid horizontal plate movement, the essence of plate tectonics, in the late Archaean.

Palaeomagnetism of the Kaapvaal Craton

The Kaapvaal Craton has been the target of approximately the same number of palaeomagnetic studies as the Pilbara, although recently few new studies have been carried out. Interest in the palaeomagnetism of the Ventersdorp Supergroup goes back to the late 1960s (Jones et al., 1967), but since then no new data have been reported. No palaeomagnetic studies from the Pongola Supergroup have been reported earlier. Large time gaps exist between subsequent pole positions on the Kaapvaal APWP, which requires a cautionary approach regarding tectonic interpretations. Nevertheless, the Kaapvaal APWP has been used in the past to make statements about Archaean tectonics (e.g. Kröner and Layer, 1992), which really stand or fall with the quality of this APWP.

Chapter 4 describes the results of a palaeomagnetic study of basalts from the Pongola and Ventersdorp Supergroups. The aim was to expand the number of Archaean pole positions for the Kaapvaal Craton and to facilitate tectonic interpretations. A pervasive medium temperature component, which was recorded by almost all studied units, is caused by remagnetisation at ca. 180 Ma during the formation of the Karoo large igneous province, which affected almost the entire Kaapvaal Craton. Further, five studied units hold a possibly Archaean high temperature magnetisation. We carried out various palaeomagnetic field tests to try to constrain the age of magnetisation, but none could convincingly demonstrate an Archaean age. We depended on the already established APWP of the Kaapvaal Craton to acquire some possible age constraints. This, however, required a quality analysis of the published Archaean pole positions. We found that only one of these had a positive conglomerate test (Wingate, 1998), although the scatter of data from this pole position is higher after tectonic correction than before, which points towards a negative fold test. The latter, however, could not be tested for the published data. The other pole positions lack solid field tests and in many cases the palaeohorizontal is unknown. We subsequently had to conclude that the quality of the Archaean palaeomagnetic data of the Kaapvaal Craton, including our new data, is too poor to construct a reliable APWP and not suitable to make meaningful tectonic interpretations.

The geomagnetic field in the late Archaean

In **Chapter 5**, our palaeomagnetic data set of the Pilbara Craton is used to study the behaviour of the late Archaean geomagnetic field. Experiments described in Chapter 5 are twofold: firstly, the palaeomagnetic data from Chapters 1 to 3 were analysed to select samples for palaeointensity determination. Secondly, the site mean data from Chapters 1 to 3 were used to study palaeosecular variation. For palaeointensity experiments, samples were chosen that show only the original NRM and no low or medium temperature overprints. To improve the success rate of the palaeointensity experiment, we developed a method to check for magnetic alteration with increasing temperature, using a Curie balance and applying repeated heating-cooling cycles at increasingly higher set point temperatures. Only the samples that showed little or no alteration were chosen as suitable samples for palaeointensity determination. The mean virtual dipole moment (VDM) at 2772 ± 2 Ma is determined at 28.1 ± 9.3 ZAm^2 (Z = zeta = 10^{21}) and at 2721 ± 4 Ma at 22.1 ± 4.2 ZAm^2, which are relatively low values compared to the present day dipole moment of ca. 80 ZAm^2. However, the late Archaean VDM values are within error of the average VDM from 1 to 84 Ma, which is 55 ± 30 ZAm^2 (Tauxe and Staudigel, 2004).

The palaeosecular variation experiment consisted of the analysis of the mean virtual geomagnetic pole (VGP) scatter of the Pilbara data and the comparison with the VGP scatter of the last 5 Myr, using real palaeosecular variation data from modern lavas (PSVRL, McElhinny and McFadden, 1997) and model predictions based on PSVRL (TK03.GAD, Tauxe and Kent, 2004). The Pilbara data were analysed per individual package and per group of packages that share a common palaeolatitude. The latter is more suitable, because the tests are more significant with a larger number of data. We find that the TK03.GAD model predictions are similar to the Pilbara data, both for individual packages and for groups of packages. We are able to conclude, for the first time, that Archaean secular variation is not significantly different from secular variation today.

Concluding, the Pilbara data strongly suggest: that the GAD hypothesis is valid in the late Archaean; that palaeointensities are lower than at present, but not significantly lower than during the period between 1 and 84 Ma; and that secular variation is comparable to that of the last 5 Myr. Therefore, the geomagnetic field seems to be stable at ca. 2.8 Ga and this either provides important constraints on the role of the solid inner core on the geomagnetic field, or questions the estimated age of the inner core. Our results imply that either a solid inner core is not necessary for a stable geodynamo, or that the solid inner core had already nucleated at ca. 2.8 Ga. At present, theoretical models cannot yet answer these questions.

Chapter 1

Palaeomagnetism of flood basalts in the Pilbara Craton, Western Australia: late Archaean continental drift and the oldest known reversal of the geomagnetic field

"They should be going that way, then again, ya never know with rocks..."

Dave 'Dynamite' Taylor

Palaeomagnetism of flood basalts in the Pilbara Craton, Western Australia: late Archaean continental drift and the oldest known reversal of the geomagnetic field

Abstract

A late Archaean (ca. 2775-2715 Ma) succession of terrestrial continental flood basalts, mafic tuffs, felsic volcanic rocks and clastic sedimentary rocks, in the Nullagine Synclinorium (and Meentheena Centrocline) of the East Pilbara Basin, Western Australia has been sampled for a palaeomagnetic study. Over 500 oriented, mostly basalt, drill cores were collected from the supracrustal succession and associated dykes. Thermal and alternating field demagnetisation revealed two distinct components. Positive fold, conglomerate and reversal tests confirm that the primary natural remanent magnetisation (NRM) is still preserved. The secondary component is interpreted as the record of remagnetisation during a major thermal event, possibly in the early Proterozoic. Analysis of the primary NRM directions results in a magnetostratigraphy and an apparent polar wander path (APWP) for the 60 Myr interval covered by the sampled succession. Assuming a geocentric axial dipole during this time interval, the APWP shows that the Pilbara Craton was drifting during the late Archaean and that drift rates probably varied significantly. In particular, a mean 27.2° shift in palaeolatitude is recorded across an unconformity that represents a relatively short time period and that marks a significant change in basalt geochemistry. This study suggests that continents moved horizontally during the late Archaean and that the rates of movement were significantly faster than in the Phanerozoic. In addition, a reversed polarity interval - with a positive reversal test - is recorded. We argue that it documents the oldest known reversals of the geomagnetic field.

Introduction

The nature of Archaean (4.0-2.5 Ga) tectonic processes is largely unknown and often controversial. Schools of thought still vary widely despite decades of research on all continents (e.g. de Wit, 1998; Hamilton, 1998). Central to all controversies concerning larger-scale tectonic processes is the question to which degree Archaean continental crust moved horizontally across the Earth's surface, in other words whether it was dominated by horizontal or vertical tectonics.

Palaeomagnetism, in conjunction with high resolution isotopic and biostratigraphic age control, has proven crucial to quantifying both the rotation and latitudinal displacement of the Earth's plates during the Phanerozoic. However, in rocks older than ca. 180 Ma the oceanic polarity record is not available, and in Precambrian rocks there is poor biostratigraphic control and commonly only widely spaced isotopic ages. In addition, Precambrian rocks are commonly deformed and metamorphosed rendering them unsuitable for palaeomagnetic studies. Therefore, with increasing age, it becomes more difficult to derive and interpret palaeomagnetic data.

In Archaean rocks, palaeomagnetic studies are even more problematic because there is an even greater paucity of well-exposed, unaltered and undeformed rocks that are suitable for palaeomagnetic studies. Further, Archaean tectonic processes are still poorly understood, which makes interpreting the meaning of any palaeomagnetic results problematic. While there is a broad consensus that the Archaean mantle was substantially hotter than today (e.g. Pollack, 1997), there is little consensus concerning larger-scale tectonic processes. For example, Hamilton (1998) argues that plate tectonic processes such as those evoked for the Phanerozoic did not occur until at least 2.6 Ga and concludes that no observational evidence for rifting, rotation and continental plate reassembly has been found to support plate tectonic activity. In contrast, de Wit (1998) argues that the evidence for plate tectonics in the late Archaean is strong, and that the process appears to dominate this time period.

Palaeomagnetic studies can make a significant contribution to this debate, provided they have sufficient geological and geochronological control, and provided that they demonstrate a primary natural remanent magnetisation (NRM). However, little is known about the Archaean geomagnetic field and certain assumptions have to be made when interpreting Archaean NRM. In particular, we have to assume that the Earth's magnetic field behaved as a geocentric axial dipole (GAD), even though it is still a topic of debate. For example, Kent and Smethurst (1998) conclude that a 25 % octupole contribution to the axial dipole field can explain the anomalous inclination distribution for the Precambrian and Palaeozoic, based on the bias towards low inclinations of known data from the Global Palaeomagnetic Database (GPMDB). However, McElhinny and McFadden (2000) claim that it is more probable that continental lithosphere had the tendency to be cycled into the equatorial belt, and that the database used by Kent and Smethurst (1998) does not allow a sufficiently random sampling of the whole Earth throughout the Precambrian and Palaeozoic.

Compared with Phanerozoic rocks, the palaeomagnetic database of Archaean rocks is very small. The Archaean shields of Canada, particularly the Superior Province, are the most extensively studied with 40 entries in the 2000 version of the GPMDB, (Buchan et al., 1998; McElhinny and Lock 1996; Zhai et al., 1994) followed by Africa, Europe and Australia (16, 11 and 8 entries in the GPMDB, respectively). Only a few studies convincingly demonstrate the timing of magnetisation through several field tests. For instance, Meert et al. (1994) show by means of a positive fold, reversal and conglomerate test that a succession
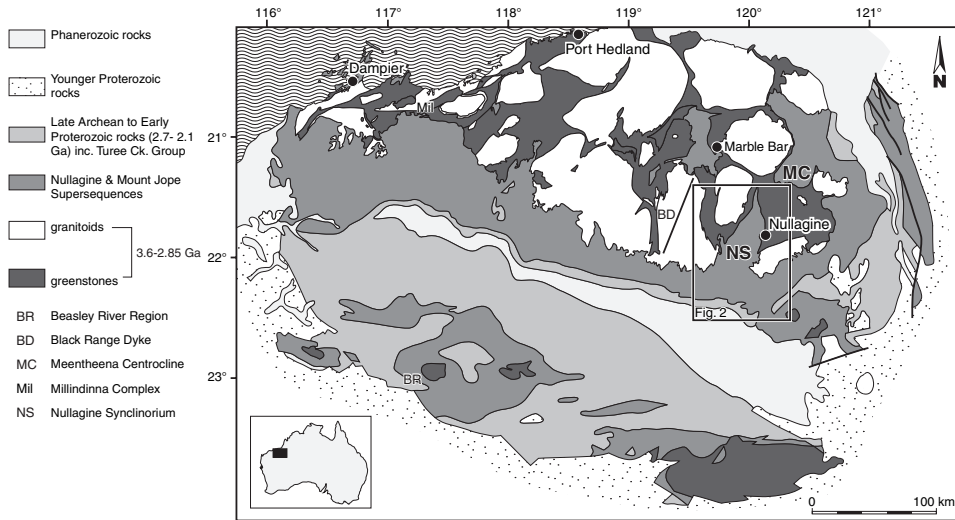
Figure 1.1
Simplified geological map of the Pilbara, showing the locations of the Beasley River Region, the Black Range Dyke, the Meentheena Centrocline, the Millindinna Complex, the Nullagine Synclinorium, and the approximate location of Figure 1.2. The Hamersley Province comprises most of the southwestern half of the map.

of the Nyanzian System (Tanzania Craton), carries an NRM of 2680 ± 10 Ma. However, many studies lack palaeomagnetic field tests and/or precise age control. Previous palaeomagnetic studies of Archaean rocks were mostly focussed on a single rock formation within a specific area and resulted in one palaeopole for that area (e.g. Morimoto et al., 1997; Wingate, 1998). When combined, results from these studies determine an apparent polar wander path (APWP) that is poorly constrained, with average time gaps of ca. 60 Myr between following palaeopoles (Idnurm and Giddings, 1988). Compared to many Phanerozoic APWPs (e.g. Laurentia, one key pole position per 20.8 Myr from the Early Cambrian to present, based on more than 3000 pole positions, cf. McElhinny and McFadden, 2000; McFadden and McElhinny, 1995; van der Voo, 1990) these Archaean APWPs are extremely crude and would be deemed meaningless in a Phanerozoic context. Therefore, to obtain meaningful Archaean APWPs, it is essential to study precisely dated Archaean successions within one geologically coherent terrain and preferably within a coherent stratigraphic section.

Over the last 20 years the Sensitive High Resolution Ion Microprobe (SHRIMP) has revolutionised Precambrian geochronology by providing ages commonly with precisions of only a few million years. When these ages are integrated into detailed geological and geophysical studies of Archaean terrains they provide a framework that is becoming suitable for high-precision palaeomagnetic studies, as we illustrate in this study.

The ca. 2775-2715 Ma Nullagine and Mount Jope Supersequences (Blake, 1993; Blake, 2001) in the Nullagine Synclinorium in the Pilbara Craton of Western Australia (Figs. 1.1, 1.2) were chosen for this study, because they comprise a well-exposed, relatively undeformed and unaltered late Archaean succession that contains an abundance of flood basalts. In addition, the succession in the study area (Figs. 1.1, 1.2) has recently been divided

Figure 1.2
Summary geological map of the Nullagine Synclinorium showing dominant lithologies, related mafic dykes (after Blake, 2001) and sample locations (see Tab. 1.2).

Figure 1.3
Summary stratigraphic column (cumulative maximum stratigraphic thickness) of the Nullagine and Mount Jope Supersequences and the lower Marra Mamba Supersequence Package in the Nullagine Synclinorium (after Blake, 2001). The figure includes (from left to right), the approximate stratigraphic position of the Meentheena Centrocline Package 1 samples (GSP61-67), the stratigraphic position of palaeomagnetic sample sites in the Nullagine Synclinorium, dominant lithologies, package numbers, summary rock ages, second-order divisions and comagmatic dyke and growth-fault orientations (with palaeomagnetic sample site numbers). Correlations with the lithostratigraphic scheme and a regional stratigraphic context are given in Table 1.1. Each basalt sample number tie line represents a single flow unit, two basalt sample sites with a single tie line represent two sample sites in the same flow unit. The exact stratigraphic positions of sites GSP 34, 35, 36, and 37 were not recorded but they are shown in their correct relative stratigraphic positions. Positions of samples GSP50, GSP 173, GSP183 and GSP 184 are estimates of their positions within the stratigraphic section of the dacite porphyry. BRS, Black Range Suite; CCS, Castle Creek Suite; FMCS; Five Mile Creek Suite; MC, Meentheena Centrocline; MM, Marra Mamba Supersequence Package; MMS, Mount Maggie Suite.

UNCONFORMITY-BASED DIVISIONS				LITHOSTRATIGRAPHIC DIVISIONS	
Chichester Range Megasequence, Regional Subdivisions (Blake, 1993)	Chichester Range Megasequence Subdivisions in the East Pilbara Basin (Blake, 1993)	Chichester Range Megasequence in the Nullagine Synclinorium (East Pilbara Basin) (Blake, 2001)		Mount Bruce Supergroup in the Nullagine Synclinorium	Mount Bruce Supergroup in the Nullagine Synclinorium
2nd Order Subdivisions or Grouped 2nd Order Subdivisions	3rd Order Subdivisions or Grouped 3rd Order Subdivisions	Super-sequences	Package Number	Formations and Members	Groups
Marra Mamba Supersequence Package			Package 12	Marra Mamba Iron Formation	Hamersley Group
			Package 11	Jeerinah Formation and basal Woodiana Member	Fortescue Group
Mount Jope Supersequence	Maddina Sequence Package	Mount Jope (2) Ss	Package 10	Maddina Basalt / Kuruna Member	
			Package 9	Maddina Basalt	
			Package 8		
	Tumbiana Sequence	Mount Jope (1) Ss	Package 7	Tumbiana Formation	
	Kylena Sequence	Nullagine Supersequence	Package 6	Kylena Basalt	
			Package 5		
Nullagine Supersequence	Taylor Creek Sequence (Hardey Seq. Package)		Package 4	Hardey Sandstone	
			Package 3		
	Hales Grave Well Sequence (Hardey Seq. Package)		Package 2	Hardey Sandstone & "quartz-plagioclase porphyry"	
	Mount Roe Sequence		Package 1	Mount Roe Basalt	
PILBARA CRATON (OLDER ARCHAEAN)					

Table 1.1
A comparison of stratigraphic subdivisions of the lower succession of the Hamersley Province in the Nullagine Synclinorium (after Blake, 2001). The right two columns are after Hickman and Lipple (1978); Thom et al. (1979); Thorne and Tyler (1996). Sequence stratigraphic/lithostratigraphic correlations are simplified.

(stratigraphically) in detail and has been precisely dated (Fig. 1.3; Blake, 2001; Blake et al., 2004).

There are few previous palaeomagnetic studies of Nullagine and Mount Jope Supersequences and associated igneous intrusions. Embleton (1978) presented the first palaeopole for the Black Range Dyke (Fig. 1.1) and the Cajuput Dyke, (SCD in Fig. 1.2) which are part of the Black Range Suite that has now been dated at 2772 ± 2 Ma (SHRIMP U-Pb zircon, Wingate, 1999). Embleton (1978) interpreted the NRM as primary based on a positive baked contact test. Schmidt and Embleton (1985) presented palaeomagnetic data for the Mount Roe Basalt (Tab. 1.1) and the Mount Jope Volcanics (broad equivalents of the Kylena Basalt to Maddina Basalt in Tab. 1.1), as well as for the older Millindinna Complex (Fig. 1.1) that was dated at 2860 ± 20 Ma (Gulson and Korsch, 1983). Schmidt and Embleton (1985) interpreted the NRM preserved in the rocks as primary, based on positive fold tests. Schmidt and Clark (1994) carried out a palaeomagnetic study of the banded-iron formations (BIF) of the Hamersley Range Megasequence, which overlies the Chichester Range Megasequence. The rocks studied are dated between 2479 ± 3 Ma (SHRIMP U-Pb zircon, Nelson, 1999) and 2449 ± 3 Ma (SHRIMP U-Pb zircon, Barley et al., 1997). They found remagnetised pole positions, which they interpreted to have been caused by burial metamorphism. The age of remagnetisation of the BIF's was estimated by Schmidt and Clark (1994) at 2200 ± 100 Ma, based on a positive fold test on folds formed during the Ophthalmia Orogeny. Sumita et al. (2001) presented the results of a study of

BIF of the Hamersley Province (Beasley River region; Fig. 1.1) and basalts of the Mount Jope Supersequence in the southern Pilbara. They found that both the BIF and their basalt samples are remagnetised and have not preserved any primary NRM directions.

The most extensive relevant work in the Pilbara recently is by Li et al. (2000). This work has focussed mostly on the BIFs of the Hamersley Province, though some basalts of the Mount Jope Supersequence were also sampled. Li et al. (2000) distinguished five phases of remanent magnetisation. The bulk of their samples revealed overprinted directions, possibly obtained during either the Ophthalmian (<2.45 - ca. 2.2 Ga) or the Ashburton (1.8-1.65 Ga) Orogenies. Li et al. (2000) note that separating Ophthalmian-related structures from Ashburton-related structures is difficult. Thus, there is a large degree of uncertainty as to the ages of their magnetic overprint directions. Li et al. (2000), however, did record a possible primary NRM direction in basalt samples from the Chichester Range Megasequence, but this was not tested.

To summarize, palaeomagnetic studies of the Hamersley Range Megasequence have revealed only remagnetised NRM directions, whereas the Chichester Range Megasequence and associated dolerite dykes appears to have preserved a primary NRM.

Aims of the Study

Important aims of our palaeomagnetic study are summarised as follows.
1. To demonstrate that there is a primary NRM in the succession.
2. To test the proposed correlations by Blake (2001) between mafic dykes and flood basalts in the area.
3. To establish a magnetostratigraphy for a Late Archaean flood basalt succession.
4. To look for evidence of geomagnetic reversals in the succession.
5. To establish a series of palaeomagnetic poles within a single, coherent stratigraphic succession for the period 2775-2715 Ma, and thus to construct a high-precision APWP for the Pilbara Craton for this time period.

Geological setting

The Mount Bruce Supergroup is a late Archaean to early Proterozoic succession of volcanic and sedimentary rocks, unconformably overlying the ca 3.5-2.85 Ga "granite-greenstone" terrain of the Pilbara Craton. The Supergroup has been divided into three groups, which, from old to young, are the Fortescue Group, the Hamersley Group, and the Turee Creek Group (e.g. MacLeod et al., 1963; Thorne and Trendall, 2001; Trendall, 1979). An unconformity-based framework for part of the lower succession of the Hamersley Province (i.e., most of the Fortescue Group or the Nullagine and Mount Jope Supersequences; Fig. 1.1, Tab. 1.1) was initiated in the 1980's to early 1990's (see Blake, 1993). More recently, Blake (2001) extended the unconformity-based divisions in the Nullagine Synclinorium of the east Pilbara and this framework is followed herein (Figs. 1.2, 1.3; Tab. 1.1; see Blake, 1993; Blake, 2001 for details).

The regional geotectonic evolution of the Nullagine and Mount Jope Supersequences is presented in detail in (Blake, 1993; Blake, 2001) and is summarised as follows. The two supersequences are interpreted as the rock record of a two-phase continental break-up in the late Archaean. The first phase, represented by the Nullagine Supersequence, was dominated by WNW-ESE directed extension (in present coordinates) that resulted in the formation of large volumes of mostly subaerial basalt, followed by the development of extensional intracontinental sedimentary basins with associated felsic and mafic volcanics and an ocean may have formed to the west of the present Craton. The

second phase of break-up, represented by the Mount Jope Supersequence, involved rifting of the southern Pilbara Craton margin, possibly along an earlier transfer fault, resulting in the eruption of large volumes of basalt, with minor felsic volcanism. In the north, the craton was buried beneath subaerial flood basalts and mafic tuff piles, whereas in the south it was buried beneath a dominantly submarine mafic succession.

Figures 1.2 and 1.3 summarise the geology of the Nullagine and Mount Jope Supersequences (and part of the Marra Mamba Supersequence Package) in the Nullagine Synclinorium. The succession comprises basalt, porphyritic felsic lava domes (?), mafic and felsic tuffs and terrigenous clastic sedimentary rock. It is metamorphosed to very low grade (prehnite–pumpellyite–epidote zone (< 200 mPa, < 300 °C); Smith et al., 1982), gently folded by two generations of folds, and cut by a complex array of normal faults (Blake, 2001).

The approximate 6 km thick (cumulative maximum thickness) succession has been divided into 11 unconformity-bound packages, and an upper package with a basal unconformity (Fig. 1.3). The packages have been numbered sequentially from oldest to youngest. Each package is interpreted as a cogenetic unit but, importantly, packages are not hierarchically identical. Package 1 is dominated by subaerial basalt, Package 2 is dominated by clastic sedimentary rock and felsic porphyry, and Packages 3 and 4 are dominated by clastic sedimentary rock with minor subaerial basalt near the top of Package 4 (Blake, 1993; Blake, 2001). Packages 5 to 10 are dominated by basalt and mafic tuff, but also contain minor felsic tuff bands. Package 11 is a marine succession that comprises mostly laminated mudrock with subordinate reworked crystal-rich felsic tuff, carbonated mafic volcarenite and chert. Package 12 is a marine succession that comprises laminated carbonaceous mudrock that passes gradationally upwards into ferruginous laminated chert.

In addition to extrusive mafic rocks, there are four physically and geochemically distinct mafic dyke suites in the area, each with a characteristic orientation (Fig. 1.2). These are the Black Range Suite (Blake, 1993) and the Mount Maggie, Five Mile Creek and Castle Creek Suites (Blake, 2001). Each dyke suite has been matched geochemically to basalts within the Nullagine or Mount Jope Supersequences in the Nullagine Synclinorium (Blake, 2001).

Initial dating of the Hamersley Province succession was dominated by the use of the Rb-Sr whole rock and mineral isochron methods which yielded mostly mean ages of 2300-2000 Ma (see summaries in Blake and McNaughton, 1984; Trendall, 1983; see also Nelson et al., 1992). Pidgeon (1984) published the first conventional zircon U-Pb age of 2768 ± 16 Ma for the felsic porphyry in Package 2 in the Nullagine Synclinorium (Fig. 1.3) and Arndt et al. (1991) provided the first SHRIMP zircon U-Pb ages for the Fortescue Group. These zircon U-Pb ages established a broad geochronological framework and showed that Rb-Sr and Pb-Pb isochrons obtained from igneous rocks probably date younger hydrothermal and/or metamorphic events rather than the age of magmatism (Blake and McNaughton, 1984; Nelson et al., 1992).

Wingate (1999) determined a mean ion microprobe baddeleyite ^{207}Pb/^{206}Pb age of 2772 ± 2 Ma from four samples each from a different dyke of the Black Range Suite including the Black Range Dyke itself. Geochemical and geological correlations (Blake, 2001) suggest that Package 1 basalt in the Nullagine Synclinorium is comagmatic with the Black Range Suite and hence is of the same age (Fig. 1.3). Blake et al. (2004) have obtained 11 high-precision SHRIMP zircon U-Pb ages from rocks within the Nullagine Synclinorium covering Package 2 to Package 11. Package 2 is dated at ca. 2766 Ma (cf. Pidgeon, 1984), the upper part of Package 4 is dated at ca. 2752 Ma, Package 5 is dated at ca. 2741 Ma, and Packages 7-10 were deposited between ca. 2725 Ma and 2715 Ma (Fig. 1.3).

Area	Package/ Dyke	Site Number	Lithology	AMG coordinates (AGD 84)	N	n	dec°	inc°	k	a95°	R	Plat°	VGP lat°	VGP long°
NS	10	U904	Basalt	50K 0803892 - 7529581	10	10	152.6	46.7	52.3	6.7	9.828	27.9	-64.6	191.5
NS	10	U907	Basalt	50K 0794956 - 7533268	10	8	147.2	48.6	49.4	8.0	7.858	29.6	-59.7	189.0
NS	10	U905	Basalt	50K 0800384 - 7528231	12	8	158.9	55.9	77.0	6.4	7.909	36.4	-66.9	167.5
NS	**10 mean**				**3**	**26**	**153.3**	**52.1**	**243.5**	**7.9**	**2.992**	**31.3**	**-64.1**	**183.5**
NS	9	U908	Basalt	50K 0790365 - 7538167	14	0	n/a	n/a	n/a	n/a	n/a	n/a	n/a	n/a
NS	9	U909	Basalt	50K 0790358 - 7538230	15	4	149.0	39.3	19.7	21.2	3.848	22.3	-61.4	203.9
NS	**9 mean**				**1**	**4**	**149.0**	**39.3**	**n/a**	**n/a**	**n/a**	**22.3**	**-61.4**	**203.9**
KB	CCS	U912	Dolerite	51K 0211344 - 7562821	27	14	127.0	53.5	102.9	3.9	13.874	34.0	-42.2	183.6
KB	**CCS mean**				**1**	**14**	**127.0**	**53.5**	**n/a**	**n/a**	**n/a**	**34.0**	**-42.2**	**183.6**
NS	8	U902	Basalt	50K 0801760 - 7550680	11	2	147.2	43.4	n/a	n/a	1.997	25.3	-59.9	197.3
NS	8	U901	Basalt	50K 0783579 - 7542746	10	7	141.5	50.0	342.6	3.3	6.982	30.8	-54.7	187.4
NS	8	U903	Basalt	50K 0804763 - 7554167	15	10	142.2	50.5	80.6	5.4	9.888	31.2	-55.2	186.6
NS	**8 mean**				**3**	**19**	**143.2**	**48.0**	**292.1**	**7.2**	**2.993**	**29.1**	**-56.7**	**190.1**
KB	FMCS	U913	Dolerite	51K 0213166 - 7563166	36	19	155.8	58.0	40.2	4.8	18.526	38.7	-63.4	165.9
KB	**FMCS mean**				**1**	**19**	**155.8**	**58.0**	**n/a**	**n/a**	**n/a**	**38.7**	**-63.4**	**165.9**
NS	7	U900	Basalt	50K 0777731 - 7542868	10	10	175.9	77.2	884.4	1.6	9.990	65.6	-46.6	122.2
NS	7	U899	Basalt	50K 0778502 - 7544894	11	8	132.0	75.7	564.4	2.3	7.988	63.0	-38.2	145.1
NS	7	U896	Basalt	51K 0190962 - 7558533	10	3	164.4	57.9	47.8	18.0	2.958	38.6	-68.8	155.5
NS	7	U898	Mafic tuff	50K 0792063 - 7561302	10	7	181.3	72.6	62.6	7.7	6.904	57.9	-54.1	118.7
NS	**7 mean**				**4**	**28**	**160.8**	**71.7**	**56.3**	**12.3**	**3.947**	**56.3**	**-52.8**	**133.7**
NS	6	U897	Basalt	50K 0809522 - 7566847	10	5	104.6	67.0	49.6	11.0	4.919	49.7	-25.9	164.1
NS	6	U888	Basalt	51K 0197002 - 7571844	10	0	n/a	n/a	n/a	n/a	n/a	n/a	n/a	n/a
NS	6	U887	Basalt	51K 0197465 - 7572443	10	0	n/a	n/a	n/a	n/a	n/a	n/a	n/a	n/a
NS	6	U886	Basalt	51K 0197449 - 7572544	10	4	165.9	61.7	96.8	9.4	3.969	42.9	-66.0	146.1
NS	6	U884	Basalt	51K 0197264 - 7572677	10	0	n/a	n/a	n/a	n/a	n/a	n/a	n/a	n/a
NS	6	U889	Basalt	51K 0198233 - 7572870	11	0	n/a	n/a	n/a	n/a	n/a	n/a	n/a	n/a
NS	5	U891	Basalt	51K 0198573 - 7573091	10	2	170.7	77.4	n/a	n/a	n/a	65.9	-45.6	125.5
NS	**5 & 6 mean**				**3**	**11**	**145.6**	**71.4**	**28.9**	**23.4**	**2.931**	**52.8**	**-47.1**	**147.1**
NS	4	U915	Basalt	50K 0796304 - 7572341	26	7	167.6	75.1	120.4	5.5	6.950	62.0	-49.1	128.7
NS	4	U916	Basalt	50K 0796058 - 7572405	5	0	n/a	n/a	n/a	n/a	n/a	n/a	n/a	n/a
NS	4	GSP52	Mafic tuff	51K 0199348 - 7577225	9	0	n/a	n/a	n/a	n/a	n/a	n/a	n/a	n/a
NS	**4 mean**				**1**	**7**	**167.6**	**75.1**	**n/a**	**n/a**	**n/a**	**62.0**	**-49.1**	**128.7**
NS	3	GSP51	Mudrock	51K 0196019 - 7584831	4	0	n/a	n/a	n/a	n/a	n/a	n/a	n/a	n/a
NS	**3 mean**				**0**	**0**								
NS	2	GSP50	Porphyry	51K 0198794 - 7589321	14	10	332.4	-70.1	29.2	9.1	9.692	54.1	51.5	326
NS	2	GSP173	Porphyry	51K 0201271 - 7588274	7	7	318.4	-74.7	78.4	6.9	6.923	61.3	41.2	325.2
NS	2	GSP184	Porphyry	51K 0201617 - 7588455	7	1	313.6	-63.7	n/a	n/a	n/a	45.3	45.6	346.8
NS	2	GSP183	Porphyry	51K 0201729 - 7588543	7	0	n/a	n/a	n/a	n/a	n/a	n/a	n/a	n/a
NS	**2 mean**				**3**	**18**	**320.9**	**-69.7**	**153.7**	**10.0**	**2.987**	**53.6**	**46.5**	**332.7**
NS	2	GSP33	Conglomerate	51K 0192952 - 7608690	40	26	n/a	n/a	n/a	n/a	n/a	n/a	n/a	n/a
NS	2	U895	Conglomerate	51K 0192871 - 7608499	10	0	n/a	n/a	n/a	n/a	n/a	n/a	n/a	n/a
MC	1	GSP67	Basalt	51K 0212666 - 7628329*	7	6	130.1	73.0	255.9	4.2	5.980	58.6	-38.6	151.0
MC	1	GSP66	Basalt	51K 0212666 - 7628329*	7	7	142.1	71.5	4898.0	0.9	6.999	56.2	-45.4	149.4
MC	1	GSP65	Basalt	51K 0212666 - 7628329*	7	6	136.6	67.2	748.0	2.5	5.993	49.9	-45.6	159.5
MC	1	GSP64	Basalt	51K 0212666 - 7628329*	7	5	137.9	70.7	117.2	7.1	4.966	55.0	-44.1	152.6
MC	1	GSP63	Basalt	51K 0212600 - 7628194*	7	7	129.1	70.5	161.5	4.8	6.963	54.7	-39.6	155.8
MC	1	GSP62	Basalt	51K 0212600 - 7628194*	7	6	132.3	70.4	175.6	5.1	5.972	54.5	-41.7	154.9
MC	1	GSP61	Basalt	51K 0212600 - 7628194*	7	7	129.4	66.5	1014.7	1.9	6.994	49.0	-41.6	162.9
NS	1	GSP37	Basalt	51K 0194857 - 7608645*	5	4	124.8	60.2	481.8	4.2	3.994	41.1	-39.9	173.8
NS	1	GSP36	Basalt	51K 0194857 - 7608645*	5	0	n/a	n/a	n/a	n/a	n/a	n/a	n/a	n/a
NS	1	GSP35	Basalt	51K 0194857 - 7608645*	5	0	n/a	n/a	n/a	n/a	n/a	n/a	n/a	n/a
NS	1	GSP34	Basalt	51K 0194857 - 7608645*	5	2	126.3	71.4	n/a	n/a	1.973	56.1	-37.8	154.8
NS	1	U894	Basalt	51K 0194425 - 7608523	10	7	125.7	63.3	139.1	5.1	6.957	44.8	-40.1	168.9
NS	1	U892	Basalt	51K 0194045 - 7608483	10	7	120.2	58.3	327.0	3.3	6.982	39.0	-36.5	176.8
NS	1	U893	Basalt	51K 0193839 - 7608409	10	10	129.1	70.0	176.0	3.7	9.949	53.9	-40.0	156.6
NS + MC	**1 mean**				**12**	**74**	**129.6**	**67.9**	**231.0**	**2.9**	**11.952**	**51.1**	**-41.2**	**159.9**
NS	BRS	U914	Gabbro	51K 0201215 - 7570357	5	0	n/a	n/a	n/a	n/a	n/a	n/a	n/a	n/a
NS	BRS	U917	Dolerite	51K 0199583 - 7561500	19	3	120.9	69.7	190.8	8.9	2.99	53.5	-35.8	159.1
NS	**BRS mean**				**1**	**3**	**120.9**	**69.7**	**n/a**	**n/a**	**n/a**	**53.5**	**-35.8**	**159.1**

Sampling

Four hundred and seventy one oriented drill cores (25 mm diameter, 5-6 cm long) were taken from the supracrustal succession in the Nullagine Synclinorium and associated comagmatic dykes in the area (Fig. 1.3, Tab. 1.2). Mafic dyke samples were taken from the Black Range, Five Mile Creek and Castle Creek Suites (Fig. 1.3; Blake, 2001). The Mount Maggie Suite (Fig. 1.3; Blake, 2001) was not sampled because it is poorly exposed. Samples were collected using a petrol drill, with an average of 9 cores per site for the supracrustal succession. Four oriented hand samples were collected (Site GSP51) and cored in the laboratory (two cores per hand sample). In addition, to enable a fold test for Package 1, 49 cores were collected from 7 sites from basalts of a stratigraphic equivalent to Package 1 in the Meentheena Centrocline (Figs. 1.1, 1.3; Tab. 1.2).

Sample sites were chosen carefully to allow collection of fresh in-situ rock in areas least likely to have been struck by lightning. Most supracrustal samples are of flood basalts with fewer samples from massive dacite porphyry, terrigenous mudrock, mafic tuff and conglomerate (Tab. 1.2). Packages 5 and 6 were sampled as one unit, because the distinction between these packages had not been made at the time of sampling.

Methods

In the field, a susceptibility meter (Scintrex K2) was used as an indication for magnetic intensity of the sampled rocks in the field. For low values, a magnetic compass was used to orient the samples, and for higher values, as a precaution a sun compass was used in addition to the magnetic compass. No significant difference were recorded between magnetic and sun compass directions (between 0-2° in all cases).

In the laboratory, the cores were cut to standard specimens of 22 mm length. The anisotropy of magnetic susceptibility was measured on an AGICO KLY-3 susceptibility bridge, which showed that the samples are not significantly anisotropic (range from 0.3 to 3.4 %). At least one specimen and occasionally two specimens of each drill core were thermally demagnetised in a magnetically shielded, laboratory-built furnace. The NRM was measured on a 2G Enterprises DC-SQUID cryogenic magnetometer. Eleven specimens were demagnetised using the alternating field (AF) technique, where demagnetisation was performed in a laboratory-built AF demagnetiser up to a peak field of 200 mT.

NRM directions were analysed and interpreted with Zijderveld diagrams (Zijderveld, 1967). Principal component analysis (Kirschvink, 1980) was used to determine the directions of the various NRM components. Mostly, no directions with a maximum angular deviation (MAD) greater than 10° were used, except for very weak samples.

Table 1.2 (opposite)
Summary of HT (high temperature) results from the Nullagine Synclinorium and the Meentheena Centrocline. Results are in stratigraphic order with each comagmatic dyke placed at the base of its associated package. The Meentheena Package 1 data are placed above the Nullagine data (in stratigraphic order) for convenience only, exact correlations are uncertain. Correlation of Meentheena Package 1 and Nullagine Package 1 basalts is based on relative stratigraphic position, flow morphologies and petrographic characteristics. Grey areas show means. Abbreviations: AMG = Australian Map Grid, N = number of specimens from each site and number of sites contributing to the mean, n = number of specimens accepted and the number of specimens contributing to the mean, dec = declination, inc = inclination, Plat = palaeolatitude, VGP lat (long) = latitude (longitude) of VGP (virtual geomagnetic pole), n/a = not applicable, KB = Kurrana Batholith, MC = Meentheena Centrocline, NS = Nullagine Synclinorium, CCS = Castle Creek Dyke Suite, FMCS = Five Mile Creek Suite, BRS = Black Range Suite. Identical AMGs with asterisk indicate sequences of sites in basalt flows directly on top of each other.

Results

Thermal demagnetisation

The NRM of all rock units shows either two or three components. A low temperature (LT) component was recorded in the temperature range of 20 °C to 300-350 °C; this component was well-developed in Packages 2, 7, 9 and 10 and in the Five Mile Creek Suite. A medium temperature (MT) component was recorded from 350 °C to approximately 450 °C; this component is well-developed in specimens from Package 7 upward and in the Five Mile Creek Suite. A high temperature (HT) component was recorded from 450°C to 580 °C; this component is well-developed in almost all rock units and rock types except in Package 3 and 9.

The LT component records the present day field direction (Figs. 1.4, 1.5), which is generally only apparent in samples with a weak magnetic intensity of the HT component. All samples are of fresh rock, so the LT present day field component is unlikely to be caused by weathering. Possibly, a (small) part of the NRM has been reset in the ambient field by high surface rock temperatures (air temperatures commonly exceed 40°C in summer) and is recorded by low coercivity or low unblocking temperature magnetite. For example, the normalised intensity versus temperature plot of sample U892.2A (Fig. 1.6c) shows a two-step intensity decay, with 20% intensity loss between the 20° to 300 °C steps, which is when the LT component unblocks. Between 300° and 500 °C only a gradual intensity decrease is observed and from 500 °C the HT component effectively starts unblocking in this sample.

The following paragraphs describe the palaeomagnetic results per package and dyke suite. Confer Table 1.2 for statistical details.

Package 1 has a well-developed HT component and magnetisations of relatively high magnetic intensity (on average 50×10^{-3} A/m, whereas most packages have an average magnetic intensity of 5 to 10×10^{-3} A/m, although compared to modern basalts, these intensities are all exceptionally low). Except for sites GSP35 and GSP36, which have been affected by lightning, the distribution of high temperature directions from both the Nullagine Synclinorium and Meentheena Centrocline samples is very well clustered (Fig. 1.5a). LT and MT components were poorly developed or did not have consistent directions in this package (e.g. Fig. 1.4a).

The Package 2 felsic porphyry showed a HT component with a consistent direction, which is antipodal to the HT components of other packages (Figs. 1.4b, 1.5b). The MT directions were poorly defined and the LT directions could rarely be determined.

Most exposed rocks in Package 3 were unsuitable for palaeomagnetic sampling. An attempt was made to acquire data from a siltstone (GSP51) but no reliable HT components were derived.

In Package 4, a mafic tuff horizon (GSP52), and a single basalt flow (U915, U916) near the top of this succession were sampled. The mafic tuff revealed only present day field directions and was unsuitable for thermal demagnetisation (i.e., they exploded above 350-400 °C). Four specimens of the basalt flow revealed a low temperature present day field direction (e.g. Fig. 1.4c) and only seven specimens revealed a consistent HT direction (Fig. 1.5c). The remaining samples from this package were affected by lightning.

No well-defined component could be derived from basalt samples from Packages 5 and 6, because the HT component is largely overprinted by a MT component of inconsistent direction, resulting in an unreliable end-vector at high temperatures. Out of seven sites, with a total of 71 samples (Tab. 1.2), only three sites, with a total of eleven samples, revealed meaningful results (e.g. Fig 1.5d).
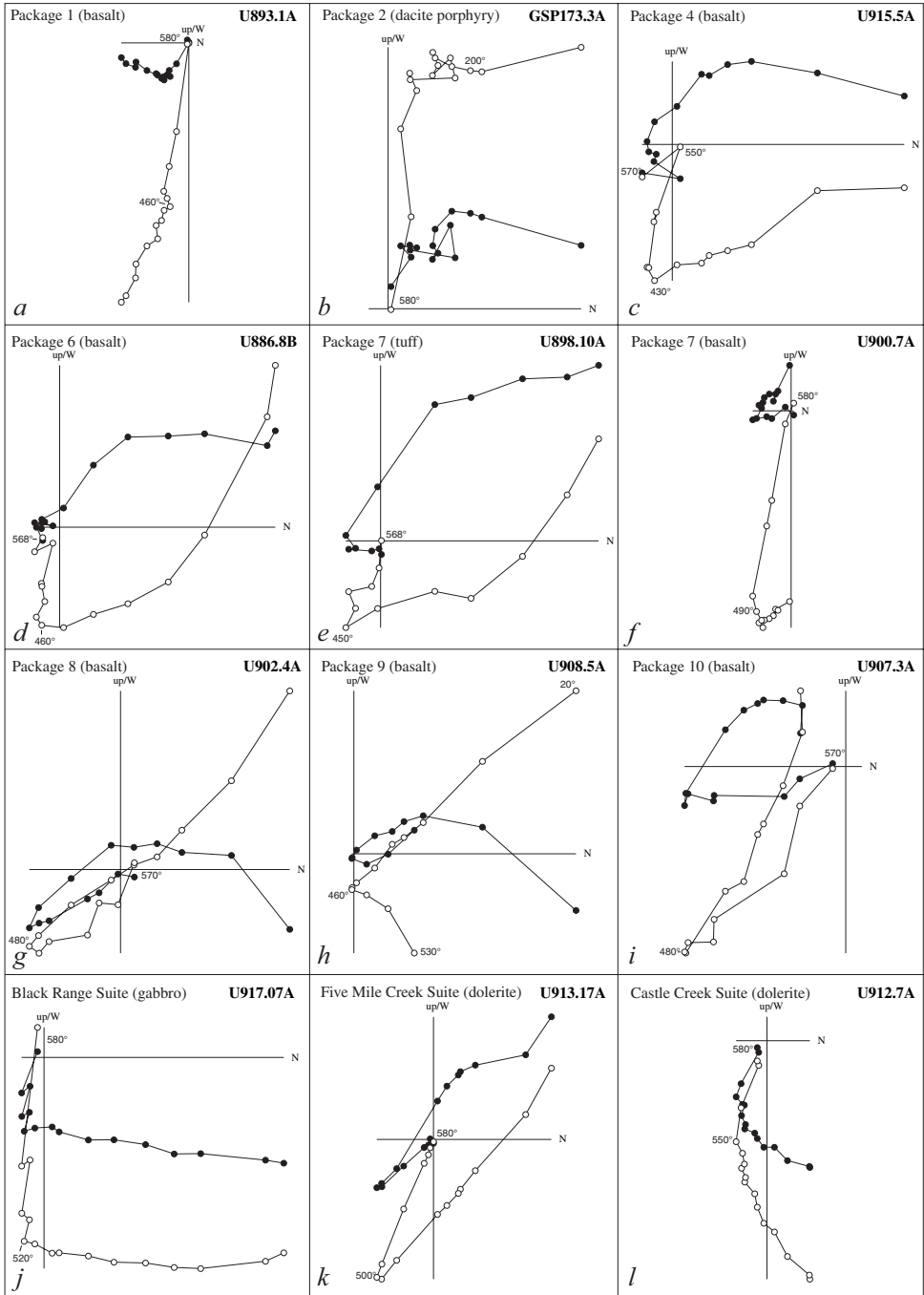
Figure 1.4

Examples of characteristic Zijderveld diagrams from each package and sampled comagmatic dykes. Key temperature steps are shown. Specimen numbers indicate location (Fig. 1.2, Tab. 1.2) followed by sample number. 1.4a, b, f, h, j, k, l show two components of magnetisation, 1.4c, d, e, g, i show three components.
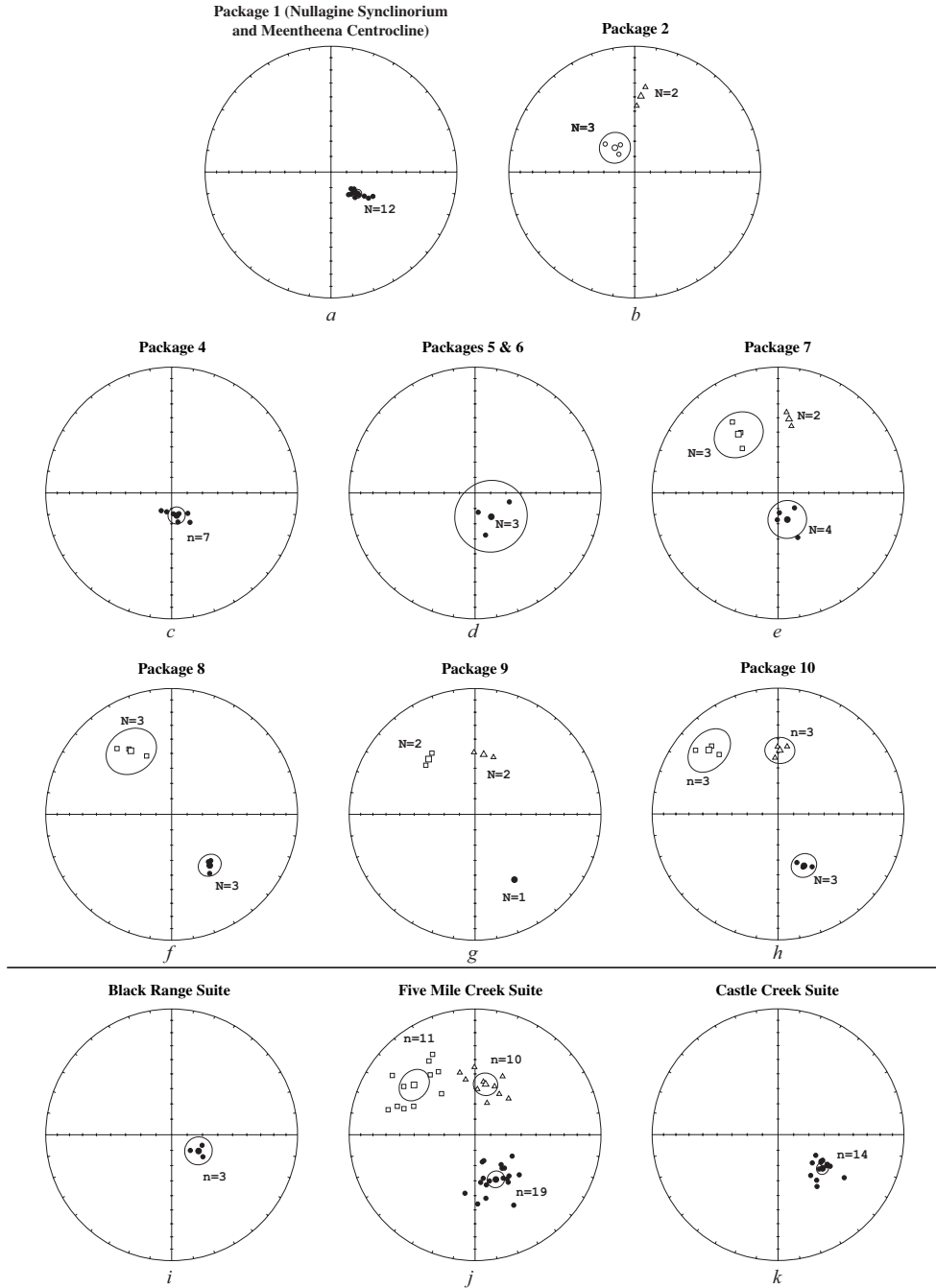
Figure 1.5
Equal area plots of results from all studied packages and dykes. 1.5a, b, d, e, f, g, h represent equal area plots of multiple sites. N = total number of sites with accepted data, small symbols are site means, larger symbols are the mean of site means with the corresponding $\alpha 95$ circles (where applicable). 1.5c, i, j, k represent single sites, n = total number of specimens, larger symbols are the sample means showing error circles. Open (closed) symbols indicate negative (positive) inclinations, circles are high temperature directions, squares are medium temperature directions and triangles are low temperature directions. Data in Tables 1.2, 1.3.

Most samples of Package 7 were taken from flood basalts and one sample set was taken from a mafic tuff (U898). Individual sites show a good clustering of the data (e.g. site U899, with k=564, Tab. 1.2), but the package mean direction has a larger spreading (k=56, Tab. 1.2). In the flood basalts, except for site U896, all three NRM components are developed (Fig. 1.4e, 1.4f) and cluster well (Fig. 1.5e). While some mafic tuff samples are affected by a present day field overprint the MT and HT components are clearly present.

In Package 8, the MT and HT directions form well-defined clusters, and the present day field overprint is generally poorly developed, but some samples show all three NRM components as illustrated in Figure 1.4g. Data from individual sites cluster well as does the package mean, both for the HT and MT directions.

Suitable fresh exposure of Package 9 basalt was not found in the Nullagine Synclinorium. The basalt is commonly strongly weathered because of its coarse grain size (see Tab. 6 in Blake, 2001). Despite this problem, the few samples from a single basalt flow unit in Package 9 (Fig. 1.3) yielded all three NRM components (e.g. Figs. 1.4h, 1.5g). The MT component is well developed at both sites, although the HT component is only consistent at site U909 (Fig. 1.5g).

In Package 10, all three components of magnetisation are recorded (e.g. Fig. 1.4i) and their directions form well-defined clusters (Fig. 1.5h). Occasionally, the NRM could not be completely removed, giving scattered directions at temperatures of 560 °C or higher, possibly because of growth of new magnetic minerals during thermal demagnetisation.

The Black Range Suite was sampled at two locations (U914, U917). The Cajuput Dyke (Fig. 1.2; site U914) was difficult to drill because it contains abundant quartz. The few samples from this site revealed only a present day field direction. A smaller dyke from the same suite (site U917) is finer grained. The demagnetisation diagrams for this site generally show a HT and a LT component (e.g. Fig. 1.4j), of which only a few consistent and reliable HT directions could be derived (Fig. 1.5i). The LT directions do not cluster.

The Five Mile Creek Suite was sampled at one location (site U913) and all three magnetisation components are present (e.g. Fig. 1.4k). The HT component is commonly present and its directions cluster reasonably (k=40), while also the LT and MT components form acceptable clusters (Fig. 1.5j).

The Castle Creek Suite was sampled at one location (site U912) and shows MT and HT components of magnetisation (Fig. 1.4l). The MT component is poorly developed and does not cluster, whereas the HT component is easily distinguished and its directions show clear clustering (Fig. 1.5).

Lightning
Previous work has shown that exposed rocks in the Pilbara have commonly been struck by lightning (Schmidt and Clark, 1994; Schmidt and Embleton, 1985). Lightning strikes can destroy or partly reset NRM (Hallimond and Herroun, 1933). Lightning strikes have been shown to disturb the remanent magnetisation of a surface area as much as 25 m^2 (Graham, 1961) and can affect rocks down to 25 metres below the surface. However, the original remanent magnetisation can usually be detected at a depth of 90 to 160 centimetres in areas struck by lightning. Since lightning commonly strikes on high and/or open places, sampling sites were chosen in narrow and deep-cutting gullies or on steep rock faces.

Following several pilot studies (van Hoof, pers. com.), careful field procedures have resulted in only 10 % of the samples showing a lightning induced remanent magnetisation.
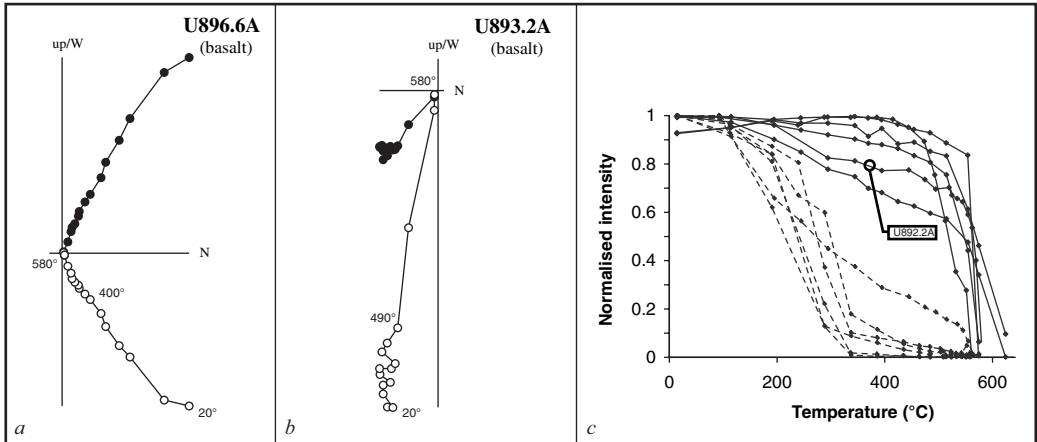
Figure 1.6
Examples illustrating the effects of lightning strikes.
a) Zijderveld diagram of a basalt sample struck by lightning, showing a characteristic steep intensity decrease at low temperatures.
b) Zijderveld diagram of a basalt sample not struck by lightning, showing a gradual intensity decrease up to 490 °C followed by a steep decrease up to 580 °C.
c) Normalised intensity *versus* temperature of selected basalt samples. The dashed lines show the intensity decay of representative samples struck by lightning (specimens U894.10, U896.6, U915.11, .15, .16 and .19). Solid lines show the intensity decay of samples not struck by lightning (specimens U892.2, .7A and .7B, U893.1, .2 and .5, and U899.5). Specimen U892.2 is pointed out to show two-step unblocking: the LT component unblocks between 20° and 300 °C and the HT component between 500° and 580 °C.
Conventions of Figures 1.6a and 1.6b as in Figure 1.4, see Figure 1.2 for specimen locations.

Lightning has the following effects on NRM, which proved to be diagnostic in the recognition of lightning induced NRM.

1. The intensity of the magnetic signal is usually much stronger (commonly by more than an order of magnitude) than the intensity of the magnetic signal of the same rock unaffected by lightning.
2. Samples affected by lightning generally reveal only one component (e.g. compare Fig. 1.6a with Fig. 1.6b).
3. The direction of this one component compared to other samples from the same site or location is random, so sampling an area around a point which has been struck by lightning should reveal a set of random directions (Graham, 1961).
4. The (normalised) magnetic intensity is observed to decrease rapidly with increasing temperature, whereas the magnetic intensity of (magnetite bearing) rocks unaffected by lightning show a gradual decrease until about 525-550 °C and then a steep decrease close to 580 °C (Fig. 1.6c).

Field tests

To help constrain the time at which the NRM was acquired, three palaeomagnetic field tests were carried out, namely a fold test, a reversal test and a conglomerate test.

A fold test could not be achieved in the Nullagine Synclinorium, because the succession dips too shallowly (mostly < 5°) and is only gently folded. However, HT data from Package 1 in the Nullagine Synclinorium can be compared with HT data from a stratigraphic equivalent of Package 1 in the Meentheena Centrocline (Fig. 1.1) to define a fold test. Directions before and after tilt correction are shown in Figure 1.7a (data in Tab.
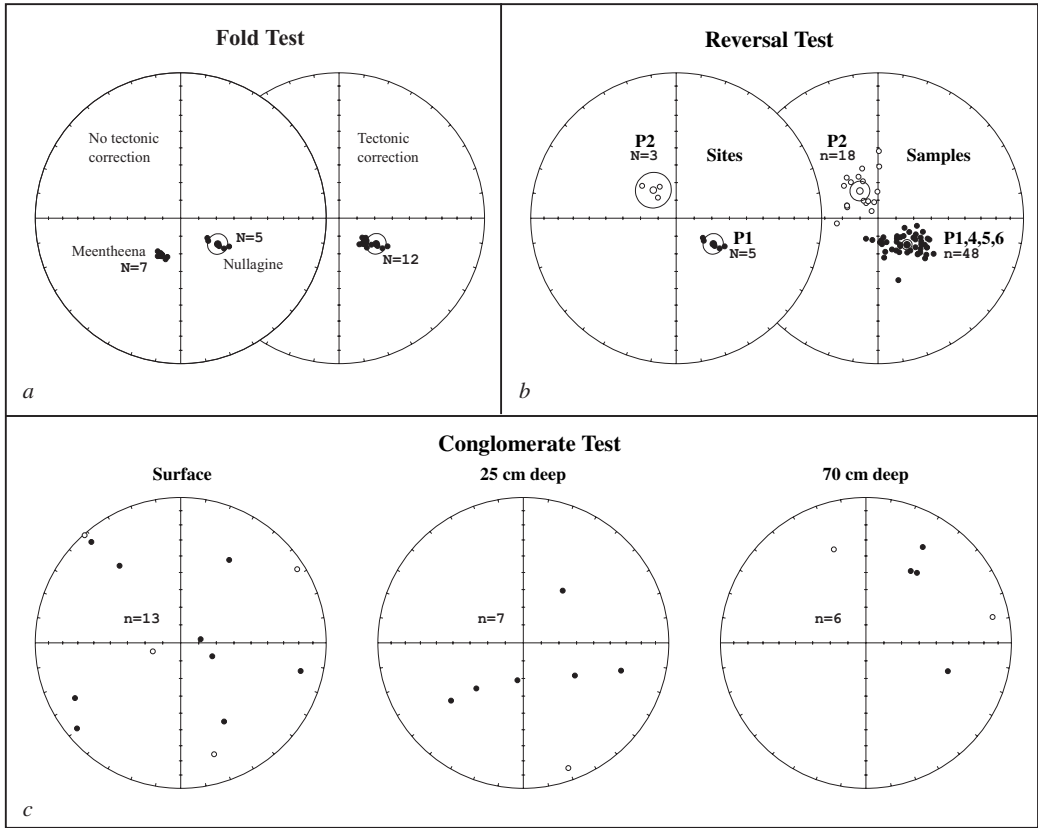
Figure 1.7
a) Equal area plots of HT directions from the fold test before and after tilt correction. Symbols represent site means. All directions are from Package 1, both from the Nullagine Synclinorium and from the Meentheena Centrocline. The $\alpha 95$ circle of the Meentheena data is too small (1.9°) to be noticed on the plot.
b) Equal area plots of HT directions from the reversal test. The left plot shows the directions of site averages of Package 1 and 2 in the Nullagine Synclinorium; the right plot shows the directions of individual samples of Package 1, 2, 4 and 5-6 from the Nullagine Synclinorium.
c) Equal area plots of HT directions from the conglomerate test, taken at three different levels. All directions are from specimens of Package 2, site GSP33 (Fig. 1.2).
Conventions as in Figure 1.5.

1.2). These data do not pass the fold test according to Definition 1 of McFadden (1990), because statistically the two groups do not belong to the same population, but in an incremental fold test using an eigenvector approach, they do give better results at 100% tilt correction (Tauxe and Watson, 1994), but the best result is obtained at ca. 130 ± 30% unfolding. The large error is caused by the small difference in bedding between Nullagine and Meentheena. One problem in applying the McFadden fold test is that the precision parameter of the Meentheena samples (k_1 = 806) is much higher than that of the Nullagine samples (k_2 = 182; so k_1/k_2 = 4.4). Ideally, the k_1/k_2 ratio should not be larger than 2. A second problem is determination of the exact dip of shallow-dipping basalt flows. Flow tops are commonly undulose at several scales and tectonic dips are difficult to estimate accurately. This may explain the misfit of site means after tilt correction in Fig. 1.7a. However,

because the incremental tilt correction gives better results at 100 % unfolding, we conclude that the HT magnetisation was most probably acquired prior to folding. The age of the folding is not exactly known. Blake (2001) describes that NNE-trending folds are thought to have formed contemporaneously with the development of the Nullagine and Mount Jope Supersequences. The age of the SE-trending folds is more problematic. While they are probably related to younger deformations that are more strongly developed around the Pilbara Craton margins, a Mount Jope Supersequence age cannot be discounted.

The discovery of magnetic reversals in the HT component of the succession allowed for a reversal test, which was carried out using two different approaches. First, the HT site means of Package 1 (Nullagine Synclinorium and Meentheena Centrocline data) were compared to those of Package 2 and the reversal test of McFadden and McElhinny (1990) was performed (Fig. 1.7b, left). With and without simulation the reversal test was found to be positive (classification B), meaning that the antipodal angle lies between 5 and 10°. The angle between the mean of the normal and the mean of the reversed polarity set is 8.0°, which is smaller than the critical angle of 9.2°. Second, a reversal test was performed on all accepted individual HT sample directions from Packages 1 to 6 (except for the Package 2 conglomerate samples; Fig. 1.7b right). This reversal test is also positive with the angle between the mean of the normal and the mean of the reverse polarity set being 6.0°, which is lower than the critical angle of 6.2°(resulting in classification B). Although no data are available for the sedimentary successions of Packages 3 and 4, the reversed interval is stratabound, which is additionally suggestive of a primary magnetisation.

A conglomerate test was carried out on basalt clasts (cobbles to boulders) in a conglomerate that overlies Package 1 basalts. Field relationships, petrographic data and unpublished geochemical data show that the basalt clasts were derived from Package 1 basalts. Basalt clasts were sampled (one core per clast) and thermally demagnetised (Tab. 1.2). The succession above the conglomerate was also sampled (Package 2 massive dacite porphyry to Package 10), making this conglomerate test an intraformational conglomerate test (McElhinny and McFadden, 2000). The test was carried out at two sites approximately 100 m apart. The characteristic remanent magnetisation (ChRM) of specimens from the first site (U895: Figs. 1.2, 1.3) shows no preferred orientation. However, from the strong magnetic intensity of these samples and from the intensity decay curves we interpret these samples as having been struck by lightning.

The second site (GPS33; Figs. 1.2, 1.3) was sampled at the surface and, following blasting, at depths of 25 cm and 70 cm below the original surface (Fig. 1.7c). Samples from basalt clasts at this site mostly have much lower magnetic intensities than the U895 basalt clast samples. In addition, the magnetic intensity of these basalt clasts was mostly two orders of magnitude lower than the intensities of the underlying Package 1 basalts, an observation similar to that of Shipunov et al. (1998). Of a total of 40 samples, 14 (35 %) are interpreted as affected by lightning. Of the 21 basalt clasts sampled at the surface, 8 (38 %) are affected by lightning. At 25 cm below the surface 3 (30 %) of the 10 clasts samples are affected by lightning. At 70 cm below the surface 3 (33 %) of the 9 clasts samples are affected by lightning. Hence, blasting to a depth of 70 cm made little difference to the percentage of samples affected by lightning.

The ChRM of the samples of GSP33 from the surface that were not affected by lightning has no preferred orientation (Fig. 1.7c). The test for uniform randomness of Watson, 1956 requires the resultant (R) of all N individual directions to be smaller than a critical value R_0. In this case, N = 13, R_0 = 5.75 and R = 3.150, so R < R_0, meaning that there is at least

a 95% probability that the directions come from a random population. Further, an alternative and more sensitive conglomerate test by Shipunov et al. (1998), which allows for the inclusion of a known secondary component or reference vector for the studied area, is also positive, with $\rho_0 = 0.263$ and $\rho = 0.207$, so $\rho < \rho_0$. The reference vector used in the calculations is 132.5°/68.0°, the average direction of NRM of Package 1, 4 and 5-6.

The ChRMs from 25 cm below the surface give a negative Watson test for uniform randomness and the test of Shipunov was also negative, with $N = 7$, $R_0 = 4.18$, $R = 4.939$, $\rho_0 = 0.362$ and $\rho = 0.686$ (Fig. 1.7c). The ChRMs from the 70 cm below the surface also did not pass the Watson test for uniform randomness, with $N = 6$, $R_0 = 3.85$ and $R = 4.211$. However, the test of Shipunov with $\rho_0 = 0.392$ and $\rho = 0.258$ is positive. When all accepted samples from the surface, 25 cm and 70 cm depth are pooled, both the test of Watson ($N = 26$, $R_0 = 8.18$ and $R = 9.621$) and the test of Shipunov ($\rho_0 = 0.186$ and $\rho = 0.348$) are negative.

The results of the conglomerate test after the blasting are unclear and it is possible that the ChRM has been (partly) reset by the shock wave from the blasting (shock induced remagnetisation?). Although the clasts from 70 cm below the surface pass the test of Shipunov, the negative results from 25 cm below the surface make the validity of the data after the blasting uncertain and are thus disregarded. However, since the ChRM in the basalt clasts not struck by lightning from the surface is random, the conglomerate test is interpreted as positive. Together with the positive fold test and positive reversal test, we conclude that the ChRM preserved in the rocks from Packages 1 to 10 is a primary NRM.

Thus, the HT component of the accepted basalt, dolerite and dacite porphyry samples is interpreted to have been acquired during or shortly after the cooling of the rocks in the late Archaean and is a record of the geomagnetic field at that time. The HT component of the accepted mafic tuff samples (U898) is interpreted as the result of lock-in of free magnetite grains during consolidation of the tuff and is also a record of the geomagnetic field in the late Archaean.

Discussion
Dyke to Package correlations

From earlier palaeomagnetic correlations it could be deduced that the Black Range Suite (BR in Fig. 1.8) was possibly of similar age as the Chichester Range Megasequence. This follows from data presented by Schmidt and Embleton (1985), although they used a different lithostratigraphic terminology. New geochemical evidence shows that the Black Range Suite is most probably comagmatic with Package 1 (Blake, 2001). This is supported by the palaeomagnetic data presented herein (Tab. 1.2). Further, the Five Mile Creek Suite correlates geochemically to Package 8 and the Castle Creek Suite to Package 9 or 10 (Blake, 2001). From our palaeomagnetic data, these correlations are less apparent (Tab. 1.2), but when the results of Package 8 to 10 are averaged as one group (see below), the Five Mile Creek and Castle Creek Suite results fall in this group and do not contradict the proposed correlations. More sampling of the dykes is needed, however, to convincingly confirm the proposed correlations palaeomagnetically.

The medium temperature (MT) and high temperature (HT) components

The evaluation of all package means, including both the HT and the MT directions (if applicable) with their corresponding α95 made it apparent that there are five distinct groups of data (Tabs. 1.2, 1.3), which have significantly different mean directions (Tab. 1.4). These groups are:
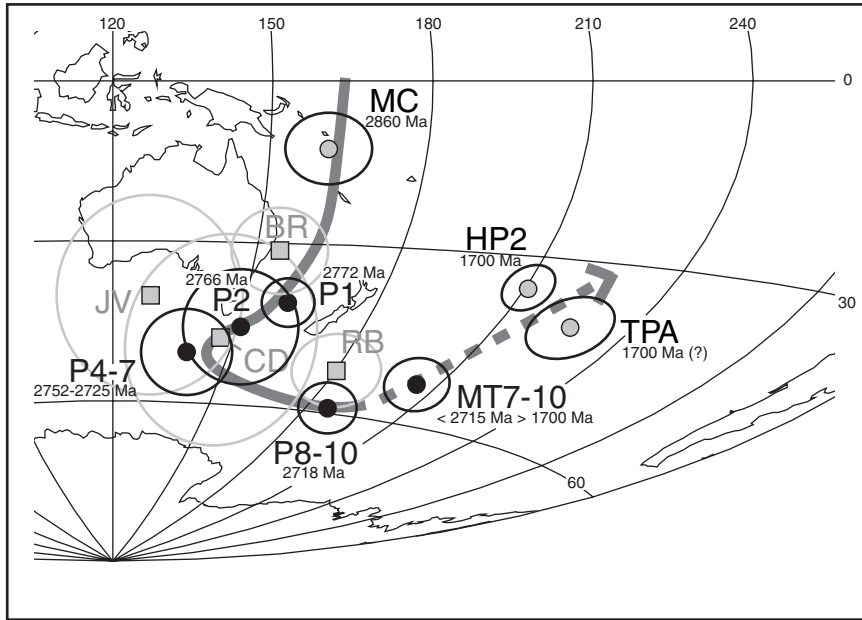
Figure 1.8
Aitoff projection of the apparent polar wander path (APWP) for the Pilbara from ca. 2860 to ca. 1700 (?) Ma showing approximate pole ages. Dashed part of the APWP is speculative. APWP is based on this study and published data. Square symbols are poles not included in the APWP. Circular symbols are poles included in the APWP, of which the black filled circles are poles from this study. Poles comprising the APWP are MC (Millindinna Complex, Schmidt and Embleton, 1985), P1 (Nullagine and Meentheena Package 1 HT data and the Black Range Suite HT data), P2 (Package 2 HT data), P4-7 (Packages 4 to 7 HT data), P8-10 (Packages 8 to 10 HT data and Five Mile Creek Suite and Castle Creek Suite HT data), MT7-10 (medium temperature directions), TPA (Mt. Tom Price iron ore, Schmidt and Clark, 1994) and HP2 (Hamersley Province F3 pole, Li et al., 2000). Each package pole is a grouped mean of the mean site data, including comagmatic dykes (cf. Tab. 1.4). Poles not included in the path are BR (Black Range Dyke) and CD (Cajuput Dyke, Embleton, 1978), RB (Mount Roe Basalt) and JV (Mount Jope Volcanics, Schmidt and Embleton, 1985).

1. P1, which comprises the HT directions of Package 1 samples plus the HT directions of Black Range Dyke Suite samples;
2. P2, which comprises the HT directions of Package 2 samples;
3. P4-7, which comprises the HT directions of Packages 4, 5, 6 and 7 samples;
4. P8-10, which comprises the HT directions of Packages 8, 9 and 10 samples plus the HT directions of the Five Mile Creek Suite and the Castle Creek Suite samples.
5. MT7-10, which comprises the MT directions of Packages 7, 8, 9 and 10 plus the MT directions of the Five Mile Creek Suite samples (Tab. 1.3).

Based on the positive field tests, the HT component is interpreted as the primary NRM. It follows therefore that the age of the HT component is the same as the age of cooling of the basalt, dolerite and dacite porphyry samples. These ages have been determined by high-precision geochronology and bracket the ages of the four HT groups as follows. P1 magnetisation is ca. 2772 Ma, P2 is ca. 2766 Ma, P4-7 is bracketed between ca. 2752 Ma and ca. 2725 Ma, and P8-10 is bracketed between ca. 2718 Ma and ca. 2715 Ma (Fig. 1.8).

The direction of the MT component is in all cases reversed with respect to the direction of the HT component and has a relatively shallow inclination, in contrast to the relatively steep inclination of the HT components. Whereas the HT directions of Package 7 and 8 are

Package/ Dyke	Site Number	N	n	dec°	inc°	k	a95°	R	Plat°	VGP lat°	VGP long°
10	U904	10	6	315.7	-25.5	24.9	13.7	5.800	13.4	47.1	34.1
10	U907	10	8	315.3	-34.0	34.2	9.6	7.795	18.6	48.1	26.4
10	U905	12	3	307.7	-18.4	19.0	29.1	2.895	9.4	38.3	35.6
10 mean		**3**	**17**	**312.7**	**-26.0**	**84.2**	**13.5**	**2.976**		**not calculated**	
9	U908	5	3	324.8	-40.3	56.6	16.5	2.965	23.0	57.6	21.7
9	U909	5	3	314.9	-43.9	345.8	6.6	2.994	25.7	48.8	15.8
9 mean		**2**	**6**	**320.0**	**-42.2**	**n/a**	**n/a**	**1.995**		**not calculated**	
8	U902	11	6	326.9	-38.0	103.0	6.6	5.951	21.3	59.3	25.1
8	U901	10	3	333.5	-46.0	63.6	15.6	2.969	27.4	65.4	12.2
8	U903	15	8	320.3	-31.6	97.1	5.6	7.928	17.1	52.4	30.3
8 mean		**3**	**17**	**327.3**	**-39.8**	**64.6**	**15.5**	**2.969**		**not calculated**	
FMS	U913	36	11	310.1	-35.1	24.6	7.6	10.556	19.4	43.4	23.9
FMS mean		**1**	**11**	**310.1**	**-35.1**	**n/a**	**n/a**	**n/a**		**not calculated**	
7	U900	10	7	327.3	-33.4	25.8	12.1	6.767	18.2	59.1	31.0
7	U899	11	7	321.3	-52.6	23.2	12.8	6.742	33.2	54.2	3.3
7	U896	10	0	n/a	n/a	n/a	n/a	n/a	n/a	n/a	n/a
7	U898	10	6	328.3	-43.0	21.4	14.8	5.766	25.0	60.8	17.7
7 mean		**3**	**20**	**326.0**	**-43.0**	**66.5**	**15.2**	**2.970**		**not calculated**	
Total MT		**12**	**71**	**320.0**	**-37.1**	**52.0**	**6.1**	**11.788**	**20.7**	**53.2**	**23.9**

Table 1.3
Summary of MT (medium temperature) results from the Nullagine Synclinorium. Consistent MT directions were found only in Packages 7, 8, 9 and 10 and the FMCS. Results are grouped by package and comagmatic dyke suite. See Table 1.2 for additional sample data and explanation of abbreviations.

clearly different (Tab. 1.2), the MT directions are similar, and therefore all MT directions are grouped in MT7-10. Hence, MT7-10 is interpreted as the result of a (re)magnetisation that is younger than the HT magnetisation. Remagnetisation in the Pilbara has previously been ascribed to either burial metamorphism (e.g. Schmidt and Clark, 1994; Sumita et al., 2001) and/or orogenic activity (e.g. Li et al., 2000). However, if the MT remagnetisation was caused by the thermal effects of regional-scale burial metamorphism or a regional-scale orogenesis, it should have been detected throughout the succession, not in the upper 4 packages only. Because no data were acquired higher than Package 10, the full stratigraphic distribution of the MT component is unknown. While the MT component is interpreted as the result of a "thermal" event, the exact nature and scale of the event is unknown.

Li et al. (2000) describe phases of remanence acquired possibly at the end of the Ophthalmian Orogeny (ca. 2200 Ma) and during the late Ashburton Orogeny (ca. 1700 Ma). The MT component of this study is different from both of these remagnetisations and hence cannot readily be ascribed to either orogenic phase with any certainty. The pole of the MT direction plots approximately midway between the P8-10 pole (ca. 2715-2718 Ma) and the ca. 1700 Ma pole of the Hamersley BIFs (TPA and HP2, Fig. 1.8, Li et al., 2000; Schmidt and Clark, 1994). However, appropriate field tests should be done before the age of the MT7-10 magnetisation can be constrained more accurately and more confidently.

Group	N	dec°	inc°	min lat°	max lat°	av lat°	latp°	longp°	a95°	dp°	dm°
TPA	1	308.8	-9.3	0.0	10.6	4.7	-37.4	220.3	n/a	5.7	11.3
HP2	9	304.2	-18.1	6.9	11.8	9.3	-35.3	211.9	3	n/a	n/a
MT7-10	12	320.0	-37.1	16.7	25.2	20.7	-53.2	203.9	5.3	n/a	n/a
JV	5	n/a	n/a	n/a	n/a	n/a	-40.5	128.7	n/a	19.9	20.8
P8-10	9	146.8	49.9	26.2	35.7	30.7	-59.1	186.3	6.1	n/a	n/a
P4-7	8	157.5	72.2	46.2	70.6	57.3	-50.4	138.2	12.5	n/a	n/a
P2	3	320.9	-69.7	40.6	70.0	53.5	-46.5	152.7	15.2	n/a	n/a
P1	13	129.0	68.0	47.4	55.0	51.1	-40.8	159.8	3.7	n/a	n/a
CD	9	145.0	71.0	38.7	78.1	55.4	-46.0	146.0	22.0	n/a	n/a
BR	16	115.0	72.0	48.3	67.0	57.0	-32.0	154.0	9.0	n/a	n/a
RB	4 (12)	320.0	-53.8	28.5	41.2	34.3	-52.4	178.0	n/a	6.4	9.1
MC	1 (8)	265.0	-65.1	40.8	54.4	47.1	-11.9	161.3	n/a	6.8	8.4

Table 1.4
Summary of grouped palaeolatitude and palaeopole positions from this study (Group name in bold) and from previously published data (Group name in normal print). Group definitions are given in the caption to Figure 1.8 and in the text. Site means contributing to each group mean are given in Tables 1.2 and 1.3 and each group is plotted in Figure 1.8. N = number of sites contributing to the grouped mean (site means given in Tables 1.2 and 1.3), N in italics = number of localities with number of sites between brackets, dec° = declination, inc° = inclination, min lat° = minimum palaeolatitude, max lat° = maximum palaeolatitude, min, max and ave lat° = minimum, maximum and average palaeolatitude respectively, latp = latitude of pole position, longp = longitude of pole position, a95 = confidence circle at the 95% level, *dp* and *dm* define the oval of 95% confidence about the mean pole.

Apparent polar wander

Table 1.2 is an overview of the HT component data of all sampled rock units. Table 1.3 summarises the directions of MT7-10. Virtual geomagnetic pole (VGP) positions have been calculated for the HT and MT components, both from the mean of each site and from the mean of each package and dyke suite. The palaeomagnetic poles for the grouped data (Tab. 1.4), which were calculated from the VGPs of the site means, are plotted in Figure 1.8, which also includes previously published relevant palaeomagnetic poles (cf. also Tab. 1.4). Although P2 plots within the 95% confidence limit of both P1 and P4-7, its average pole position plots half way between these groups.

There is some overlap of the relevant part of the previous APWP and the new APWP of this study within their 95% confidence limit (Fig. 1.8). The previous poles plot on the APWP, but in an inconsistent order. For instance, BR, CD and RB in Figure 8 are all similar in age (analogues to P1, 2772 ± 2 Ma) yet plot on three distinctly different positions on the new APWP. BR and CD have overlap with the P1 pole, but RB overlaps with P8-10.

In contrast, the palaeopoles from this study follow a consistent time path and have smaller errors (Tab. 1.4). These differences may be attributed to the limited number of localities, sites or samples per site in previous studies, which resulted in larger errors on the mean average magnetic directions, and hence in less precise pole determinations. From the new APWP (Fig. 1.8), it becomes apparent that there has been considerable rotation, from at least Package 1 to Package 7. The distance between P4-7 and P8-10 on the APWP resembles a phase of latitudinal drift.

Magnetostratigraphy

Magnetostratigraphic schemes have been developed for many Phanerozoic flood basalt provinces and have proven useful in stratigraphic divisions and correlations (e.g. Marsh et al., 1997; Reidel and Hooper, 1989; Saunders et al., 1997; Westphal et al., 1998).

This paper presents the first magnetostratigraphic scheme for an Archaean flood basalt succession (Fig. 1.9). Two particular components of this scheme may prove useful in assisting stratigraphic correlations within the Nullagine and Mount Jope Supersequences across the Pilbara Craton. These are:

> 1. The normal-reverse-normal primary NRM up-stratigraphy (Fig. 1.9); and
> 2. The major shift in palaeolatitude across the Packages 7/8 boundary (Fig. 1.9, see below).

Implications of changes in palaeolatitude

The palaeolatitudes of individual site means and grouped means are plotted from oldest to youngest in Figure 1.9. Although the mean pole positions of groups P1, P2 and P4-7 differ, they have average palaeolatitudes that have overlapping errors, which implies that either no (significant) latitudinal movement has taken place, or that it cannot be resolved with the current amount of data.

There is a significant change in palaeolatitude (average 27.2°) at the Package 7/8 boundary between P4-7 and P8-10 (Fig. 1.9). Geochemical data from the Nullagine Synclinorium show that this boundary also coincides with a major change in the composition of mafic rocks. For this reason, Blake (2001) split the Mount Jope Supersequence into two second-order packages in the Nullagine Synclinorium (Tab. 1.1). The difference in mean SHRIMP zircon ages from above and below this boundary is 3 Myr (95% confidence error range of 0-10 Myr, Blake et al., 2004). Assuming an Earth of current radius, the average shift is 3025 km, which in 3 million years gives a rate of shift of palaeolatitude of 100 cm per year. However, taking into account errors in average palaeolatitude and age, the maximum rate of shift is instantaneous motion (if Package 7 and 8 are of the same age) and the minimum possible rate is a shift of 12 cm per year. Importantly, these are all minimum estimates, since longitudinal shift is unconstrained.

The geological meaning of this 27.2° shift in palaeolatitude is unknown and fundamentally different explanations are possible depending on different assumptions. These are summarized as follows.

Option 1.

The Earth did not have a purely geocentric axial dipole (GAD) in the late Archaean. Long-term contributions of non-dipole fields and the change of this contribution through time could generate an apparent shift in palaeolatitude. For example, if an octupole contribution to the dipole field changed from 0 to 40 %, this would result in an apparent latitudinal shift of ca. 25° (cf. Fig. 4 of van der Voo and Torsvik, 2001). The likelihood of long-term non-dipole fields through geological time is a topic of debate (cf. van der Voo and Torsvik, 2001 and references herein), but as an option it cannot be ruled out. However, since the shift in palaeolatitude is sustained in Packages 9 and 10, a sudden change in octupole contribution (or other non-dipole contribution) must have remained stable for at least ca. 3 Myr. This interpretation has no precedent throughout geological history and is not regarded as the most likely option.

Option 2.

The shift in palaeolatitude is the result of true polar wander (TPW). The nature and validity of TPW is still a topic of debate. Kirschvink et al. (1997) argue that fast apparent motion of continents in the Cambrian was the result of a 6° Myr^{-1} shift of the Earth's spin axis with respect to the geographic reference frame. However, Meert (1999) finds no compelling palaeomagnetic support for this model, although the author states that a
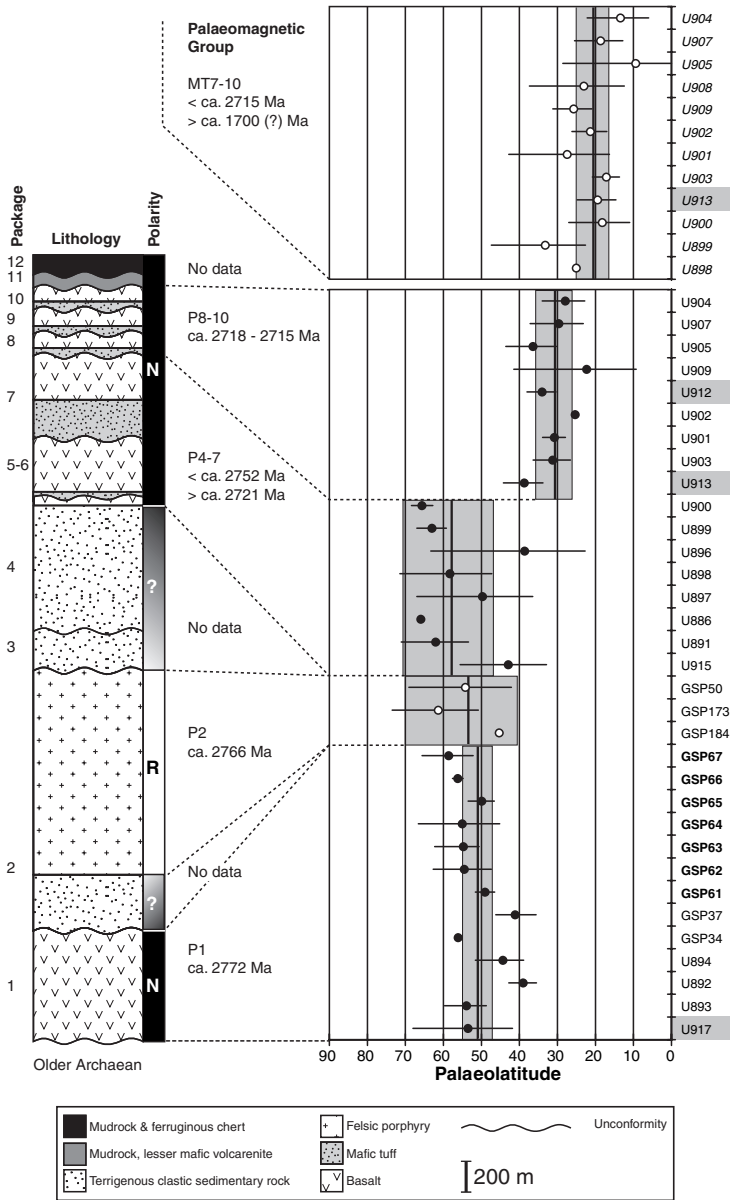
Figure 1.9
Mean palaeolatitudes for the Nullagine and Mount Jope Supersequences in the Nullagine Synclinorium and Package 1 of the Meentheena Centrocline. The lower right column shows site mean HT (high temperature) palaeolatitudes (in degrees) linked to the stratigraphic column. Sample site numbers in grey boxes indicate dykes and site numbers in bold indicate Meentheena data. The upper right column shows site mean MT (medium temperature) palaeolatitudes with the site numbers in italics. HT and MT site means are in stratigraphic order with dyke sites at the base of their comagmatic package. The exact position of the Meentheena data in this column is uncertain and has been placed above the Nullagine Package 1 data for convenience only. Site mean palaeolatitudes are represented by a circle with a horizontal bar representing the α95 (after Fisher, 1953) Closed (open) symbols represent normal (reversed) intervals. Five groups of palaeolatitudes (four HT means, one MT mean) have been distinguished and their means are the means of their constituent sites (see Tab. 1.4). Groups are defined in the text and in the caption to Figure 1.8. Group means are given by thick black vertical lines and their a95 by the grey boxes. The five groups have been linked to the stratigraphic column by dashed lines. N indicates normal polarity, R indicates reversed polarity.

relatively small contribution of TPW cannot entirely be ruled out. Courtillot and Besse (1987) note that TPW is a continuous process and argue that TPW only comes to a standstill during periods of low reversal frequency and during episodes of continental break-up. Aspects of our data are not consistent with TPW being an explanation of the 27° shift in palaeolatitude. These include an apparent low reversal frequency (see below) and the relatively fast and sudden shift across the Package 7/8 boundary. While TPW cannot be discounted, observations to date do not support it as an explanation for the documented shift in palaeolatitude. As a special case, inertial interchange TPW could explain the sudden shift in palaeolatitude. In this scenario, unbalance of the Earth's landmasses cause the lithosphere and mantle to rotate ca. 90° with respect to the Earth's spin axis (cf. e.g. Kirschvink et al., 1997), which results in rapid TPW. IITPW is a topic of considerable controversy, which so far has not even been proven. Therefore, we retain a conservative interpretation and we feel that the burden of proof is with the advocates of non-dipole fields and/or (II)TPW.

Option 3.

The Earth had a GAD and the latitudinal shift is the result of plate movement. Possible drift rates across the Package 7/8 boundary (as discussed above) range from fast Phanerozoic drift rates (e.g. Meert et al., 1993) to drift rates that are up to an order of magnitude faster than any known Phanerozoic drift rate. In a Phanerozoic plate tectonic setting, rapid drift rates are commonly associated with fast spreading following continental rifting. Blake and Barley (1992) and Blake (1993) proposed a broad 2 stage rifting to rifted setting for the development of the Nullagine and Mount Jope Supersequences. Their proposed first stage, represented by the Nullagine Supersequence could not be confirmed by our palaeomagnetic data in terms of latitudinal drift, because the palaeolatitude results of Package 1 to 4 are not significantly different. However, there is evidence for rotation during this phase (Fig. 1.8), as is confirmed by a change in declination from 129.0° in P1 to 157.5° in P4-7 (Tab. 1.4). However, their second stage of rifting is supported by our palaeomagnetic data. Indeed, the shift in palaeolatitude between Package 7 and 8 was used by Blake (2001) to divide the Mount Jope Supersequence in the Nullagine Synclinorium into two parts (Fig. 1.3). The recorded 3025 km of drift in a single event represents a phase of rapid horizontal movement.

The cause(s) of this possible event is unknown. In a Phanerozoic-style plate tectonic setting the implied drift distance is not unlikely but the implied great rapidity of drift is unlike any known Phanerozoic setting. If this interpretation is correct, it has fundamental implications for models of plate movement during the late Archaean. It suggests that at least some late Archaean crust moved thousands of kilometres across the Earth but at a rate incompatible with modern-style plate tectonics. Whereas in Phanerozoic successions flood basalt volcanism may be associated with mantle plumes, in the Late Archaean, mantle plumes are not necessarily a prerequisite for the formation of flood basalts (Blake, 1993). With a hotter late Archaean mantle, it is conceivable that a different style of tectonism took place.

Finally, it is conceivable that the observed drift is a result of a combination of the above-mentioned options. To summarise, the palaeomagnetic shift of 27.2° across the Package 7/8 boundary could be the result of apparent polar wander, and indicates a phase of rapid horizontal tectonic movement between ca. 2721 Ma and ca. 2718 Ma, although other explanations cannot be ruled out. Work in progress, i.e. additional sampling of Packages 7 and 8 at different locations, will aid in further constraining the drift rate.

Geomagnetic reversals

The antipodal directions of Package 2 with respect to Package 1 beneath and Package 4 above are interpreted as the record of two geomagnetic reversals, one which occurred between 2772 ± 2 Ma and ca. 2766, and one between ca. 2766 Ma and ca. 2741 Ma (Fig. 1.3). Following the Package 2 reversal there is no record of magnetic reversals in the section studied. This interval without geomagnetic reversals has a minimum duration of 26 Myr (from ca. 2741 Ma to ca. 2715 Ma). While reversals may have occurred during this period, and have not been recorded, this period of single polarity is comparable in duration with the Cretaceous Normal Superchron (CNS, ca. 30 Myr, Cande and Kent, 1995). A discussion about the occurrence and importance of Superchrons during the Archaean, however, is beyond the scope of this paper.

The oldest Archaean geomagnetic reversal reported to date is from the Kaap Valley pluton of South Africa (Layer et al., 1996). The authors sampled a variety of rock types of different ages and argued that, if all end vectors were plotted together and contoured, a pattern of higher density distributions of directions was found, but a reversal test was not carried out. The exact age of the Kaap Valley pluton reversal could not be further constrained as being younger than 3224 Ma and older than ca. 2000 Ma.

The magnetic reversals in the Nullagine Supersequence are, however, the oldest unambiguous and precisely dated Archaean reversals, and importantly, they are stratabound and recorded in a single continuous stratigraphic section. This implies that there is no uncertainty about the relative age of the rocks and the normal-reverse-normal sequence. In addition, the data presented here pass the reversal test and the encountered NRM is demonstratively primary. The next younger reported reversal occurs at 2680 ± 10 Ma in the Tanzania Craton (Meert et al., 1994).

It is also likely that a period of reversed polarity occurred between ca. 2700 and ca. 1700 million years ago, since the MT directions have all reverse directions. This is consistent with palaeomagnetic data from the ca. 2500 Ma Hamersley banded iron formations (BIFs) (e.g. Li et al., 2000; Schmidt and Clark, 1994), which have reverse directions as well.

Implications for the Vaalbara hypothesis

Recently, Cheney, 1996 put forward the hypothesis that between 2.7 and 2.1 Ga the Pilbara and Kaapvaal were part of the same continent, named 'Vaalbara'. Zegers et al. (1998) made a palaeomagnetic reconstruction showing that the Vaalbara supercontinent may have existed between 3.1 and 2.7 Ga. Wingate (1998) compared the mean palaeolatitude of 34.3 ± 6.4° from the interpreted 2772 ± 2 Ma Mount Roe Basalt (Package 1 is part of the Mount Roe Basalt; Tab. 1.1) as published by Schmidt and Embleton (1985) with the slightly older palaeolatitude of the 2782 ± 5 Ma (concordant SHRIMP U-Pb, zircon, Wingate, 1999) Derdepoort Basalts, Kaapvaal Craton. Wingate (1998) found a mean palaeolatitude of 64.5 ± 17.5° (95 % confidence limit) for the Derdepoort Basalts and concluded that it is unlikely that the Kaapvaal Craton and the Pilbara Craton were part of the same Vaalbara continent at 2.77 to 2.78 Ga since there is a gap of 6.3° between the minimum palaeolatitude of the Derdepoort basalts and the maximum palaeolatitude of the Mount Roe Basalt (Fig. 1.10).

Now, with better-constrained data from this study, a similar palaeolatitude reconstruction has been made. With a mean palaeolatitude of 51.1 ± 3.9° for Package 1, the data fall well within the range of 64.5 ± 17.5° for the palaeolatitude of the Derdepoort Basalts (Fig. 1.10). Earlier studies of the Black Range and Cajuput Dykes (Embleton, 1978) gave palaeolatitudes similar to those found in this study, but were not included in the
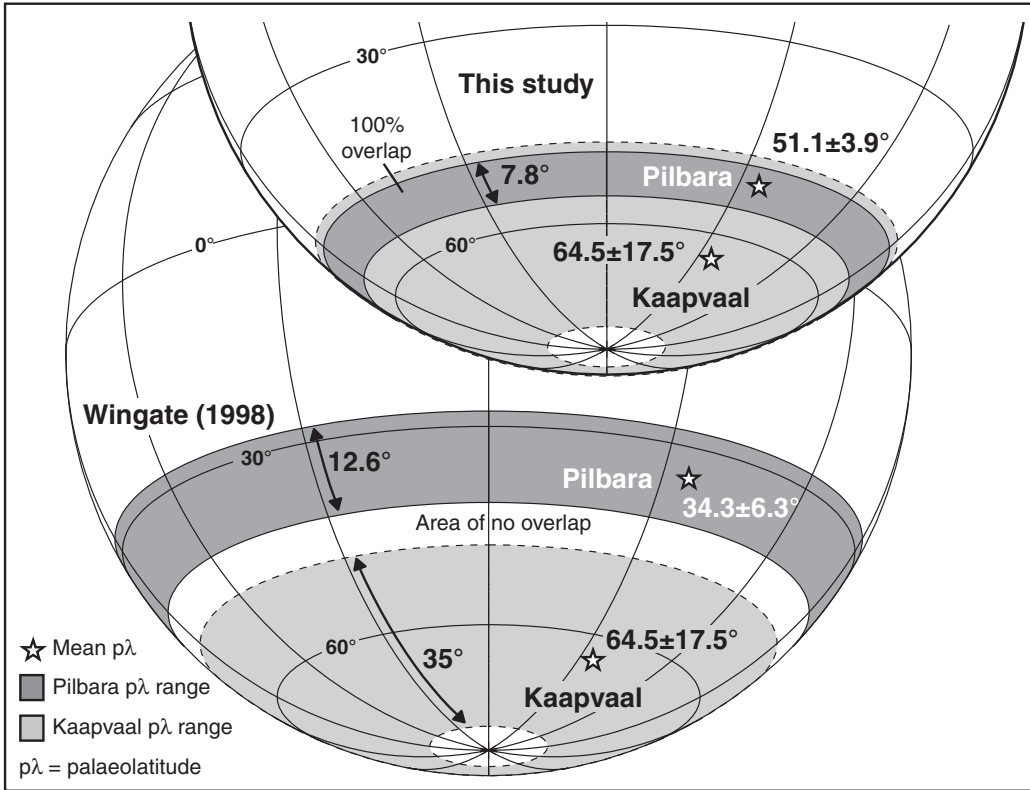
Figure 1.10
Palaeolatitude reconstructions for the Pilbara and Kaapvaal Cratons at 2.78-2.77 Ga after Wingate (1998, lower globe) compared to this study (upper globe). Reconstructions are based on average palaeolatitudes, which are indicated by stars and the corresponding 95% confidence limits, which are indicated by grey areas. The possible range of Kaapvaal Craton palaeolatitudes in the reconstruction of Wingate compared with the possible range of Pilbara Craton palaeolatitudes from (Schmidt and Embleton, 1985) do not overlap. However, the possible range of Kaapvaal Craton palaeolatitudes does overlap with the possible range of Package 1 palaeolatitudes from this study.

reconstructions of Figure 1.10. The new data imply that the Vaalbara hypothesis cannot be rejected at 2.78 to 2.77 Ga, however, since longitude is not constrained in palaeolatitude reconstructions, the Pilbara and Kaapvaal Cratons could still have been situated up to 180° away from each other. Further, because of a minimum age difference of 3 Myr and an average age difference of 10 Myr between the Kaapvaal and Pilbara basalts, matching palaeolatitudes do not prove the Vaalbara hypothesis at 2.78 to 2.77 Ga, since this study shows that large amounts of drift may occur within a few million years in the late Archaean. Finally, the errors on the Kaapvaal Craton palaeolatitude determinations are still significant and therefore more sampling is needed. Nevertheless, we conclude that with the data available at this moment, the Vaalbara hypothesis cannot be rejected.

Conclusions

This study has demonstrated that a meaningful APWP can be constructed for a late Archaean succession. Importantly, there is no ambiguity about the relative ages of the obtained pole positions, since the data come from a single stratigraphic succession. Further,

the availability of precise, robust geochronology within the succession enables the determination of absolute ages for the palaeomagnetic poles. The results of this study are summarised as follows.

1. Based on positive field tests and the ability to distinguish between lightning affected directions, overprint directions and high temperature directions, we conclude that the high temperature NRM component is of primary origin, acquired at the time of cooling.

2. Late Archaean-aged dyke suites can be palaeomagnetically correlated to flood basalt packages, providing additional evidence for comagmatic relationships.

3. Contrary to the suggestion of Wingate (1998), the Vaalbara hypothesis cannot be rejected for the 2.78-2.77 Ga interval, since the palaeolatitude of Package 1 lies well within the 95% confidence limits of the palaeolatitude of the Derdepoort Basalts.

4. Within a ca. 60 Myr succession, the geomagnetic field has reversed at least twice. It appears that the geomagnetic field in the late Archaean was mostly of single polarity. However, there are significant time intervals that have not been sampled (e.g. Package 3 and most of Package 4, ca. 2766- < 2752 Ma; Fig. 1.3). These may contain additional geomagnetic field reversals.

5. It is possible to generate meaningful palaeopole positions for almost all packages within the Nullagine and Mount Jope Supersequences, and to construct a consistent APWP.

6. A major palaeomagnetic break occurs at the Package 7/8 boundary, demonstrating the unconformable nature of this boundary. Assuming that this break reflects plate movement, this result supports the tectonic model for rifting of the Mount Jope Supersequence (Blake, 1993; Blake, 2001; Blake and Barley, 1992). The results indicate a possible average drift rate as high as 100 cm per year, which is an order of magnitude faster than the modern plate tectonic drift rate.

Acknowledgements

Chapter 2

A palaeomagnetic study of the Nullagine and Mount Jope Supersequences, East Pilbara and Marble Bar Basins, Western Australia: rapid continental drift in the late Archaean?

A palaeomagnetic study of the Nullagine and Mount Jope Supersequences, East Pilbara and Marble Bar Basins, Western Australia: rapid continental drift in the late Archaean?

Abstract

Palaeomagnetic studies of late Archaean terrains can play a crucial role describing early Earth geodynamic processes. The amount of late Archaean terrain is limited and there is an even greater paucity of unmetamorphosed terrain, which is a prerequisite for the survival of primary natural remanent magnetisation (NRM). The ca. 2775 – 2715 Ma Nullagine and Mount Jope Supersequences of the Pilbara Craton, Western Australia, constitute one of the few late Archaean successions that have been preserved in near pristine conditions. Recent palaeomagnetic studies have shown that primary NRM is still present. Flood basalts, and to a lesser extend mafic tuff and dacite porphyry have been sampled in the East Pilbara and Marble Bar Basins and have been stepwise demagnetised for a palaeomagnetic study. Our palaeomagnetic data confirm the proposal of Blake (2004) that the subdivision in 12 unconformity bound packages, as defined for the Nullagine Synclinorium, can be extrapolated to other parts of the East Pilbara Basin and to the Marble Bar Basin. The geomagnetic field is shown to have reversed at least four times during the formation of the studied succession, which compared to the Phanerozoic is still a low reversal frequency. A palaeolatitude shift of 14.4° is found across a boundary that also marks a major geochemical change. The average speed of this shift is 4.8° Myr^{-1} or ca. 50 cm yr^{-1}. We think that the shift represents a rapid phase of horizontal movement, possibly in combination with true polar wander, a fundamental observation for late Archaean geodynamic processes.

Introduction

In the Phanerozoic, plate tectonics are responsible for the constant movement and reorganisation of the lithosphere. Reconstructing the displacement history of the Earth's plates is mainly done with the aid of palaeomagnetism, as it plays a key role in quantifying rotational and latitudinal movement. In the Phanerozoic, these reconstructions benefit from the contribution of biostratigraphic and isotopic age control and, until ca. 150 Ma, also from the oceanic polarity record. Studies focussing on older terrains encounter the problems of increasingly poor age control and the increasing difficulties of finding suitable unmetamorphosed rocks that have preserved the primary natural remanent magnetisation (NRM).

For the late Archaean, there is still no consensus about whether or not plate tectonic processes were active. The discussion focuses on horizontal (e.g. de Wit, 1998 and references therein) versus vertical movement (e.g. Hamilton, 1998 and references therein). Indeed, for a long time the discussion has lacked key evidence for one or the other mechanism. Palaeomagnetic studies are crucial in this discussion, but these studies are severely hampered by the limited availability of exposed Archaean terrain. Often, Archaean terrains are metamorphosed to high grades, while also the availability of high precision ages is very limited.

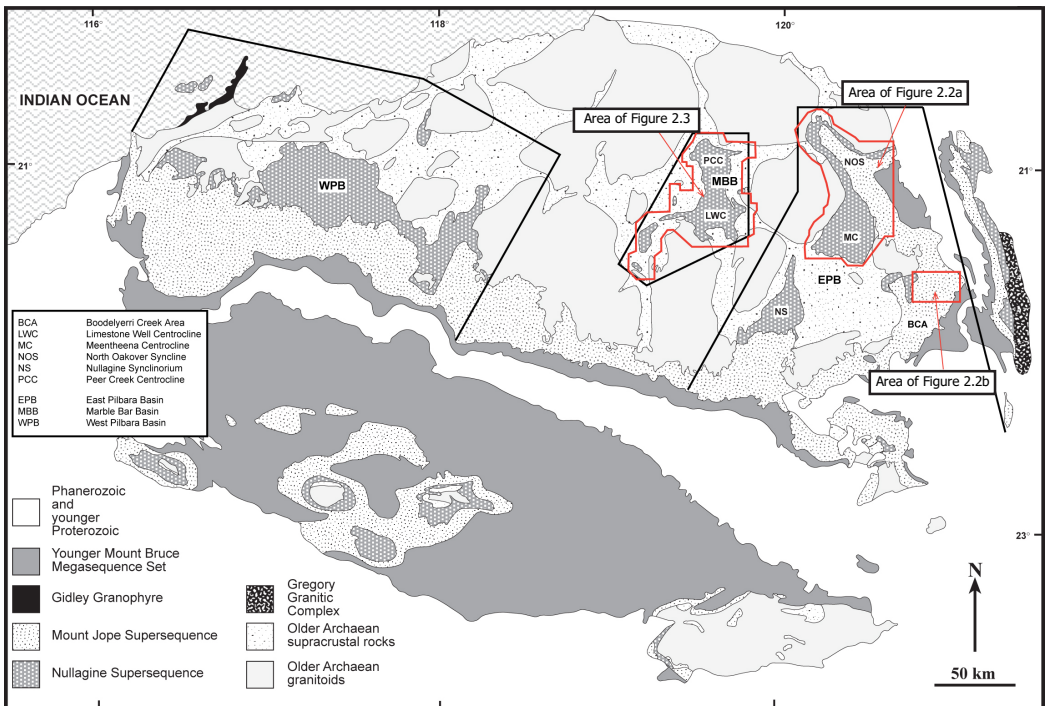The Nullagine and Mount Jope Supersequences of the Pilbara Craton, Western

Figure 2.1
Simplified geological map of the Pilbara (Blake, 2001), showing the approximate location of Figures 2.2 and 2.3. The Hamersley Province comprises most of the south-western half of the map.

Australia, form an exception. The succession is preserved in near pristine conditions and has been well dated (e.g. Arndt et al., 1991; Blake et al., 2004). The Nullagine and Mount Jope Supersequences (Fig. 2.1) have recently been the focus of a palaeomagnetic study (Strik et al., 2003). The succession was sampled in the Nullagine Synclinorium, which is a part of the East Pilbara Basin. An important conclusion was that the unconformity-bound packages defined for the Nullagine Synclinorium (Blake, 2001) have preserved a primary NRM. This conclusion is based on positive results for the conglomerate, fold and reversal tests. The main conclusion, i.e. that the Pilbara underwent ca. 3025 km of horizontal drift between ca. 2718 and ca. 2715 Ma is fundamental in the light of the discussion of horizontal versus vertical movement.

In this paper, we aim to provide support for expanding the subdivision in unconformity-bound packages, as defined for the Nullagine Synclinorium by Blake (2001), to the East Pilbara and Marble Bar Basins (Blake, 2004), by palaeomagnetically testing this correlation. The new palaeomagnetic data add to the (magneto)stratigraphy of Strik et al. (2003), while the significantly increased number of data helps to further constrain the apparent polar wander path (APWP) for the Pilbara Craton between ca. 2775 and 2715 Ma. The data also show that a correlation between the East Pilbara and Marble Bar Basins is not straightforward. We present palaeomagnetic evidence for an older flood basalt unique to the Marble Bar Basin. Finally, the study confirms and refines the high drift rate found by Strik et al. (2003) and shows that the movement is regional rather than confined to the Nullagine Synclinorium.

Geological setting

The ca. 6000 m thick 2.775-2.715 Ga Nullagine and Mount Jope Supersequences (Fig. 2.1) rest unconformably on the ca. 3.5 to 2.9 Ga granite-greenstone terrain of the Pilbara Craton, Western Australia. Historically, the rocks of the Nullagine and Mount Jope Supersequences, which make up the lower part of the Mount Bruce Megasequence Set, have been divided on the basis of a lithostratigraphic framework. Since unconformities have been shown to exist throughout the Nullagine and Mount Jope Supersequences, Blake (1993; 2001) developed an unconformity-based sequence-stratigraphic framework, which will be used here.

The unconformity-based subdivision into 12 genetically distinct packages was developed for the Nullagine Synclinorium (Blake, 2001), which is part of the East Pilbara Basin (Fig. 2.1). The rock types within each package are interpreted as consisting of cogenetic units. They have been numbered from old to young, from 1 to 12, and are not given names until they can confidently be correlated on a regional scale (Blake, 2001). The Nullagine Supersequence (Figs. 2.2, 2.3, 2.4) encompasses a thick subaerial flood basalt package (Package 1) with a thick succession of terrigenous sedimentary and felsic volcanic rocks on top (Package 2 to 4). The Mount Jope Supersequence (Figs. 2.2, 2.3, 2.4) is made up of six packages of subaerial flood basalts, all preceded by mafic tuff successions (Package 5 to 10) and a mudrock-dominated marine succession on top (Package 11 and 12). Blake (2001) divided the Mount Jope Supersequence into two second-order packages in the Nullagine Synclinorium (Fig. 2.4), based on a major palaeolatitude shift (Strik et al., 2003) and major changes in the geochemistry of mafic rocks across the Packages 7/8 boundary.

A third-order subdivision was made for other parts of the East Pilbara Basin (Blake, 1990), comprising the Meentheena Centrocline, the Northwest Oakover Syncline and the
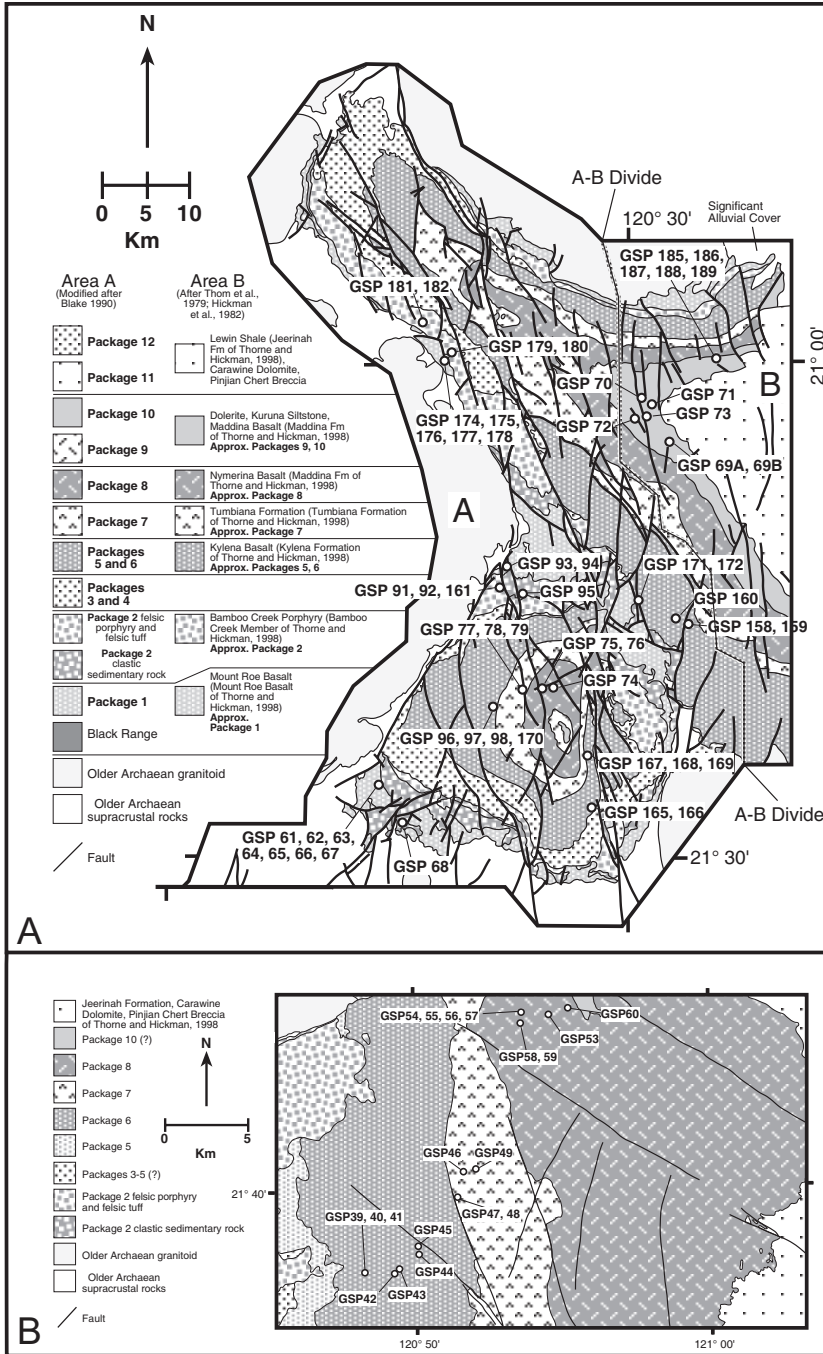
Figure 2.2
Summary geological maps of (A) the Meentheena Centrocline and the North Oakover Syncline (after Blake, 2004, Blake, 1990; Hickman et al., 1982; Thom et al., 1979) and (B) the Boodelyerri Creek Area (after Blake, 2004, Thorne and Hickman, 2001), showing dominant lithologies and sample locations (see Tab. 2.1).
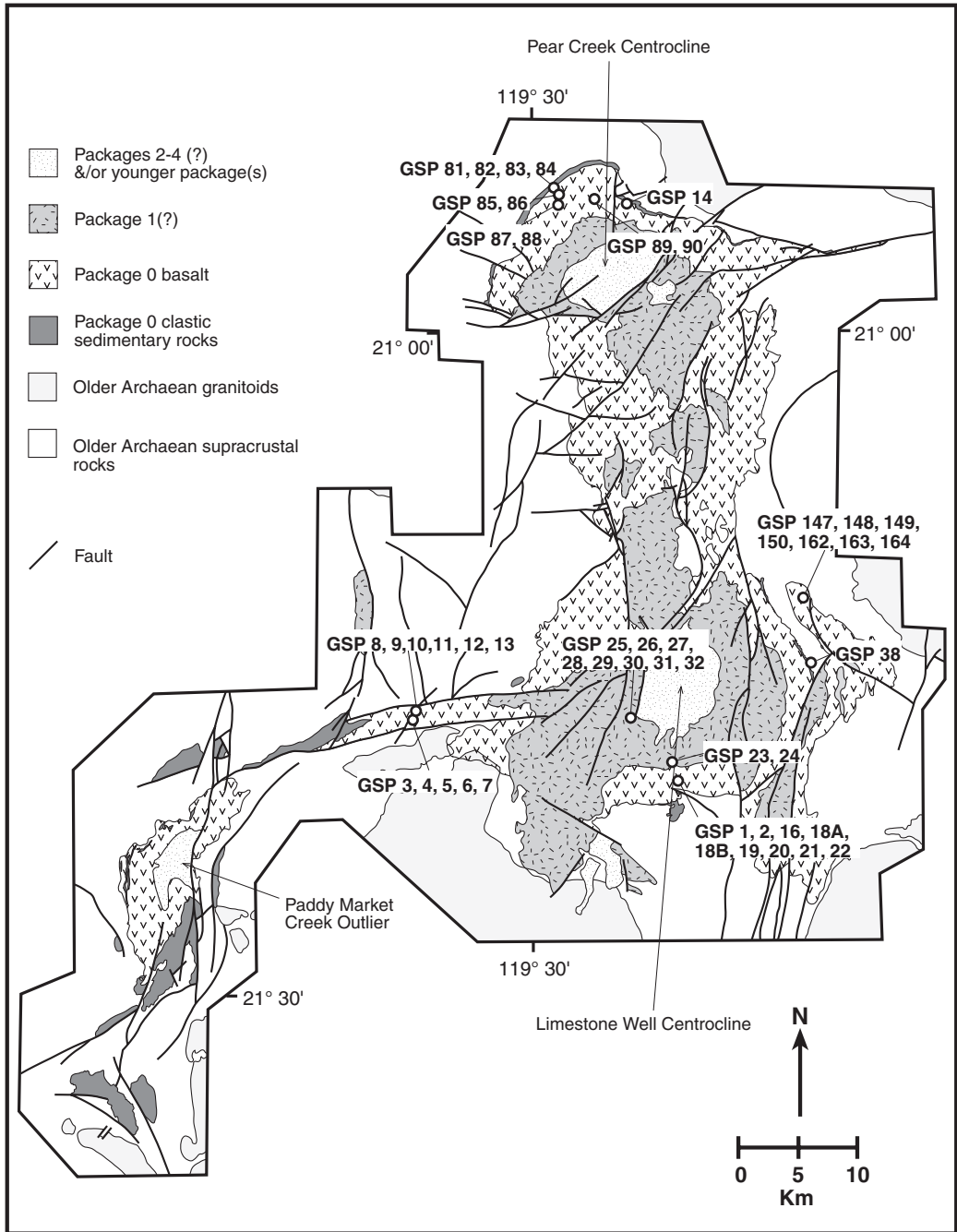
Figure 2.3
Summary geological map of the Marble Bar Basin, showing dominant lithologies (after Blake, 1993; Blake, 2004) and sample locations (see Tab. 2.1).
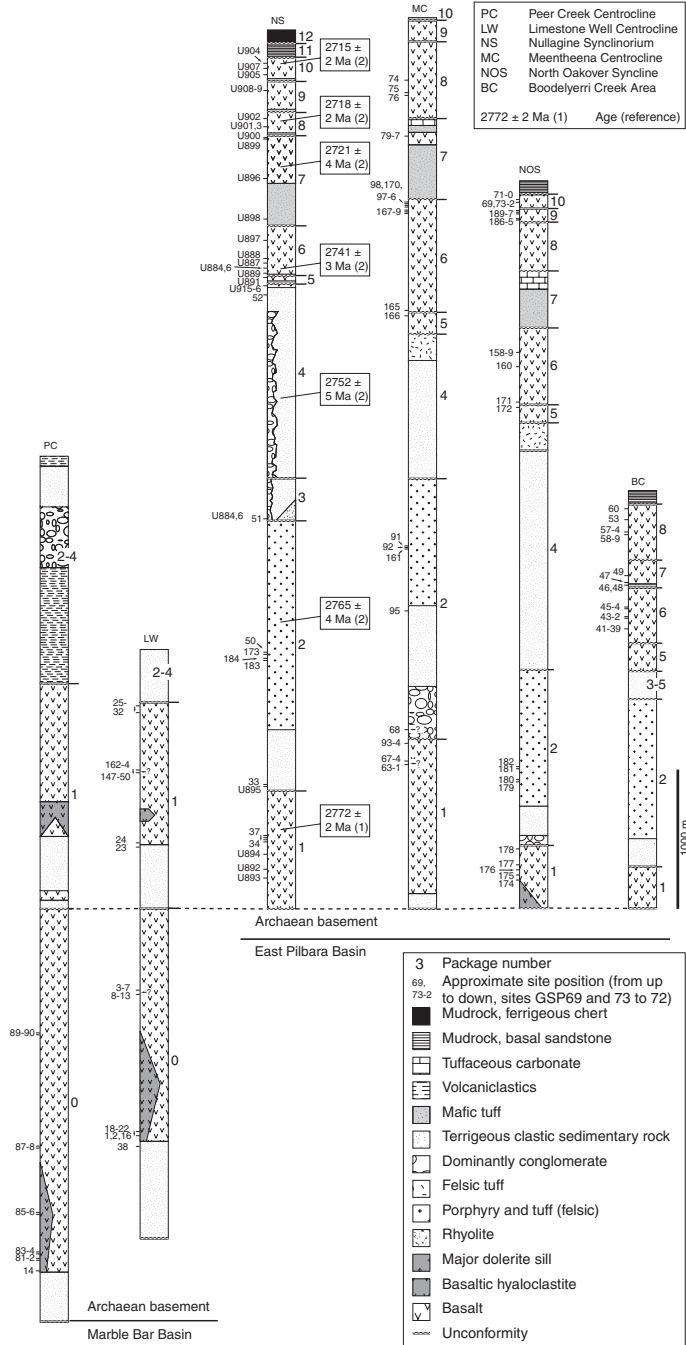
Figure 2.4
Summary stratigraphic columns (cumulative maximum stratigraphic thickness) of the Nullagine (Package 0 to 6) and Mount Jope (Package 7 to 11) Supersequences and the lower Marra Mamba Supersequence Package (Package 12) for the various areas in the Marble Bar and East Pilbara Basins (after Blake, 2001; Blake, 2004). The figure includes approximate sample site positions, dominant lithologies, package numbers, and summary rock ages. The dashed line connects the base of Package 1 unconformity. Age references: (1) Pb-Pb baddeleyite on cogenetic mafic dykes, Wingate, 1999; (2) U-Pb SHRIMP zircon, Blake et al., 2004.

Boodalyerri Creek Area, (cf. Fig. 2.1) and also for the Marble Bar Basin. A correlation between the package subdivision in the Nullagine Synclinorium, and the third order subdivision of the East Pilbara and Marble Bar Basins is currently being developed (Blake, 2004). When we use the package subdivision outside the Nullagine Synclinorium anywhere in our paper, we refer to this work in progress.

Blake (1993) interpreted the deposition of the Nullagine and Mount Jope Supersequences each as the geological record of a major phase of continental break-up in the late Archaean. The author concluded that, during the deposition of the Nullagine Supersequence, the general trend was that of WNW-ESE crustal extension with the possible development of a rift and an ocean at what is now the western margin of the Pilbara Craton. The Mount Jope Supersequence formed during a period of NNE-SSW extension with a rift and an ocean at the southern margin of the Craton.

For Archaean standards, the geochronology of the studied succession is very detailed: nine of the twelve packages have high precision ages (see also Fig. 2.4). Wingate (1999) determined a mean ion microprobe baddeleyite $^{207}Pb/^{206}Pb$ age of 2772 ± 2 Ma from four samples, each from a different dyke of the Black Range Suite, including the Black Range Dyke itself. Geochemical, geological and palaeomagnetic correlations (Blake, 2001; Strik et al., 2003) suggest that the Package 1 basalt in the Nullagine Synclinorium is comagmatic with the Black Range Suite and hence is of the same age. Package 1 itself yielded an age of 2775 ± 10 Ma (U-Pb SHRIMP on zircon, Arndt et al., 1991). The felsic porphyry of Package 2 is dated at 2765 ± 4 Ma, Package 3 is dated at 2766 ± 3Ma, Package 4 at 2752 ± 5 Ma, Package 5 at 2741 ± 3 Ma, Package 7 at 2721 ± 4 Ma, Package 8 at 2718 ± 3 Ma, Package 10 at 2715 ± 2 Ma and Package 11 2715 ± 2 Ma (all U-Pb SHRIMP zircon, Blake et al., 2004).

Methods

Samples (Ø 25 mm) were taken in the field using a petrol engine drill and they were orientated with both a magnetic and sun compass. The sun compass directions have been used in the sample analyses, although generally there was no significant difference in sun and magnetic compass direction. In the laboratory, all samples were cut to standard speci-mens of 22 mm length. Generally, one specimen of each drill core was thermally demagnetised in a magnetically shielded, laboratory-built furnace. The NRM was measured on a 2G Enter-prises DC-SQUID cryogenic magnetometer or occasionally on a JR5 spinner magnetometer. Thermal demagnetisation was done in 16 temperature steps (20, 100, 200, 300, 350, 400, 450, 480, 500, 525, 530, 540, 550, 560, 568, and 575 or 580 °C). Occasionally, an additional step of 590 °C was done. Sixty-three specimens were demagnetised using the alternating field (AF) technique, in which demagnetisation was carried out with a laboratory-built AF demagnetiser up to a peak field of 200 mT.

NRM directions were analysed and interpreted using Zijderveld diagrams (Zijderveld, 1967) and principal component analysis (Kirschvink, 1980). No directions with a maximum angular deviation (MAD) greater than 10° were used.

Results

The subdivision in unconformity bound packages for the Nullagine Synclinorium (Blake, 2001) and the hereto-related palaeomagnetic data of Strik et al. (2003) forms a reference framework for the results presented here. Correlation of the packages to the third order subdivision in the East Pilbara and Marble Bar Basins is based on geological mapping

(e.g. Blake, 1990) and work in progress (Blake, 2004). In this paper, we follow the subdivision in unconformity bound and subsequently numbered packages, assuming it is valid for the whole East Pilbara Basin as well as for the Marble Bar Basin. Therefore, the results will be presented in categories of assumed packages. Subsequently, the data are compared to the palaeomagnetic data from the Nullagine Synclinorium, which is an important check for the validity of the palaeomagnetic package correlations.

The sampled rocks of the East Pilbara and Marble Bar Basins reveal up to three components of remanent magnetisation. Firstly, a present day field component has been recorded in all sampled packages. It is generally removed after heating at 350 °C. Secondly, a consistent medium temperature (MT) component that generally unblocks between 350 and 480 °C was found in Package 1 and in Packages 6 to 10. Finally, in all sampled packages a high temperature (HT) component was recorded, with unblocking between 200-480 °C and a maximum temperature of 580 °C, with the starting temperature of the HT unblocking spectrum depending on the amount of MT component contribution.

The third-order subdivision of the Nullagine Supersequence in the Marble Bar Basin does not correlate in a straightforward way to the packages defined in the Nullagine Synclinorium, nor to the East Pilbara Basin. The Marble Bar Basin developed separately from the East Pilbara Basin and is the only basin that, instead of one, has two well-developed, thick flood basalt units in the Nullagine Supersequence. Further the Mount Jope Supersequence is absent. Initially, we thought that the unit overlying the older Archaean terrain would palaeomagnetically correlate to Package 1. However, all sites in the lower unit of the Marble Bar Basin appeared to have a nearly 180 degree different HT direction with respect to the HT direction of Package 1 in the Nullagine Synclinorium. The only exception is a sequence we sampled in the eastern part of the Marble Bar Basin (sites GSP147-150 and GSP162-164), which we thought to be part of the lower flood basalt unit as well (Figs. 2.3, 2.4). It has HT directions similar to those of Package 1 in the Nullagine Synclinorium and therefore does not correlate to the lower flood basalt unit of the Marble Bar Basin. The geologic relation between this eastern sequence and the lower flood basalt unit is unclear, however. The area is bounded by faults and it is not unthinkable that sites GSP147-150 and GSP162-164 are in fact part of the upper flood basalt unit, as suggested in Figure 2.4. This upper flood basalt unit of the Marble Bar Basin was thought to represent a Package 2-aged sequence without equivalent in the East Pilbara Basin (e.g. Blake, 1993). The HT directions from this upper unit (sites GSP24-32), however, are nearly identical to the HT direction of Package 1 in the Nullagine Synclinorium. Therefore, a "Package 0" is introduced, which represents the lower flood basalt unit of the Marble Bar Basin, excluding the eastern (Flying Fox, or FF) sequence, and Package 1 in the Marble Bar Basin is represented by the upper flood basalt unit, including the FF sequence, (cf. Fig. 2.4).

Demagnetisation results

The following describes the palaeomagnetic results per package, and a comparison is made with the results of the palaeomagnetic study of the Nullagine Synclinorium by Strik et al. (2003).

Package 0: Basalts, sandstone and hyaloclastite of this package were sampled in the Marble Bar Basin. Zijderveld diagrams show a consistent direction after tectonic correction has been applied (Fig. 2.5, y-z). A present day field component is apparent in seven of the 33 sampled sites (Fig. 2.6j), but no significant consistent MT directions are preserved. Reliable HT directions are present in 28 sample sites (Tab. 2.1, Fig. 2.6j). The hyaloclastite of sites
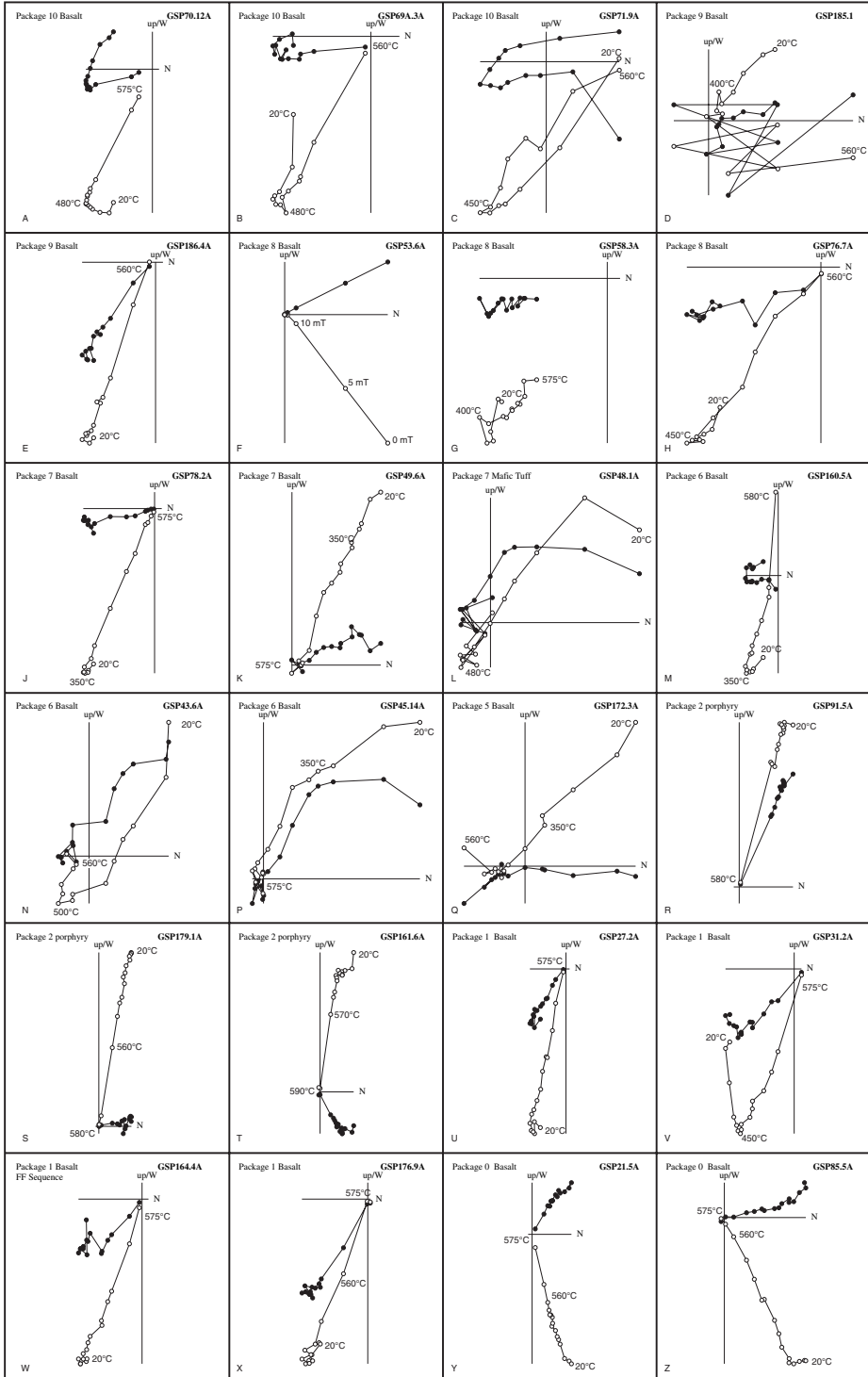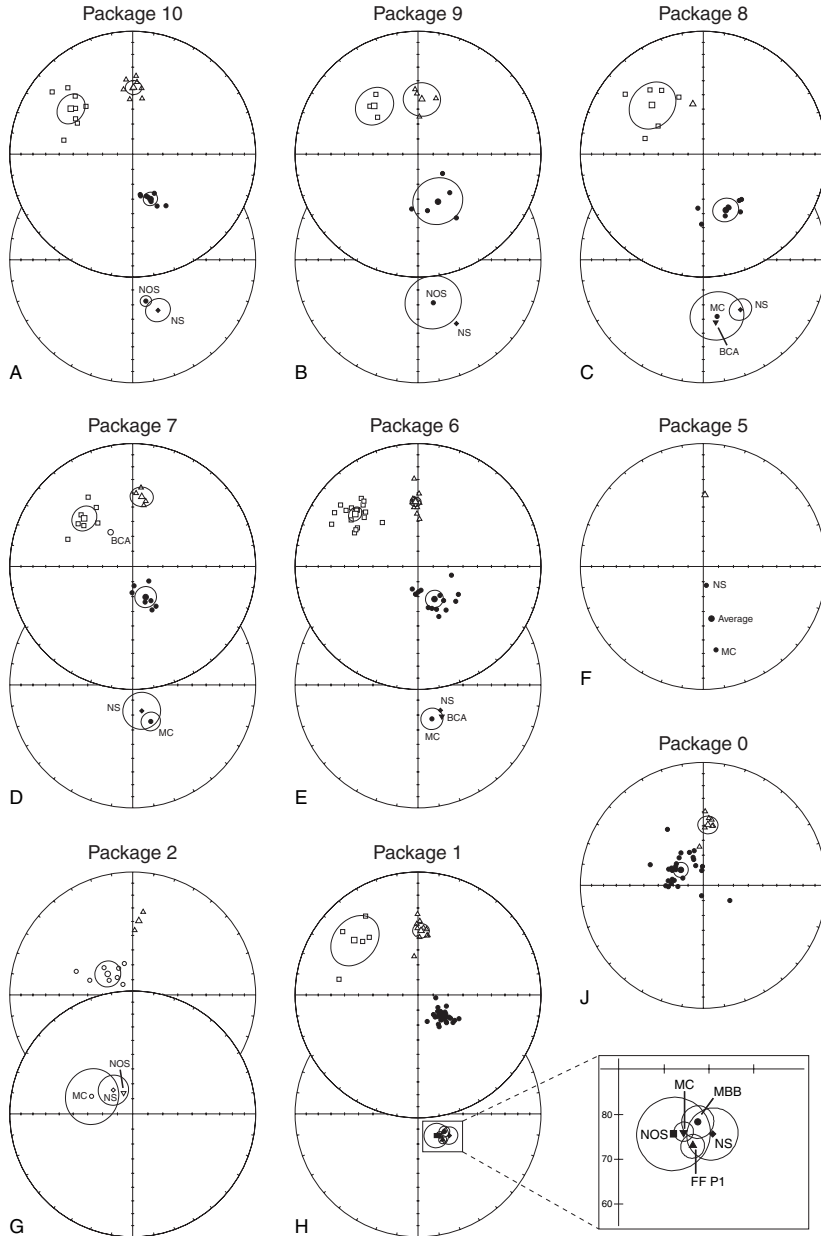
Figure 2.6
Equal area plots of results from all studied packages. All diagrams are equal area plots of multiple sites. N = total number of sites with accepted data, small symbols are site means, larger symbols are the mean of site means with the corresponding α95 circles (where applicable). Open (closed) symbols indicate negative (positive) inclinations, circles are high temperature directions, squares are medium temperature directions and triangles are low temperature directions. Data in Tables 2.1, 2.2.

Figure 2.5 (opposite)
Examples of characteristic Zijderveld diagrams from each package. Key temperature/field steps are shown. Specimen numbers indicate location (Fig. 2.2, Tab. 2.1) followed by sample number.

Area	Package	Site Number	Lithology	AMG coordinates (AGD 84)	Strike/Dip	N	n	dec°	inc°	k	a95°	R	Plat°	VGP lat°	VGP long°
NOS	10	GSP71	Basalt	51K 242817 - 7670512	290/03 N	10	10	162.0	60.6	46.5	7.2	9.806	41.6	-64.5	153.0
NOS	10	GSP70	Basalt	51K 241713 - 7671205	290/03 N	12	12	160.5	59.7	388.8	2.2	11.972	40.6	-64.4	156.5
NOS	10	GSP69B	Basalt	51K 244902 - 7666287	295/03 N	7	7	169.2	61.7	677.2	2.3	6.991	42.9	-66.4	140.6
NOS	10	GSP69A	Basalt	51K 244972 - 7666272	295/03 N	7	7	169.4	62.7	597.1	2.5	6.990	44.1	-65.4	139.0
NOS	10	GSP73	Basalt	51K 242266 - 7669152	subhor.	10	0	n/a	n/a	n/a	n/a	n/a	n/a	n/a	n/a
NOS	10	GSP72	Basalt	51K 240916 - 7668901	subhor.	10	10	151.0	60.2	98.9	4.9	9.909	41.1	-58.3	164.6
NS	10	U904	Basalt	50K 803892 - 7529581	subhor.	10	10	152.6	46.7	52.3	6.7	9.828	27.9	-64.6	191.5
NS	10	U907	Basalt	50K 794956 - 7533268	subhor.	10	8	147.2	48.6	49.4	8.0	7.858	29.6	-59.7	189.0
NS	10	U905	Basalt	50K 800384 - 7528231	subhor.	12	8	158.9	55.9	77.0	6.4	7.909	36.4	-66.9	167.5
	10 mean					**9**	**62**	**158.0**	**57.3**	**115.2**	**5.2**	**7.939**	**37.9**	**-64.9**	**163.4**
NOS	9	GSP185	Basalt	51K 250351 - 7675774	066/16 S	8	3	186.6	53.0	90.5	13.0	2.978	33.6	-76.1	97.0
NOS	9	GSP186	Basalt	51K 250317 - 7675850	066/16 S	7	5	140.5	56.6	66.6	9.4	4.940	37.2	-52.2	176.5
NOS	9	GSP187	Basalt	51K 250170 - 7675943	066/16 S	7	2	170.4	51.5	n/a	n/a	n/a	32.2	-75.9	156.1
NOS	9	GSP188*	Basalt	51K 250143 - 7675931	066/16 S	7	1	123.9	25.4	n/a	n/a	n/a	13.4	-36.1	209.1
NOS	9	GSP189	Basalt	51K 250121 - 7675971	066/16 S	7	2	128.2	69.2	n/a	n/a	n/a	52.8	-39.4	158.6
NS	9	U909	Basalt	50K 790358 - 7538230	subhor.	15	4	149.0	39.3	19.7	21.2	3.848	22.3	-61.4	203.9
	9 mean					**5**	**16**	**157.1**	**55.5**	**23.8**	**16.0**	**4.832**	**36.0**	**-64.0**	**167.1**
MC	8	GSP74	Basalt	51K 232063 - 7639814	070/08 S	15	4	161.8	43.6	72.8	10.8	3.959	25.5	-72.8	193
MC	8	GSP75	Basalt	51K 231048 - 7639677	095/10 S	15	13	185.7	53.6	6.6	17.4	11.189	34.1	-76.2	100.2
MC	8	GSP76	Basalt	51K 230589 - 7639737	095/10 S	11	9	154.8	50.7	124.4	4.6	8.936	31.4	-65.3	181
BCA	8	GSP60	Basalt	51K 284609 - 7613065	subhor.	11	0	n/a	n/a	n/a	n/a	n/a	n/a	n/a	n/a
BCA	8	GSP53	Basalt	51K 283471 - 7612649	subhor.	12	0	n/a	n/a	n/a	n/a	n/a	n/a	n/a	n/a
BCA	8	GSP57	Basalt	51K 281898 - 7612725*	subhor.	7	0	n/a	n/a	n/a	n/a	n/a	n/a	n/a	n/a
BCA	8	GSP56	Basalt	51K 281898 - 7612725*	subhor.	8	1	154.2	50.0	n/a	n/a	n/a	30.8	-65.2	183.8
BCA	8	GSP55	Basalt	51K 281898 - 7612725*	subhor.	7	0	n/a	n/a	n/a	n/a	n/a	n/a	n/a	n/a
BCA	8	GSP54	Basalt	51K 281898 - 7612725*	subhor.	7	0	n/a	n/a	n/a	n/a	n/a	n/a	n/a	n/a
BCA	8	GSP58	Basalt	51K 281732 - 7611993*	subhor.	7	4	181.4	42.4	25.3	18.6	3.882	24.5	-86.8	97.6
BCA	8	GSP59	Basalt	51K 281732 - 7611993*	subhor.	7	0	n/a	n/a	n/a	n/a	n/a	n/a	n/a	n/a
NS	8	U902	Basalt	50K 801760 - 7550680	subhor.	11	2	147.2	43.4	n/a	n/a	1.997	25.3	-59.9	197.3
NS	8	U901	Basalt	50K 783579 - 7542746	subhor.	10	7	141.5	50.0	342.6	3.3	6.982	30.8	-54.7	187.4
NS	8	U903	Basalt	50K 804763 - 7554167	subhor.	15	10	142.2	50.5	80.6	5.4	9.888	31.2	-55.2	186.6
	8 mean					**8**	**50**	**158.5**	**49.1**	**47.1**	**8.2**	**7.851**	**30.0**	**-68.9**	**182.1**
MC	7	GSP79	Basalt	51K 228781 - 7639463	023/15 E	10	10	151.8	64.2	589.2	2.0	9.985	46.0	-56.3	156.7
MC	7	GSP78	Basalt	51K 228667 - 7639456	023/15 E	14	12	160.8	64.9	440.5	2.1	11.975	46.9	-60.1	147.2
MC	7	GSP77	Basalt	51K 228554 - 7639452	023/13 E	14	11	164.1	63.3	15.6	11.9	10.358	44.8	-63.1	145.8
BCA	7	GSP49*	Basalt	51K 279149 - 7603472	subhor.	10	8	327.2	-62.9	39.2	9.0	7.821	44.3	54.8	343
BCA	7	GSP47*	Basalt	51K 278215 - 7601882	subhor.	10	3	157.1	79.1	146.4	10.2	2.986	68.9	-40.7	131.5
BCA	7	GSP46	Mafic tuff	51K 278526 - 7603301	subhor.	20	0	n/a	n/a	n/a	n/a	n/a	n/a	n/a	n/a
BCA	7	GSP48*	Mafic tuff	51K 278052 - 7601808	subhor.	10	3	165.4	55.5	172.1	9.4	2.988	36.0	-70.8	159.2
NS	7	U900	Basalt	50K 777731 - 7542868	subhor.	10	10	175.9	77.2	884.4	1.6	9.990	65.6	-46.6	122.2
NS	7	U899	Basalt	50K 778502 - 7544894	subhor.	11	8	132.0	75.7	564.4	2.3	7.988	63.0	-38.2	145.1
NS	7	U896	Basalt	51K 190962 - 7558533	subhor.	10	3	164.4	57.9	47.8	18.0	2.958	38.6	-68.8	155.5
NS	7	U898	Mafic tuff	50K 792063 - 7561302	subhor.	10	7	181.3	72.6	62.6	7.7	6.904	57.9	-54.1	118.7
	7 mean					**7**	**61**	**161.6**	**68.5**	**84.0**	**6.6**	**6.929**	**51.8**	**-56.2**	**140.2**

Table 2.1

Summary of HT (high temperature) results from the East Pilbara and Marble Bar Basins. Results per area are in stratigraphic order where possible. The results of the various areas are placed above each other for convenience only, exact correlations are uncertain. Bold type set show means. Abbreviations: AMG = Australian Map Grid, N = number of specimens from each site and number of sites contributing to the mean, n = number of specimens accepted and the number of specimens contributing to the mean, dec = declination, inc = inclination, Plat = palaeolatitude, VGP lat (long) = latitude (longitude) of VGP (virtual geomagnetic pole), n/a = not applicable, BCA = Boodalyerri Creek Area, LW = Limestone Well Centrocline, MC = Meentheena Centrocline, NOS = North Oakover Syncline, NS = Nullagine Synclinorium, PC = Peer Creek Centrocline , Identical AMGs with asterisk indicate sequences of sites in basalt flows directly on top of each other. Site codes with asterisk are used if the HT directions have not been used for the calculation of the mean. Results of all sites from the Nullagine Synclinorium and GSP61 to GSP67 have been published in Strik et al. (2003) and are shown because they are included in the package means. Continued on next two pages.

Area	Package	Site Number	Lithology	AMG coordinates (AGD 84)	Strike/Dip	N	n	dec°	inc°	k	a95°	R	Plat°	VGP lat°	VGP long°
NOS	6	GSP158	Basalt	51K 247300 - 7646816	335/09 E	8	8	147.2	55.2	196.0	4.0	7.964	35.7	-58.0	176.5
NOS	6	GSP159	Basalt	51K 247300 - 7646816	335/09 E	7	6	157.4	53.6	393.0	3.4	5.987	34.1	-66.3	172.8
NOS	6	GSP160	Basalt	51K 245926 - 7647382	335/09 E	7	4	161.5	60.5	32.9	16.2	3.909	41.5	-64.5	154.0
NOS	6	GSP171	Mafic tuff	51K 241482 - 7649337	173/08 W	7	0	n/a	n/a	n/a	n/a	n/a	n/a	n/a	n/a
MC	6	GSP98	Basalt	51K 225502 - 7637606	352/14 E	8	6	185.0	71.6	18.9	15.8	5.735	56.4	-54.8	115.5
MC	6	GSP170	Basalt	51K 225564 - 7637556	352/14 E	7	3	184.2	71.5	159.4	9.8	2.987	56.2	-55.0	116.3
MC	6	GSP97	Basalt	51K 225437 - 7637656	352/14 E	8	5	156.6	58.8	22.5	14.4	5.778	39.5	-63.0	162.7
MC	6	GSP96	Basalt	51K 225343 - 7637693	352/14 E	8	6	132.7	55.6	68.1	9.3	4.941	36.1	-46.4	179.8
MC	6	GSP167	Basalt	51K 235802 - 7631777	173/63 W	7	7	194.3	74.6	143.0	5.1	6.958	61.1	-49.0	110.0
MC	6	GSP168	Basalt	51K 235832 - 7631768	173/63 W	7	6	172.5	74.1	17.9	16.3	5.721	60.3	-50.7	126.3
MC	6	GSP169	Basalt	51K 235769 - 7632152	170/62 W	8	7	178.6	73.2	333.6	3.3	6.982	58.9	-52.5	121.6
MC	6	GSP165	Basalt	51K 236312 - 7626431	205/18 W	8	4	124.7	57.2	23.2	19.5	3.871	37.8	-40.0	178.5
BCA	6	GSP45	Basalt	51K 275847 - 7598852	subhor.	14	0	n/a	n/a	n/a	n/a	n/a	n/a	n/a	n/a
BCA	6	GSP44	Basalt	51K 275815 - 7598574	subhor.	8	0	n/a	n/a	n/a	n/a	n/a	n/a	n/a	n/a
BCA	6	GSP43	Basalt	51K 274691 - 7597559	subhor.	7	3	143.0	61.6	41.6	19.4	2.952	42.8	-52.7	167.7
BCA	6	GSP42	Basalt	51K 274090 - 7597133	subhor.	9	2	142.8	65.8	n/a	n/a	n/a	48.0	-50.3	160.1
BCA	6	GSP41	Basalt	51K 272889 - 7597436	subhor.	8	0	n/a	n/a	n/a	n/a	n/a	n/a	n/a	n/a
BCA	6	GSP40	Hyaloclastite	51K 272751 - 7597429	subhor.	7	0	n/a	n/a	n/a	n/a	n/a	n/a	n/a	n/a
BCA	6	GSP39	Hyaloclastite	51K 272491 - 7597389	subhor.	8	0	n/a	n/a	n/a	n/a	n/a	n/a	n/a	n/a
NS	6	U897	Basalt	50K 809522 - 7566847	subhor.	10	5	104.6	67.0	49.6	11.0	4.919	49.7	-25.9	164.1
NS	6	U886	Basalt	51K 197449 - 7572544	subhor.	10	4	165.9	61.7	96.8	9.4	3.969	42.9	-66.0	146.1
	6 mean					**15**	**58**	**153.2**	**65.8**	**44.0**	**5.8**	**14.682**	**48.0**	**-55.7**	**150.8**
NOS	5	GSP172	Basalt	51K 241638 - 7649180	168/08 W	7	7	171.3	31.9	12.2	18.0	6.507	17.3	-80.7	234.2
MC	5	GSP166	Basalt	51K 236417 - 7625883	205/18 W	7	0	n/a	n/a	n/a	n/a	n/a	n/a	n/a	n/a
NS	5	U891	Basalt	51K 198573 - 7573091	subhor.	10	2	170.7	77.4	n/a	n/a	n/a	65.9	-45.6	125.5
	5 mean					**2**	**9**	**171.2**	**54.7**	**n/a**	**n/a**	**1.844**	**35.2**	**-68.6**	**138.8**
NS	4	U915	Basalt	50K 796304 - 7572341	subhor.	26	7	167.6	75.1	120.4	5.5	6.950	62.0	-49.1	128.7
	4 mean					**1**	**7**	**167.6**	**75.1**	**n/a**	**n/a**	**n/a**	**62.0**	**-49.1**	**128.7**
MC	2	GSP91	Porphyry	51K 226052 - 7650595	040/20 SE	10	10	292.6	-48.9	164.7	3.8	9.945	29.8	29.4	7.2
MC	2	GSP92	Porphyry	51K 225854 - 7650582	040/20 SE	7	6	288.8	-59.8	159.3	5.3	5.969	40.7	27.6	354.5
MC	2	GSP161	Porphyry	51K 225665 - 7650520	040/20 SE	7	6	301.9	-71.7	82.1	7.4	5.939	56.5	35.0	335.2
NOS	2	GSP182	Porphyry	51K 216881 - 7680038	304/15 NE	7	0	n/a	n/a	n/a	n/a	n/a	n/a	n/a	n/a
NOS	2	GSP181	Porphyry	51K 216455 - 7679722	304/15 NE	7	6	345.3	-68.5	80.4	7.5	5.938	51.8	57.1	317.1
NOS	2	GSP179	Porphyry	51K 219910 - 7676547	312/25 NE	7	5	317.0	-80.6	52.1	10.7	4.923	71.7	33.7	315.2
NOS	2	GSP180	Porphyry	51K 219868 - 7676505	326/21 NE	7	0	n/a	n/a	n/a	n/a	n/a	n/a	n/a	n/a
NS	2	GSP50	Porphyry	51K 198794 - 7589321	subhor.	14	14	332.4	-70.1	29.2	9.1	9.692	54.1	51.5	326.0
NS	2	GSP173	Porphyry	51K 201271 - 7588274	subhor.	7	7	318.4	-74.7	78.4	6.9	6.923	61.3	41.2	325.2
NS	2	GSP184	Porphyry	51K 201617 - 7588455	subhor.	7	1	313.6	-63.7	n/a	n/a	n/a	45.3	45.6	346.8
	2 mean					**8**	**51**	**310.1**	**-68.4**	**42.8**	**8.6**	**7.836**	**51.6**	**41.5**	**337.3**
MC	2	GSP68*	Conglomerate	51K 215391 - 7623982	340/25 E	23	23	315	28.7	1.8	32.8	10.985	n/a	n/a	n/a
LW	1	GSP25	Basalt	50K 767635 - 7643347	332/14 E	11	8	111.6	69.7	243.3	3.6	7.971	53.5	-29.7	159.1
LW	1	GSP26	Basalt	50K 767429 - 7643505	332/14 E	9	9	124.5	67.6	212.0	3.5	8.962	50.5	-38.0	161.3
LW	1	GSP27	Basalt	50K 767429 - 7643505	332/14 E	8	8	122.4	68.8	718.5	2.1	7.990	52.2	-36.4	159.6
LW	1	GSP28	Basalt	50K 767286 - 7643426*	332/14 E	7	7	132.5	69.8	144.8	5.0	6.959	53.7	-41.7	155.4
LW	1	GSP29	Basalt	50K 767286 - 7643426*	332/14 E	7	5	126.0	68.5	1144.7	2.3	4.997	51.8	-38.6	159.4
LW	1	GSP30	Basalt	50K 767286 - 7643426*	332/14 E	6	6	129.4	69.2	191.3	4.9	5.974	52.8	-40.3	157.4
LW	1	GSP31	Basalt	50K 767143 - 7643347	332/14 E	7	7	127.9	66.5	453.0	2.8	6.987	49.0	-40.5	162.5
LW	1	GSP32	Basalt	50K 767143 - 7643347	332/14 E	7	7	128.3	60.3	144.5	5.0	6.958	41.2	-42.3	172.6
LW	1	GSP24	Basalt	50K 770457 - 7639104	258/17 N	7	7	99.2	78.1	267.8	3.7	6.978	67.1	-23.1	144.2
LW	1	GSP23	Silt/sandstone	50K 770220 - 7638795	260/16 N	4	0	n/a	n/a	n/a	n/a	n/a	n/a	n/a	n/a
LW	1	GSP162	Basalt	50K 781775 - 7652781	111/15 S	7	6	145.1	66.2	381.7	3.4	5.987	48.6	-51.0	156.7
LW	1	GSP163	Basalt	50K 781720 - 7652790	111/15 S	7	7	132.7	69.0	188.1	4.4	6.968	52.5	-42.2	156.9
LW	1	GSP164	Basalt	50K 781696 - 7652810	111/15 S	7	7	133.5	64.3	105.4	5.9	6.943	46.1	-44.9	164.9
LW	1	GSP147	Basalt	50K 781652 - 7652819	111/15 S	7	5	132.8	66.8	113.9	7.2	4.965	49.4	-43.4	160.8
LW	1	GSP148	Basalt	50K 781660 - 7652857	111/15 S	7	5	137.6	67.5	61.5	9.8	4.935	50.4	-45.9	157.9
LW	1	GSP149	Basalt	50K 781665 - 7652903	111/15 S	8	8	125.6	64.6	218.2	3.8	7.968	46.5	-39.5	166.2

Table 2.1 (continued)

Area	Package	Site Number	Lithology	AMG coordinates (AGD 84)	Strike/Dip	N	n	dec°	inc°	k	a95°	R	Plat°	VGP lat°	VGP long°
LW	1	GSP150	Basalt	50K 781658 - 7652955	111/15 S	7	5	146.3	64.6	1300.8	2.1	4.997	46.5	-52.8	158.9
NOS	1	GSP178	Basalt	51K 219568 - 7676094	326/21 E	7	0	n/a	n/a	n/a	n/a	n/a	n/a	n/a	n/a
NOS	1	GSP177	Basalt	51K 219353 - 7675765	326/21 E	7	3	122.2	74.4	597.4	5.0	2.997	60.8	-33.7	150
NOS	1	GSP176	Basalt	51K 219181 - 7675678	306/15 N	15	11	134.3	63.5	54.8	6.2	10.817	45.1	-45.6	166.5
NOS	1	GSP175	Basalt	51K 219018 - 7675625	306/15 N	7	4	161.0	71.4	167.9	7.1	3.982	56.1	-52.2	137.6
NOS	1	GSP174	Basalt	51K 218927 - 7675571	306/15 N	7	5	141.7	73.4	231.1	5.0	4.983	59.2	-43.1	146.1
MC	1	GSP94*	Basalt	51K 226537 - 7652982	098/24 S	8	8	132.7	54.7	30.9	10.1	7.774	35.2	-46.5	181.0
MC	1	GSP93*	Basalt	51K 226664 - 7653075	098/24 S	8	6	124.5	46.4	40.0	10.7	5.875	27.7	-39.5	191.3
MC	1	GSP67	Basalt	51K 212666 - 7628329*	345/26 E	7	6	130.1	73.0	255.9	4.2	5.980	58.6	-38.6	151.0
MC	1	GSP66	Basalt	51K 212666 - 7628329*	345/26 E	7	7	142.1	71.5	4898.0	0.9	6.999	56.2	-45.4	149.4
MC	1	GSP65	Basalt	51K 212666 - 7628329*	345/26 E	7	6	136.6	67.2	748.0	2.5	5.993	49.9	-45.6	159.5
MC	1	GSP64	Basalt	51K 212666 - 7628329*	345/26 E	7	5	137.9	70.7	117.2	7.1	4.966	55.0	-44.1	152.6
MC	1	GSP63	Basalt	51K 212600 - 7628194*	345/28 E	7	7	129.1	70.5	161.5	4.8	6.963	54.7	-39.6	155.8
MC	1	GSP62	Basalt	51K 212600 - 7628194*	345/28 E	7	6	132.9	70.4	175.6	5.1	5.972	54.5	-41.7	154.9
MC	1	GSP61	Basalt	51K 212600 - 7628194*	345/28 E	7	7	129.4	66.5	1014.7	1.9	6.994	49.0	-41.6	162.9
NS	1	GSP37	Basalt	51K 194857 - 7608645*	350/13 E	5	4	124.8	60.2	481.8	4.2	3.994	41.1	-39.9	173.8
NS	1	GSP34	Basalt	51K 194857 - 7608645*	350/13 E	5	2	126.3	71.4	n/a	n/a	1.973	56.1	-37.8	154.8
NS	1	U894	Basalt	51K 194425 - 7608523	350/12 E	10	7	125.7	63.3	139.1	5.1	6.957	44.8	-40.1	168.9
NS	1	U892	Basalt	51K 194045 - 7608483	350/16 E	10	7	120.2	58.3	327.0	3.3	6.982	39.0	-36.5	176.8
NS	1	U893	Basalt	51K 193839 - 7608409	350/10 E	10	10	129.1	70.0	176.0	3.7	9.949	53.9	-40.0	156.6
	1 mean					**32**	**218**	**130.7**	**68.3**	**207.0**	**1.8**	**31.850**	**51.5**	**-41.4**	**158.5**
PC	0	GSP90	Basalt	50K 765529 - 7686812	070/28 S	7	6	325.5	63.9	56.9	9.0	5.912	45.6	16.5	95.1
PC	0	GSP89	Basalt	50K 765454 - 7686832	070/28 S	8	8	339.1	76.1	125.4	5.0	7.994	63.7	3.9	110.4
PC	0	GSP88	Basalt	50K 762392 - 7686373	035/44 SE	8	5	189.5	83.0	15.1	20.3	4.736	76.2	-34.5	116.8
PC	0	GSP87	Basalt	50K 762368 - 7686443	035/44 SE	7	4	119.9	69.7	38.0	15.1	3.921	53.5	-34.3	158.1
PC	0	GSP86	Basalt	50K 762461 - 7687281	035/44 SE	7	6	345.3	66.3	512.5	3.0	5.990	48.7	19.2	109.3
PC	0	GSP85	Basalt	50K 762426 - 7687252	035/44 SE	7	7	337.3	66.3	159.8	4.8	6.962	48.7	17.5	104.3
PC	0	GSP84	Basalt	50K 762347 - 7687315	035/44 SE	7	4	340.0	70.3	273.2	5.6	3.989	54.4	12.8	107.7
PC	0	GSP83	Basalt	50K 762343 - 7687328	035/44 SE	7	6	357.6	77.5	173.8	5.1	5.971	66.1	3.0	118.5
PC	0	GSP82	Basalt	50K 762063 - 7687732	035/44 SE	7	4	353.9	80.2	96.2	7.8	4.958	70.9	-1.9	117.5
PC	0	GSP81	Basalt	50K 762058 - 7687748	035/44 SE	7	7	339.6	71.8	274.4	3.7	6.978	56.7	10.6	108.3
LW	0	GSP07	Basalt	50K 749404 - 7643594*	055/46 SE	6	5	295.7	67.2	270.0	4.7	4.985	49.9	-1.0	84.0
LW	0	GSP06	Basalt	50K 749404 - 7643594*	055/46 SE	7	5	279.5	70.5	244.0	4.9	4.984	54.7	-12.0	83.8
LW	0	GSP05	Basalt	50K 749404 - 7643594*	055/46 SE	7	3	304.6	67.8	57.0	16.5	2.965	50.8	3.1	88.0
LW	0	GSP04	Basalt	50K 749404 - 7643594*	055/46 SE	6	3	267.8	66.8	132.7	10.7	2.985	49.4	-17.4	76.4
LW	0	GSP03	Basalt	50K 749404 - 7643594*	055/46 SE	9	8	299.7	69.1	116.1	5.2	7.940	52.6	-0.5	87.6
LW	0	GSP13	Basalt	50K 749688 - 7644249*	265/74 N	5	3	289.4	75.7	66.6	15.2	2.970	63.0	-10.5	93.6
LW	0	GSP12	Basalt	50K 749688 - 7644249*	265/74 N	9	7	277.3	66.6	120.0	5.5	6.950	49.1	-11.4	77.9
LW	0	GSP11	Basalt	50K 749688 - 7644249*	265/74 N	7	4	273.0	68.8	516.3	4.0	3.994	52.2	-14.9	80.1
LW	0	GSP10	Basalt	50K 749688 - 7644249*	265/74 N	9	5	281.0	69.0	138.9	6.5	4.971	52.5	-10.4	82.0
LW	0	GSP09	Basalt	50K 749688 - 7644249*	265/74 N	7	5	267.1	73.2	116.4	7.1	4.966	58.9	-19.6	86.2
LW	0	GSP08	Basalt	50K 749688 - 7644249*	265/74 N	7	3	269.4	65.1	180.8	9.2	2.989	47.1	-15.8	74.4
LW	0	GSP22	Basalt	50K 770852 - 7637517*	260/23 N	7	1	327.3	45.1	n/a	n/a	n/a	26.6	32.5	84.7
LW	0	GSP21	Basalt	50K 770852 - 7637517*	260/23 N	7	7	298.5	66.1	334.2	3.3	6.982	48.5	1.3	83.9
LW	0	GSP20	Basalt	50K 770852 - 7637517*	260/23 N	7	6	297.0	64.6	233.8	4.4	5.979	46.5	0.4	81.0
LW	0	GSP19	Basalt	50K 770852 - 7637517*	260/23 N	7	4	297.6	67.2	187.2	6.7	3.984	49.9	0.0	84.8
LW	0	GSP18B	Basalt	50K 770852 - 7637517*	260/23 N	7	3	291.3	51.8	10.3	40.5	2.806	32.4	5.2	67.5
LW	0	GSP18A	Basalt	50K 770852 - 7637517*	260/23 N	8	6	308.6	67.2	88.9	7.1	5.944	49.9	5.5	89.3
LW	0	GSP16	Basalt	50K 770822 - 7637462	260/23 N	10	4	318.7	65.7	55.1	12.5	3.946	47.9	11.5	92.8
LW	0	GSP02	Basalt	50K 770822 - 7637493*	260/23 N	9	0	n/a	n/a	n/a	n/a	n/a	n/a	n/a	n/a
LW	0	GSP01	Basalt	50K 770822 - 7637493*	260/23 N	6	0	n/a	n/a	n/a	n/a	n/a	n/a	n/a	n/a
PC	0	GSP14A*	Hyaloclastite	50K 768095 - 7686388*	113/36 S	7	1	349.0	63.7	n/a	n/a	n/a	45.3	23.0	111.2
PC	0	GSP14B*	Hyaloclastite	50K 768095 - 7686388*	113/36 S	8	8	185.4	78.1	5.7	25.3	6.779	67.1	-43.6	116.7
LW	0	GSP38	Sandstone	50K 782224 - 7647492	247/30 N	5	0	n/a	n/a	n/a	n/a	n/a	n/a	n/a	n/a
	0 mean					**28**	**140**	**304.6**	**72.0**	**31.7**	**4.9**	**27.147**	**57.0**	**-1.5**	**93.6**

Table 2.1 (continued)

GSP14A-B only show inconsistent HT directions. Package 0 appears to have no equivalent in the East Pilbara Basin, with its mean HT direction showing a nearly 180 degree declinational difference from the Nullagine Synclinorium Package 1 HT direction.

Package 1: Basalts and silt- to sandstones of Package 1 were sampled in the Marble Bar Basin, and also in the North Oakover Syncline and the Meentheena Centrocline of the East Pilbara Basin. Zijderveld plots show consistent and straightforward demagnetisation behaviour (Fig. 2.5, v-x). A present day field overprint is occasionally recognised while a MT component is only sporadically apparent. The dispersion of MT data is relatively high (Fig. 2.6h, Tab. 2.2). All sites show well-defined HT directions, except for a site in a sedimentary unit (GSP23) and basalt site GSP178 (Tab. 2.2). The HT directions of sites GSP93 and 94 are less well defined and are not included in the Package 1 mean HT direction. The remaining 20 sites have a very consistent HT component. The data from the upper flood basalt unit of the Marble Bar Basin ("MBB P1" in Fig. 6h) are nearly identical to the Package 1 data of the East Pilbara Basin areas. Data from sites GSP147-150 and GSP162-164 ("FF P1" in Fig. 2.6h) also show a similar direction. The average of the Package 1 data, combined with the Package 1 data from the Nullagine Synclinorium and the Meentheena Centrocline (Strik et al., 2003), has relatively high precision (k = 207.0, Fig. 2.6h, Tab. 2.2).

Package 2: The massive dacite porphyry of this package was sampled in the Meentheena Centrocline and in the North Oakover Syncline. Zijderveld plots of Package 2 samples are consistent and nearly always show only one (HT) component (Fig. 2.5, r-t). In two from a total of seven sites, a present day field component is preserved (Fig. 2.6g) and in none of the sites a MT component is recorded. The HT directions have a reversed polarity consistent with Package 2 data of the Nullagine Synclinorium (Tab. 2.1, Fig. 2.6g). The package means of the respective sampling areas differ more from each other than the means of e.g. Package 1 (cf. Fig. 2.6g and h), but the number of Package 2 sample sites is relatively limited.

No suitable sites were found to sample Package 3, just like in the Nullagine Synclinorium. Also, no suitable sites were found to sample Package 4, therefore no comparison could be made to Package 4 results from the Nullagine Synclinorium.

Package 5: Only two basalt sites in the Meentheena Centrocline were thought to be suitable to sample Package 5, but these reveal poor results. Site GSP166 revealed no consistent directions and site GSP172 was largely overprinted by the present day field (Figs. 2.5q and 2.6f). No MT component is recognised and the HT directions do not form well-defined clusters (k = 12.2, cf. Tab. 2.1). This is similar to the Nullagine Synclinorium, which also revealed poor results for Package 5 (Tab. 2.1, Fig. 2.6f).

Package 6: Basalts, hyaloclastite and mafic tuff of Package 6 were sampled in the Meentheena Centrocline and in the Boodalyerri Creek Area. In the Nullagine Synclinorium, only poor results were obtained for Package 6 and unfortunately, the results for the Boodalyerri Creek Area are very similar. At high temperature steps, the Zijderveld plots are often chaotic (Fig. 2.5p). Some samples were af-demagnetised to check for possible oven effects, but similarly poor results were obtained. Clear present day field and MT directions can be distinguished (Fig. 2.5, n-p, Tab. 2.2). Occasionally, a HT component is recorded (Tab. 2.1), of which the direction is comparable to that of Package 6 in the Nullagine Synclinorium (Fig. 2.6e). Results from Package 6 in the Meentheena Centrocline are better: Zijderveld diagrams show a clear HT component (Fig. 2.5m), although significant alteration occurs at temperatures of 560 °C and higher. All but the mafic tuff site (GSP171) show consistent HT directions (Tab. 2.1). A present day field component and a MT component

Package	Site Number	N	n	dec°	inc°	k	a95°	R	Plat°	VGP lat°	VGP long°
10	GSP70	12	5	281.5	-42.4	13.3	21.8	4.698	24.5	18.6	370.6
10	GSP72	10	5	315.7	-44.7	16.0	19.8	4.749	26.3	49.3	374.2
10	GSP71	10	4	308.7	-40.1	52.1	12.9	3.942	22.8	42.6	378.4
10	GSP69A	7	3	266.4	-20.0	1.4	99.9	1.584	10.3	0.4	379.6
10	GSP69B	7	1	301.7	-44.6	n/a	n/a	n/a	26.2	36.8	372.9
10	U904	10	6	315.7	-25.5	24.9	13.7	5.800	13.4	47.1	34.1
10	U907	10	8	315.3	-34.0	34.2	9.6	7.795	18.6	48.1	26.4
10	U905	12	3	307.7	-18.4	19.0	29.1	2.895	9.4	38.3	35.6
10 mean		**8**	**35**	**301.5**	**-35.0**	**18.6**	**13.2**	**7.624**	**19.3**	**35.7**	**21.0**
9	GSP187	7	1	312.4	-53.4	n/a	n/a	n/a	34.0	46.2	362.9
9	U908	5	3	324.8	-40.3	56.6	16.5	2.965	23.0	57.6	21.7
9	U909	5	3	314.9	-43.9	345.8	6.6	2.994	25.7	48.8	15.8
9 mean		**3**	**7**	**317.8**	**-46.0**	**98.2**	**12.5**	**2.980**	**27.4**	**51.1**	**12.8**
8	GSP74	15	1	307.5	-21.0	n/a	n/a	n/a	10.9	38.7	33.5
8	GSP75	15	7	285.0	-49.4	46.5	8.9	6.871	30.3	23	365.5
8	GSP58	7	3	301.9	-54.3	20.3	28.1	2.9	34.8	37.8	362.8
8	U902	11	6	326.9	-38.0	103.0	6.6	5.951	21.3	59.3	25.1
8	U901	10	3	333.5	-46.0	63.6	15.6	2.969	27.4	65.4	12.2
8	U903	15	8	320.3	-31.6	97.1	5.6	7.928	17.1	52.4	30.3
8 mean		**6**	**28**	**313.4**	**-41.1**	**20.7**	**15.1**	**5.759**	**23.6**	**46.8**	**17.3**
7	GSP77	14	2	292.7	-42.3	n/a	n/a	n/a	24.5	28.5	373.3
7	GSP47	10	2	315.0	-40.4	n/a	n/a	1.989	23.1	48.5	380.1
7	GSP46	20	20	309.9	-47.0	64.3	4.1	19.705	28.2	44.4	372
7	GSP48	10	7	308.0	-43.0	152.2	4.9	6.961	25.0	42.4	376.2
7	U900	10	7	327.3	-33.4	25.8	12.1	6.767	18.2	59.1	31.0
7	U899	11	7	321.3	-52.6	23.2	12.8	6.742	33.2	54.2	3.3
7	U898	10	6	328.3	-43.0	21.4	14.8	5.766	25.0	60.8	17.7
7 mean		**7**	**51**	**314.8**	**-43.7**	**55.3**	**8.2**	**6.892**	**25.5**	**48.5**	**15.7**
6	GSP98	8	4	296.1	-22.8	295.1	5.4	3.990	11.9	28.4	388.1
6	GSP170	7	3	302.8	-20.3	70.7	14.8	2.972	10.5	34.2	32
6	GSP97	8	3	298.0	-41.2	54.9	16.8	2.964	23.6	33.1	375.3
6	GSP96	8	1	302.5	-41.2	n/a	n/a	n/a	23.6	37.2	376.2
6	GSP159	7	3	321.0	-52.0	59.2	16.2	2.966	32.6	53.7	364
6	GSP160	7	6	304.9	-34.1	216.9	4.6	5.977	18.7	38.4	383.1
6	GSP165	8	3	312.3	-40.5	44.7	18.7	2.955	23.1	46	378.9
6	GSP167	7	1	312.8	-33.1	n/a	n/a	n/a	18.1	45.6	386.1
6	GSP168	7	6	320.2	-28.7	41.0	10.6	5.878	15.3	51.8	32.7
6	GSP169	8	6	318.3	-33.4	22.9	14.3	2.960	18.2	50.8	387.5
6	GSP171	7	4	307.9	-26.7	34.9	15.8	3.914	14.1	40.1	29.6
6	GSP45	14	14	300.6	-41.0	26.1	7.9	13.503	23.5	35.5	376.8
6	GSP44	8	3	314.6	-38.1	94.3	12.8	2.979	21.4	47.9	382.5
6	GSP43	7	6	312.5	-32.8	99.6	6.7	5.950	17.9	45.3	387
6	GSP42	9	5	311.4	-28.7	58.6	10.1	4.932	15.3	43.7	390.1
6	GSP41	8	1	308.4	-20.7	n/a	n/a	n/a	10.7	39.5	34.8
6	GSP40	7	4	316.1	-38.5	43.5	14.1	3.931	21.7	49.4	382.4
6	GSP39	8	3	320.4	-31.6	36.5	20.7	2.945	17.1	52.5	390.7
6 mean		**18**	**76**	**309.9**	**-33.9**	**60.0**	**4.5**	**17.716**	**18.6**	**43.2**	**24.4**
2	GSP68	23	11	305.7	-33.8	49.1	6.6	10.796	18.5	39.1	383.4
2 mean		**1**	**11**	**305.7**	**-33.8**	**n/a**	**n/a**	**n/a**	**18.5**	**39.1**	**23.4**
1	GSP177	7	1	310.1	-21.1	n/a	n/a	n/a	10.9	41.2	34.1
1	GSP176	15	2	314.0	-37.5	n/a	n/a	n/a	21.0	47.2	21.7
1	GSP175	7	1	281.2	-34.8	n/a	n/a	n/a	19.2	16.8	15.7
1	GSP93	8	8	319.8	-38.5	36.8	9.3	7.810	21.7	52.7	22.0
1	GSP94	8	3	326.4	-24.0	62.5	15.7	2.968	12.6	56.8	40.0
1 mean		**5**	**15**	**310.7**	**-32.1**	**23.7**	**16.0**	**4.831**	**17.4**	**43.4**	**25.6**
Total MT		**48**	**223**	**310.0**	**-37.1**	**32.6**	**3.7**	**46.560**	**20.7**	**43.7**	**21.2**

Table 2.2
Summary of MT (medium temperature) results from the East Pilbara Basin. Consistent MT directions were found only in Packages 1, 2, 6, 7, 8, 9 and 10. Results are grouped by package. See Table 2.1 for additional sample data and explanation of abbreviations. Sites without results have been omitted.

are commonly developed as well (Fig. 2.6e, Tab. 2.2). The mean HT direction of Package 6 in the Meentheena Centrocline is comparable but more precisely defined (Fig. 2.6e) than that of the mean of the Nullagine Synclinorium and the mean of the Boodalyerri Creek Area.

Package 7: Basalts and mafic tuff of this package were sampled in the Meentheena Centrocline and in the Boodalyerri Creek Area. In the latter, two mafic tuff sites (GSP46 and 48) and two basalt sites (GSP47 and 49) were sampled. Zijderveld diagrams reveal both present day field and MT directions (e.g. Fig. 2.5p, see also Tab. 2.2), but only the basalt samples have a HT component, which is well developed in GSP49 (Fig. 2.5k). The GSP49 HT direction has a reversed polarity with respect to the Package 7 HT mean direction in the Nullagine Synclinorium (Tab. 2.1, Fig. 2.6d). GSP47 seems to have a normal polarity, but the HT data of this site are of poor quality. Package 7 data from the Meentheena Centrocline reveal only occasional present day field and MT components; the HT component is well developed (Fig. 2.5j) and has a normal polarity (Tab. 2.1, Fig. 2.6d). Compared to Package 7 in the Nullagine Synclinorium, the Meentheena Centrocline HT mean has a similar direction (Fig. 2.6d).

Package 8: Basalts of Package 8 were sampled in the Meentheena Centrocline and in the Boodalyerri creek Area. The sample sites in the latter area (GSP53-60) were heavily affected by lightning (cf. Fig. 2.5f) and only five out of 66 samples generated useful results (cf. Tab. 2.1). Twenty-eight samples had to be measured on the JR5 spinner magnetometer, due to the high magnetic intensity of these samples (between 8 and 114 Am^{-1} for the first temperature step), which exceeds the range of the DC-SQUID magnetometer. Of the five accepted samples, one shows a present day field component, three show a MT component and all five have a HT component. Sampling in the Meentheena Centrocline was more successful, because all three sampling sites (GSP77-79) gave consistent results. For these sites, only MT and HT components are found (Tabs. 2.1, 2.2, Fig. 2.6c). The Package 8 HT mean of the Meentheena Centrocline is almost identical to that of the Boodalyerri Creek Area and the $\alpha95$ overlaps with the Package 8 HT mean of the Nullagine Synclinorium (Fig. 2.6c).

Package 9: Basalts of this package were sampled in the North Oakover Syncline. In other areas Package 9 is either absent or has no suitable outcrop. Many Zijderveld diagrams show a present day field component, but after heating to 400 °C the demagnetisation results are scattered (Fig. 2.5d). Of 36 samples, only 13 reveal consistent HT directions (e.g. Fig. 2.5e, see also Tab. 2.1), and seven MT component directions are recorded (Tab. 2.2). Only one HT direction is obtained for site GSP188, which has not been included in the Package 9 mean. In the Nullagine Synclinorium, the results were not much better, possibly because Package 9 consists of unusually coarse-grained basalt, which makes it more susceptible to weathering. The Package 9 HT means of the North Oakover Syncline and the Nullagine Synclinorium do not correlate well, (Fig. 2.6b), perhaps because secular variation has not sufficiently been averaged out.

Package 10: Basalts of Package 10 were sampled in the North Oakover Syncline. This is the only area of the East Pilbara Basin other than the Nullagine Synclinorium where Package 10 basalt is found. Zijderveld plots show that a present day field component, a MT and a HT component are recorded (Fig. 2.5, a-c). Site GSP73 was affected by lightning, but all other sites give good results (Tabs. 2.1, 2.2) and have consistent present day field, MT and HT components (Fig. 2.6a). Occasionally, a "very high temperature" component was observed, which does not go towards the origin and is probably due to some oxidation in the oven.

Compared to the results from the Nullagine Synclinorium, the HT directions have a steeper inclination in the sites from the North Oakover Syncline, although the a95 circles still overlap (Fig. 2.6a).

Field tests

Strik et al. (2003) concluded that the HT component preserved in the rocks of the Nullagine Synclinorium represents a primary NRM. This is based on positive conglomerate, reversal and fold tests. In this paper, we present results of an intraformational conglomerate test in the Meentheena Centrocline, a Package 1 – Package 2 and a Package 2 – Package 6 reversal test for the East Pilbara and Marble Bar Basins, and a fold test for Package 0 in the Marble Bar Basin.

Clasts derived from Package 1 basalts are included in a Package 2 conglomerate. Twenty-three of these clasts were sampled and thermally demagnetised. The magnetic intensity is weak; on average 1×10^{-3} A/m, which is ca. 50 times less than the average Package 1 intensity. Eleven out of 23 samples show a clear present day field overprint while 11 samples show MT directions (Fig. 2.7, see also Tab. 2.2). The HT component is poorly defined, and in some case the maximum angular deviation was larger than 10°. The Watson test for uniform randomness (Watson, 1956) gives a negative result, with critical value $R_0 = 7.69$ being smaller than the calculated value $R = 10.99$ (Fig. 2.7). The Shipunov conglomerate test (Shipunov et al., 1998), which allows a know reference vector for the studied area to be used, however, gives positive results in two tested cases. First the Package 1 HT mean direction (130.7°/68.3°) was used. The critical number $\rho_0 = 0.198$ is greater than the calculated $\rho = 0.059$. Secondly, the Package 6 HT mean direction (153.2°/65.8°) was used. The critical number $\rho_0 = 0.198$ is again greater than the calculated $\rho = 0.046$. We are not convinced, however, that the HT component may have been influenced by the MT

Conglomerate Test

n = 23   Site: GSP68,   Package 2

Watson test
$R_0 = 7.69$ $R = 10.99$
$R > R_0$ Result: **Negative**

Shipunov test
Vector used: 153.2/65.8 (= Package 6 mean)
$\rho_0 = 0.198$ $\rho = 0.046$
$\rho < \rho_0$ Result: **Positive**

Vector used: 130.7/68.3 (= Package 1 mean)
$\rho_0 = 0.198$ $\rho = 0.059$
$\rho < \rho_0$ Result: **Positive**

△ pdf
□ MT
○ HT
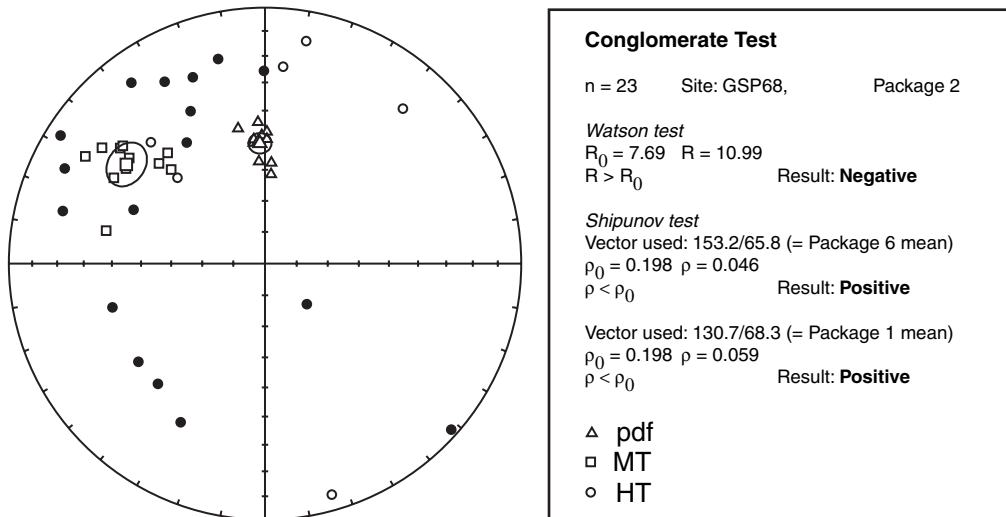
Figure 2.7
Equal area plot of the LT, MT and HT directions from the conglomerate test at site GSP68. Conventions as in Figure 2.5. The statistical details of the test are in the box on the right. The Shipunov test proved positive for all used reference vectors, but the Watson test is negative. Abbreviation: pdf = present day field.

component, since it seems that more directions plot in the same quadrant as the MT mean than in other quadrants of the equal area plot (Fig. 2.7). Therefore, we interpret the result of the conglomerate test as indeterminate.

Since Package 2 has a reversed polarity with respect to Package 1, the reversal test of McFadden and McElhinny (1990) can be applied. The HT means of Packages 1 and 2 of the East Pilbara and Marble Bar Basins were used (cf. Tab. 2.1). The angle between the mean of the normal (Package 1) and the reversed (Package 2) polarity set is 0.2°, and the large critical angle is 8.7°, which means that the reversal test is passed with classification B. If the reversal test is performed on the HT means of Package 2 and Package 6, the critical angle is 9.9°. The angle between the mean of the normal (Package 6) and the reversed (Package 2) polarity set is 9.3°, which again means that the reversal test is passed with classification B.

Package 0 is locally folded by a narrow belt that runs in an S-shape from the south-west to the northeast of the Marble Bar Basin (Fig. 2.3). Package 1 is not affected by this fold and unconformably overlies Package 0. Two limbs of an anticline from the fold belt were sampled for a fold test. Sites GSP03 - 07 are situated in the southern limb of the anticline, with an average plunge of 46.3° towards 054.8°. Sites GSP08 - 13 are situated in the northern
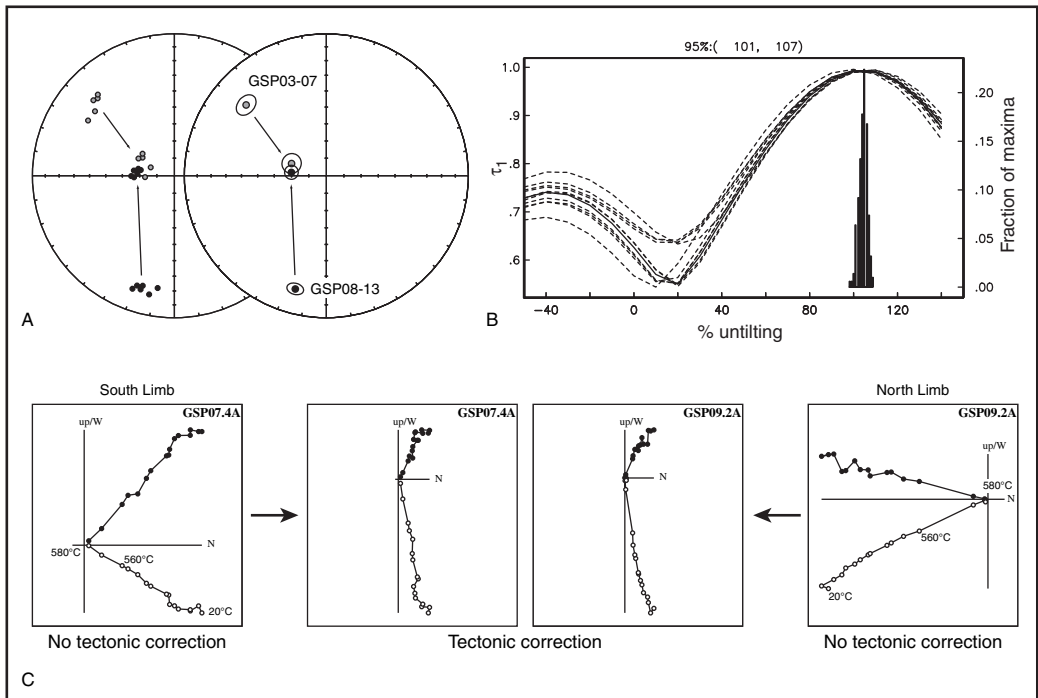
Figure 2.8
Equal area plots of HT directions from the fold test before and after tilt correction. Symbols represent site means. All directions are from Package 0, From the Marble Bar Basin. The left plot shows the fold test for the site means, where N represents the number of sites. The right plot is the fold test for the means of all individual samples, from the two limbs of the fold, where n represents the total number of samples per limb. Grey symbols are data from the South limb and black symbols are data from the North limb.
Results from the applied fold test of Tauxe & Watson (1994). Best grouping occurs between 101 and 107 % of untilting.
Zijderveld diagrams of two selected samples from the South and North limb of the fold, before and after tectonic correction. After tectonic correction, the diagrams are nearly identical.

limb of the anticline, with an average plunge of 74.4° towards 264.5°. Figure 2.8a shows equal area plots of individual site means and the mean of the site means before and after tectonic correction. Before tectonic correction, inclinations are shallow and the northern and southern limb data plot ca. 115° apart. After tectonic correction is applied, inclinations are steep and declinations are nearly the same. When the non-parametric fold test of Tauxe and Watson (1994) is applied, the best results are obtained between 101 and 107 % of unfolding (Fig. 2.8b). Bearing in mind that flood basalts commonly have an undulose surface, exact bedding determination is complicated, which explains why the best results are not obtained for exactly 100% unfolding. Zijderveld diagrams of samples from this fold show very regular unblocking and the agreement between the northern and southern limb after tectonic correction is remarkable (Fig. 2.8c). Hence, the fold test is positive and since this fold was formed before the formation of Package 1, the timing of the magnetisation of Package 0 is constrained to be older than 2772 ± 2 Ma.

Based on the positive reversal tests and a positive Package 0 fold test, together with positive field tests from the Nullagine Synclinorium from Strik et al. (2003), we conclude that the HT component is a primary component acquired at the time of formation of the rocks.

Discussion

Package correlations

The suggested package subdivision of the East Pilbara and Marble Bar Basins in a similar way as the Nullagine Synclinorium (Blake, 2004), is confirmed by the palaeomagnetic data. The pattern is very consistent, except for the additional Package 0 in the Marble Bar Basin. Basalts interpreted as Package 1 have statistically identical directions as Package 1 in the Nullagine Synclinorium. Package 2 is reversed in all sampled sites of all areas, which is an important fact for the correlation. Area means of Packages 6, 7, 8 and 10 are indistinguishable (Fig. 2.6). Slight differences could be caused by secular variation or an insufficient number of sampled flows. In the case of Package 5, the poor quality of HT directions and the small number of sampling sites result in a poor correlation. Finally, the coarse grained nature of Package 9 basalts and its susceptibility to weathering and hence its poor outcrop quality explain the difficulties to unambiguously correlate Package 9 in the Nullagine Synclinorium to its possible equivalent in the North Oakover Syncline. Based on the palaeomagnetic data, we conclude that the subdivision in packages in the Nullagine Synclinorium can indeed be extrapolated to the East Pilbara Basin. The same applies to the Marble Bar Basin, with the exception that there is an additional lower flood basalt sequence (Package 0), clearly older than Package 1.

Package 0 and Package 1 in the Marble Bar Basin

The presence of Package 0 in the Marble Bar Basin is an unexpected and interesting outcome of this study. A textbook version of the positive fold test demonstrates that the HT component records the primary NRM. Package 0 is the only package that has been affected by tight folding, and locally has a significant angular unconformity, which emphasises the fact that Package 0 is older than Package 1. There is a lack of geochronological control in the Marble Bar Basin and it can therefore not be excluded that Package 0 is even significantly older than Package 1.

The palaeomagnetic data for the lower flood basalt sequence (Package 0) show a 173.9° difference to the declination of the upper sequence (Package 1) in the Marble Bar

Basin, and also to Package 1 in the East Pilbara Basin. The inclination, however, is not reversed, so a reversal of the geomagnetic (dipole) field cannot explain the data. A systematic orientation error during sampling and/or processing is highly unlikely, among other reasons because a present day field component can be identified. A number of speculations can be made to explain the 173.9° rotation, but we have no definite answer.

The first option is that Package 0 is in fact significantly older than the Nullagine Supersequence, enabling a substantial rotation phase over an extended period of time. There are no structural indications for a 173.9° rotation of the Marble Bar Basin as a separate block, but for the Pilbara Craton as a whole a significant rotation cannot be excluded, although it will be difficult to prove.

The second option is that the rotation is caused by a large excursion of the geomagnetic field or major no-dipole behaviour. With respect to the Package 1 data, Package 0 does seem to have a larger spreading of site averages (cf. Fig. 2.6, h-j), but a more complete track of a possible excursion is not recorded in the rocks sampled so far.

The third option is that of true polar wander (TPW) or even inertial interchange TPW (IITPW). Kirschvink et al. (1997) explain anomalously fast rotation and latitudinal drift between 523 and 508 Ma, with an IITPW event. This (much debated) event is supposed to have been caused by an unstable distribution of the Earth's landmasses, causing the lithosphere and mantle to rotate ca. 90° with respect to the Earth's spin axis. Meert (1999), however, explains the same event with rapid continental drift, possibly combined with TPW. The remarkable direction of Package 0 could be explained by IITPW, since a ca. 75° shift of the magnetic North towards the equator would cause the declination of Package 1 to flip ~180° with respect to Package 0 while the inclination will stay the same, as observed. If IITPW requires a 90° shift of the spin axis, it would require the Pilbara to have been located relatively close to the trace of pole rotation. Only this position will result in apparent ca. 180° rotation, whereas if the Pilbara were located 90° away from the trace of pole rotation, the IITPW event would have been recorded as a large amount of (apparent) latitudinal shift. However, to prove that IITPW has occurred, or any form of TPW for that matter, it is essential to have data from at least two, but preferably much more parts of lithosphere that have moved independently of each other. If the apparent polar wander paths (APWP) reflect the same shift at the same time, it would effectively support (II)TPW.

The most reasonable option of the three mentioned above, is a ca. 180° rotation of the Pilbara block. Given enough time, large block rotations are not unlikely and the process is not controversial. A large excursion is not unthinkable, but it is difficult to explain why this process does not affect the inclination, and why the change in declination is so extensive. IITPW or a large amount of TPW is controversial and difficult to prove, so it is also not thought to be the most likely interpretation.

Palaeomagnetic groups

Strik et al. (2003) defined several palaeomagnetic groups of packages, based on statistical similarities of HT directions in the Nullagine Synclinorium. The MT component forms a separate group, which is interpreted as a younger magnetic overprint. This same grouping is also justified with our additional data, since some packages, e.g. Package 6 and Package 7, can still not be statistically distinguished from each other. The proposed groups of Strik et al. (2003) are therefore maintained (Tab. 2.3), with the addition of Package 0 as a separate group, and the MT component group will from now be called MT (instead of MT7-10, Strik et al., 2003), since a MT component was recognised in all packages, although

Group	N	dec°	inc°	min lat°	max lat°	av lat°	latp°	longp°	a95°
TPA	1	308.8	-9.3	0.0	10.6	4.7	-37.4	220.3	8.3
HP2	9	304.2	-18.1	6.9	11.8	9.3	-35.3	211.9	3.0
MT	47	310.1	-37.1	18.2	23.3	20.7	43.8	21.2	3.7
JV	5	n/a	n/a	n/a	n/a	n/a	-40.5	128.7	14.6
P8-10	21	158.0	53.7	29.9	39.1	34.2	-66.4	170.7	5.8
P4-7	25	157.7	66.2	42.6	55.3	48.6	-56.7	146.0	6.5
P2	8	311.1	-67.9	40.7	65.2	51.6	41.5	337.3	12.5
P1	32	130.7	68.3	49.0	54.1	51.5	-41.4	158.5	2.7
P0	28	304.6	72.0	49.8	65.0	57.0	-1.5	93.6	8.2
CD	9	145.0	71.0	38.7	78.1	55.4	-46.0	146.0	22.0
BR	16	115.0	72.0	48.3	67.0	57.0	-32.0	154.0	9.0
RB	*4 (12)*	320.0	-53.8	28.5	41.2	34.3	-52.4	178.0	6.5
MC	*1 (8)*	265.0	-65.1	40.8	54.4	47.1	-11.9	161.3	5.2

Table 2.3
Summary of grouped palaeolatitude and palaeopole positions from this study (Group name in bold) and from previously published data (Group name in normal print). Group definitions are given in the caption to Figure 2.8 and in the text. Site means contributing to each group mean are given in Tables 2.1 and 2.2 and each group is plotted in Figure 2.8. N = number of sites contributing to the grouped mean (site means given in Tables 2.1 and 2.2), N in italics = number of localities with number of sites between brackets, dec° = declination, inc° = inclination, min lat° = minimum palaeolatitude, max lat° = maximum palaeolatitude, min, max and ave lat° = minimum, maximum and average palaeolatitude respectively, latp = latitude of pole position, longp = longitude of pole position, a95 = confidence circle at the 95% level.

it could not be reliably determined in Packages 3, 4 and 5 mainly because of the limited number and low quality of data available for these packages. Based on high precision geochronology (Blake et al., 2004), time frames for the palaeomagnetic groups can be given. Summarising, the grouping is as follows:

P0 (> 2772 Ma ?): includes the Package 0 HT data from the Marble Bar Basin.

P1 (ca. 2772 Ma): includes all the Package 1 HT data of the East Pilbara and Marble Bar Basins.

P2 (ca. 2766 Ma): includes all Package 2 massive dacite porphyry HT data of the East Pilbara Basin.

P4-7 (from ca. 2752 Ma to ca. 2725 Ma): includes all Packages 4 to 7 HT data of the East Pilbara Basin.

P8-10 (from ca. 2718 Ma to ca. 2715 Ma): includes all Packages 8 to 10 HT data of the East Pilbara Basin.

MT (ca. 2.0 Ga?): includes MT data of Packages 1, 2 and 6 to 10 of the East Pilbara Basin.

The medium temperature (MT) component

Previously, Strik et al. (2003) reported that it was unlikely that regional scale burial metamorphism was the cause of the MT remagnetisation in the Nullagine Synclinorium. If this had been the case, the remagnetisation should have been developed in the whole sequence, and not only in Packages 7 to 10. This argument is no longer tenable, because the MT component is now seen in Packages 1, 2 and 6 as well. It is noted, however, that the MT overprint is only occasionally present in Package 1, not in Package 0 and also not in samples from the Package 2 massive dacite porphyry. Magnetic intensities of samples from Packages 0, 1 and 2 are commonly more than a factor 10 higher than magnetic intensities in the rest

of the Nullagine and Mount Jope Supersequences. At present, it is unclear whether or not this is related to the presence of a MT component.

Proterozoic aged magnetic overprints have been reported for late Archaean and early Proterozoic rocks of the Pilbara. There is some debate on to which process may have caused remagnetisation. For example, Schmidt and Embleton (1985) and, more recently, Sumita et al. (2001) argue that regional scale burial metamorphism has caused remagnetisation of the Early Proterozoic banded iron formations (BIF) of the Hamersley Province at ca. 2200 Ma. Li et al. (2000), however, describe two phases of Proterozoic remagnetisation, and argue that (1) the same remagnetisation as described by Schmidt and Embleton (1985) has probably been caused by thermal/chemical effects during the Ashburton Orogeny, at ca. 1700 Ma, an age which is based on fold test data. The other phase of remagnetisation (2) described by Li et al. (2000) may have been caused by thermal/chemical effects during the Ophthalmian Orogeny at ca. 2200 Ma. There is some doubt about the age of the folding related to the remagnetisation described in (2), however, because Li et al. (2000) mention the possibility that this remagnetisation is in fact younger than the ca. 1700 Ma remagnetisation of (1).

The MT component of this study clearly does not pass the conglomerate test (Fig. 2.7), confirming that the age of remagnetisation is younger than the formation of the Nullagine and Mount Jope Supersequences. All MT directions were determined without applying tectonic correction. In the Nullagine Synclinorium, tectonic correction was not applied because the bedding at the sampled locations is sub-horizontal. At site GSP68 in the Meentheena Centrocline, however, the bedding plunges 25° towards 070°. Without tectonic correction, the MT mean of GSP68 is 305.7°/-33.8°, which is similar to the MT mean of the Nullagine Synclinorium, whereas when tectonic correction is applied, the mean is 296.1°/-17.8°, which differs significantly from the MT mean of the Nullagine Synclinorium. Therefore, it seems plausible that the remagnetisation has been acquired after the tilting of the strata, which timing is essentially unknown, but is possibly related to rifting during the formation of the Mount Jope Supersequence (Blake, 2001).

The magnetic overprint direction recorded by the MT component, does not correspond to any of the two phases of remagnetisation reported by Li et al. (2000), so it cannot readily be correlated to the Ophthalmian or Ashburton Orogenies. The MT group plots approximately halfway between the P8-10 pole and the ca. 1700 Ma pole of the Hamersley BIFs (TPA and HP2, Fig. 2.9b, Li et al., 2000; Schmidt and Embleton, 1985). This may be an indication that the MT magnetisation is older than ca. 1700 Ma. Regional scale burial metamorphism cannot be fully excluded as an explanation for the MT remagnetisation. Remagnetisation due to thermal effects during orogenic activity also remains a possible cause of the MT remagnetisation. Recent $^{39}Ar/^{40}Ar$ dating in the Marble Bar Basin points out to a ca. 2.0 Ga heating event, which is most probably equivalent to the age of MT magnetisation.

Geomagnetic reversal and magnetostratigraphy

The study of Strik et al. (2003) revealed only one reversed polarity interval in the Nullagine and Mount Jope Supersequences in the Nullagine Synclinorium. The Package 2 massive dacite porphyry has a consistently reversed polarity with respect to Package 1 and Package 4 basalts; so a reversal (N-R) took place between 2772 ± 2 Ma and 2765 ± 4 Ma, and the field reversed back (R-N) between 2765 ± 4 Ma and 2741 ± 3 Ma. So, the duration of this reversed interval is ill constrained (0-30 Myr). The reversed polarity interval is confirmed by this study, because Package 2 also has a reversed polarity in both the North Oakover
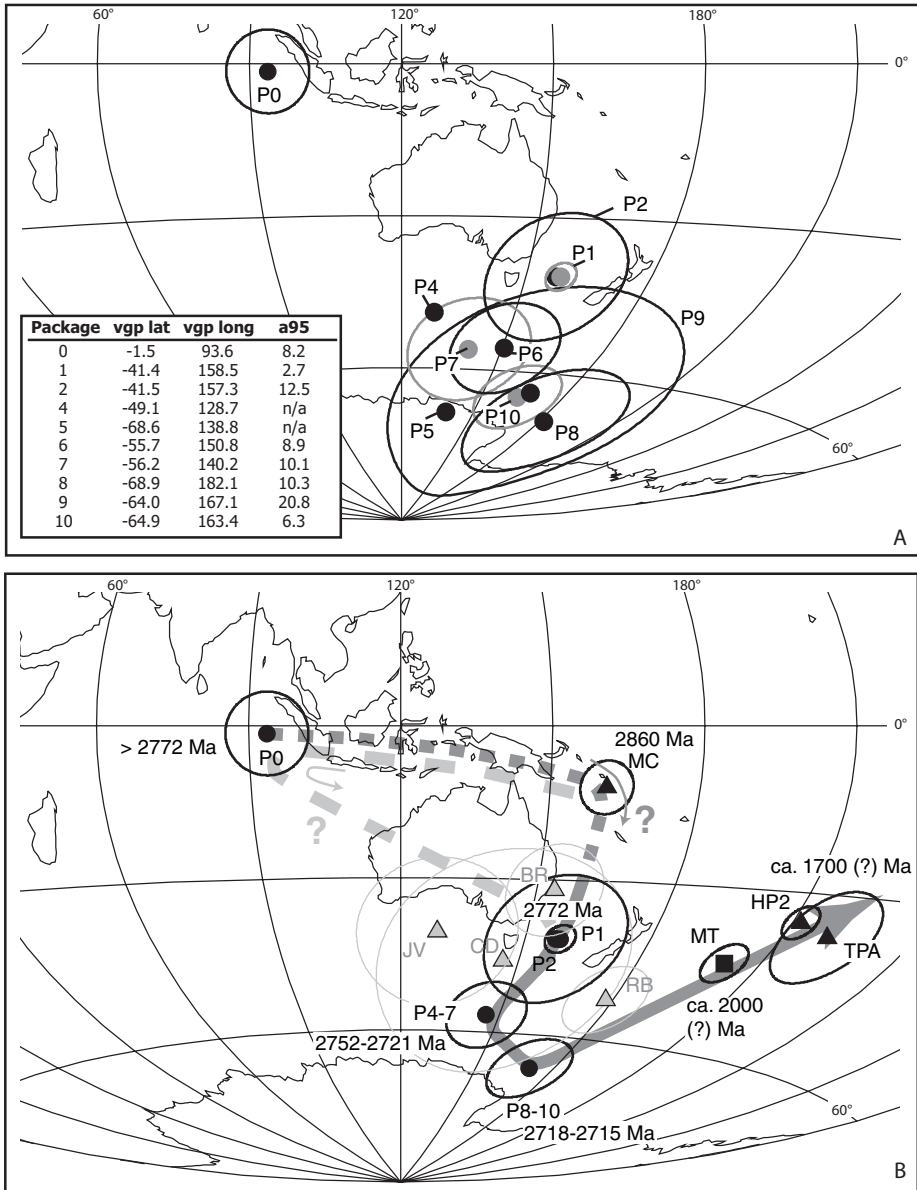
The table within figure A:

Package	vgp lat	vgp long	a95
0	-1.5	93.6	8.2
1	-41.4	158.5	2.7
2	-41.5	157.3	12.5
4	-49.1	128.7	n/a
5	-68.6	138.8	n/a
6	-55.7	150.8	8.9
7	-56.2	140.2	10.1
8	-68.9	182.1	10.3
9	-64.0	167.1	20.8
10	-64.9	163.4	6.3

Figure 2.9

a) Aitoff projection showing the HT pole positions of Packages 0 to 10 with a95 confidence limits. Poles of Packages 1, 7 and 10 are grey to enhance readability. Data in box.

b) Aitoff projection of the apparent polar wander path (APWP) for the Pilbara from ca. 2860 to ca. 1700 (?) Ma showing approximate pole ages. Dashed part of the APWP is speculative. APWP is based on this study and published data. Square symbols are poles not included in the APWP. Circular symbols are poles included in the APWP, of which the black filled circles are poles from this study. Poles included in the APWP are MC (Millindinna Complex, Schmidt and Embleton, 1985), P0 (Package 0 HT data), P1 (Package 1 HT data), P2 (Package 2 HT data), P4-7 (Packages 4 to 7 HT data), P8-10 (Packages 8 to 10 HT data), MT (medium temperature directions), TPA (Mt. Tom Price iron ore, Schmidt and Clark, 1994) and HP2 (Hamersley Province F3 pole, Li et al., 2000). Each package pole is a grouped mean of the mean site data (cf. Tab. 2.3). Poles not included in the path are BR (Black Range Dyke) and CD (Cajuput Dyke, Embleton, 1978), RB (Mount Roe Basalt) and JV (Mount Jope Volcanics, Schmidt and Embleton, 1985). There are two possible paths from P0 or MC to P1, because of the unknown age of P0.

Syncline and Meentheena Centrocline (cf. Fig. 2.6, f-h, see also Tab. 2.1). Further, this study revealed an additional reversed interval in Package 7 at ca. 2721 Ma (Fig. 2.6d, Tab. 2.1), which is probably of short duration since it is only found in one flow unit. The existence of such a short reversed interval makes it possible that other reversals have been missed, although it seems apparent, considering the large number of sampled locations, that the polarity of the Earth's magnetic field was dominantly normal in the interval from 2741 Ma or older to 2715 Ma or younger. So far, no reversals have been found between 2741 and 2721 Ma.

Apparent polar wander

The HT component data (Tab. 2.1) of all sampled sites were used to calculate virtual geomagnetic pole positions (VGP). This has been done for the mean of each site and subsequently mean VGP positions have been determined for each package (Fig. 2.9a). The poles from Package 0 to Package 10 follow a consistent path, although the poles of Packages 4, 5 and 9 are less accurately defined. The pole of Package 0 has a totally different position than those of Packages 1 to 10, because of the 173.9° declinational difference between the Package 0 and Package 1 means.

The VGPs of the site means were also used to calculate the mean VGP positions for the groups defined above. These are compared to previously published relevant pole positions for the Pilbara Craton (Tab. 2.3) and an APWP is plotted (Fig. 2.9b). The trend of the APWP shown by the individual package pole positions (Fig. 2.9a) is clearer when the division in palaeomagnetic groups is made. The groups have statistically different pole positions, with P2 having a reversed polarity. The pole for the Millindinna Complex (Schmidt & Embleton, 1985, MC in Figure 2.9b) was taken as the starting point of the APWP, as this is the closest known Pilbara Craton pole position for rocks older (2860 ± 20 Ma, Gulson and Korsch, 1983) than the Nullagine Supersequence. Significant apparent polar wander occurred between the formation of the Millindinna Complex and the extrusion of Package 10, caused by both rotation and latitudinal shift. The end point of our APWP is defined by the overprint directions from the BIFs of the Hamersley Province, which are estimated at ca. 1700 Ma (Li et al., 2000).

Palaeolatitude

Average palaeolatitudes and corresponding error have been calculated for all site means (Tabs. 2.1, 2.2) and have been plotted in Figure 2.10. The average palaeolatitude per palaeomagnetic group has been calculated from these data (cf. Tab. 2.3) and is indicated as well. The palaeolatitudes of groups P0, P1, P2 and P4-7 all plot within error, but the actual averages show a decrease in palaeolatitude from 57.0° at P0 to 48.6° at P4-7, a change of ca. 5 cm yr^{-1} during ca. 20 Myr.

A significant shift in palaeolatitude occurs between P4-7 and P8-10, an observation previously made by Strik et al. (2003) in the Nullagine Synclinorium. This shift is now confirmed for the East Pilbara Basin. The increased database results in a reduction of the shift across the Package 7/8 boundary from 27.2° (Strik et al., 2003) to 14.4°. The average age difference between Package 7 and Package 8 is 3 Myr, which gives a rate of shift of ca. 50 cm yr^{-1}. Taking into account the errors in age (from 0 to 10 Myr) and palaeolatitude determination (from 3.5°, which is the minimum palaeolatitude of P4-7 and the maximum of P8-10 to 36.3°, which is the maximum of P4-7 and the minimum of P8-10), the minimum velocity is ca. 4 cm yr^{-1} and the maximum is instantaneous movement, because the errors in
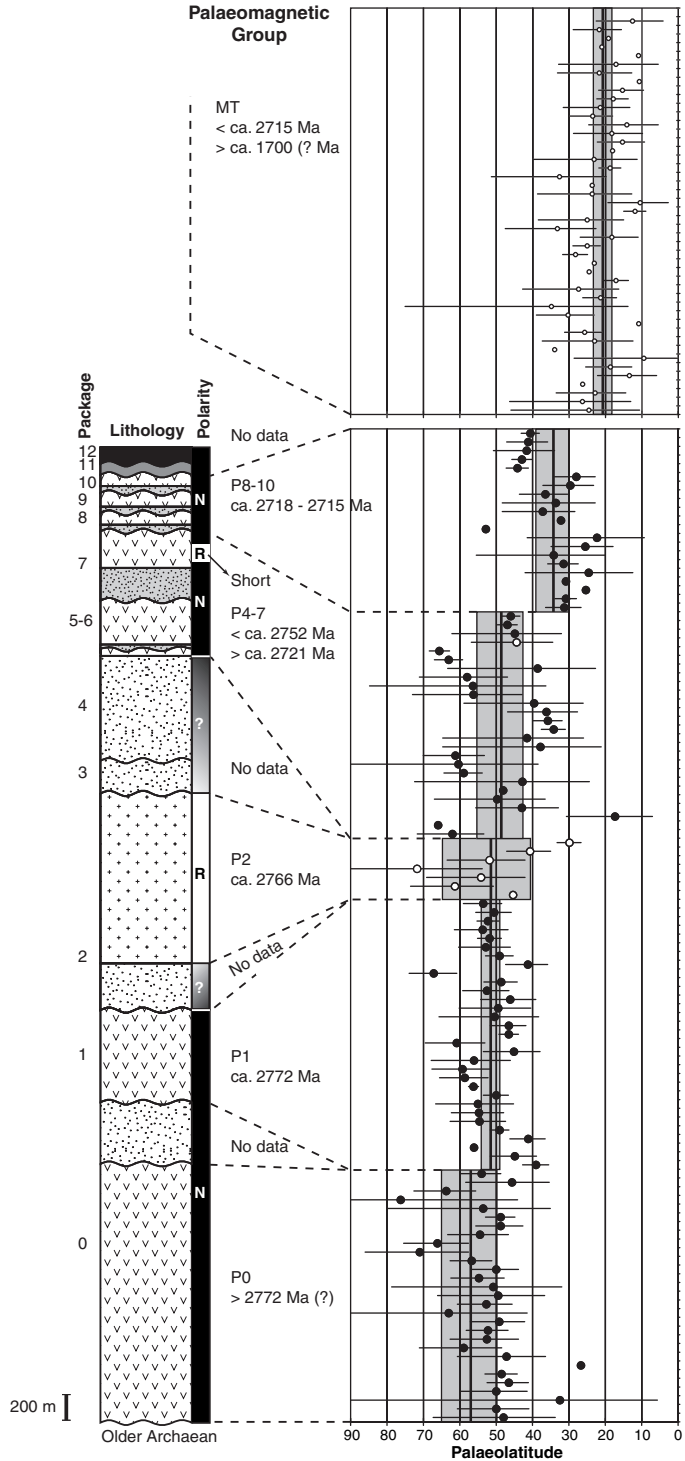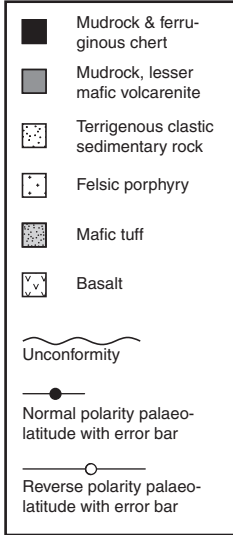
age overlap. These are all minimum estimates, because longitudinal movement is unconstrained.

The significance of a 14.4° shift of palaeolatitude within a relatively short geological time interval is not straightforward. Strik et al. (2003) propose three possible fundamentally different scenarios, which still apply with the inclusion of our new data, however, the direction for P0 puts a slightly different perspective on the proposed options. Option zero is that no geocentric axial dipole (GAD) was present in the late Archaean. This option implies that any palaeomagnetic direction from the late Archaean is meaningless. This option is not assumed.

Option 1. The occurrence of long-term multipole contributions. Nowadays, the axial dipole is dominant and it is thought that second-order contributions to the field average out over a sufficient time interval. This interval might be as long as several 100 kyr (e.g. Merrill et al., 1996), but not as long as millions of years. If this were not the case in the late Archaean, for instance a long-term contribution of an octupole field changing in amplitude/ contribution over the Package 7/8 boundary could explain the palaeolatitude shift. A change in octupole contribution from 0 to 15 % would cause the apparent palaeolatitude to change from 50° to 35°, while the real palaeolatitude remains 50° (cf. van der Voo and Torsvik, 2001). A shift of 15° would then be recorded without any actual continental movement taking place. If this is the case for the Pilbara at ca. 2718 Ma, the changed octupole contribution must have been maintained for at least 3 Myr, since low palaeolatitudes are recorded for Package 9 and 10 as well.

Long-term multipole contributions to the field are presently a topic of debate (cf. van der Voo and Torsvik, 2001), but cannot be excluded. Uranus and Neptune, for example, have a quadrupole contribution that is about equal to the dipole contribution (Stevenson, 2003). These planets have magnetic fields generated by a dynamo, although the mechanism that drives the dynamo is different than on Earth. Possibly, Earth did not have a solid inner core in the late Archaean. According to Labrosse et al. (2001), the inner core is probably not older than 1.0 ± 0.5 Ga and cannot exceed 2.5 Ga according to the model calculations. According to Bloxham (2000), a smaller inner core does not significantly change the behaviour of the magnetic field, but what happens when the inner core is absent is still unclear. So far, no indications exist that the absence of an inner core hampers a main-dipole field, although the mechanism that drives the geodynamo would be different than when an inner core is present. Therefore, a change in long-term octupole contribution to explain the shift in palaeolatitude is possible, but we cannot prove this with our current data.

Figure 2.10 (opposite)
Mean palaeolatitudes for the Nullagine and Mount Jope Supersequences in the East Pilbara Basin and mean palaeolatitudes for the Nullagine Supersequence in the Marble Bar Basin. The lower right column shows site mean HT (high temperature) palaeolatitudes (in degrees) linked to the stratigraphic column of the Nullagine Synclinorium for comparison. The upper right column shows site mean MT (medium temperature) palaeolatitudes with the site numbers in italics. An attempt was made to show HT and MT site means in strati-graphic order, although the exact position of the various areas with respect to each other is uncertain and have been placed on top of each other for convenience only. Site mean palaeolatitudes are represented by a circle with a horizontal bar representing the α95. Open (closed) symbols represent negative (positive) palaeolatitudes. Six groups of palaeolatitudes (five HT means, one MT mean) have been distinguished and their means are the means of their constituent sites (see Tab. 2.3). Groups are defined in the text and in the caption to Figure 2.9. Group means are given by thick black vertical lines and their α95 by the grey boxes. The six groups have been linked to the stratigraphic column of the Nullagine Synclinorium (for illustration purposes only) by dashed lines. N indicates normal polarity, R indicates reversed polarity. Package 0 has been added to the stratigraphic column of the Nullagine Synclinorium only for convenience and is not intended to be geologically meaningful.

Option 2. The shift in palaeolatitude is caused by true polar wander (TPW). Kirschvink et al. (1997) argue that a rapid plate reorganisation in the Cambrian between 523 and 508 Ma resulted in ca. 90° TPW (which they called inertial interchange TPW (IITPW)), which yields a minimum shift rate of 6° Myr^{-1} (67 cm yr^{-1}). Meert (1999), however, argues for actual plate movement in the Cambrian of 20 to 40 cm yr^{-1} combined with TPW, as a result of enhanced plate movement caused by lower mantle thermal anomalies. The 4.8° Myr^{-1} of latitudinal shift of our study is similar to the observed 6° Myr^{-1} for the Cambrian. Strik et al. (2003) argue that TPW is not a likely explanation for the observed shift in palaeolatitude. We observed a slow reversal rate, which, following the reasoning of Courtillot and Besse (1987), would mean that TPW is unlikely, since the authors argue that TPW comes to a standstill during periods of low reversal frequency. The Nullagine and Mount Jope Supersequences are interpreted as the rock record of continental break-up (Blake, 1993; Blake, 2001). According to Courtillot and Besse (1987), TPW also ceases during periods of continental break-up, although Meert (1999) argues that rapid plate movement driven by lower-mantle thermal anomalies might actually induce TPW. Therefore, it is not impossible that TPW has caused the shift across the Package 7/8 boundary, especially not if one is prepared to accept IITPW as an explanation for the discrepant pole position of P0, but it is controversial and cannot be proven.

Option 3. The 14.4° shift in palaeolatitude is the result of horizontal plate movement. Assuming an Earth with current radius, a 14.4° change in latitude across the Package 7/8 boundary resembles 1600 km of drift, with an average speed of ca. 50 cm yr^{-1}. The minimum speed, considering the errors of age and palaeolatitude determination, is ca. 4 cm yr^{-1}. The minimum is an acceptable Phanerozoic drift rate, but the average is extremely fast, even faster than drift rates proposed by Meert (1999) for the Cambrian.

The hypothesis of horizontal plate movement fits with the model of Blake and Barley (1992) and Blake (1993), who propose that the Nullagine and Mount Jope Supersequences resemble a two-stage record of continental rifting. Our data show mainly rotation during the development of the Nullagine Supersequence, which records the first stage of rifting. Rotation continued during the development of the successive Mount Jope Supersequence 1 (cf. Fig. 2.3), which records the beginning of the second stage. The second stage of rifting is supported by the palaeomagnetic data (Figs. 2.9, 2.10). Rapid horizontal movement took place between the extrusion of the Package 7 and Package 8 flood basalts. Packages 8 to 10 were formed within a 3 Myr interval and with the available palaeomagnetic data so far, it is not possible to point out any trends within this interval. It is conceivable, however, that movement continued during the formation of Packages 8 to 10. As noted by Strik et al. (2003), the amount of rifting is feasible in a Phanerozoic tectonic setting; however, the high speed of rifting has no equivalent in the Phanerozoic. If this option were correct, it has major implications for geodynamic models for late Archaean lithosphere.

As a final option, it is possible that a combination of the above options explains the rapid latitudinal shift. Especially rapid continental movement together with TPW is conceivable. However, since long term multipole contribution and (II)TPW are still controversial topics, we maintain a conservative approach. The observed palaeolatitude shift fits with the independently developed geotectonic model of Blake and Barley (1992) and Blake (1993) based on field observations, which makes a strong case for actual rapid horizontal motion of the Pilbara Craton in the late Archaean.

Conclusions

Our palaeomagnetic data confirm that the subdivision of the Nullagine and Mount Jope Supersequences into 12 unconformity bound packages in the Nullagine Synclinorium (Blake, 2001) can be expanded to other areas of the East Pilbara Basin, as suggested by Blake (2004). The correlation of the package subdivision to the Marble Bar Basin is also confirmed here, with the addition that the Marble Bar Basin's lower flood basalt sequence, here denoted Package 0, is older than any of the packages described in the Nullagine Synclinorium, which follows from our palaeomagnetic data. The deviating direction of Package 0 with respect to younger palaeomagnetic directions is not unequivocally explained. Large-scale (block) rotation is the favoured option, although a mechanism such as inertial interchange true polar wander may be a possible solution. Geomagnetic reversals have occurred during the formation of the Nullagine and Mount Jope Supersequence, but the reversal frequency seems to be low. We cannot exclude, however, that reversed intervals have been missed, especially in the sedimentary sequences. The APWP constructed by Strik et al. (2003) is confirmed and further refined. The palaeomagnetic data are in agreement with the two-stage rifting model proposed by Blake and Barley (1992) and Blake (1993). For the first stage, our data show rotation, but indications for rifting are unresolved. For the second stage, our data reveal a rapid change in palaeolatitude across the Package 7/8 boundary, which may resemble a phase of horizontal movement, with an average speed of ca. 50 cm yr^{-1}. Part of the change in latitude may be caused by true polar wander and/or a change in non-dipole contribution, but we conservatively assume that continental drift is the main cause of the observed change in pole position across the Package 7/8 boundary.

Acknowledgements

Chapter 3

Palaeomagnetism of the late Archaean Nullagine and Mount Jope Supersequences, Western Australia: evidence for block rotation and rapid continental drift of the Pilbara Craton

Palaeomagnetism of the late Archaean Nullagine and Mount Jope Supersequences, Western Australia: evidence for block rotation and rapid continental drift of the Pilbara Craton

Abstract

Recent palaeomagnetic studies of the circa 2775-2715 Ma Nullagine and Mount Jope Supersequences of the Australian Pilbara Craton have given new insight in geodynamic processes and the behaviour of the geomagnetic field in the late Archaean, highlighting fast horizontal drift and demonstrating the oldest known geomagnetic field reversal. Here, we discuss a palaeomagnetic study of the Nullagine and Mount Jope Supersequences in the West Pilbara Basin. Close to 500 oriented rock cores and hand specimens were taken, mainly from flood basalts. Stepwise progressive thermal demagnetisation revealed two ancient components of magnetisation, a medium and a high temperature component. The data confirm the oldest known geomagnetic field reversal that occurred between 2772 ± 2 Ma and 2765 ± 4 Ma. Further, the data show solid evidence for the second oldest reversal of the geomagnetic field at circa 2721 ± 4 Ma. Moreover, these data allowed a positive reversal test (classification B) and demonstrates that the high temperature component has preserved the original natural remanent magnetisation (NRM). Stratigraphic units of the Nullagine and Mount Jope Supersequences can now be palaeomagnetically correlated throughout the northern Pilbara. We develop a model for the tectonic evolution of the Pilbara between 2775 and 2715 Ma, integrating our palaeomagnetic data with a tectonic model based on field evidence. The model shows significant rotation of the Pilbara Craton between 2775 and 2721 Ma. Further, it shows rapid horizontal plate movement between 2721 and 2715 Ma.

Introduction

Recent palaeomagnetic studies of the Hamersley Province, Pilbara Craton, Australia (Fig. 3.1), have proven to be a powerful contribution to the understanding of geophysical and tectonic processes that were active during the development of the late Archaean (ca. 2772-2715 Ma) flood basalt dominated Nullagine and Mount Jope Supersequences (Strik et al., 2003, Strik, 2004). The palaeomagnetic studies have revealed late Archaean geomagnetic reversals; they have provided evidence for fast horizontal plate movement in the late Archaean; and have contributed to correlate stratigraphic units in the northeastern Pilbara. This paper presents a palaeomagnetic study of the northwestern Pilbara, and aims to construct a tectonic model for the evolution of the northern Pilbara by combining a tectonic model based on geological field evidence (Blake, 1993; Blake and Barley, 1992) with palaeomagnetic data. Further, the paper aims to test craton-wide correlations of packages within the Nullagine and Mount Jope Supersequences (Fig. 3.2, Blake, 2004) with palaeomagnetic data from the northwestern Pilbara.

The stratigraphic framework for the Nullagine and Mount Jope Supersequences is subdivided into 12 unconformity bound packages in the Nullagine Synclinorium (Fig. 3.1, Blake, 1993; Blake, 2001), where the succession appears to be most complete (Blake, 2001) and many packages are dated with high-precision geochronology (Fig. 3.3, Blake et al., 2004). This subdivision prompted a detailed palaeomagnetic study of the Nullagine
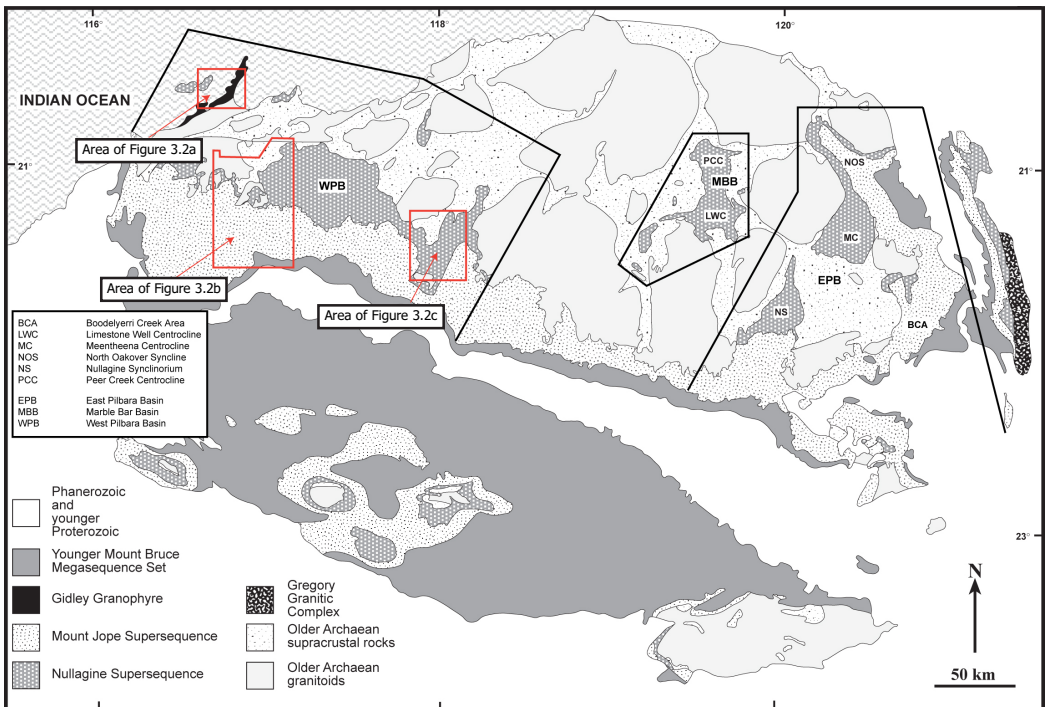
Figure 3.1
Simplified geological map of the Pilbara (Blake, 2001), showing the locations of East Pilbara Basin, the Marble Bar Basin, the Nullagine Synclinorium, the West Pilbara Basin and the approximate location of Figure 3.2. MBB = Marble Bar Basin, EPB = East Pilbara Basin, NS = Nullagine Synclinorium, WPB = West Pilbara Basin. The Hamersley Province comprises most of the southwestern half of the map.
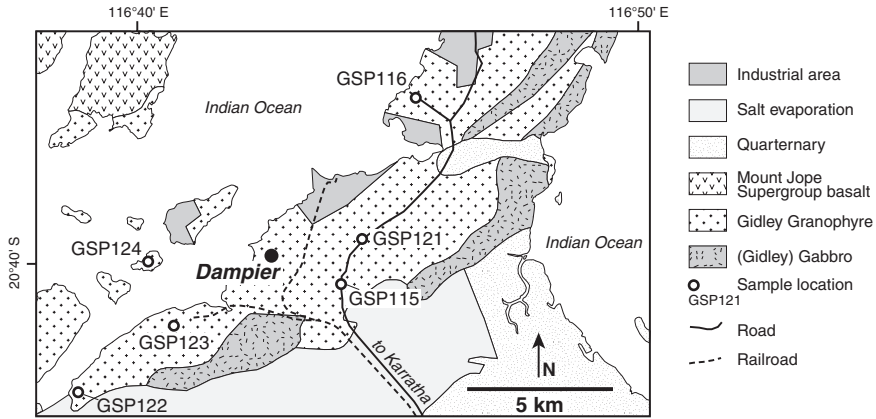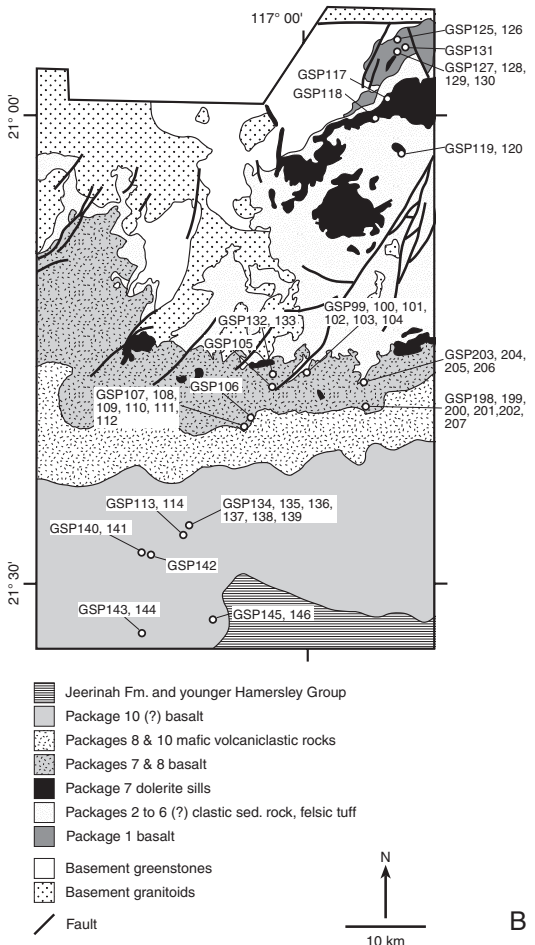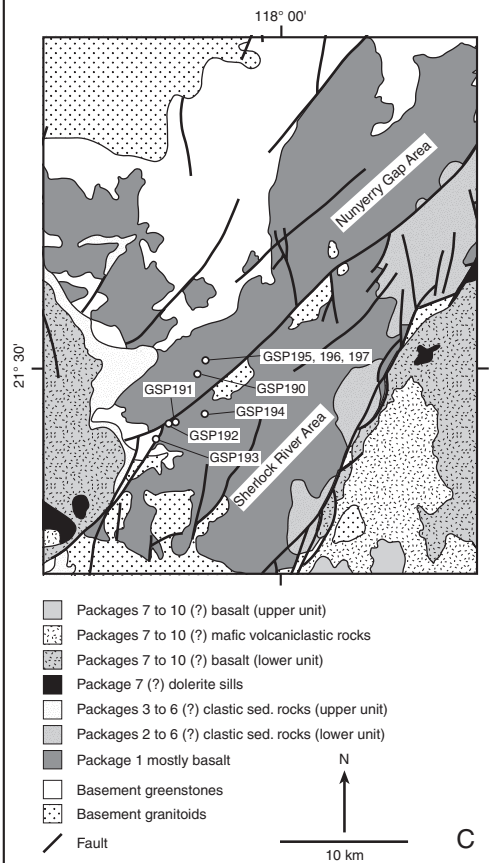
Figure 3.2
Summary geological maps of sample areas in the West Pilbara Basin showing dominant lithologies and sample locations (see Tab. 3.1). A) Sample locations of the Gidley Granophyre in the Dampier Area (geology after Hickman, 1997). B) Sample locations in the Harding River Area (geology after Blake, 2004). C) Sample locations in the Nunyerri Gap and Sherlock River Areas (geology after Blake, 2004).

Synclinorium (Strik et al., 2003), and serves as a basic framework for (palaeomagnetic) correlation of the package subdivision outside the Nullagine Synclinorium.

The stratigraphy of the Nullagine and Mount Jope Supersequences is not straightforward. During formation of the succession active tectonics were taking place. The succession was not deposited in a single basin, as was once supposed (e.g. Trendall, 1968; Trendall, 1983). Instead, it was formed in multiple depositional systems (e.g. Blake and Barley, 1992; Tyler and Thorne, 1990), complicating the correlation of individual packages of the Nullagine and Mount Jope Supersequences throughout the Hamersley Province. Three main basins have been identified in the northern Pilbara (Blake, 1984a; Blake, 1984b), namely the East Pilbara Basin (EPB), the Marble Bar Basin (MBB) and the West Pilbara Basin (WPB). Subsequently, a framework to correlate the packages defined in the Nullagine Synclinorium (EPB) to other parts of the northern Pilbara has been developed (Blake, 2004). Correlation gets increasingly complicated towards the west. So far, the EPB and MBB are successfully correlated to the succession of the Nullagine Synclinorium (Blake, 2004; Strik, 2004). Here, we will integrate the palaeomagnetic results for the WPB with the earlier established sequences.

Stratigraphy, methods and sampling

The WPB stratigraphy differs from the stratigraphic framework of the Nullagine Synclinorium, because a number of flood basalt dominated packages are missing, or are sediment dominated instead (Figs 3.2, 3.3). There are no flood basalts in (possible) Packages 4 to 6, and further, Package 9 is absent (Fig. 3.3). The Package 2 porphyry present in the EPB is not present in the WPB, and the Gidley Granophyre and the Cooya Pooya dolerite sills, possible equivalents to Package 7, are only present in the WPB. Finally, the WPB possibly contains flood basalts of Package 11, and these are not present in the EPB either.

For this study, 456 oriented rock core samples were taken from WPB Packages 1, 7, 8, 10 and a possible Package 11, mostly from natural exposure (Figs. 3.2, 3.3). Occasionally (rail) road cuts were sampled. The rock core samples are taken from Packages 1, 7, 8, 10 and 11 flood basalts, Package 7 mafic sills and Package 10 komatiites and mafic tuff. Further, 38 hand specimens were taken from the Gidley Granophyre and the Cooya Pooya dolerite sills, at road cuts and quarries.
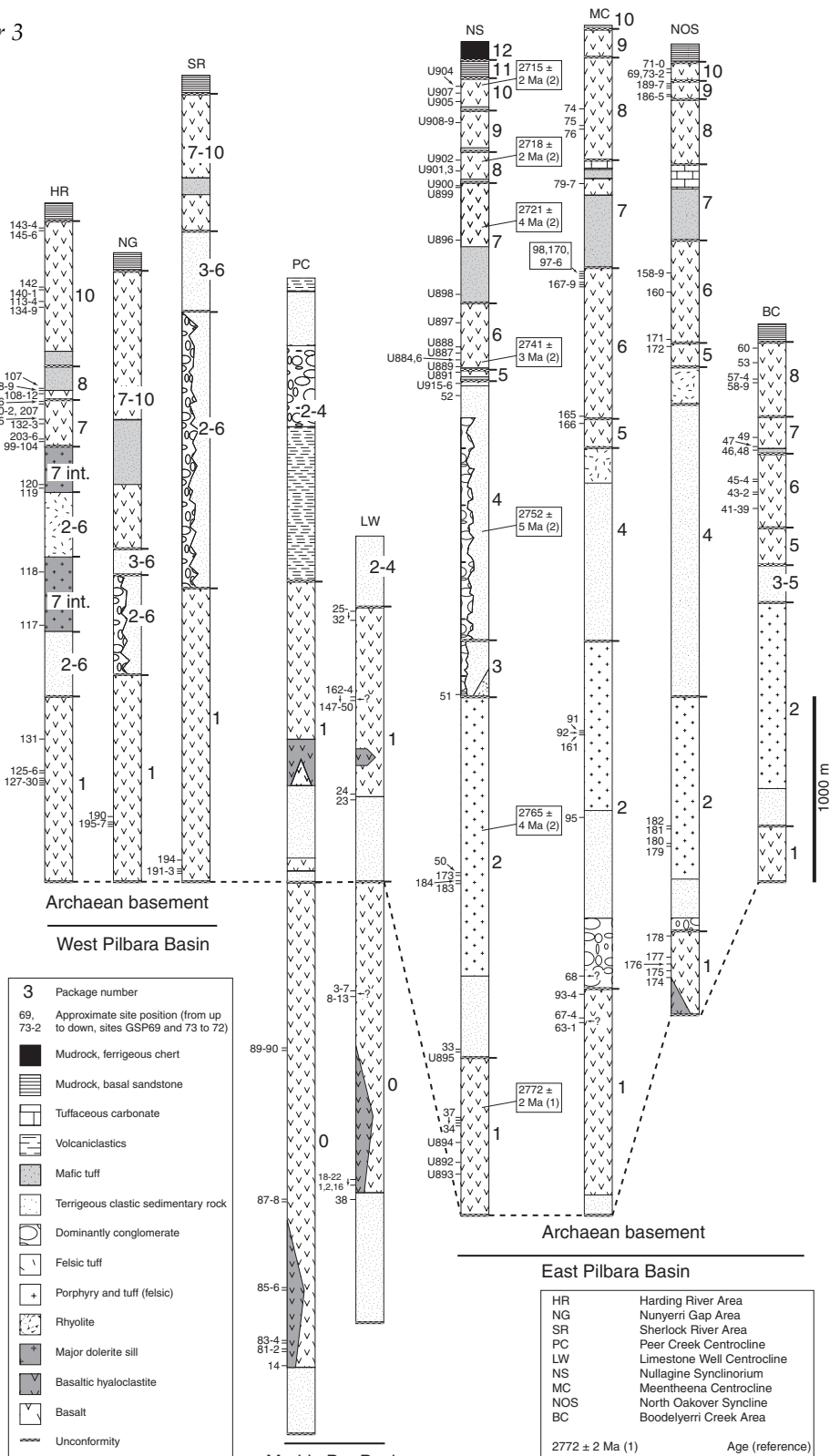
In the laboratory, the hand specimens were cored and all cores were cut to standard specimens of 22 mm length. One specimen of each core was thermally demagnetised in a magnetically shielded, laboratory-built furnace. The NRM was measured on a 2G Enterprises DC-SQUID cryogenic magnetometer.

NRM directions were analysed and interpreted with Zijderveld diagrams (Zijderveld, 1967). Principal component analysis (Kirschvink, 1980) was used to determine the directions of the various NRM components. No directions with a maximum angular deviation (MAD) greater than 10° were used.

Results

Thermal demagnetisation

The sampled rocks of the West Pilbara Basin (WPB) reveal up to three components of remanent magnetisation. Firstly, a present day field component has been recorded in all sampled flood basalt packages and intrusives. It is generally removed after heating at 350 °C. Secondly, a medium temperature (MT) component that generally unblocks between 350 and 480 °C can be isolated from 28 out of 66 sites. The MT component is present in all

West Pilbara Basin

Marble Bar Basin

East Pilbara Basin

3	Package number
69, 73-2	Approximate site position (from up to down, sites GSP69 and 73 to 72)
	Mudrock, ferrigeous chert
	Mudrock, basal sandstone
	Tuffaceous carbonate
	Volcaniclastics
	Mafic tuff
	Terrigeous clastic sedimentary rock
	Dominantly conglomerate
	Felsic tuff
	Porphyry and tuff (felsic)
	Rhyolite
	Major dolerite sill
	Basaltic hyaloclastite
	Basalt
	Unconformity

HR	Harding River Area
NG	Nunyerri Gap Area
SR	Sherlock River Area
PC	Peer Creek Centrocline
LW	Limestone Well Centrocline
NS	Nullagine Synclinorium
MC	Meentheena Centrocline
NOS	North Oakover Syncline
BC	Boodelyerri Creek Area
2772 ± 2 Ma (1)	Age (reference)

sampled units. Finally, a high temperature (HT) component has been recorded in all sampled units. It generally starts unblocking at 480 °C, and occasionally at lower temperatures, depending on the contribution of the LT and MT overprints. At 580 °C, almost all samples are completely demagnetised, which indicates that magnetite is the most probable carrier of NRM.

Below, the results per sampled package/unit are discussed from old to young. Site statistics of the HT component are summarised in Table 3.1, and of the MT component in Table 3.2; Figure 3.4 shows characteristic Zijderveld diagrams for the studied rocks, and Figure 3.5 shows the mean site direction per package.

Flood basalts of Package 1 were sampled in the Harding River Area (Fig. 3.2b) and in the Nunyerri Gap and Sherlock River Areas (Fig. 3.2c) of the WPB. All sites in the Harding River Area show consistent MT and HT directions (Tabs. 3.1, 3.2, Fig. 3.5), although the uppermost sample site (GSP131) shows reversed HT directions (Fig. 3.5). Five out of eight Nunyerri Gap and Sherlock River sites reveal a clear MT component, although the number of accepted samples per site varies (Tab. 3.2). For four Nunyerri Gap sites HT directions can be isolated, but site means vary significantly (Fig. 3.5; Tab. 3.1). None of the Sherlock River sites reveal HT directions. Contrary to the usual temperature interval of 350° to 480°C in which the MT component is developed in the EPB, the WPB Package 1 MT component can usually be isolated between 100 to 400°C (Fig. 3.4l, m). Since there is often a present day field overprint, which is removed in at least part of this temperature interval, it cannot be excluded that the directions of the MT component are influenced by this overprint.

Flood basalts of Package 7 were sampled in the Harding River Area, as well as Package 7 related mafic sills (Cooya Pooya Dolerite, see Fig. 3.2 and Tab. 3.1 for sample codes). Further, Package 7 related felsic volcanics (Gidley Granophyre) were sampled in the Dampier Area (Fig. 3.2a). From the 18 sampled basalt flows, only 7 revealed HT directions (Tab. 3.1) and similar results were obtained for the MT directions (Tab. 3.2). Many Zijderveld diagrams are chaotic, without clearly defined vectors, although some show consistent demagnetisation behaviour (Fig. 3.4g). The Gidley Granophyre specimens hardly reveal any consistent MT and HT directions (Tabs. 3.1, 3.2), although occasionally reliable HT directions can be interpreted (Fig. 3.4h). Better results were obtained for the Cooya Pooya Dolerite. A consistent HT component can be interpreted for all sampled sites (Tab. 3.1). The MT component is poorly developed (Tab. 3.2) and most Zijderveld plots show a single component (Fig. 3.4j, k). The Cooya Pooya Dolerite consists of a lower and an upper intrusion, and will from hereon be referred to as lower and upper sill. The upper sill has similar HT directions as the Package 7 flood basalts, whereas the lower sill has directions that are reversed and antipodal (Fig. 3.5; Tab. 3.1). The mean direction from the flood basalts does not significantly vary from the mean direction of the intrusions (Fig. 3.5; Tab. 3.1) and are therefore averaged to calculate a single Package 7 pole position.

Flood basalts of Package 8 were sampled in the Harding River Area. Most sites have a consistent HT component (Tab. 3.1). The MT direction can occasionally be isolated (Fig. 3.5, Tab. 3.2), but generally there is significant overlap of this component with the present

Figure 3.3 (opposite)
Summary stratigraphic columns (cumulative maximum stratigraphic thickness) of the Nullagine and Mount Jope Supersequences in the Harding River, Nunyerri Gap and Sherlock River Areas, as well as previously sampled locations (after Blake 2004), with the approximate stratigraphic positions of the palaeomagnetic sample sites. The Nullagine Supersequence comprises Packages 1 to 6 and The Mount Jope Supersequence comprises Packages 7 to 11. Age references: (1) Pb-Pb baddeleyite, Wingate, 1999, (2) U-Pb SHRIMP Blake et al., 2004.

Area	Package	Site Number	Lithology	AMG coordinates (AGD 84)	Strike/dip	N	n	dec°	inc°	k	a95°	R	Plat°	VGP lat°	VGP long°
HR	11 (?)	GSP143	basalt	50K 479675 - 7615872	315/08 NE	9	9	137.4	77.7	75.4	6.0	8.894	66.4	-37.6	136.8
HR	11 (?)	GSP144	basalt	50K 479982 - 7615433	315/08 NE	9	3	159.1	58.8	30.8	22.6	2.935	39.5	-64.7	156.8
	mean 11 (?)					**2**	**2**	**152.8**	**68.5**	**n/a**	**n/a**	**1.969**	**51.8**	**-51.5**	**143.8**
HR	10	GSP145	basalt	50K 488249 - 7617328	subhor.	10	0	n/a	n/a	n/a	n/a	n/a	n/a	n/a	n/a
HR	10	GSP146	basalt	50K 488380 - 7617475	subhor.	7	0	n/a	n/a	n/a	n/a	n/a	n/a	n/a	n/a
HR	10	GSP142	basalt	50K 480974 - 7625127	315/08 NE	7	3	164.7	75.1	33.6	21.6	2.941	62.0	-48.2	127.5
HR	10	GSP141	basalt	50K 479917 - 7625403	315/08 NE	7	2	154.1	62.0	n/a	n/a	1.982	43.2	-59.4	155.5
HR	10	GSP140	basalt	50K 479857 - 7625447	315/08 NE	7	5	136.5	54.6	76.6	8.8	4.948	35.1	-49.7	177.3
HR	10	GSP114	basalt	50K 484972 - 7627529	subhor.	8	0	n/a	n/a	n/a	n/a	n/a	n/a	n/a	n/a
HR	10	GSP113	basalt	50K 484997 - 7627609	subhor.	9	1	166.3	57.5	n/a	n/a	n/a	38.1	-69.6	149.1
HR	10	GSP134	basalt	50K 485815 - 7628033	subhor.	8	2	150.0	72.9	n/a	n/a	1.998	58.4	-47.2	139.5
HR	10	GSP136	basalt	50K 485681 - 7628599	315/08 NE	7	2	128.9	39.7	n/a	n/a	1.944	22.5	-42.8	195.5
HR	10	GSP135	basalt	50K 485559 - 7629046	315/08 NE	8	1	129.8	46.1	n/a	n/a	n/a	27.5	-44.2	188.9
HR	10	GSP139	komatiite	50K 485534 - 7629176	315/08 NE	8	1	123.2	51.3	n/a	n/a	n/a	32.0	-38.8	182.4
HR	10	GSP138	komatiite	50K 485583 - 7629388	315/08 NE	7	0	n/a	n/a	n/a	n/a	n/a	n/a	n/a	n/a
HR	10	GSP137	komatiite	50K 485603 - 7629457	315/08 NE	8	0	n/a	n/a	n/a	n/a	n/a	n/a	n/a	n/a
HR	10	GSP107	mafic tuff	50K 492312 - 7640449	subhor.	6	0	n/a	n/a	n/a	n/a	n/a	n/a	n/a	n/a
	mean 10					**14**	**8**	**140.3**	**58.3**	**29.1**	**10.4**	**7.754**	**39.0**	**-52.4**	**166.9**
HR	8	GSP198	basalt	50K 507262 - 7642578	085/5.8 S	6	0	n/a	n/a	n/a	n/a	n/a	n/a	n/a	n/a
HR	8	GSP199	basalt	50K 507371 - 7642673	085/5.8 S	7	4	119.8	41.1	78.8	10.4	3.962	23.6	-34.7	192.5
HR	8	GSP108	basalt	50K 492325 - 7640458	319/11 NE	7	5	139.5	44.9	137.9	6.5	4.971	26.5	-52.8	190.8
HR	8	GSP109	basalt	50K 492380 - 7640500*	319/11 NE	3	3	146.2	44.9	180.0	9.2	2.989	26.5	-58.8	190.7
HR	8	GSP110	basalt	50K 492418 - 7640563	319/11 NE	8	5	141.6	46.8	25.5	15.4	4.843	28.0	-54.6	188.2
HR	8	GSP111	basalt	50K 492461 - 7640589	319/11 NE	5	4	122.6	43.3	97.2	9.4	3.969	25.2	-37.5	190.9
HR	8	GSP112	basalt	50K 492464 - 7640592	319/11 NE	5	4	108.6	38.8	156.4	7.4	3.981	21.9	-24.3	191.7
	mean 8					**7**	**6**	**129.2**	**44.1**	**52.4**	**9.3**	**5.905**	**25.9**	**-43.8**	**191.0**
HR	7	GSP106	basalt	50K 493185 - 7641598	subhor.	10	0	n/a	n/a	n/a	n/a	n/a	n/a	n/a	n/a
HR	7	GSP105	basalt	50K 495805 - 7645380	subhor.	10	8	195.5	47.9	449.2	2.6	7.984	29.0	-74.0	58.8
HR	7	GSP132	basalt	50K 495995 - 7646990	300/5.5 NE	13	6	148.7	68.7	100.7	6.7	5.950	52.1	-50.9	147.4
HR	7	GSP133	basalt	50K 496123 - 7646601	300/5.5 NE	8	0	n/a	n/a	n/a	n/a	n/a	n/a	n/a	n/a
HR	7	GSP101	basalt	50K 500547 - 7646430	subhor.	8	0	n/a	n/a	n/a	n/a	n/a	n/a	n/a	n/a
HR	7	GSP100	basalt	50K 500550 - 7646454	subhor.	7	7	164.9	70.0	105.4	5.9	6.943	53.9	-55.4	132.7
HR	7	GSP99	basalt	50K 500508 - 7646602	subhor.	10	2	145.1	74.1	n/a	n/a	1.937	60.3	-43.9	140.2
HR	7	GSP102	basalt	50K 500120 - 7646900*	subhor.	7	0	n/a	n/a	n/a	n/a	n/a	n/a	n/a	n/a
HR	7	GSP103	basalt	50K 499958 - 7647370	subhor.	7	0	n/a	n/a	n/a	n/a	n/a	n/a	n/a	n/a
HR	7	GSP104	basalt	50K 499769 - 7647607	subhor.	10	0	n/a	n/a	n/a	n/a	n/a	n/a	n/a	n/a
HR	7	GSP201	basalt	50K 507635 - 7642727	085.8/5.8 S	7	0	n/a	n/a	n/a	n/a	n/a	n/a	n/a	n/a
HR	7	GSP202	basalt	50K 507686 - 7642759	085.8/5.8 S	8	0	n/a	n/a	n/a	n/a	n/a	n/a	n/a	n/a
HR	7	GSP200	basalt	50K 507409 - 7643184	085.8/5.8 S	7	0	n/a	n/a	n/a	n/a	n/a	n/a	n/a	n/a
HR	7	GSP207	basalt	50K 506962 - 7643331	085.8/5.8 S	7	3	149.4	38.3	62.2	15.8	2.968	21.5	-61.6	200.9
HR	7	GSP206	basalt	50K 507398 - 7645186	085.8/5.8 S	7	7	149.8	58.1	58.1	8.0	6.897	38.8	-58.8	166.2
HR	7	GSP203	basalt	50K 507047 - 7645839	085.8/5.8 S	7	0	n/a	n/a	n/a	n/a	n/a	n/a	n/a	n/a
HR	7	GSP204	basalt	50K 506798 - 7645970	085.8/5.8 S	8	0	n/a	n/a	n/a	n/a	n/a	n/a	n/a	n/a
HR	7	GSP205	basalt	50K 506601 - 7645979	085.8/5.8 S	7	5	162.1	68.9	123.4	6.9	4.986	52.3	-56.0	136.7
	mean 7		**basalt**			**18**	**7**	**160.9**	**62.1**	**25.0**	**12.3**	**6.760**	**43.4**	**-61.0**	**146.3**
HR	7	GSP120	mafic sill	50K 512041 - 7673398	320/02 NE	7	7	166.8	72.4	131.4	5.3	6.954	57.6	-52.2	128.6
HR	7	GSP119	mafic sill	50K 511788 - 7673204	320/02 NE	6	6	175.6	64.7	81.8	7.5	5.939	46.6	-64.2	124.1
HR	7	GSP118	mafic sill	50K 508878 - 7677632	subhor.	13	10	346.7	-65.8	70.3	5.8	9.872	48.0	60.9	315.5
HR	7	GSP117	mafic sill	50K 510344 - 7679863	subhor.	8	5	320.6	-68.4	86.3	8.3	4.954	51.6	46.8	332.2
DA	7	GSP115[*]	granophyre	50K 471925 - 7713746	230/14 NW	7	1	357.8	-44.2	n/a	n/a	n/a	25.9	84.4	317.4
DA	7	GSP116[*]	granophyre	50K 474493 - 7720083	230/14 NW	4	1	124.2	52.1	n/a	n/a	n/a	32.7	-39.3	180.8
DA	7	GSP121	granophyre	50K 472641 - 7715258	230/14 NW	4	1	167.7	68.8	n/a	n/a	n/a	52.2	-57.0	130.6
DA	7	GSP122	granophyre	50K 462839 - 7710006	230/14 NW	5	0	n/a	n/a	n/a	n/a	n/a	n/a	n/a	n/a
DA	7	GSP123	granophyre	50K 466146 - 7712257	230/14 NW	5	0	n/a	n/a	n/a	n/a	n/a	n/a	n/a	n/a
DA	7	GSP124	granophyre	50K 465278 - 7714459	230/14 NW	5	0	n/a	n/a	n/a	n/a	n/a	n/a	n/a	n/a
	mean 7		**intrusive**			**10**	**5**	**163.9**	**68.5**	**195.6**	**5.5**	**4.980**	**51.8**	**-56.6**	**135.3**
	MEAN 7		**all**			**28**	**12**	**162.0**	**64.8**	**39.5**	**7.0**	**11.722**	**46.7**	**-59.3**	**141.3**

Table 3.1
See next page for explanation.

Area	Package	Site Number	Lithology	AMG coordinates (AGD 84)	Strike/dip	N	n	dec°	inc°	k	a95°	R	Plat°	VGP lat°	VGP long°
HR	1	GSP131	basalt	50K 512567 - 7686094	320/20 NE	8	7	271.0	-58.4	34.4	10.4	6.825	39.1	13.8	350.1
HR	1	GSP126	basalt	50K 511651 - 7686984	320/20 NE	8	7	90.3	60.9	437.7	2.9	6.986	41.9	-14.0	167.2
HR	1	GSP125	basalt	50K 511632 - 7686995	320/20 NE	7	4	117.3	57.3	163.1	7.1	3.982	37.9	-33.9	174.7
HR	1	GSP129	basalt	50K 511865 - 7685658	320/20 NE	7	4	135.9	69.4	24.2	19.1	3.876	53.1	-43.5	152.3
HR	1	GSP127	basalt	50K 511623 - 7685943	320/20 NE	7	5	90.0	67.1	35.2	13.1	4.886	49.8	-15.8	159.2
HR	1	GSP128	basalt	50K 511741 - 7685642	320/20 NE	9	8	113.6	56.9	52.9	7.7	7.868	37.5	-30.9	175.1
HR	1	GSP130	basalt	50K 511614 - 7685457	320/20 NE	8	4	115.0	70.1	51.8	12.9	3.942	54.1	-31.4	155.6
NG	1	GSP196	basalt	50K 597712 - 7622787	010/10 E	7	7	189.2	78.7	594.6	2.5	6.990	68.2	-42.9	113.3
NG	1	GSP197	basalt	50K 597687 - 7622875	010/10 E	7	5	181.2	64	16.6	19.3	4.759	45.7	-65.8	115.9
NG	1	GSP195	basalt	50K 597351 - 7622822	010/10 E	7	2	155.3	59.7	n/a	n/a	1.976	40.6	-61.7	160.0
NG	1	GSP190	basalt	50K 596927 - 7621919	010/10 E	8	5	119.2	54.8	41.4	12.0	4.903	35.3	-35.6	179.1
SR	1	GSP194	basalt	50K 597248 - 7619073	360/12 E	8	0	n/a	n/a	n/a	n/a	n/a	n/a	n/a	n/a
SR	1	GSP191	basalt	50K 595115 - 7618495	180/2.5 W	7	0	n/a	n/a	n/a	n/a	n/a	n/a	n/a	n/a
SR	1	GSP192	basalt	50K 594789 - 7618467	180/2.5 W	7	0	n/a	n/a	n/a	n/a	n/a	n/a	n/a	n/a
SR	1	GSP193	basalt	50K 593575 - 7617435	360/12 E	7	0	n/a	n/a	n/a	n/a	n/a	n/a	n/a	n/a
	mean 1					**15**	**11**	**121.9**	**66.5**	**28.3**	**8.7**	**10.647**	**49.0**	**-36.9**	**160.0**

Table 3.1(continued)
Summary of HT (high temperature) results from the West Pilbara Basin. Results per area are in stratigraphic order where possible. The results of the various areas are placed above each other for convenience only, exact correlations are uncertain. Bold type set show means. Abbreviations: AMG = Australian Map Grid, N = number of specimens from each site and number of sites contributing to the mean, n = number of specimens accepted and the number of specimens contributing to the mean, dec = declination, inc = inclination, Plat = palaeolatitude, VGP lat (long) = latitude (longitude) of VGP (virtual geomagnetic pole), n/a = not applicable, WPB = West Pilbara Basin, NG = Nunyerri Gap Area and SR = Sherlock River Area. Site codes with asterisk are used if the HT directions have not been used for the calculation of the mean. AMG coordinates with asterisk are estimated positions from the topographic map. See also Figure 3.2 for sample locations.

day field component (Fig. 3.4f), or with the HT component (Fig. 3.4e), or both. The inclination of the HT component is fairly constant, although the declination is more variable (Fig. 3.5; Tab. 3.1) and shows somewhat of a girdle, possibly caused by partial overprint of the MT direction.

Flood basalts, komatiites and mafic tuff of Package 10 were sampled in the Harding River Area. The overall results for this package are disappointing, and many site means are based on only a few accepted directions, both for the MT and HT components (Tabs. 3.1, 3.2). Zijderveld diagrams are either chaotic or show unblocking at lower temperatures (Fig. 3.4d). However, some specimens have a stable HT component (Fig. 3.4c), and the site means are fairly consistent (Fig. 3.5). As for Package 8, MT directions could only occasionally be isolated (Fig. 3.5) and there may be overlap with the present day field and HT directions.

Two flood basalt flows from Package 11 (?) were sampled in the Harding River Area. Alternatively, these flows may represent the top of Package 10. A HT component is present in most samples (Tab. 3.1, Fig. 3.4a, b), but specimens appear to alter at high temperatures, causing spurious directions and often impeding a straight decay towards the origin (Fig. 3.4b). The MT component has too much overlap with the present day field and HT directions and cannot confidently be derived (Tab. 3.2, Fig. 3.4a, b).

Reversal test
The apparent antipodal directions between the Package 7 lower and upper sills allow a reversal test. The individual HT directions rather than the site means were grouped to ensure a statistically relevant result. The lower sill comprises 15 south-up directions and the upper sill 13 north-down directions with similar statistical values (Fig. 3.6). The angle between the normal and the reversed polarity set is 5.2°, and the critical angle is 6.8°, which is a positive reversal test with classification B. This implies that the primary NRM of Package 7 is still preserved. The positive Package 7 reversal test in the WPB is the first robust field

Area	Package	Site Number	N	n	dec°	inc°	k	a95°	R	Plat°	VGP lat°	VGP long°
	mean 11 (?)		**2**	**0**	**n/a**	**n/a**	**n/a**	**n/a**	**n/a**	**n/a**	**n/a**	**n/a**
HR	10	GSP114	8	1	332.8	-23.4	n/a	n/a	n/a	12.2	62.4	42.0
HR	10	GSP137	8	4	314.5	-45.0	15.1	24.4	3.8	26.6	48.3	10.5
	mean 10		**14**	**2**	**324.8**	**-34.5**	**n/a**	**n/a**	**1.948**	**19.0**	**56.3**	**23.4**
HR	8	GSP199	7	2	305.3	-24.8	n/a	n/a	1.992	13.0	37.3	26.7
HR	8	GSP110	8	1	344.5	-29.5	n/a	n/a	n/a	15.8	74.3	45.0
	mean 8		**7**	**2**	**324.5**	**-28.6**	**n/a**	**n/a**	**1.907**	**15.2**	**56.1**	**31.3**
HR	7	GSP106	10	2	325.9	-19.7	n/a	n/a	1.961	10.1	55.4	40.4
HR	7	GSP201	7	3	330.4	-32.7	15.6	32.3	2.872	17.8	61.9	29.0
HR	7	GSP202	8	3	330.0	-25.5	19.8	28.4	2.899	13.4	60.4	37.6
HR	7	GSP200	7	4	334.0	-44.1	52.3	12.8	3.943	25.9	65.8	11.2
HR	7	GSP206	7	2	331.6	-32.2	n/a	n/a	1.997	17.5	63.0	30.2
	mean 7 basalts		**18**	**5**	**330.2**	**-30.9**	**73.4**	**9.0**	**4.945**	**16.7**	**61.7**	**30.7**
HR	7	GSP120	7	2	318.6	-30.8	n/a	n/a	1.925	16.6	50.7	26.3
HR	7	GSP119	6	2	336.7	-12.7	n/a	n/a	1.976	6.4	63.1	56.7
HR	7	GSP118	13	1	312.3	-34.8	n/a	n/a	n/a	19.2	45.3	20.7
DA	7	GSP121	8	3	322.7	-33.6	16.4	31.5	2.878	18.4	54.8	23.9
DA	7	GSP122	5	1	334.0	-41.5	n/a	n/a	n/a	23.9	65.8	14.3
DA	7	GSP123	5	3	324.4	-37.8	57.8	16.4	2.965	21.2	56.8	19.3
DA	7	GSP124	5	1	340.9	-47.4	n/a	n/a	n/a	28.5	71.0	358.5
	mean 7 intrusives		**10**	**7**	**326.9**	**-34.5**	**34.7**	**10.4**	**6.827**	**19.0**	**59.0**	**23.6**
	MEAN 7		**28**	**12**	**328.3**	**-33.0**	**46.5**	**6.4**	**11.763**	**18.0**	**60.2**	**26.4**
HR	1	GSP131	8	5	322.3	-43.4	35.5	13.0	4.887	25.3	55.2	12.5
HR	1	GSP126	8	2	338.2	-19.2	n/a	n/a	1.986	9.9	66.3	51.6
HR	1	GSP125	7	5	332.8	-32.2	27.1	15.0	4.852	17.5	64.1	30.1
HR	1	GSP129	7	1	342.6	-31.6	n/a	n/a	n/a	17.1	73.1	37.3
HR	1	GSP127	7	3	328.4	-18.7	277.3	7.4	2.993	9.6	57.6	42.7
HR	1	GSP128	9	9	312.2	-24.9	31.5	9.3	8.746	13.1	43.8	28.9
HR	1	GSP130	8	4	337.5	-32.3	54.6	12.5	3.945	17.5	68.5	32.3
NG	1	GSP197	7	2	313.3	-32.7	n/a	n/a	1.982	17.8	46.0	24.2
NG	1	GSP190	8	3	315.9	-8.3	17.9	30.1	2.888	4.2	43.9	43.6
SR	1	GSP191	7	3	302.8	-42.7	77.1	14.1	2.974	24.8	37.7	12.6
SR	1	GSP192	7	2	309.8	-30.4	n/a	n/a	1.994	16.3	42.4	25.1
SR	1	GSP193	7	3	306.9	-29.1	198.4	8.8	2.990	15.6	39.5	25.1
	mean 1		**15**	**12**	**322.1**	**-29.4**	**27.9**	**8.4**	**11.606**	**15.7**	**53.7**	**28.9**
	Total MT		**66**	**28**	**325.1**	**-31.3**	**33.1**	**4.8**	**27.183**	**16.9**	**56.9**	**27.7**

Table 3.2
Summary of MT (medium temperature) results from the West Pilbara Basin. Results are grouped per package. Conventions as for Table 3.1.

test for the Mount Jope Supersequence. Together with positive field tests from the Nullagine Supersequence of the MBB and EPB (Strik et al., 2003; Strik, 2004), we conclude that the HT directions of the Nullagine and Mount Jope Supersequences in the WPB represent the primary NRM.

Discussion

Reliability of the WPB data set

Our careful sample strategy, which has proven to be effective in the East Pilbara Basin (EPB) and the Marble Bar Basin (MBB), has not prevented that the amount of useful data from the WPB is relatively limited. Out of 494 rock cores, 181 proved to hold useful HT directions, which is a success rate of 37 %. This is in contrast with the EPB and the MBB, where 60 % of the analysed specimens contained a meaningful HT direction. There is no significant difference in specimens affected by lightning, but rather, there is a higher percentage of chaotic demagnetisation behaviour at higher temperatures. Further, the MT
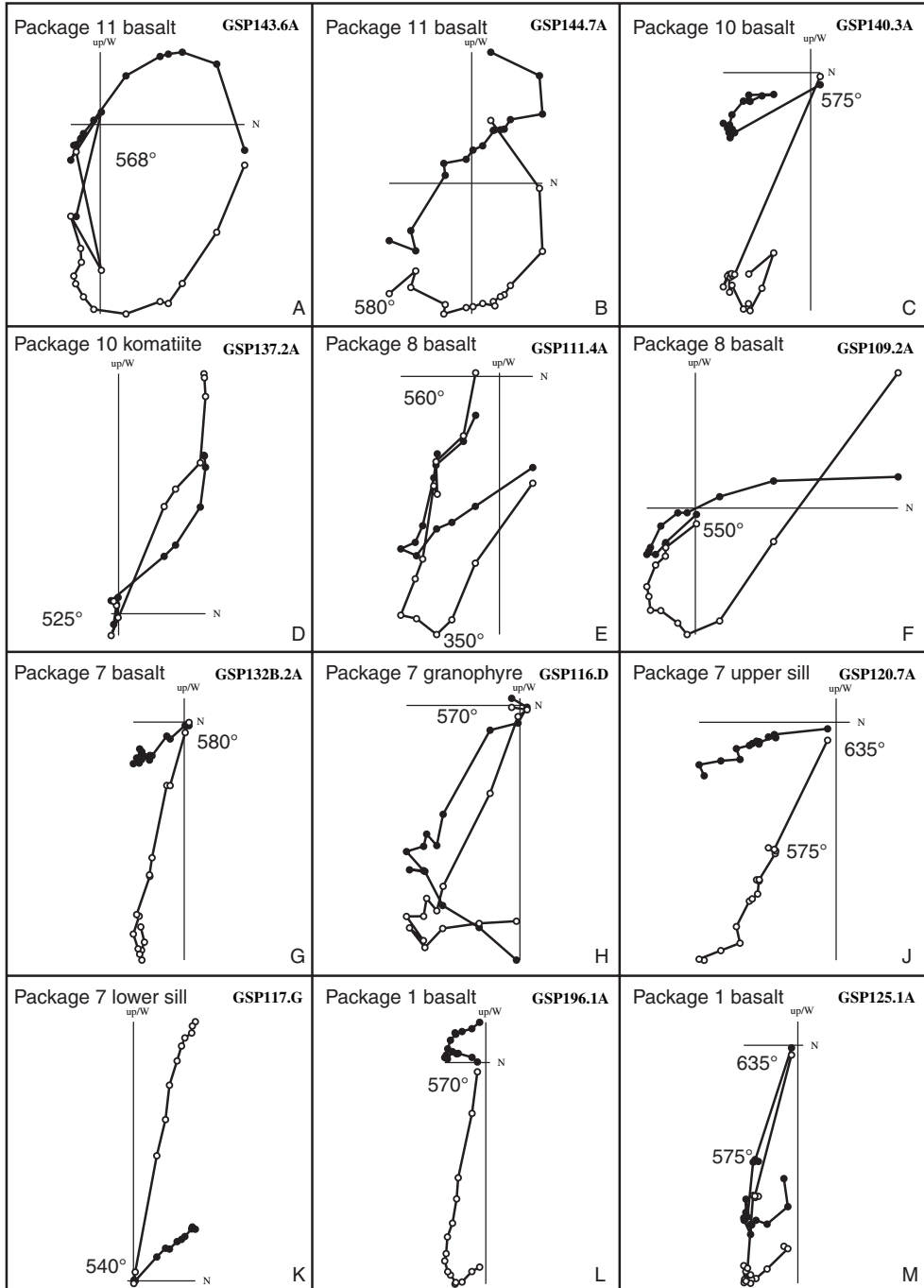
Figure 3.4
Examples of characteristic Zijderveld diagrams from each sampled package. Key temperature steps are shown. Specimen numbers indicate location (Fig. 3.2, Tab. 3.1) followed by sample number.
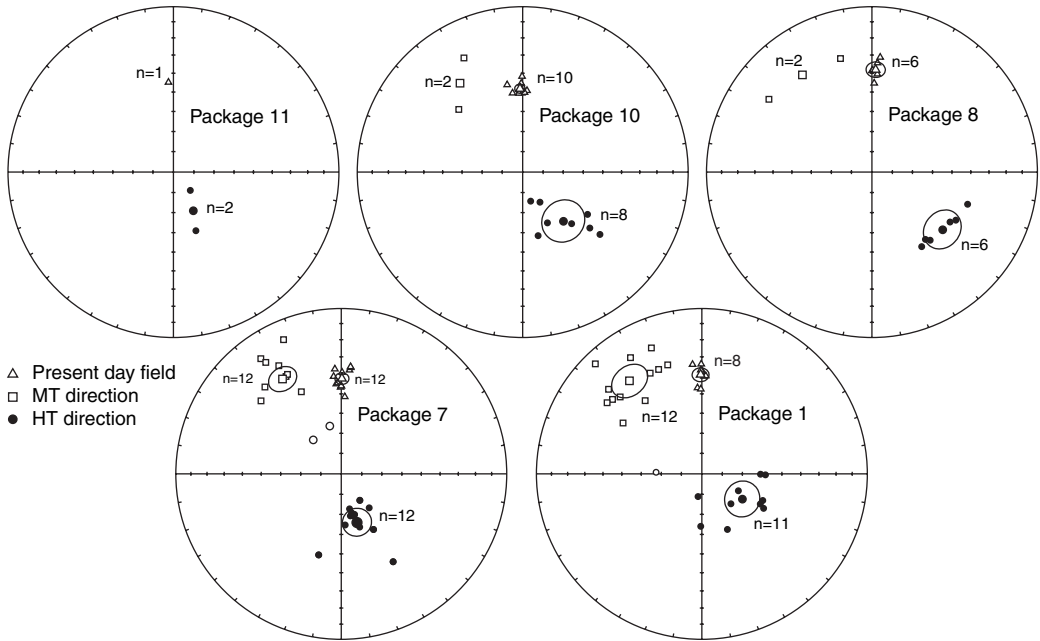
Figure 3.5
Equal area plots of results from all studied packages. N = total number of sites with accepted data, small symbols are site means, larger symbols are the mean of site means with the corresponding α95 circles (where applicable). Open (closed) symbols indicate negative (positive) inclinations. Statistics of the data are listed in Tables 3.1 and 3.2.

component shows larger overlap with the present day field and HT component in the WPB and the directions are less well-defined. This has likely been caused by the more complex thermal history of the WPB as can be deduced from a recent geochronological study of the West and Central Pilbara using the $^{40}Ar/^{39}Ar$ technique (Beintema, 2003). This study reveals that most samples have severely disturbed age spectra with Proterozoic overprinting, and that the effect is significantly stronger in the West Pilbara than revealed by similar studies in the East Pilbara (e.g. Zegers, 1996). Additionally, a metamorphic study of the Hamersley Province (Smith et al., 1982) shows that the metamorphic grade increases from ca. 118° longitude towards the west. On the basis of our palaeomagnetic and the $^{40}Ar/^{39}Ar$ data, we suggest that the metamorphic grade increases more rapidly towards the west than appears from the metamorphic study.

The higher metamorphic grade has as a consequence that the package mean directions for the WPB are less well-determined than those of the EPB and the MBB, with generally more scatter and hence lower k values. This is especially true for the Package 7 flood basalt mean (Tab. 3.1) and the Package 10 mean, which display a low number of reliable HT directions. Constructing an apparent polar wander path (APWP) for the Pilbara Craton based solely on the WPB data is not straightforward (Fig. 3.7), but when the data are compared with the earlier and more robust set of EPB and MBB data, meaningful correlations can still be made, especially because the WPB data are consistent per package. In the following section, the data of Package 0 to 10 from the EPB and the MBB are compared to the data of the five flood basalt dominated packages present in the WPB.
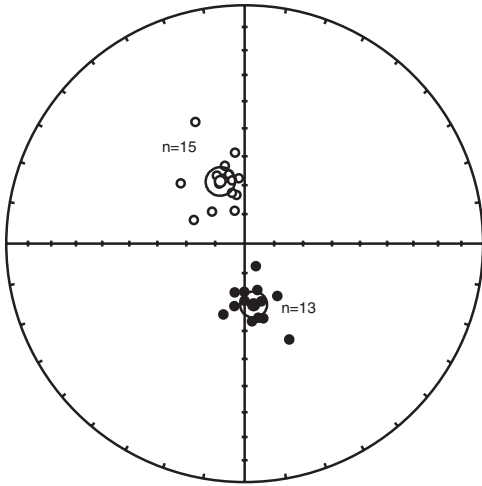
Package 7 lower and upper sill reversal test					
Sill	N	dec	inc	k	a95	rsum
Lower	15	338.6	-67.1	61.3	4.9	14.772
Upper	13	171.6	68.9	85.6	4.5	12.860

Classification B, angle between N and R = 5.2°
Critcal angle = 6.8°

Figure 3.6
Equal area plot of the HT directions from the Package 7 lower and upper sills, used for the reversal test. The lower sill revealed 15 reversed directions, whereas the upper sill has 13 normal directions. Test results (in box) show that the test is positive, with classification B.

Palaeomagnetic correlation

Package 0 is geochemically similar to Package 1, but palaeomagnetic data revealed that it only occurs in the MBB and not in the EPB (Strik, 2004). Package 0 has a completely different pole position than Package 1 (Fig. 3.7). None of the sampled packages in the WPB have pole positions similar to that of Package 0, which confirms that Package 0 flood basalts are confined to the MBB.

The pole position of Package 1 in the WPB (WPB1, Fig. 3.7) overlaps with the EPB and MBB (P1) pole position (Fig. 3.7). Also, the palaeolatitude of WPB1 is similar to that of P1 (Tab. 3.3). This means that Package 1 can successfully be correlated throughout the northern Pilbara, not only based on the bounding unconformities and similar lithology correlation criteria of Blake (2004), but also based on the palaeomagnetic data.

Package 2 to Package 6 do not contain any flood basalts or otherwise suitable rocks for palaeomagnetic sampling in the WPB.

The correlation of Package 7 rocks is twofold. Firstly, the WPB Package 7 flood basalts can be correlated to the EPB based on bounding unconformities and similar lithology (Blake, 2004). The palaeomagnetic data show that the WPB Package 7 flood basalt pole position is, although less well-determined, in good agreement with the EPB Package 7 pole (Tab. 3.3). Secondly, the WPB Package 7 dolerite sill and flood basalt pole positions plot within error and can be combined to form one single pole position for Package 7 in the WPB (WPB7, Fig. 3.7, Tab 3.3). Further, the Package 7 dolerite sills only occur in the WPB and can be correlated with EPB flood basalts based on chemical similarity only. The pole position of the dolerite sills is within error of the pole position of Package 7 in the EPB (Fig. 3.5), and the palaeolatitude is identical (Tab. 3.3), and as a result the palaeomagnetic data confirm that the sills are of Package 7 time. Subsequently, if WPB7 is compared to the combined pole position of Packages 4 to 7 of the EPB (P4-7, Fig. 3.7), it appears that WPB7 and P4-7 are almost identical, which means that Package 7 can confidently be correlated across the northern Pilbara based on the palaeomagnetic data.
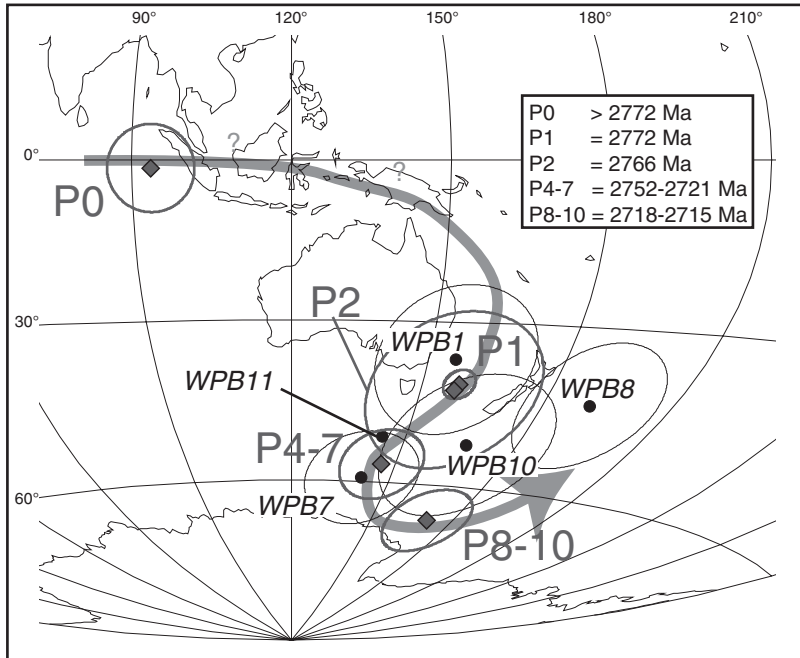
Figure 3.7
Aitoff projection of the apparent polar wander path of the East Pilbara and Marble Bar Basins (combined), compared to the pole positions from the five studied West Pilbara Basin packages. Diamonds represent Marble Bar and East Pilbara pole positions, circles represent West Pilbara Basin pole positions. Statistics of the pole positions are listed in Table 3.3. P0, Package 0; P1, Package 1; P2, Package 2; P4-7, combined pole for Packages 4 to 7; P8-10, combined pole for Packages 8 to 10; WPB1, West Pilbara Basin Package 1; WPB7, West Pilbara Basin Package 7; WPB8, West Pilbara Basin Package 8; WPB10, West Pilbara Basin Package 10; WPB11, West Pilbara Basin Package 11.

Palaeomagnetic correlation of Package 8 is more complicated. There is a significant difference in Package 8 pole position between the EPB and the WPB (Tab. 3.3). The combined Packages 8 to 10 pole position for the EPB (P8-10) does not overlap with the Package 8 WPB pole position (WPB8, Fig. 3.7). The differences in VGP positions from Package 8 reveal the poorer quality of the WPB Package 8 data, which may be caused by an incomplete removal of the secondary component from the WPB Package 8 data (cf. Figs. 3.4f, 3.5), perhaps indicative of a higher metamorphic grade in the WPB. Importantly, however, the observed shift in palaeomagnetic pole position across the P7-8 boundary in the EPB (Strik et al., 2003, Strik, 2004), is also observed in the WPB. This, together with the bounding unconformities and similar lithology correlation criteria of Blake (2004), and the empirical fact that WPB Package 8 is younger than Package 7, still supports the correlation between Package 8 in the EPB and the WPB.

Package 9 of the EPB has no equivalent in the WPB (Blake, 2004). Package 10, however, is extruded in the WPB. The palaeomagnetic data cannot confirm nor reject a craton-wide correlation of Package 10, because the WPB Package 10 (WPB10) pole position differs from the EPB Package 10 pole position, although the WPB10 palaeolatitude is nearly identical to Package 10 in the EPB. Part of the discrepancy between WPB10 and the EPB Package 10 pole position may again be caused by the larger overlap of the MT component in the WPB, as mentioned for Package 8.

Area	Package	Pole code	N	dec	inc	k	a95	R sum	plat	Pole lat	Pole lon
WPB	**11**	**WPB11**	2	152.8	68.5	n/a	n/a	1.969	51.8	-51.5	143.8
EPB	10	P8-10	9	158.0	57.3	115.2	5.2	7.939	37.9	-64.9	163.4
WPB	**10**	**WPB10**	8	140.3	58.3	29.1	10.4	7.754	39.0	-52.4	166.9
EPB	9	P8-10	5	157.1	55.5	23.8	16.0	4.832	36.0	-64.0	167.1
EPB	8	P8-10	8	158.5	49.1	47.1	8.2	7.851	30.0	-68.9	182.1
WPB	**8**	**WPB8**	6	129.2	44.1	52.4	9.3	5.905	25.9	-43.8	191.0
EPB	7	P4-7	7	161.6	68.5	84.0	6.6	6.929	51.8	-56.2	140.2
WPB	**7 sill***	**WPB7**	5	163.9	68.5	195.6	5.5	4.980	51.8	-56.6	135.3
WPB	**7 basalt**	**WPB7**	7	160.9	62.1	25.0	12.3	6.760	43.4	-61.0	146.3
WPB	**7 mean**	**WPB7**	12	162.0	64.8	39.5	7.0	11.722	46.7	-59.3	141.3
EPB	6	P4-7	15	153.2	65.8	44.0	5.8	14.682	48.0	-55.7	150.8
EPB	5	P4-7	2	171.2	54.7	n/a	n/a	1.844	35.2	-68.6	138.8
EPB	4	P4-7	1	167.6	75.1	n/a	n/a	n/a	62.0	-49.1	128.7
EPB	2	P2	7	311.1	-67.9	37.4	10.0	6.840	50.9	42.5	337.7
EPB + MBB	1	P1	32	130.7	68.3	207.0	1.8	31.850	51.5	-41.4	158.5
WPB	**1**	**WPB1**	11	121.9	66.5	28.3	8.7	10.647	49.0	-36.9	160.0
MBB	0	P0	28	304.6	72.0	31.7	4.9	27.147	57.0	-1.5	93.6
EPB	*8 to 10*	*P8-10*	*21*	*158.0*	*53.7*	*47.5*	*4.7*	*20.579*	*34.2*	*-66.4*	*170.7*
EPB	*4 to 7*	*P4-7*	*25*	*157.7*	*66.2*	*38.5*	*4.7*	*24.377*	*48.6*	*-56.7*	*146.0*
EPB	*2*	*P2*	*7*	*311.1*	*-67.9*	*37.4*	*10.0*	*6.840*	*50.9*	*42.5*	*337.7*
EPB + MBB	*1*	*P1*	*32*	*130.7*	*68.3*	*207.0*	*1.8*	*31.850*	*51.5*	*-41.4*	*158.5*
MBB	*0*	*P0*	*28*	*304.6*	*72.0*	*31.7*	*4.9*	*27.147*	*57.0*	*-1.5*	*93.6*

* includes 1 Package 7 granophyre mean

Table 3.3
Summary of package mean directions for all northern Pilbara basins. The West Pilbara Basin codes are in bold type. The grouped East Pilbara and Marble Bar Basins data are printed in italic type. Conventions as for Table 3.1.

The (possible) WPB Package 11 flood basalts have no equivalent in the EPB. Alternatively, these flood basalts form the top of Package 10, but the Package 11 pole position (WPB11) is significantly different from WPB10 (Tab. 3.3, Fig. 3.7). WPB11, however, is not well-determined, because it is based on only two sampled flows and therefore any conclusions about the relevance of the Package 11 pole position are unfounded at this stage.

Magnetostratigraphy of the Nullagine and Mount Jope Supersequences
Previous work has shown that most rocks of the Nullagine and Mount Jope Supersequences have the same polarity (Strik et al., 2003, Strik, 2004). So far, only Package 2 and Package 7 have revealed reversed intervals. The Package 2 reversal is well established throughout the EPB, but the Package 7 reversal was recorded in only one basalt flow in the EPB and is possibly of short duration. In the WPB, we find that the uppermost sampled Package 1 flow has a reversed polarity (Tab. 3.1). This may imply that the Package 2 reversal of the EPB in fact started earlier, namely during the extrusion of the uppermost Package 1

flood basalts. The alternative, namely that the top of Package 1 in the WPB is remagnetised by the intrusion of the (reversed) lower sill of Package 7 is unlikely, since Package 1 and the Package 7 lower sill are separated by ca. 300 meters of sediment. More importantly, the magnetic directions between the reversed Package 1 and Package 7 lower sill are significantly different (Tab. 3.1), yet are consistent with the EPB results, confirming the oldest documented reversal of the geomagnetic field.

The Package 7 reversal of the EPB is now confirmed by the reversed polarity of the Package 7 lower sill. A crude but workable magnetostratigraphy now exists for the Nullagine and Mount Jope Supersequences in the northern Pilbara: Between at least 2772 Ma to 2766 Ma, polarity changed from normal to reversed. Between 2766 Ma and 2741 Ma polarity changed back to normal again. The rock record of much of this period consists of sedimentary rock, which has not been sampled (pilot studies only revealed a present day field direction), so additional reversals may have been missed. Between 2741 Ma and 2715 Ma or younger, the field was dominantly normal, with the exception of the short reversed interval in Package 7 between ca. 2724 and 2721 Ma. This suggests that the reversal frequency from 2772 Ma to 2715 Ma was most probably low, but no firm indications exist that the magnetic field in terms of reversals behaved differently in the late Archaean than in the Phanerozoic.

Tectonic evolution of the Nullagine and Mount Jope Supersequences

A ca. 15° shift in pole position across the Package 7/8 boundary is recorded throughout the northern Pilbara. Three options were brought forward to explain the cause and the meaning of this rapid shift, namely non-dipole behaviour, rapid true polar wander (TPW), and rapid horizontal plate movement (Strik, 2004). We have argued earlier (Strik et al., 2003), that the latter option, horizontal plate movement, is the most likely cause. The shift in palaeolatitude represents a rapid phase of rifting with an average speed of ca. 50 cm yr^{-1} (Strik, 2004), and this is reconfirmed by the additional data from the WPB. Horizontal plate movement fits the tectonic model for the development of the Nullagine and Mount Jope Supersequences (Blake, 1993; Blake and Barley, 1992). With the new data from the WPB we now have an extra argument to strengthen the model of rapid horizontal plate movement.

The dataset for the Nullagine and Mount Jope Supersequences shows that the northern Pilbara moved as a whole block during the development of the Nullagine Supersequence and the formation of Package 7, since VGP positions from the EPB to the WPB are (close to) identical. The tectonic model of Blake (1993); Blake and Barley (1992) for the development of the Nullagine Supersequence (Package 1 to 6) describes an episode of WNW-ESE directed crustal extension. A series of major NNE-SSW trending faults with considerable west-block-down movement were active during this period. The palaeomagnetic data do not reveal major latitudinal movement during this episode. However, a maximum of 11.5° or ca. 1300 km of latitudinal movement from Package 1 to Package 7 is still possible within the errors of palaeolatitude determination (2.5 cm yr^{-1}). Further, the data reveal strong indications for a circa 30° rotation of the northern Pilbara as a whole, until Package 7 times (Fig. 3.8).

The rest of the Mount Jope Supersequence, from Package 8 onward, was possibly deposited during the development of a WNW-ESE trending rift. The palaeomagnetic data confirm this phase by the observed latitudinal shift across the Package 7-8 boundary, which represents ca. 1600 km of northward drift (Fig. 7.8). The VGP positions from the EPB and WPB, however, are not identical anymore, which is most probably related to the contribution

EPB	East Pilbara Basin
WPB	West Pilbara Basin
SRFC	Sherlock River Fault Complex

(IV) Present day

(III) > 1600 km of N-ward rifting between 2721 and 2718 Ma

Package 8, 2718 Ma

spreading rift

Package 1, 2772 Ma

Package 7, 2721 Ma

Transfer fault (?)

(I) WNW-ESE crustal extension between 2772 and 2724 Ma

(II) Ca. 30° counter-clockwise rotation between 2772 and 2721 Ma of northern Pilbara (EPB + WPB)
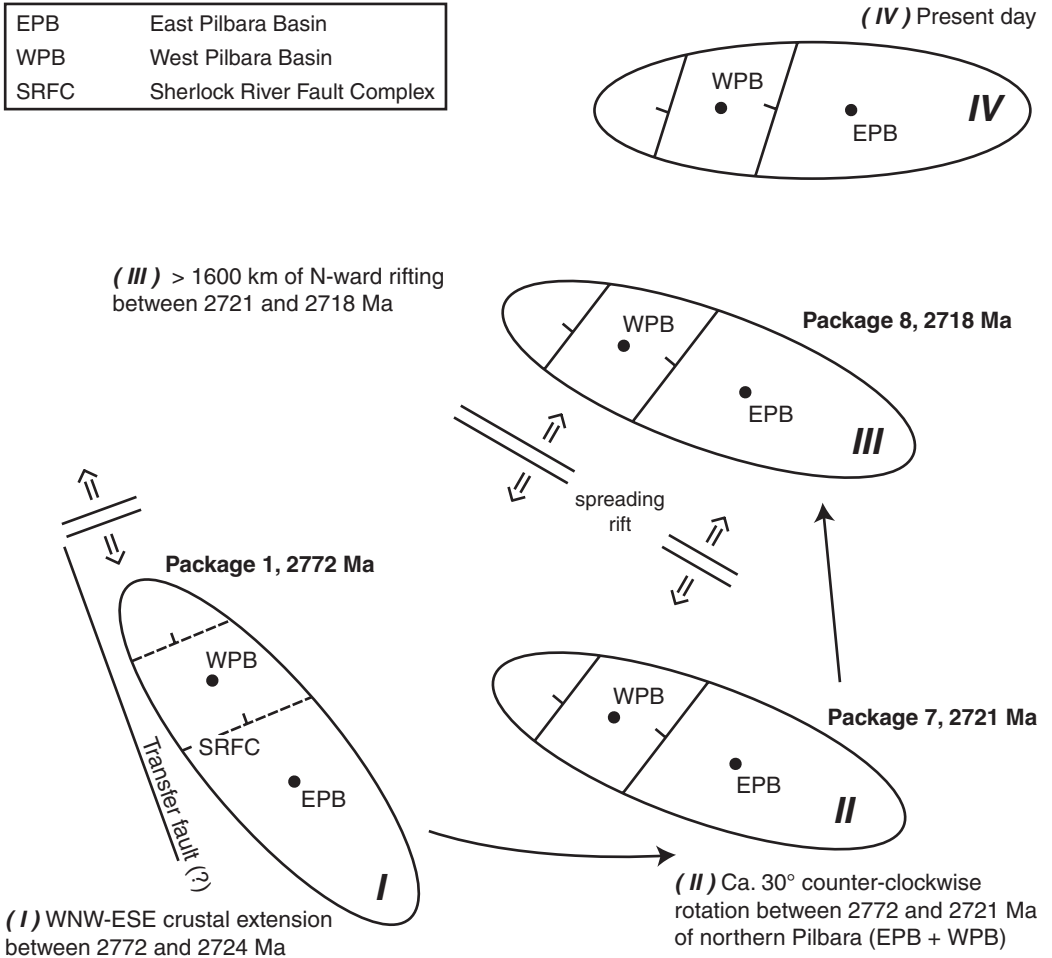
Figure 3.8
Tectonic model for the evolution of the Nullagine and Mount Jope Supersequences of the northern Pilbara Craton. The model integrates the tectonic model of Blake (1993); Blake and Barley (1992) based on geologic field evidence with the palaeomagnetic data of the studied sequence.

of the MT component to the HT component in WPB8 and 10, as discussed above. However, the change in palaeolatitude position through time is similar for the EPB and WPB (Tab. 3.3), which justifies the model.

Concluding, rapid apparent polar wander is well explained by the palaeomagnetic shift representing a phase of rapid horizontal movement of the Pilbara, which fits with the models based on geological evidence. These models are now extended with a rotational phase between the formation of Packages 1 and 7, and a quantification of the amount of drift.

Conclusions

The palaeomagnetic dataset from the Nullagine and Mount Jope Supersequences in the West Pilbara Basin has proven to be consistent, albeit with a lower success rate than for the Marble Bar and East Pilbara Basins.

The ca. 2721 Ma Package 7 geomagnetic reversal that is observed in a single lava flow in the East Pilbara Basin has been confirmed by a Package 7 dolerite sill in the West Pilbara Basin, which highlights the significance of this reversal and makes this the second oldest well-documented stratabound reversal. It passes the reversal test and confirms the primary nature of the NRM.

Individual packages of the Nullagine and Mount Jope Supersequences can be correlated throughout the northern Pilbara based on palaeomagnetic data, thus reinforcing the stratigraphic correlations of Blake (2004).

Finally, the ca. 15° latitudinal shift recorded across the Package 7/8 boundary throughout the northern Pilbara is most probably caused by rapid horizontal plate movement. This is in agreement with an established model for the tectonic evolution of the Nullagine and Mount Jope Supersequences (Blake, 1993; Blake and Barley, 1992) and is supported by a consistent palaeomagnetic dataset based on a total of 235 sample sites throughout the northern Pilbara. Additional evidence for large-scale tectonic movement is provided by a block rotation of the Pilbara Craton during the formation of Packages 1 to 7.

Acknowledgements

Chapter 4

Palaeomagnetism of the Neoarchaean Pongola and Ventersdorp Supergroups and an appraisal of the 3.0-1.9 Ga apparent polar wander path of the Kaapvaal Craton, Southern Africa.

"nihil nec optimum"

The senior Aliaga staff 2003

Palaeomagnetism of the Neoarchaean Pongola and Ventersdorp Supergroups and an appraisal of the 3.0-1.9 Ga apparent polar wander path of the Kaapvaal Craton, Southern Africa.

Abstract

The style of tectonic processes of the young Earth is a topic of intense debate, and palaeomagnetism provides the only robust tests with which to settle theoretical disputes based on the rock record that infer large scale horizontal motions between palaeocontinents. A possible apparent polar wander path (APWP) of the Kaapvaal Craton, which shows great distances between subsequent pole positions adjacent pole positions, can be interpreted as evidence for such horizontal displacements in the Archaean-Proterozoic between ca. 3.2 and 1.9 Ga. There are, however, significant uncertainties build into this APWP. Currently, the published APWP for the Kaapvaal Craton comprises up to eight pole positions between 3.0 and 1.9 Ga, that for example between 2.8 and 2.7 Ma already span possible horizontal motions exceeding 6500 km. The aim of our research is to increase the pole density within this interval and in doing so to test the robustness of the Kaapvaal APWP within this time frame. More than 250 samples of basalt, diamictite and dolerite of the Neoarchaean Pongola (ca. 2.95-2.85 Ga) and Ventersdorp (ca. 2.71-2.70 Ga) Supergroups of the Kaapvaal Craton were sampled both at surface and in an underground mine. Thermal demagnetisation revealed two magnetic components. A high temperature component is present in three Pongola formations and in two Ventersdorp formations; these may be recorders of the primary natural remanent magnetisation. Because of lack of precise geochronology and positive field tests, this magnetisation can only be constrained as older than ca. 2.05 Ga. A medium temperature overprint in many samples probably records remagnetisation at ca. 180 Ma, during the emplacement of basalts and dolerites of the Mesozoic Karoo Large Igneous Province. This remagnetisation appears to have affected a vast area of the Kaapvaal Craton. Our new pole positions, together with those published previously, demonstrate that the Neoarchaean APWP of the Kaapvaal Craton is poorly defined. Direct comparisons between the APWP of the Kaapvaal Craton with APWPs of other Archaean cratons to determine relative motions between Archaean continents, based on these data, are premature.

Introduction

The Kaapvaal Craton of southern Africa encompasses some of the best-preserved parts of stable continental crust of Neoarchaean age (3.0-2.5 Ga). The dominant mode of tectonism during this age is still a topic of intense debate (e.g. Bédard et al., 2003; de Wit, 1998; Hamilton, 1998; McCall, 2003). Here, we intend to contribute to this debate using palaeomagnetism. We studied the Neoarchaean Pongola and Ventersdorp Supergroups, because these successions contain abundant basalts, rocks that are usually good recorders of the geomagnetic field. The degree of metamorphism of these rocks is relatively low, generally at lower greenschist facies, which provides a reasonable possibility that the original natural remanent magnetisation (NRM) has been preserved. Locally, however, the degree of metamorphism is substantially higher. Also, parts of the Kaapvaal Craton have been subjected to various regional Neoarchaean, Proterozoic and Phanerozoic tectonothermal events (cf. e.g. Eglington and Armstrong, 2004; Poujol et al., 2003), including: the intrusion of the vast Bushveld Complex at ~2.057 Ga; the Vredefort Meteorite Impact at 2.017 ± 5 Ga (Eglington and Armstrong, 2004); the Waterberg Igneous Province (~1.87-1.98 Ga); the Natal-Namaqua Collision Event (~1.040 Ga); and the formation of the Karoo Large Igneous Basalt Province (~0.182 Ga). It is uncertain to what extent these events may have affected the original NRM, but widespread remagnetisation has been recognised in previous palaeomagnetic studies (e.g. Layer et al., 1988b).

The aim of this study is to obtain new palaeomagnetic pole positions for the Pongola and Ventersdorp Supergroups and to increase the resolution of the existing Neoarchaean apparent polar wander path (APWP) of the Kaapvaal Craton. In turn this may provide information about its tectonic history. Naturally, our work requires demonstrating that the NRM preserved in the rocks is of primary origin. In addition, possible secondary overprints may give insight into the subsequent thermal history of (a part of) the craton. Based on our results, a quality analysis of a new APWP is presented. Finally, there have been suggestions, based on lithostratigraphical, geochronological, and palaeomagnetic data, that the Kaapvaal and Pilbara Cratons may once have been part of the same continent called Vaalbara (e.g. Cheney, 1996; Strik et al., 2003; Wingate, 1998; Zegers et al., 1998). Here, we examine the validity of this hypothesis further.

Palaeomagnetic studies of the Kaapvaal Craton are limited and of variable quality. Previous studies are often only recorded as unpublished PhD-theses and/or were carried out before progressive demagnetisation became routine procedure. The Global Palaeomagnetic Database (GPMDB, see URL in references) lists only three Archaean pole positions for the Kaapvaal Craton between 3.2 and 2.5 Ga (Tab. 4.1). Further, six presumed primary pole positions are published for the period between ca. 3.0 to 1.9 Ga, but these are not listed in the GPMDB (Tab. 4.1). Reconstructions of an APWP are further limited by the small number of radiometric dates that are available (Tab. 4.1). Thus, a reliable APWP for this time period does not exist. However, the palaeomagnetic data set for the Kaapvaal Craton has earlier been referred to as evidence for large amounts of rifting in the Archaean (e.g. Kröner and Layer, 1992; Layer et al., 1989) and has even been used to estimate minimum rift speeds. These conclusions stand or fall with the quality of the palaeomagnetic data, which will be reviewed thoroughly in this paper, together with our new data.

Supergroup	Group/Intrusive	Subgroup	Formation	Dominant lithology	Pmag ref.	Age, method [reference]
Younger	Post-Waterberg			dolerite	a	1879-1872 Ma, U-Pb baddeleyite [1]
Younger	Bushveld Complex			ultramafic	b*	2059 ± 1 Ma, U-Pb titanite [2]
Younger	Postmasburg		Ongeluk	lava	c	2222 ± 13 Ma, Pb-Pb [3]
Younger	Younger rocks			various		2642 ± 3 Ma, Pb evap. [4]
Younger	Mbabane Pluton			granitoid	d*	2687 ± 6 Ma, ^{40}Ar/^{39}Ar, hornblende [5]
Ventersdorp	(Pniel)		Allanridge	flood basalt	this study	(older than 2642 ± 3 Ma)
Ventersdorp	(Pniel)		Bothaville	sediments		
Ventersdorp	Platberg		Rietgat	mafic volcanics		
Ventersdorp	Platberg		Makwassie	porphyry		2709 ± 4 Ma, U-Pb zircon [6]
Ventersdorp	Platberg		Goedgenoeg	porphyry		
Ventersdorp	Platberg		Kameeldoorns	sediments		
Ventersdorp	Klipriviersberg		Edenville	subaerial flood basalt		
Ventersdorp	Klipriviersberg		Loraine	subaerial flood basalt		
Ventersdorp	Klipriviersberg		Jeanette	subaerial flood basalt		
Ventersdorp	Klipriviersberg		Orkney	subaerial flood basalt		
Ventersdorp	Klipriviersberg		Alberton	subaerial flood basalt		2714 ± 8 Ma, U-Pb zircon [6]
Ventersdorp	Klipriviersberg	East Driefontein	Westonaria	subaerial flood basalt	this study	
Ventersdorp	Klipriviersberg	East Driefontein	Venterspost	subaerial flood basalt		
Ventersdorp	correlation uncertain		Derdepoort	flood basalt	e*	2782 ± 5 Ma, U-Pb, zircon [7]
Unconformity / various intrusions	Gabarone Complex			granite	f	2783 ± 2 Ma, U-Pb zircon evap. [8]
Unconformity / various intrusions	Modipe Gabbro			gabbro	g	> 2783 Ma
Unconformity / various intrusions	Usushwana Complex			gabbro, pyroxenite		2875 ± 40 Ma, ^{40}Ar/^{39}Ar, hornblende [9] / 2871 ± 30, Sm-Nd [10]
Unconformity / various intrusions	Post-Pongola			dolerite	this study	Age unknown
Pongola	Mozaan	Nkoneni	Ntanyana	sediments, BIF, minor volcanics		
Pongola	Mozaan	Nkoneni	Gabela	sediments, BIF, minor volcanics		
Pongola	Mozaan	Nkoneni	Bongaspoort	sediments, BIF, minor volcanics		
Pongola	Mozaan	Odwaleni	Kiphunyawa	sediments, BIF, minor volcanics	this study	
Pongola	Mozaan	Odwaleni	Tobolsk	sediments, BIF, minor volcanics	this study	
Pongola	Mozaan	Odwaleni	Delfkom	sediments, BIF, minor volcanics		
Pongola	Mozaan	Dwaalhoek	Hlashana	sediments, BIF, minor volcanics		
Pongola	Mozaan	Dwaalhoek	Thalu	sediments, BIF, minor volcanics		
Pongola	Mozaan	Dwaalhoek	Ntombe	sediments, BIF, minor volcanics		
Pongola	Mozaan	Dwaalhoek	Singeni	sediments, BIF, minor volcanics		< 2837 ± 5 Ma, U-Pb zircon [11]
Pongola	Nsuze	Ozwana	Mkuzane	mafic volcanics		
Pongola	Nsuze	Ozwana	Langfontein	mafic volcanics		
Pongola	Nsuze	Bivane	Agatha	mafic volcanics	this study	2984 ± 2.6 Ma [12], 2940 ± 22 Ma, U-Pb Zircon [10]
Pongola	Nsuze	Bivane	White Mfolozi	mafic volcanics		
Pongola	Nsuze	Bivane	Nhlebela	mafic volcanics	this study	
Pongola	Nsuze	Bivane	Mantonga	mafic volcanics		(younger than 3028 ± 14 Ma)
	Older basement			granite-greenst.		3028 ± 14 Ma, Rb-Sr [13]
	Nelshoogte Pluton			granitoid	h*	3179 ± 18 Ma, ^{40}Ar/^{39}Ar, hornblende [14]

Legend (within Mozaan row block):
- +++ Felsic volcanics
- vvvv Mafic extrusive
- ^^^^ Mafic Intrusive
- Sediment
- Mixed lithology

Table 4.1
Summary lithostratigraphy and geochronology of the Pongola and Ventersdorp Supergroups, and other rock units relevant to this study. Lithology (Gold and von Veh, 1995; Kent, 1980; van der Westhuizen et al., 1991; Winter, 1976). References to published palaeomagnetic data (Pmag Ref.), poles with an asterisk (*) are listed in the GPMDB: (a) Hanson et al., 2004; (b*) Hattingh, 1986; (c) Evans et al., 1997; (d*) Layer et al., 1989; (e*) Wingate, 1998; (f) Evans, 1966; (g) Evans and McElhinny, 1966; (h*) Layer et al., 1998. Geochronology: (1) Hanson et al., 2004; (2) Buick et al., 2001; (3) Cornell et al., 1996; (4) Minimum age for the younger successions: Beukes unpubl., referenced in Tinker et al., 2002; (5) Layer et al., 1989; (6) Armstrong et al., 1991; (7) Wingate, 1998; (8) Grobler and Walraven, 1993; (9) Layer et al., 1988a; (10) Hegner et al., 1984; (11) Minimum age from felsic sill: Gutzmer et al., 1999; (12) Hegner et al., 1993; (13) Barton et al., 1983; (14) Layer, 1986; Layer et al., 1998.

Geological setting

The proto-Kaapvaal craton formed over a period of about 500 million years, between 3.6-3.1 Ga, through amalgamation of small tectonic blocks (de Wit et al., 1992; Eglington and Armstrong, 2004; Poujol et al., 2003). By 3.0- 2.9 Ga, the craton was part a relatively stable continent with a well formed 30 to 50 km thick continental crust underlain by a ca.
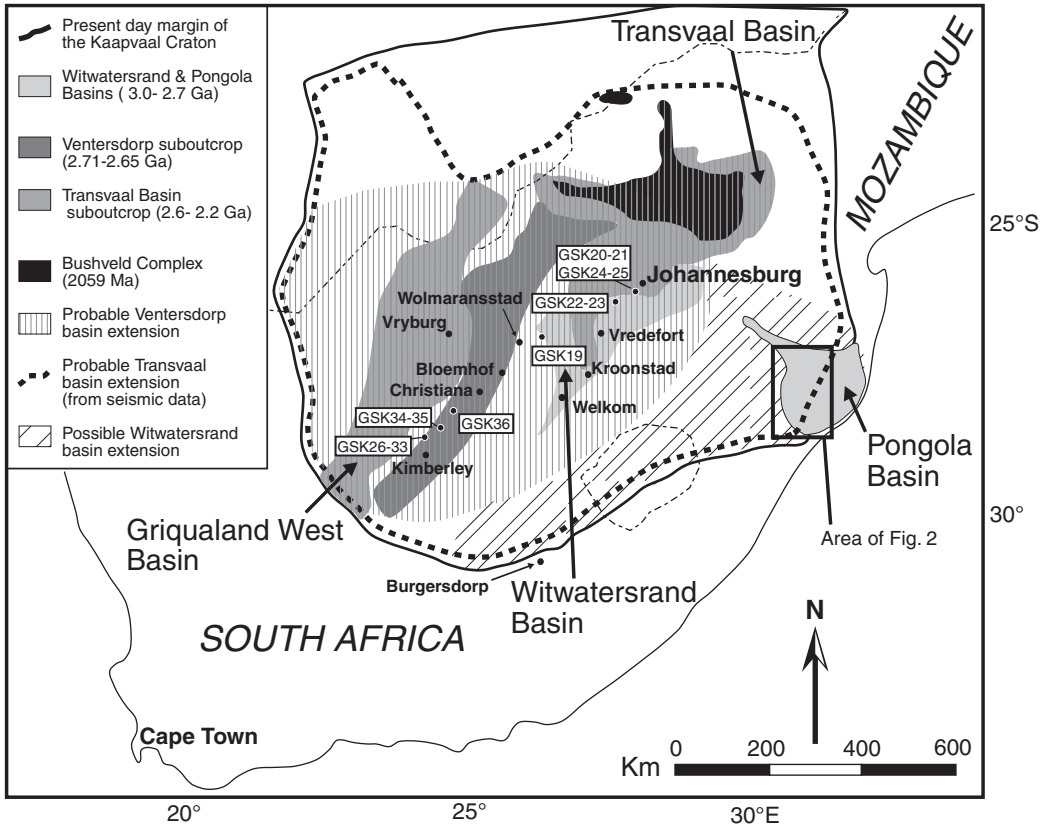
Figure 4.1
Simplified outcrop map of the Kaapvaal Craton showing probable basin extensions. Also shown are the Ventersdorp Supergroup sample locations.

250-300 km thick lithospheric mantle keel (Moser et al., 2001; Stankiewicz et al., 2002 Fouch and et, 2004; Schmitz and Bowring, 2004). Remnants of the first major sedimentary basins that were deposited across peneplained granite-greenstone basement of this continent are represented by the siliciclastics and and volcanics of the Witwatersrand-Dominion and Pongola basins. Recent dating indicates that the Pongola and Witwatersrand are contemporary deposits, possible of the same regionally extensive basin (Fig. 4.1). Below we briefly summarize their salient geological features that are also summarized in Table 4.1.

Pongola Supergroup (ca. 2.95-2.85 Ga)

The Neoarchaean Pongola Supergroup is exposed in an area of ca. 120 by 275 km in the southeast of the Kaapvaal Craton, partly in Swaziland and partly in South Africa (Fig. 4.2). The Pongola Supergroup unconformably overlies the granite-greenstone basement of the Kaapvaal Craton (e.g. Button, 1981). The sequence has an overall maximum stratigraphic thickness of ca. 12 km, comprising mainly of volcanics and clastic sediments with significant
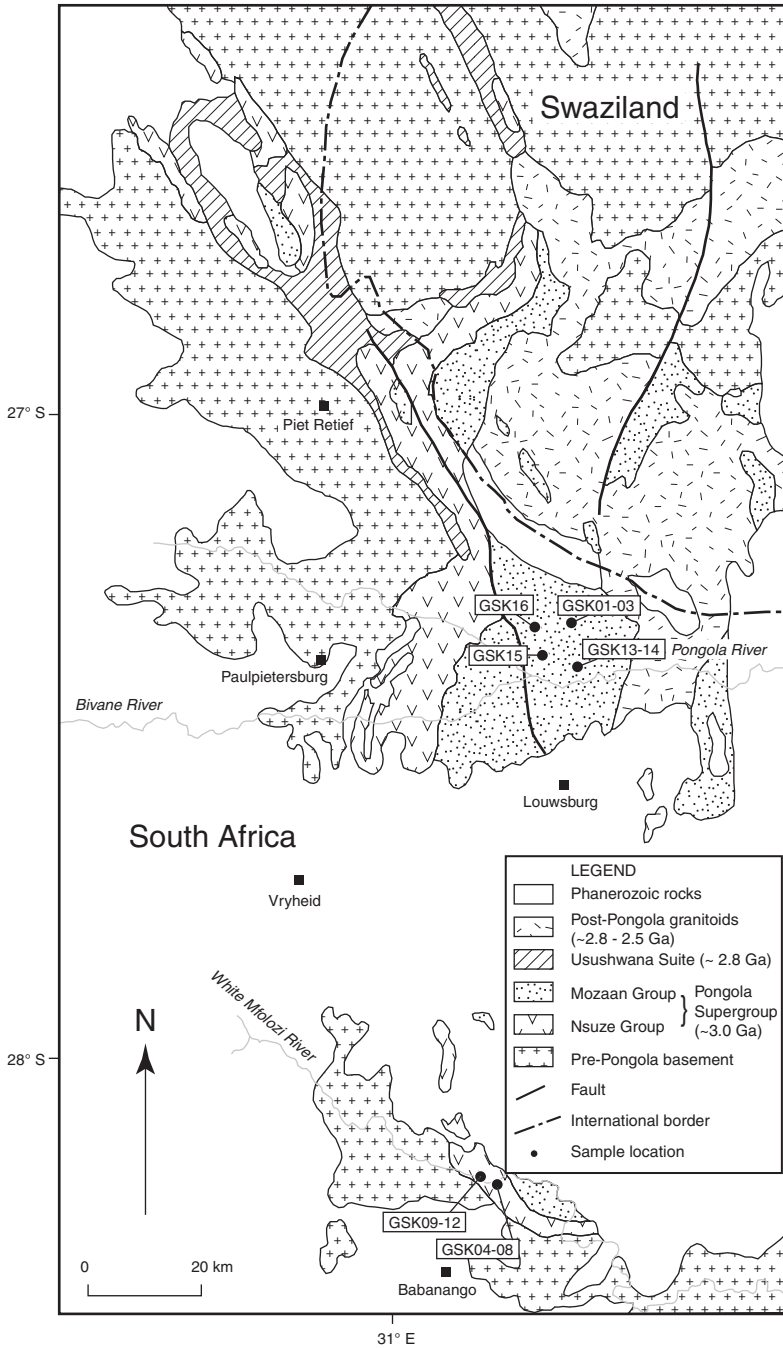
Figure 4.2
Simplified geological map of the Pongola Supergroup with sample locations. Modified after Gold & von Veh (1995).

lateral variations in thickness (Burke et al., 1985a). The Pongola Supergroup has been subdivided in the mainly volcanic Nsuze Group (e.g. Armstrong et al., 1982) and the dominantly sedimentary Mozaan Group (e.g. Beukes and Cairncross, 1991, Table 4.1). The Nsuze Group has been interpreted as the rock record of a rapid phase of rifting and filling of a rift basin (Burke et al., 1985a). The sediments of the Mozaan Group are interpreted as shallow marine shelf deposits (Beukes and Cairncross, 1991) and may be the record of thermal subsidence of the Pongola basin (Bickle and Eriksson, 1982).

The Pongola Supergroup has been affected by greenschist-facies metamorphism (Burke et al., 1985a). In general, the Pongola basin has undergone only moderate deformation, although towards the south the deformation is stronger, because of overprinting by the 1.0-1.04 Ga Natal-Namaqua orogeny (Burke et al., 1985a; Matthews, 1990).

Ventersdorp Supergroup (ca. 2.71-2.70 Ga)

The Neoarchaean Ventersdorp Supergroup extends over an area of at least 750 by 350 km (Winter, 1976) and crops out in a large part of central South Africa (Fig. 4.1). Most information about the Ventersdorp Supergroup comes from borehole and seismic data, which have shown that the extent of the Ventersdorp Supergroup is far greater than what can be deduced from surface exposure (e.g. Tinker et al., 2002; Tyler, 1979). The Ventersdorp Supergroup overlies the Witwatersrand Supergroup with a (mostly angular) unconformity (e.g. Tankard et al., 1982; Tinker et al., 2002; Winter, 1976). The Ventersdorp Supergroup reaches a total maximum thickness of ca. 8 km, of which 5.1 km exist of sub-aerial volcanics and ca. 2.9 km of sediments (van der Westhuizen et al., 1991). The Ventersdorp Supergroup has been subdivided in three groups, namely: the sub-aerial flood basalt dominated Klipriviersberg Group, the lithologically diverse Platberg Group (cf. Tab. 4.1), and the siliciclastic and flood basalt dominated Pniel Sequence.

The Klipriviersberg Group contains no sediments other than the basal conglomerate, which suggests that this group has formed in a relatively short period, during rapid basalt extrusion (cf. Eriksson et al., 2002; van der Westhuizen et al., 1991). The source of the lava maybe plume-related (Eriksson et al., 2002).

The Platberg Group unconformably overlies the Klipriviersberg Group. Formations within the Platberg Group are all conformable (van der Westhuizen et al., 1991). Volcanism related extension continued during Platberg times.

The Pniel Sequence unconformably overlies the Platberg Group and extensional tectonics most probably continued during the formation of the entire Pniel Sequence (e.g. Eriksson et al., 2002; van der Westhuizen et al., 1991), although Clendenin et al. (1988) suggest that the Allanridge basalts (cf. Tab. 4.1) formed during a period of thermal subsidence.

The rocks of the Ventersdorp Supergroup have been affected by lower greenschist facies metamorphism (e.g. Cornell, 1978; Crow and Condie, 1988); locally, the Klipriviersberg Group has experienced middle to upper greenschist facies during at ca. 1950 Ma (Layer et al., 1988b).

Methods

Two hundred and fifty-four samples from the Nhlebela Formation (Fm.), the Agatha Fm., the Tobolsk Fm., the Kiphunyawa Fm., Post-Pongola dolerite, the Westonaria Fm. and the Allanridge Fm. were collected (Tab. 4.1). Sampling in the field was carried out

using a petrol engine drill. Samples were orientated with both a magnetic and sun compass. The sun compass directions were used in the sample analyses, although generally there was no significant difference between sun and magnetic compass direction. Following earlier studies in the similar-age Pilbara Craton (e.g. Strik et al., 2003), great care has been taken to avoid sites that may have been affected by a lightning-induced isothermal remanent magnetisation (IRM). To further test this, ten oriented hand-specimens were taken from the Westonaria Fm. in the Kloof Gold Mine, Shaft number 4, 41 level, ca. 3160 meters below surface.

In the laboratory, the hand samples were cored; all cores were cut to standard specimens of 22 mm length. One specimen of each core was thermally demagnetised in a magnetically shielded, laboratory-built furnace. The NRM was measured on a 2G Enterprises DC-SQUID cryogenic magnetometer. Thermal demagnetisation was done in 16 temperature steps (20, 100, 200, 300, 350, 400, 450, 480, 500, 525, 530, 540, 550, 560, 568, and 575 °C and occasionally 590 °C)

The results of the thermal demagnetisation were plotted in Zijderveld diagrams (Zijderveld, 1967) and principal component analysis (Kirschvink, 1980) was done to interpret the directions of NRM. Only components with a maximum angular deviation (MAD) less than 10 degrees were accepted.

A modified horizontal translation Curie balance that applies a cycling field (Mullender et al., 1993) and an alternating gradient force magnetometer (AGFM MicroMag) were used to measure some magnetic properties and to help identifying the carriers of NRM of selected samples.

Results

The following section describes the results of the thermal demagnetisation of each studied rock unit in sequence from older to younger (Tab. 4.1). Apart from an occasional low-coercivity present day field component, two main components of magnetisation are present, namely:
- A medium temperature (MT) component that unblocks from between 200-350 °C and 480 °C
- A high temperature (HT) component that unblocks from between 350-500 °C and 580°C

The statistical data of all HT component directions and the data for the MT component directions are given in Tables 4.2 and 4.3, respectively.

Nsuze Group, Nhlebela Fm.

Basalt samples from the Nhlebela Fm. are from fresh exposures in a deeply incised valley where chances of lightning impact were thought to be small. However, samples from two out of four sites were severely affected by a lightning induced IRM. The two remaining sites (GSK11-12) have a similar, consistent HT component (Tab. 4.2; Figs. 4.3L-M; 4.4G). No consistent MT components are developed at this location.

Nsuze Group, Agatha Fm.

Basalts from the Agatha Fm. were sampled in the same valley as those from the Nhlebela Fm., but were not affected by a lightning overprint. A consistent HT direction is present in four out of five sites (Tab. 4.2; Figs. 4.3J-K; 4.4F). A consistent MT component is present in all sites (Tab. 4.3; Fig. 4.4F) which is fully unblocked at ca. 480-500 °C (Fig. 4.3J-K). A present day field component is sporadically developed (Fig. 4.4F).

Group	Formation	Site Number	Lithology	Coordinates (WGS 84)	Strike/ dip	N	n	dec°	inc°	k	a95°	R	Plat°	VGP lat°	VGP long°
Karroo age		GSK35	Conglo.	S28.32769 E24.71916	subhor.	11	11	131.1	-32.6	1.3	76.2	3.458	n/a	n/a	n/a
Ventersdorp Supergroup															
Pniel	Allanridge	GSK36	Basalt	S28.09500 E24.86562	subhor.	7	0	n/a	n/a	n/a	n/a	n/a	n/a	n/a	n/a
Pniel	Allanridge	GSK34	Basalt	S28.32687 E24.71856	subhor.	7	2	195.3	63.2	n/a	n/a	1.998	44.7	-69.6	352.2
Pniel	Allanridge	GSK33	Basalt	S28.46568 E24.37387	163/07 W	7	7	206.1	54.2	28.3	11.5	6.788	34.7	-67	316.8
Pniel	Allanridge	GSK32	Basalt	S28.46553 E24.37544	163/07 W	7	4	208.0	54.5	72.5	10.9	3.959	35.0	-65.4	317
Pniel	Allanridge	GSK31	Fissure	S28.46537 E24.37793	163/07 W	15	0	n/a	n/a	n/a	n/a	n/a	n/a	n/a	n/a
Pniel	Allanridge	GSK30	Basalt	S28.46524 E24.37793	163/07 W	7	6	195.0	60.2	72,5	7.9	5.931	41.1	-72.4	344.2
Pniel	Allanridge	GSK29	Basalt	S28.50963 E24.39162	subhor.	7	5	173.7	64.6	35.3	13.1	4.887	46.5	-71.4	38.1
Pniel	Allanridge	GSK28	Basalt	S28.51187 E24.39029	subhor.	7	5	180.8	63.7	33.2	13.5	4.879	45.3	-73.2	22.4
Pniel	Allanridge	GSK27	Basalt	S28.51754 E24.38674	subhor.	7	7	164.6	58.7	80.7	6.8	6.926	39.4	-73.2	69.7
Pniel	Allanridge	GSK26	Basalt	S28.51823 E24.38639	subhor.	7	7	178.1	59.6	154.0	4.9	6.961	40.4	-78	31.3
Pniel	Allanridge	GSK19	Basalt	S26.92500 E26.38473	subhor.	7	0	n/a	n/a	n/a	n/a	n/a	n/a	n/a	n/a
Pniel	**Allanridge**					**8**		**188.7**	**60.7**	**82.0**	**6.2**	**7.915**	**41.7**	**-75.0**	**0.1**
Klipriviersberg	Westonaria	GSK24	Basalt	S26.30111 E27.98459	083/20 S	7	2	124.9	81.4	n/a	n/a	1.984	73.2	-34.9	44.8
Klipriviersberg	Westonaria	GSK25	Basalt	S26.30055 E27.98294	083/20 S	8	7	78.7	80.9	29.1	11.4	6.794	72.2	-21.6	46.8
Klipriviersberg	Westonaria	GSK21	Basalt	S26.29844 E27.98459	083/20 S	9	9	40.4	69.8	22.4	11.1	8.643	53.7	2.7	50.6
Klipriviersberg	Westonaria	GSK20	Basalt	S26.30021 E27.98314	083/20 S	8	1	62.7	78.1	n/a	n/a	n/a	67.1	-14.4	48.9
Klipriviersberg	Westonaria	GSK23	Basalt	Kloof, shaft #4 41 level	151/30 SW	5	0	n/a	n/a	n/a	n/a	n/a	n/a	n/a	n/a
Klipriviersberg	Westonaria	GSK22	Basalt	Kloof, shaft #4 41 level	151/30 SW	5	0	n/a	n/a	n/a	n/a	n/a	n/a	n/a	n/a
Klipriviersberg	**Westonaria**					**4**		**66.2**	**79.1**	**84.7**	**10.0**	**3.965**	**68.9**	**-17.1**	**47.9**
Pongola Supergroup															
?	Post-Pongola	GSK15	Diorite	S27.40616 E31.22810	018/45 E	10	8	132.2	32.1	60.7	7.2	7.885	17.4	-45.0	123.6
?	**Post-Pongola**					**1**		**132.2**	**32.1**	**60.7**	**7.2**	**7.885**	**17.4**	**-45.0**	**123.6**
Mozaan	Kiphunyawa	GSK14	Diamictite	S27.42398 E31.27691	353/09 E	10	0	n/a	n/a	n/a	n/a	n/a	n/a	n/a	n/a
Mozaan	Kiphunyawa	GSK13	Diamictite	S27.42163 E31.27467	043/36 SE	10	6	148.1	19.4	101.7	6.7	5.951	10.0	-55.3	145.2
Mozaan	**Odwaleni**					**1**		**148.1**	**19.4**	**101.7**	**6.7**	**5.951**	**10.0**	**-55.3**	**145.2**
Mozaan	Tobolsk	GSK16	Basalt	S27.37628 E31.22210	011/21 E	7	5	52.8	-64.8	198.5	5.4	4.980	46.7	44.7	161.1
Mozaan	Tobolsk	GSK03	Basalt	S27.35403 E31.26595	258/67 N	7	3	119.5	-35.5	642.7	4.9	2.997	19.6	-14.9	153.2
Mozaan	Tobolsk	GSK02	Basalt	S27.35469 E31.26517	279/71 N	7	3	75.2	16.6	67.4	15.1	2.970	8.5	9.0	106.8
Mozaan	Tobolsk	GSK01	Basalt	S27.35487 E31.26487	251/33 N	7	6	257.4	69.8	71.3	8.0	5.930	53.7	-29.0	349.9
Mozaan	**Tobolsk**					**4**		**89.1**	**-9.1**	**1.3**	**n/a**	**1.658**	**n/a**	**n/a**	**n/a**
Nsuze	Agatha	GSK08	Basalt	S28.23298 E31.18613	318/25 NE	8	8	272.5	51.6	82.1	6.2	7.915	32.2	-12.7	331.2
Nsuze	Agatha	GSK07	Basalt	S28.23304 E31.18602	318/25 NE	7	7	274.0	49.8	180.7	4.5	6.967	30.6	-10.8	330.2
Nsuze	Agatha	GSK06	Basalt	S28.23341 E31.18554	318/25 NE	7	5	273.2	46.8	318.8	4.3	4.987	28.0	-10.3	327.6
Nsuze	Agatha	GSK05	Basalt	S28.23372 E31.18527	318/25 NE	7	1	289.2	57.2	n/a	n/a	n/a	37.8	-3.5	342.8
Nsuze	Agatha	GSK04	Basalt	S28.23267 E31.18661	318/25 NE	7	0	n/a	n/a	n/a	n/a	n/a	n/a	n/a	n/a
Nsuze	**Agatha**					**4**		**276.7**	**51.5**	**157.6**	**7.3**	**3.981**	**32.2**	**-9.4**	**333.0**
Nsuze	Nhlebela	GSK09	Basalt	S28.24441 E31.16114	312/26 NE	8	0	n/a	n/a	n/a	n/a	n/a	n/a	n/a	n/a
Nsuze	Nhlebela	GSK10	Basalt	S28.24457 E31.16147	312/26 NE	8	0	n/a	n/a	n/a	n/a	n/a	n/a	n/a	n/a
Nsuze	Nhlebela	GSK11	Basalt	S28.24426 E31.16164	312/26 NE	8	7	317.0	47.1	63.4	7.6	6.905	28.3	20.1	351.4
Nsuze	Nhlebela	GSK12	Basalt	S28.24385 E31.16154	312/26 NE	8	2	336.4	44.1	n/a	n/a	1.976	25.9	31.3	6.2
Nsuze	**Nhlebela**					**2**		**327.0**	**46.0**	**n/a**	**n/a**	**1.985**	**27.4**	**25.9**	**358.4**

Table 4.2
Summary of HT (high temperature) results from the Pongola and Ventersdorp Supergroups. Results are in stratigraphic order. Grey areas show means. Abbreviations: N = number of specimens from each site and number of sites contributing to the mean, n = number of specimens accepted, dec = declination, inc = inclination, Plat = palaeolatitude, VGP lat (long) = latitude (longitude) of VGP (virtual geomagnetic pole), n/a = not applicable.

Mozaan Group, Tobolsk Fm.

Basalts from the Tobolsk Fm. were sampled at two locations and four sites (Fig. 4.2). A HT component has a consistent direction per site, but site averages are not consistent

Group	Formation	Site Number	Lithology	N	n	dec°	inc°	k	a95°	R	Plat°	VGP lat°	VGP long°
Ventersdorp Supergroup													
Pniel	Allanridge	GSK34	Basalt	7	6	339.5	-54.0	71.8	8.0	5.930	34.5	71.5	270.0
Pniel	Allanridge	GSK33	Basalt	7	2	325.0	-64.7	n/a	n/a	1.990	46.6	57.3	251.1
Pniel	Allanridge	GSK32	Basalt	7	7	324.1	-54.0	69.1	7.3	6.913	34.5	59.0	273.9
Pniel	Allanridge	GSK30	Basalt	7	4	313.7	-49.3	41.6	14.4	3.928	30.2	49.9	280.3
Pniel	Allanridge	GSK29	Basalt	7	5	345.6	-54.8	47.5	11.2	4.916	35.3	76.0	261.5
Pniel	Allanridge	GSK28	Basalt	7	2	330.2	-51.4	n/a	n/a	1.999	32.1	64.1	279.1
Pniel	Allanridge	GSK27	Basalt	7	3	336.5	-60.3	55.3	16.7	2.964	41.2	67.0	254.6
Pniel	Allanridge	GSK26	Basalt	7	2	342.1	-63.0	n/a	n/a	1.986	44.5	68.6	241.4
Pniel	Allanridge	GSK19	Basalt	7	3	328.0	-38.4	37.2	20.5	2.946	21.6	60.4	299.7
Klipriviersberg	Westonaria	GSK24	Basalt	7	6	339.4	-47.4	60.4	8.7	5.917	28.5	71.6	286.3
Klipriviersberg	Westonaria	GSK25	Basalt	8	6	331.7	-49.8	54.0	9.2	5.907	30.6	64.8	281.5
Klipriviersberg	Westonaria	GSK21	Basalt	9	4	320.8	-51.6	23.2	19.5	3.871	32.2	55.5	278.6
Ventersdorp				**20**	**12**	**331.0**	**-53.6**	**78.7**	**4.9**	**11.860**	**34.1**	**64.7**	**272.6**
Pongola Supergroup													
?	Post-Pongola	GSK15	Diorite	10	3	333.0	-48.8	227.9	8.2	2.991	29.7	66.2	289.2
Mozaan	Kiphunyawa	GSK13*	Diamictite	10	7	282.7	-38.9	6.5	25.6	6.080	22.0	20.7	286.5
Mozaan	Tobolsk	GSK16	Basalt	7	6	316.7	-69.5	55.7	9.1	5.910	53.2	49.0	250.0
Mozaan	Tobolsk	GSK03	Basalt	7	7	339.5	-46.0	216.6	4.1	6.972	27.4	71.8	296.5
Mozaan	Tobolsk	GSK02	Basalt	7	8	331.9	-47.7	99.9	5.6	7.930	28.8	65.2	291.3
Mozaan	Tobolsk	GSK01	Basalt	7	4	329.9	-51.6	36.8	15.3	3.919	32.2	63.5	283.3
Nsuze	Agatha	GSK08	Basalt	8	8	334.3	-56.3	155.0	4.5	7.955	36.9	66.8	272.8
Nsuze	Agatha	GSK07	Basalt	7	7	324.3	-55.3	140.4	5.1	6.957	35.8	59.0	277.8
Nsuze	Agatha	GSK06	Basalt	7	7	337.1	-58.1	270.7	3.7	6.978	38.8	68.3	266.2
Nsuze	Agatha	GSK05	Basalt	7	6	328.6	-62.0	507.1	3.0	5.990	43.2	60.7	262.0
Nsuze	Agatha	GSK04	Basalt	7	1	316.8	-37.8	n/a	n/a	1.000	21.2	50.3	301.4
Pongola				**16**	**10**	**328.9**	**-52.6**	**57.6**	**6.4**	**9.844**	**33.2**	**63.1**	**278.2**
All				**34**	**22**	**330.1**	**-53.2**	**70.5**	**3.7**	**21.702**	**33.8**	**64.0**	**275.2**

Table 4.3
Summary of MT (medium temperature) results from the Kaapvaal Craton. Consistent MT directions were found only in both the Pongola and the Ventersdorp Supergroups. Results are grouped by formations and supergroups. Data in bold are site averages. See Table 4.2 for additional sample data and explanation of abbreviations. Sites with an asterisk (*) are not included in the mean.

(Tab. 4.2; Fig. 4.4E and cf. Fig. 4.3G and 4.3H). The HT direction means do not form a confined cluster, with or without tectonic correction. The MT directions, however, show a consistent direction when no tectonic correction is applied (Tab. 4.3; Fig. 4.4E). A present day field component is not recognised in this formation.

Mozaan Group, Kiphunyawa Fm.

Diamictite samples from the Kiphunyawa Fm. were taken at two sites, which were sampled to allow for a fold test. GSK13 shows consistent HT, MT and present day field components (Tabs. 4.2, 4.3; Fig. 4.4D). Figure 4.3F shows a sample in which the MT component is well preserved. Three samples of site GSK14, however, appear to be affected by lightning and the remaining seven have chaotic demagnetisation paths. Therefore, the fold test could not be carried out.

Post-Pongola dolerite

A fine-grained Post-Pongola (exact age unknown) was sampled at one site. A consistent HT component is present in eight out of ten samples (Tab. 4.2, Figs. 4.3E, 4.4C).
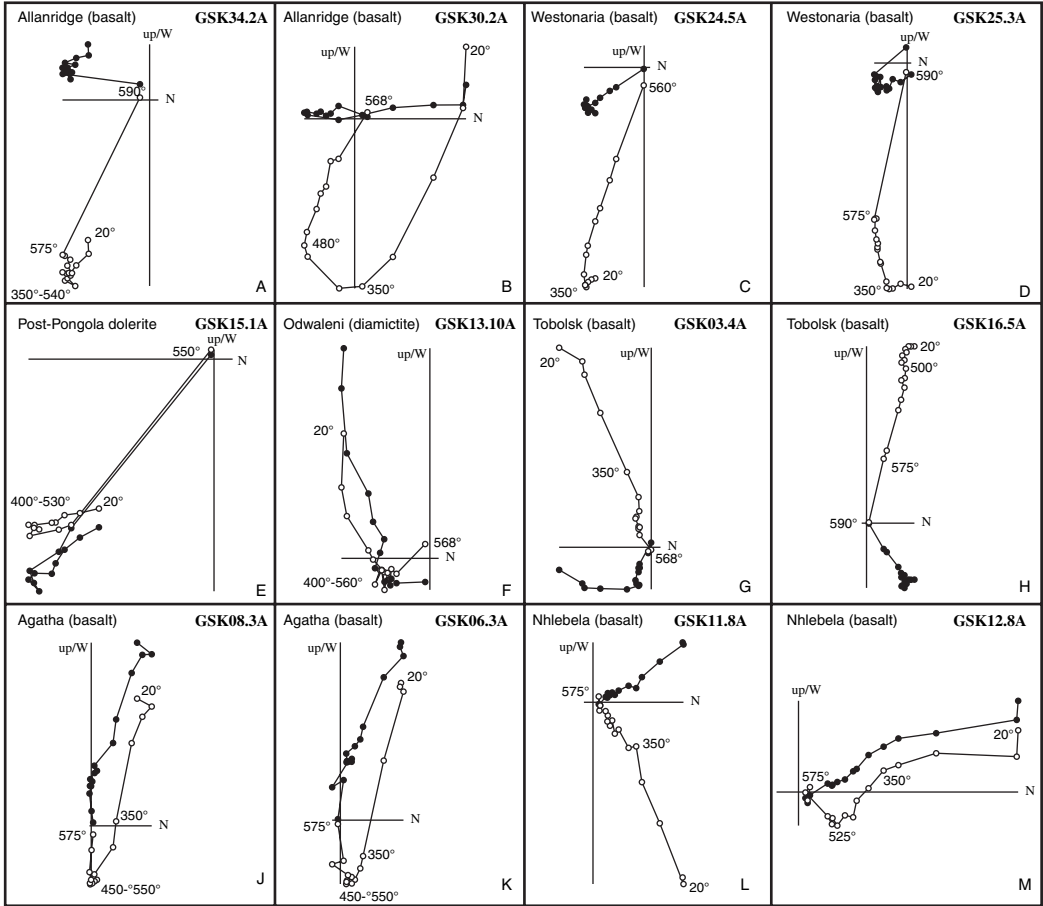
Figure 4.3
Selection of characteristic Zijderveld diagrams of samples from all studied formations. Key temperature steps are shown. Specimen numbers indicate location (Figs. 4.1, 4.2, Tab. 4.2) followed by sample number.

Three samples also show a consistent MT direction (Tab. 4.3; Figs. 4.3E; 4.4C). No present day field component is recorded.

Klipriviersberg Group, Westonaria Fm.

Thermal demagnetisation of hand samples from Westonaria Fm. basalts, taken from the Kloof Gold Mine, resulted in chaotic Zijderveld plots. It is doubtful that the samples have been affected by the elevated temperatures (> 50 °C) in the mine, though the shocks from the blasting of the hallways may have affected the NRM. No components from these underground samples could be isolated. Nevertheless, basalt samples taken from a quarry generated better results. Some 60% of these samples have consistent HT directions (Tab. 4.2; Fig. 4.4B) and ca. 40% have consistent MT directions (Tab. 4.3; Fig. 4.4B). The present day field direction is only occasionally present. Zijderveld diagrams show clear progressive demagnetisation paths (Fig. 4.3C-D).

Allanridge Basalt (AR)

Westonaria Basalt (WE)

Ventersdorp Supergroup

Pongola Supergroup

Kiphunyawa Diamictite (KD)

Tobolsk Basalt (TB)

Post-Pongola Dolerite (PD)

△ present day field
□ MT component
● HT bedding corrected
▼ HT *in situ*

Agatha Basalt (AB)

Nhlebela Basalt (NB)
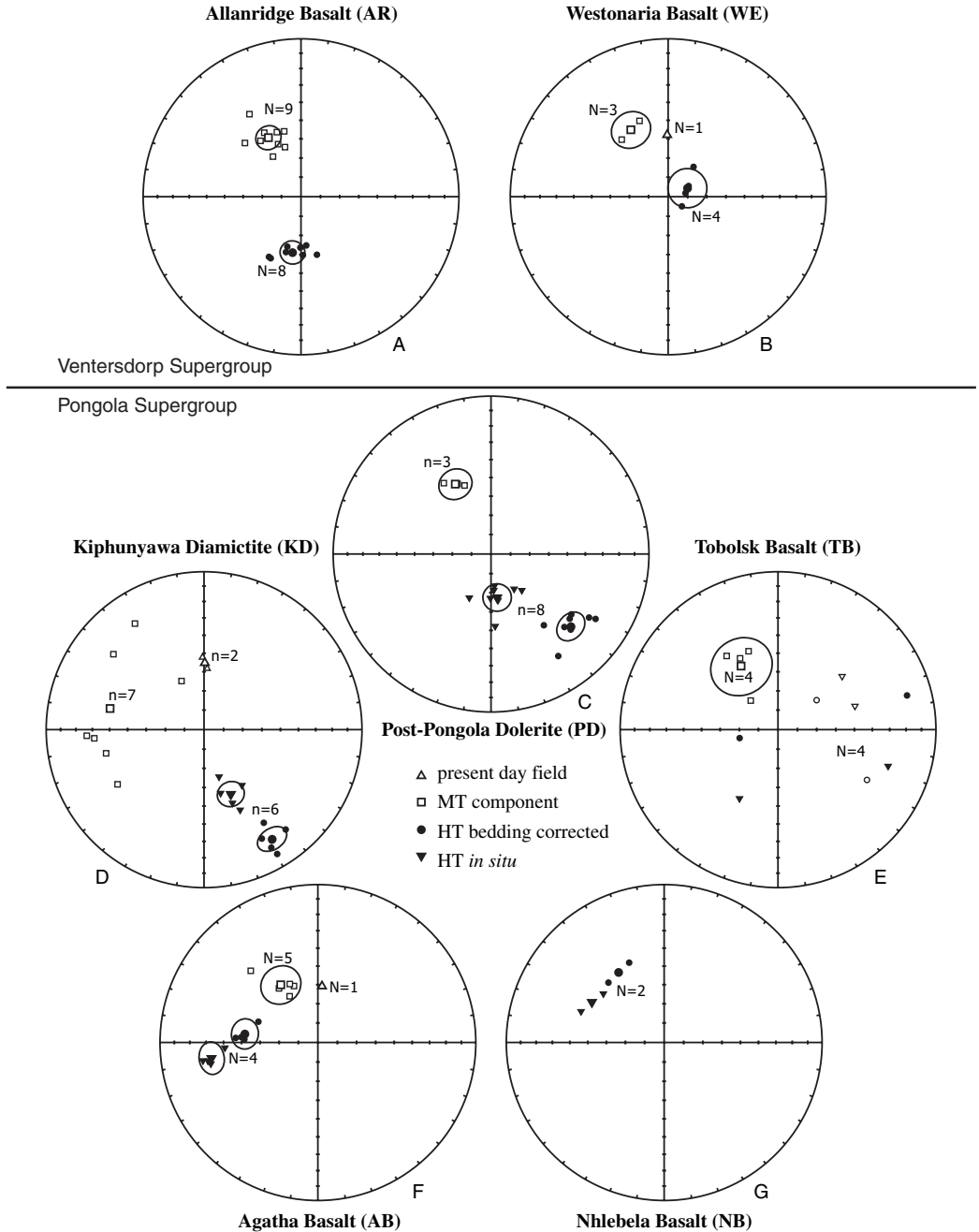
Figure 4.4
Equal area plots of results from all studied packages and dykes. 4.4A, B, E, F and G represent equal area plots of multiple sites. N = total number of sites with accepted data, small symbols are site means, larger symbols are the mean of site means with the corresponding α_{95} circles (where applicable). 4.4C and D represent single sites, n = total number of specimens, larger symbols are the site means showing error circles. Open (closed) symbols indicate negative (positive) inclinations, circles are tectonically corrected high temperature (HT) directions, inverted triangles are in situ HT directions, squares represent the secondary (MT) overprint, and triangles are a present day field overprint.

Pniel Sequence, Allanridge Fm.

Basalts from the Allanridge Fm. were sampled at four different locations and at a total of eleven sites (cf. Fig. 4.1; Tab. 4.2). At most sites, the quality of results is good, with one exception: site GSK36 was affected by lightning. Site GSK31 was sampled to allow for a "breccia test". Here, a fissure filled with randomly oriented blocks of basalt embedded in a younger basalt matrix allows an experiment similar to a conglomerate test. Random orientations of HT directions of the basalt blocks would indicate that the preserved NRM in sites away from the fissure might have preserved their original NRM. However, Zijderveld
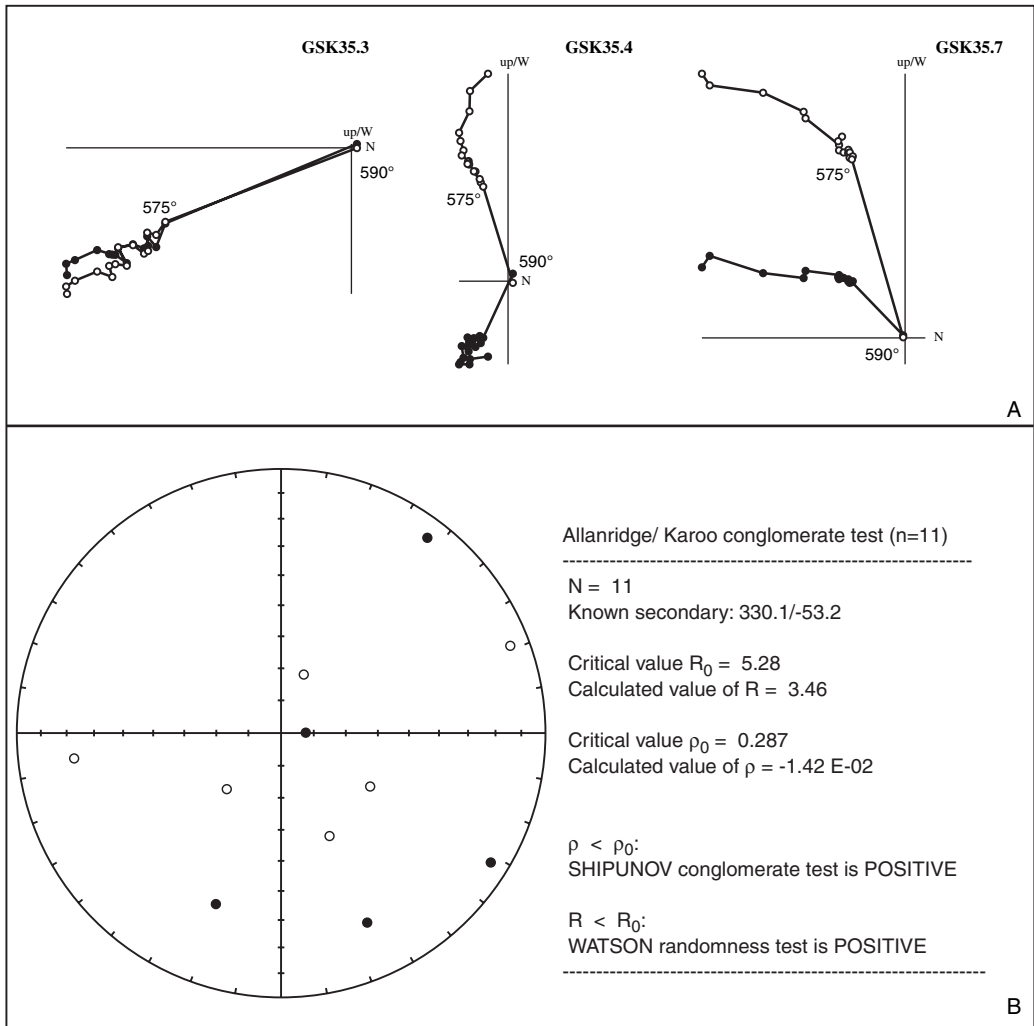
Figure 4.5
A) Zijderveld diagrams of selected conglomerate samples. Unblocking is gradual until 575 °C, followed by rapid unblocking at the next temperature step (590 °C).
B) Equal area plot of HT directions from the conglomerate test, including the statistical data. Both Watson and Shipunov tests are positive. Conventions as in Figure 4.4.

diagrams from site GSK31 show a chaotic pattern and no HT components can be isolated. The "breccia test" is therefore inconclusive. The remaining sites in the Allanridge Fm. show well-developed HT components (Fig. 4.3A-B) that have a consistent direction (Tab. 4.2; Fig. 4.4A). The MT component is also clearly present (Fig. 4.3B) and also has a consistent direction (Tab. 4.3; Fig. 4.4A).

Field tests

Three formations were sampled with the intention to apply a fold test, namely the Tobolsk Fm., the Kiphunyawa Fm., and the Westonaria Fm. Of these, the Tobolsk Fm. is the only formation that does not have a consistent HT component site mean, either before, or after tectonic correction (Fig. 4.4E). This implies that the fold test cannot be carried out. Further, one site from the two Kiphunyawa Fm. sites is affected by lightning induced IRM, which means that here too, the fold test cannot be carried out. Finally, only one of two sample locations in the Westonaria Fm. generated results. Again this prevents the application of the fold test.

Although the breccia test was inconclusive, lower Permian (295-255 Ma) Karoo Supergroup conglomerates that unconformably overlie the Allanridge Fm. close to the town of Winsorton (Site GSK35, Fig. 4.1), give better results. Eleven boulders of various rock types all have stable demagnetisation paths and unblock at 580°C (Fig. 4.5A). The HT directions are plotted in Figure 4.5B. The Watson test for uniform randomness (Watson, 1956) gives a positive result when applied to these HT directions. The Shipunov conglomerate test (Shipunov et al., 1998) gives a positive result as well, where the used vector is a known secondary component, namely the mean of all MT directions (cf. Tab. 4.3). These results imply that the magnetisation preserved in the Allanridge basalts is at least older than 275 ± 20 Ma. However, the possibility that the preserved NRM is of primary origin cannot be confirmed by field tests at this stage.

Carriers of natural remanent magnetisation

Progressive thermal demagnetisation (Fig. 4.3) shows that no remanence remains after heating at 580 °C. Haematite is therefore excluded as carrier of the NRM. Intensity decay curves typically show one or two plateaux (Fig. 4.6). Where there are two plateaus, the first intensity drop occurs between 200 and 350 °C and the second intensity drop starts at ca. 540 °C, followed by a steep decline to zero at 580 °C. Where there is only one plateau, intensity is stable until ca. 540 °C, after which it steeply declines to zero at 580 °C. The component that unblocks at 580 °C is SD magnetite, and the small unblocking window suggests it is probably very fine grained. IRM acquisition data (Fig. 4.7) show a best-fit of two components, which have overlapping coercivity spectra. The high coercivities (high Hc) are not indicative of haematite (because samples unblock at 580 °C), but instead suggest slightly oxidised magnetite (van Velzen and Zijderveld, 1995). The decrease in intensity at 350 °C may indicate inversion of maghemite (Dankers, 1978).

Experiments with the Curie balance show that the contribution of SD magnetite to the bulk magnetic material of the sample is unusually low, and the samples show mainly paramagnetic behaviour (Fig. 4.8). The intensity of the NRM in the Kaapvaal specimens is particularly low: on average, the magnetic intensity of the specimens does not exceed 5-10 x 10^{-3} A/m, an observation that was also made for Neoarchaean flood basalts of the Pilbara Craton (e.g. Strik et al., 2003). By contrast, in modern basalts such as those from Iceland,
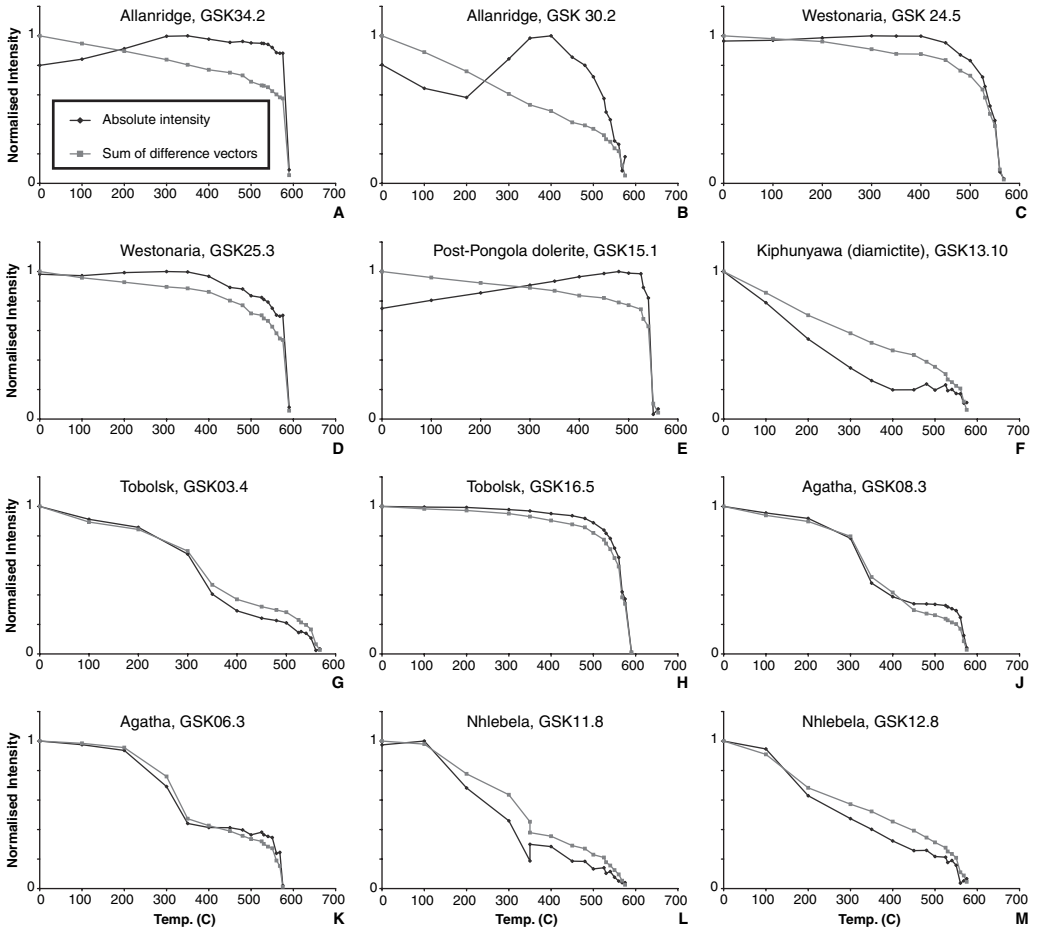
Figure 4.6
Normalised magnetic intensity *versus* temperature. The diagrams correspond to the Zijderveld diagrams of Figure 4.3, in the same order. Diagrams show either a fast decrease in intensity, starting at ca. 540 °C (Fig 4.6A-F, H) or two decreases, of which one at ca. 300-350 °C and the other at ca. 540 °C (Fig 4.6G, J-M). Black graphs represent the absolute intensity decay, grey graphs represent the decay of the sum of difference vectors.

magnetic intensities of 10 A/m in standard specimens are common. For the Archaean, samples with high intensities are usually affected by a lightning induced IRM.

Discussion

Timing of the MT component magnetisation

From the 34 sites of this study, 23 show internally consistent MT component directions. These 23 MT site mean directions appear to be consistent when no tectonic correction is applied (Tab. 4.3). The presence of a consistently common MT component in both the Pongola and Ventersdorp Supergroup samples, suggests a large-scale and even craton-wide remagnetisation event. This event cannot be related to well-established orogenic events, since the MT directions are only consistent prior to any tectonic correction. There is
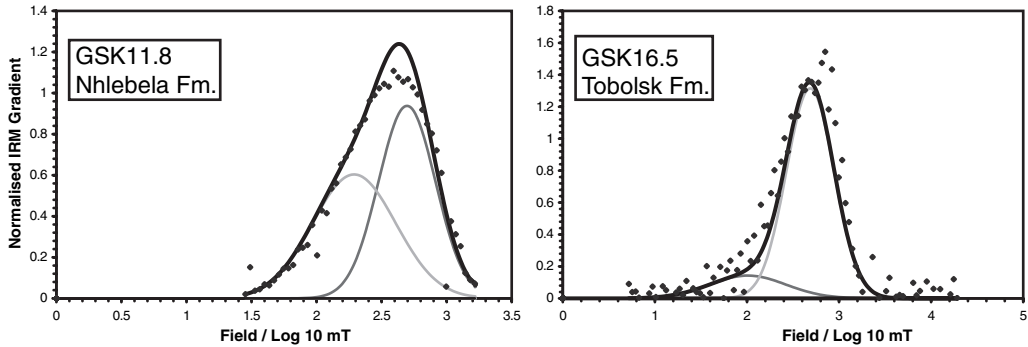
Figure 4.7
Normalised IRM acquisition gradient *versus* field for selected samples. See Figure 4.3 for corresponding Zijderveld diagrams of these samples. Most samples are too weakly magnetised to be measured above the noise limits. IRM analysis from the Tobolsk and Nhlebela formations show a best fit for two overlapping components. Program used was IRMUNMIX V2.2 (Heslop et al., 2002).

significant evidence for thermo-tectonic events at around 2.0 Ga: the formation of the Bushveld Complex at ca. 2059 ± 1 Ma (U-Pb, titanite, Buick et al., 2001); the 2017 ± 5 Ma Vredefort impact (Reimold et al., 2002); and the 1.87-1.93 Ga related basaltic magmatism of the Waterberg-Soutpansberg rifts (Hanson et al., 2004). In addition, much of the craton cover may have been effected by fluid-induced alteration during the Keiss orogeny along the western margin of the craton (Duana et al., 1988). Further low temperature overprinting event(s) have affected the eastern Kaapvaal Craton as far south as the Barberton Mountain Land, as indicated by $^{40}Ar/^{39}Ar$ biotite dates of ~ 2.0 Ga Layer et al., 1989) and ~2.0 Ga Rb/Sr dates on carbonates (de Ronde and de Wit, 1994; Weiss and Wasserberg, 1987).

However, the pole position of the MT component of our samples does not coincide with the pole position of the Bushveld Complex (Fig. 4.9A), nor with the less well constrained poles of the Vredefort Dome, Limpopo direction A and the in situ Witwatersrand pole (cf. Layer et al., 1988b). This implies that the MT overprint observed in our study has a different, and likely younger age.

Significant younger candidates for this are the high-grade metamorphic events related to collision of the Natal-Namaqua terrains along the southern and western margins of the Kaapvaal craton. It is known from thermochronology on lower crustal xenoliths in kimberlites from the Archaean craton, that this orogenesis significantly increased the cratonic geotherm at ~1.0 Ga across a wide area. (Schmitz and Bowring, 2004). The palaeomagnetic pole position of Natal-Namaqua (Onstott et al., 1986), however, does not overlap with the MT pole of this study either (Fig. 4.9A).

A second regional event is the significantly younger emplacement of the Jurassic flood basalts, and massive dolerite dykes and sills of the Karoo Large Igneous Province (LIP) (Erlank, 1984; Hunter and Reid, 1987; Uken and Watkeys, 1997) The bulk of the lavas are preserved in Lesotho, but significant areas in northern South Africa, Zimbabwe, and Namibia were also covered. In addition, the dolerite swarms and thick extensive sills occur throughout southern Africa (Erlank, 1984). The pole position of the Karoo basalts (Tab. 4.4) and dolerites can be presumed to be primary, based on positive reversal tests (Hargraves and Rehacek, 1997) and is dated at about 180 Ma (combined $^{40}Ar/^{39}Ar$, Hargraves and Rehacek, 1997 and U-Pb zircon and baddeleyite, Duncan et al., 1997; Encarnacion et al., 1996). This position overlaps with the pole position of the MT component in our Archaean
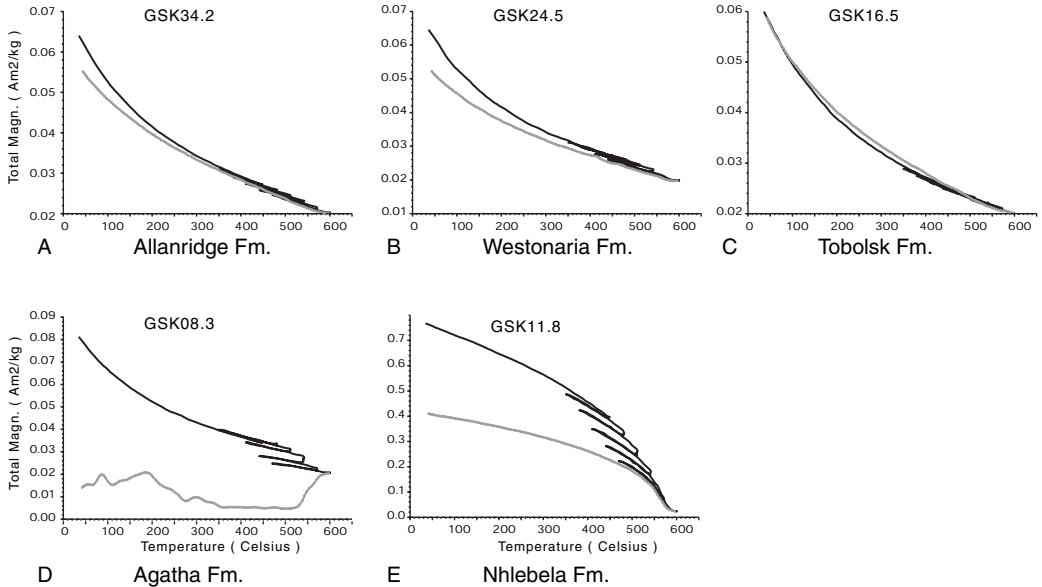
Figure 4.8
Total magnetisation *versus* temperature of selected samples, measured on the Curie balance. Stepwise heating was applied. All steps are in black, except the cooling curve from 600 °C to room temperature, which is drawn in grey. Most samples show pronounced paramagnetic behaviour, except for the Nhlebela Fm. sample. The contribution of (SD) magnetite to the total induced magnetization appears to be small.

samples (Tab. 4.4, Fig 4.9A). The MT pole position is based on 22 sites (Tab. 4.3). The near coincidence of the MT and Karoo pole positions, and the post folding origin of the MT directions, leads us to conclude that the Pongola and Ventersdorp Supergroups were partly remagnetised at 180 Ma, during the extensive Karoo igneous event, which is now generally accepted to be related to the regional mantle plume responsible for the initial break-up of the southern Gondwana supercontinent (Stern and de Wit, 2004; Storey, 1995; White and McKenzie, 1995). Given the size of our sample area, the Karoo igneous event apparently affected a vast part of the Kaapvaal Craton. Our data indicate that regional remagnetisation during this event has affected at least 240,000 km^2 between Johannesburg, Kimberley and the Pongola Basin. This implies that palaeomagnetic studies will be tampered by this event, and that possibly some regions or rock types are entirely remagnetised with a Karoo-age overprint.

Significance of the high temperature (HT) directions

The positive conglomerate test implies that the age of the HT component of the Allanridge Basalt is at least older than ca. 290 Ma. In addition, the existence of a ca. 180 Ma consistent magnetic overprint (MT) suggests that possibly all HT directions from the Pongola and Ventersdorp Supergroups are older than 180 Ma. This leaves a gap of ca. 2.5 Gyr during which the HT magnetisations may have been recorded. A case can be made that most HT directions in our samples are pre-folding. The studied sequences do not appear to have been affected by any major tectonic activity after ca. 2000 Ma (cf. e.g. Eglington and Armstrong, 2004; Layer et al., 1989; Tankard et al., 1982), except for the southern Pongola Basin that was significantly deformed during the Natal-Namaqua orogeny. Indeed, the

pole position for the Agatha Fm. slightly overlaps with the Natal-Namaqua pole (Fig. 4.9A) and a possible ca. 1.0 Ga remagnetisation for this formation can therefore not be excluded. The other HT component poles, however, do not coincide with any pole positions related to the most obvious regional thermo-tectonic events that could have been the cause of remagnetisation. So, if we assume that the HT component is the result of remagnetisation, it must have occurred prior to ca. 2000 Ma. Furthermore, the remagnetisation event(s) must have been local (as opposed to regional), since all studied formations have different tilt-corrected HT poles.

The pole position for the diamictite of the Kiphunyawa Fm. is similar to that of the sampled Post-Pongola dolerite of unknown age. Therefore, it cannot be excluded that the intrusion has remagnetised the diamictite. Further, the Tobolsk lava has consistent HT directions at each site, but the mean of sites is not consistent, neither pre- nor post-folding. This is indicative of early remagnetisation. The remaining Nhlebela, Westonaria and Allanridge Formations, do not show any direct evidence for remagnetisation and the primary NRM could still be preserved in our samples.

A possible apparent polar wander path (APWP) for the Kaapvaal Craton

Constructing an APWP for the Kaapvaal Craton based on published data for the interval between 3.0 and 1.9 Ga, results in a path defined by eight presumed primary pole positions (Fig. 4.9A). Due to this limited number, a cautious approach must be taken when comparing the four possible primary pole positions from our study with this APWP. The pole positions from the Nsuze Group, the Nhlebela (NB) and Agatha (AB) Formations plot relatively close to the 2875 ± 40 Ma (Tab. 4.1) Usushwana Complex (UC) pole position. The pole positions of the Westonaria (WE) and Allanridge (AR) Formations plot closest to the 2782 ± 5 Ma (Tab. 4.1) Derdepoort Basalt (DB) pole (Fig. 4.9A). If the pole positions of the Nhlebela, Agatha, Westonaria and Allanridge Formations are treated as primary then a substantial amount of drift of the Kaapvaal Craton must have taken place in the Neoarchaean. The palaeolatitude of the Pongola Supergroup averages around 30 degrees latitude, whereas the Ventersdorp palaeolatitude averages around 55 degrees, implying a minimum of 3000 km of displacement in ca. 200 Myr (at an average rate of ca. 1.5 cm yr^{-1}). A similar amount of drift (but at a much greater rate of ca. 100 cm yr^{-1}) has recently been recorded in a palaeomagnetic study of the Neoarchaean of the Pilbara Craton, western Australia. Here, Strik et al. (2003) have demonstrated that ca. 3000 km of drift occurred within 3 Myr, between 2721 Ma and 2718 Ma during the formation of the Neoarchaean Nullagine and Mount Jope Supersequences.

Figure 4.9 (opposite)
A) Aitoff projection of a possible apparent polar wander path (APWP) for the Kaapvaal Craton from ca. 3200 to ca. 1900 Ma (grey arrow) showing approximate pole ages. Bold poles NB, AB, KD, PD, WE, AR and MT from this study. NP (Layer, 1986; Layer et al., 1998); UC (Layer et al., 1988a); GC (Evans, 1966); MG (Evans and McElhinny, 1966); DB (Wingate, 1998); MP (Layer et al., 1989), MP$_N$ is the normal, published direction, MP$_R$ is the reversed direction to allow for a more reasonable APWP; OL (Evans et al., 1997); BC (Hattingh, 1986); WD (Hanson et al., 2004); NN (Onstott et al., 1986) and KB from (Hargraves and Rehacek, 1997). See legend for code explanation.
B) Nelshoogte Pluton site VGP positions and mean pole position (Layer, 1986; Layer et al., 1998). Although the mean pole has a small α_{95}, the VGPs have large errors; therefore, the precision parameter is small ($k = 9$).
C) Modipe Gabbro site VGP position and mean pole position (Evans and McElhinny, 1966). The precision parameter is relatively low ($k = 22.4$) and samples have been measured without progressive demagnetisation.
D) Usushwana Complex site VGP position and mean pole position (Layer et al., 1988a). The large spreading of the VGP directions result in an inaccurate mean pole determination. The distribution of VGPs is not Fisherian.
E) Derdepoort Basalt site VGP position and mean pole position (Wingate, 1998). Site VGPs are often well-determined, but the mean pole position underestimates the real distribution. The precision parameter is higher in situ than tilt corrected.
F) Mbabane Pluton site VGP position and mean pole position (Layer et al., 1989), which shows large individual errors.

Code	N	Dec (°)	Inc (°)	plat (°)	latp (°)	longp (°)	a95 (°)	Age (Ma)	Ref.
KB	6	156.0	53.0	33.6	69.2	278.3	3.3	183 ± 5	1
MT	20	330.7	-54.0	34.5	64.5	273.6	4.3	183 ± 5	
WD	nya	nya	nya	nya	-15.6	197.1	8.9	1879-1872	2
BC	6	195.6	-40.0	22.8	-39.5	227.0	10.9	2050 ± 12	3
OL	20	264.8	-21.1	10.9	0.5	280.7	5.3	2222 ± 13	4
MP	5	65.4	8.9	4.5	19.7	105.7	9.4	2687 ± 6	5, 6
AR	8	188.7	60.7	41.7	-75.0	0.1	8.8	~2708 ± 4	
WE	4	66.2	79.1	68.9	-17.1	47.9	18.8	2714 ± 8	
DB	8	222.7	76.6	64.5	-39.6	4.7	17.5	2782 ± 5	7
MG	10	154.5	85.0	80.1	-32.8	30.8	10.4	> 2783	8
UC	18	304.3	52.7	33.3	9.2	347.0	7.6	2875 ± 40	5, 9
PD	1	132.2	32.1	17.4	-45.0	123.6	n/a	unknown	
KD	1	148.1	19.4	10.0	-55.3	145.2	n/a	unknown	
AB	4	276.7	51.5	32.2	-9.4	333.0	8.9	2940 ± 22 ?	
NB	2	327.0	46.0	27.4	25.9	358.4	n/a	2984 ± 2.6 ?	
NP	17	293.1	7.0	3.5	17.6	309.8	9.0	3197 ± 18	5, 10

Table 4.4
Summary palaeomagnetic results (this study and published data) for the Kaapvaal Craton between 3.2 and 2.0 Ga. latp = latitude of pole position, longp = longitude of pole position, see Table 4.2 for explanation of other abbreviations. Confer Figure 4.9 for explanation of codes. Nya = not yet available. Palaeomagnetic references: (1) Hargraves and Rehacek, 1997; (2) Hanson et al., 2004; (3) Hattingh, 1986; (4) Evans et al., 1997; (5) Layer, 1986; (6) Layer et al., 1989; (7) Wingate, 1998; (8) Evans and McElhinny, 1966; (9) Layer et al., 1988a; (10) Layer et al., 1998.

When the Post-Pongola dolerite (PD) and the Kiphunyawa Fm (KD) pole positions are compared to the above-suggested APWP, it is apparent that they plot far away from the trajectory between the Usushwana Complex (UC) pole and the Derdepoort basalt (DB) pole (Fig. 4.9A). If the UC and DB poles are indeed primary, it provides an additional indication that the Kiphunyawa Fm. (KD) is remagnetised by the adjacent Post-Pongola (PD) dolerite. The age of this remagnetisation is not known.

Assessment of the Kaapvaal Craton APWP
The age of the pole positions presented in this study are poorly constrained. Other than a positive conglomerate test on a Permian Karoo Supergroup conglomerate, a preserved primary direction cannot be confirmed by robust palaeomagnetic tests. Much of the interpretation of the APWP therefore relies on the nine published pole positions. Between 3.0 and 1.9 Ga the most important of these poles are: the Usushwana Complex (UC) pole, the Modipe Gabbro (MG) pole, the Derdepoort Basalt (DB) pole and the Mbabane Pluton (MP) pole (Tab. 4.4). In addition, the ca. 3.2 Ga Nelshoogte Pluton (NP) pole is listed in the GPMDB, and we tentatively consider it as a starting point for the APWP of the eastern Kaapvaal craton. We caution that no solid conclusions can be drawn from the path between 3.2 and 2.9 Ga, since at 3.2 the eastern Kaapvaal Craton had not yet completely amalgamated and stabilised, and stabilization of the entire craton probably only occurred around 2.9 Ga

(e.g. de Wit et al., 1992; Moser et al., 2001). The relevant pole positions are discussed below from oldest to youngest.

The pole position for the Nelshoogte Pluton is not confirmed by any field tests and no palaeo-horizontal can be determined. Although the Nelshoogte data show both normal and reversed directions, the reversal test is indeterminate (Layer, 1986; Layer et al., 1998). With an average α_{95} of 33.7 (average from 14 sites, 3 sites had only one accepted direction), the site VGPs are not well constrained (Fig. 4.9B). Further, given the wide range of NRM intensities including unusually high intensities (> 1.0 A/m), part of the data is likely affected by lightning. The precision parameter for the mean pole position ($k = 9$) questions the statistical relevance of the Nelshoogte Pluton pole position. The criterion used to accept this pole position as a primary position relies only on the fact that the average direction does not coincide with younger pole positions. The primary nature of the Nelshoogte Pluton pole position can therefore not be verified.

The Usushwana pole position cannot be subjected to rigorous palaeomagnetic tests either (Layer et al., 1988a), and no palaeo-horizontal can be determined. The Usushwana pole position has been inferred as primary because its direction does not coincide with any younger pole positions. Although the position is slightly better determined ($k = 22$) than for the Nelshoogte Pluton (Tab. 4.4), the spreading of site VGPs is still large (Fig. 4.9C) and does not conform to a Fisher distribution ($M_e = 1.292$, cf. Fisher, 1953; Tauxe, 1998). This implies that the mean pole has no statistical meaning and can thus not be demonstrated to be primary.

The palaeomagnetic data for the Modipe Gabbro (as well as the adjacent Gaborone Complex) were acquired without progressive demagnetisation, and no palaeo-horizontal can be determined. Directions were measured once "stable endpoints" were reached (Evans and McElhinny, 1966), (GC, Fig 4.9A, Evans, 1966). The Gaborone Complex pole has a very low precision parameter ($k = 7.04$) that has previously been considered unreliable (Wingate, 1998); and we concur with that. The determination of the Modipe Gabbro pole (Fig. 4.9D) is slightly better ($k = 22.4$). However, given the used demagnetisation method, the Modipe Gabbro pole position cannot be considered much more reliable than the pole for the Gaborone Complex. Also, no field tests can confirm a primary NRM, so this assumption remains untested.

The pole position for the Derdepoort basalt is interpreted as primary based on a positive conglomerate test (Wingate, 1998). However, the site VGPs are dispersed and show a stretched band from the equator to the pole, and there seem to be two distinct groups within the distribution (Fig. 4.9E). The large α_{95} (17.5°) of the mean pole underestimates the real distribution. Further, the precision parameter of the mean pole position decreases from $k = 46$ in situ to $k = 29$ with tectonic correction, which is suggestive of a negative fold test. Therefore, the primary nature of the pole position for the Derdepoort basalt cannot be demonstrated convincingly with the available data.

No palaeomagnetic tests are available to test the validity of the primary nature of the Mbabane Pluton pole position (Layer et al., 1989) and no palaeo-horizontal can be determined. The pole position is based on five site VGPs, with an average α_{95} of 23.8° per VGP, which does not result in a well-determined pole position (Fig. 4.9F). Individual specimens from the Mbabane Pluton vary in intensity, and many exceed 1.0 A/m (cf. Layer, 1986), which, in our experience, is almost invariably indicative of a lightning induced IRM for these Archaean rocks. Without field tests, the only indication that the Mbabane Pluton

pole position may be primary is that it does not coincide with younger pole positions. Hence, there is no solid basis for assuming that this pole is primary.

Palaeoproterozoic pole positions for the Kaapvaal Craton appear better defined. Pole positions for the Ongeluk lavas (OL), the Bushveld Complex (BC) and the Post-Waterberg dolerites (WD) (Fig. 4.9A and cf. Tab. 4.1) have been successfully subjected to a conglomerate (breccia) test, a fold test, and a reversal test respectively.

In summary, there are no robust pole positions for the Archaean Kaapvaal Craton that can confidently be called primary. The argument that a pole position could be primary, because it does not correspond with a younger pole on the APWP, relies on a solidly established and detailed APWP. This is not the case yet for the Kaapvaal Craton. Both published data and our new data are of similar variable quality that preclude construction of a reliable Archaean APWP for the Kaapvaal Craton. This implies that estimates of amounts and speed of rifting of the Kaapvaal Craton between 3.0 and 1.9 Ga, as made above and by e.g. Kröner and Layer (1992); Layer et al. (1989), must be considered with utmost caution, just because solid proof is lacking.

Also, in comparing the present Archaean APWP of the Kaapvaal Craton to that of other cratons, interpretation must be considered with great care. Based on the currently available palaeomagnetic data, for example, the Archaean connection between the Kaapvaal and Pilbara Cratons (Strik et al., 2003; Wingate, 1998; Zegers et al., 1998), albeit permissible, has a low level of confidence. Whereas pole positions that determine the APWP of the Pilbara Craton have relatively high precision for at least some intervals, this is not the case yet for the Kaapvaal Craton. The large time gaps between pole positions of the Kaapvaal Craton therefore still allow for multiple and competing tectonic interpretations.

Conclusions

This study has demonstrated the following:
- Five out seven studied formations have provided a mean pole based on a stable HT remanent magnetisation, namely the Nhlebela, Agatha, Westonaria and Allanridge Formations, and a Post-Pongola dolerite. Basalts from the Tobolsk Formation are almost certainly remagnetised, probably early in their tectonic history. The diamictite of the Kiphunyawa Formation was probably remagnetised during the intrusion of a Post-Pongola dolerite of unknown age.
- The age of the characteristic (HT) remanent magnetisation (ChRM) can be constrained to be at least ca. 290 Ma for the Allanridge Fm. based on a positive Karoo Supergroup-aged conglomerate test. For the Nhlebela, Agatha and Westonaria Formations, the ChRM is older than 180 Ma, which is a dated secondary overprint that coincides with the pole position of Karoo Supergroup basalts and dolerites and the onset of the break-up of Gondwana
- There appears to be little effect on the craton of the ca. 1.0 Ga Natal-Namaqua orogeny. The only exception comes from the Agatha Formation that may have been affected by this event. Given that no other major tectonic phase occurred after ca. 2000 Ma and that the pole positions of the four formations are all different, the HT magnetisation is likely pre-folding. Because these pole positions do not correspond to the poles for the Bushveld Complex or the Vredefort impact, it is possible that the primary NRM is still preserved, although no field tests can confirm this.

- A major part of the Kaapvaal Craton has been affected by a remagnetisation event related to the magmatism of the Karoo LIP. A consistent remagnetisation overprint was found in 22 sites, both in the Pongola and in the Kaapvaal Supergroup. It can be estimated at 180 Ma, which is the age of the coinciding pole position of the Karoo basalts.
- The quality of existing palaeomagnetic data do not allow construction of a reliable Archaean APWP for the Kaapvaal Craton, because no field tests can confirm inferred primary pole positions. This implies that available palaeomagnetic data cannot convincingly determine drift rates for the Kaapvaal Craton and cannot test a possible Archaean "*Vaalbara*" connection between the Kaap*vaal* and Pil*bara* Cratons.

Acknowledgements

Chapter 5

Similarity between the late Archaean and current geodynamo: secular variation and palaeointensity analysis of 2.8-2.7 Ga flood basalts from the Pilbara Craton, Australia

Similarity between the late Archaean and current geodynamo: secular variation and palaeointensity analysis of 2.8-2.7 Ga flood basalts from the Pilbara Craton, Australia

Abstract

The character of the magnetic field in the Archaean is an important factor in determining the nature of the early Earth's geodynamo, a time possibly without a solid inner core. The database of accurate Archaean palaeointensity estimates is small and even less is known about Archaean secular variation. We used recent palaeomagnetic studies of the ca. 2775-2715 Ma flood basalt dominated Nullagine and Mount Jope Supersequences of the Pilbara Craton, Australia, for an analysis of palaeosecular variation and for palaeointensity measurements, for which we used the recently developed IZZI protocol. The dipole moment at 2772 ± 2 Ma is determined at 28.1 ± 9.3 ZAm^2, and at 2721 ± 4 Ma at 22.1 ± 4.2 ZAm^2. These values are at the low end, although within error, of the average dipole moments between 84 and 1 Ma, (55 ± 30 ZAm^2). Analysis of palaeosecular variation suggests that in the late Archaean the geodynamo operated in a similar way as during the last 5 Myr. Together with low but not anomalous palaeointensities and the occurrence of geomagnetic reversals, we must conclude that the Archaean geodynamo worked no different than today. This may imply, but cannot prove, that the growth of the solid inner core commenced before 2775 Myr ago.

Introduction

Variations of the magnetic field intensity and secular variation are important factors determining the nature of the geodynamo. The present day geodynamo is generated by outer core convection. The behaviour of the magnetic field strongly depends on, firstly, the role of core mantle boundary (CMB) processes, which according to recent numerical dynamo models influence secular variation, reversals and excursions, and reversal frequency, (e.g. Glatzmaier et al., 1999; Glatzmaier and Roberts, 1995; Kuang and Bloxham, 1997). Secondly, the solid inner core has been argued to have a stabilising effect on the magnetic field (Hollerbach and Jones, 1993), while the growth of the solid inner core plays a role in maintaining the magnetic field (Buffett and Bloxham, 2002; Labrosse et al., 2001).

So far, the age of inner core nucleation has not been determined unambiguously. Labrosse and Macouin (2003) estimate the age at 1.0 ± 0.3 Ga, with a maximum of 2.5 Ga. The maximum age, however, can be as high as 3.0 Ga if radioactive elements are present in the core. Consequently, the late Archaean (3.0-2.5 Ga) may lack a solid inner core. Investigating the behaviour of the Earth magnetic field of the late Archaean can therefore provide crucial information about the significance of the inner core for the geodynamo. Without the stabilising function of the inner core, the geomagnetic field may show a more chaotic behaviour, and high reversal frequencies and large secular variation may occur (cf. Gubbins et al., 2003; Hollerbach and Jones, 1993).

Palaeosecular variation (PSV) and field intensity of the last 5 Myr for example are well studied (Constable and Johnson, 1999; McElhinny and McFadden, 1997; Tauxe et al., 2003), but until now no large or coherent dataset was available to determine secular variation in the late Archaean. In addition, very few reliable palaeointensity estimates exist (cf. Valet, 2003). Recent palaeomagnetic studies of the ca. 2775-2715 Ma flood basalt dominated Nullagine and Mount Jope Supersequences, Pilbara Craton, Australia (Strik, 2004; Strik et al., 2003) have generated a data set of 141 sites. The NRM is of primary nature, based on positive fold, reversal and conglomerate tests and the occurrence of the oldest geomagnetic reversals indicate a dipole dominated (GAD) field. We therefore think that this database is an excellent candidate for PSV analysis.

Here, we present an analysis of PSV and the results from palaeointensity measurements on sister samples of those used by Strik (2004); Strik et al. (2003). Selection of samples was based on NRM behaviour (single component magnetisation) and on detailed Curie balance measurements, which we have optimised for detection of alteration. The palaeointensity measurements were done using the recently developed IZZI (In-field, Zero-field; Zero-field, In-field) protocol (Yu et al., 2004), which resulted in a field strength estimate for both the Nullagine and the Mount Jope Supersequence. The virtual geomagnetic pole (VGP) scatter of both individual and grouped units from these sequences were analyzed and compared to the palaeosecular variation database for lavas (PSVRL) of the last 5 Myr (McElhinny and McFadden, 1997) and model predictions (using TK03.GAD, Tauxe and Kent, 2004) for similar palaeolatitudes as indicated by the real data. The outcome of the combined intensity, secular variation, and palaeomagnetic data of Strik (2004); Strik et al. (2003), questions a relatively young age of solid inner core nucleation or its role in the behaviour of the geomagnetic field.

Geology and sampling

The geology of the Nullagine and Mount Jope Supersequences is described in detail by Blake (1993) and Blake (2001) and is here briefly summarised. The two supersequences
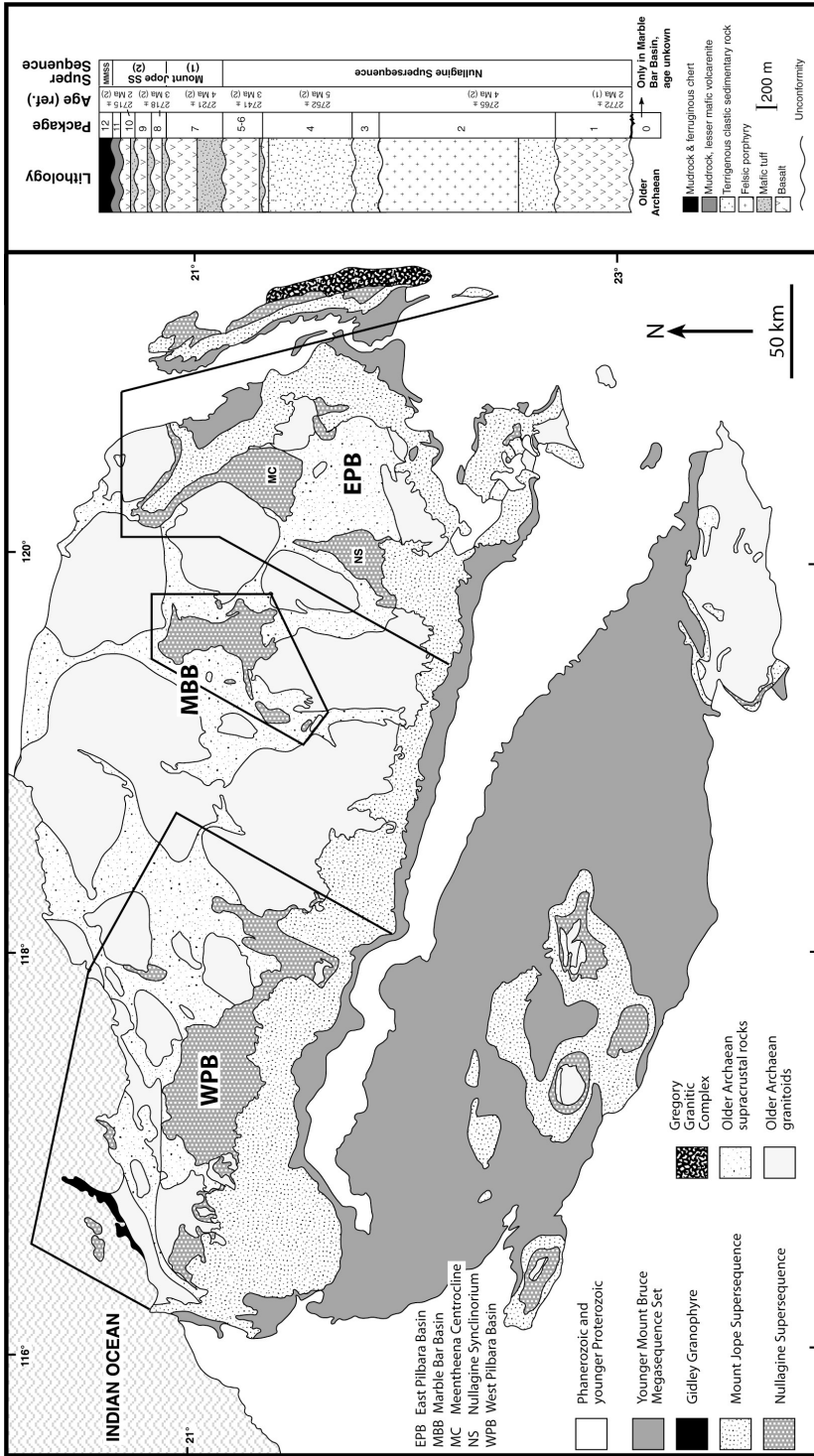
Figure 5.1
Simplified geological map of the Pilbara Craton and simplified lithostratigraphic column of the Nullagine Synclinorium, modified after Blake (2001). The stratigraphy of the Nullagine Synclinorium is shown, because here the succession is most complete. Age references: (1) Pb-Pb baddeleyite, Wingate, 1999; (2) U-Pb SHRIMP zircon, Blake et al., 2004.

are interpreted as the rock record of two phases of continental break-up. The first phase is marked by the extrusion of large volumes of subaerial flood basalts, followed by development of extensional sedimentary basins and associated felsic and mafic volcanics. The second phase is associated with mafic and minor felsic volcanism (Fig. 5.1). The Nullagine and Mount Jope Supersequences have been subdivided into 12 Packages in the Nullagine Synclinorium (Fig. 5.1), based on regional unconformities (Blake, 2001). These Packages are provisionally numbered from 1 to 12 until their full regional extent is known. A regional correlation is currently in progress (Blake, 2004) and recent palaeomagnetic work (Strik, 2004; Strik et al., 2003) seems to confirm the stratigraphic framework of Blake (2004). The palaeomagnetic work also demonstrated the existence of an older flood basalt package, which uniquely occurs in the Marble Bar Basin (Fig. 5.1) and which is provisionally named Package 0. The Nullagine and Mount Jope Supersequences have recently been dated with high precision (Fig. 5.1, Blake et al., 2004; Wingate, 1999). The succession is generally only gently folded and the metamorphic grade does not exceed 200 MPa and 300 °C (Smith et al., 1982).

The samples used for palaeointensity determination were taken from the Meentheena Centrocline in the East Pilbara Basin (Fig. 5.1). Rock core samples were initially collected for NRM analysis (Strik, 2004; Strik et al., 2003), and the most promising specimens of these rock core samples were selected for palaeointensity determination. For this study, we selected flood basalt specimens from Package 1 (GSP61-63, 65, and 66); felsic porphyry samples from Package 2 (GSP91); and flood basalt samples from Package 7 (GSP77-79). Samples for PSV analysis come from 141 sites distributed over the East Pilbara, Marble Bar and West Pilbara Basins (Strik, 2004; Strik et al., 2003).

Methods

Preselection of palaeointensity samples

Ideal samples for palaeointensity determination are samples that have a single (primary) component of NRM, have mainly (pseudo)single domain grains and do not show alteration upon heating. In practice, good specimens are hard to obtain and many palaeointensity experiments have a low success rate. For this study, we first identified sites for which at least three samples had a single NRM component. A modified horizontal translation Curie balance that applies a cycling field (Mullender et al., 1993) was used to study the degree of alteration of samples upon heating. Small amounts of material (60 to 120 mg) were crushed to a coarse powder and subjected to a number of heating-cooling cycles during which the magnetic field fluctuated between 150 and 300 mT. The total magnetic moment of the samples was measured every 10 seconds. Samples were first heated to 450 °C, maintained at the set point for 10 minutes and cooled down to 350 °C. The cycle was repeated for 480, 510, 540 and 570 °C, each time leaving the sample for 10 minutes at the set point and subsequently cooled down to 100 °C less. A final heating step to 600 °C was carried out, after which the sample was cooled down to room temperature. Samples that showed large amounts of alteration were discarded as candidates for palaeointensity measurements, except for a few test cases.

Palaeointensity determination using the IZZI protocol

We used the so-called IZZI protocol (Tauxe et al., 2004; Yu et al., 2004) for our palaeointensity experiment, which uses double and triple heating. For every other temperature step the order of the double heating procedure is changed. For the first

temperature step, the specimens are heated and cooled in zero-field first, then in-field (ZI) and for the next temperature step, specimens are heated and cooled in-field first, then zero-field (IZ). Following the ZI step, specimens are reheated a third time to the same temperature and are cooled in zero-field. This is the so-called pTRM tail check, which tests whether the pTRM gained during the in-field step can completely be removed by reheating to the same temperature (Riisager and Riisager, 2001; Tauxe and Staudigel, 2004). Finally, between ZI steps, the specimen is reheated to a lower temperature and cooled in the laboratory field. The pTRM gained in this step is compared to the same lower temperature in-field step, which is called the pTRM check (Coe et al., 1978). A difference between these two steps can indicate experimental noise, but large changes usually imply alteration of the specimen. The applied field for our experiments was 20 µT. The used temperature steps were from 250 to 450 °C in 50 °C steps; 480, 500, 510 and 520 °C; from thereon we used 5 °C increments until 580 °C; and a final step of 600 °C.

Palaeosecular variation analysis

The data set for analysis of secular variation includes 141 site mean directions (electronic appendix on website, Strik, 2004). We only used sites of which the site mean direction is based on three or more directions; on average, the site means were based on 6.2 directions per site. The statistical model for PSV of Tauxe and Kent (2004), developed for the GAD of the last 5 Myr (TK03.GAD), was used to generate a set of directions for latitudes equal to palaeolatitudes of the late Archaean data set. It is possible to draw a specified number of Gauss coefficients from the model. The Gauss coefficients are converted to a local declination, inclination and intensity series. Subsequently, these were converted to virtual geomagnetic poles (VGPs). The angular standard deviation (ASD) of the VGPs of the model data was compared to the ASD of the late Archaean data set.

Results

Curie balance measurements

At first glance, many samples generate similar results for the measurements on the Curie balance (Fig. 5.2). Generally, samples show a weak magnetisation and the paramagnetic contribution to the total magnetisation is prominent. The differences lie in the interval between 350 and 600 °C. With increasing temperature, some samples clearly show alteration, such as GSP21.5, 63.6, 179.2 and U901.1 (Fig. 5.2). Also, for these samples it is apparent that alteration progresses with time. For example, when samples are kept at 540 °C for 10 minutes, sample GSP21.5 clearly loses magnetic moment, whilst sample U901.1 gains magnetic moment during the 10 minutes at set point. These samples are therefore not suitable for palaeointensity determination, because they will alter during the repeated exposure to high temperatures. Other samples, like GSP69A.2, 78.8 and 158.1 show little evidence for alteration in the Curie balance plots (Fig. 5.2).

Despite the apparent lack of alteration, however, the paramagnetic contribution to the total magnetic moment is significant. Although the paramagnetic behaviour does not contribute to the pTRM acquisition, it actually masks the small part of ferrimagnetic contribution that is present (clearly visible in e.g. GSP78.3, less obvious in e.g. GSP69A.2, Fig. 5.2). To visualise the ferrimagnetic behaviour, the paramagnetic moment was subtracted from the total magnetic moment. To do this, first the specific (mass dependent) paramagnetic and diamagnetic susceptibilities were determined, using least square fitting. The susceptibility is proportional to the inverse of the temperature, according to Curie-Weiss
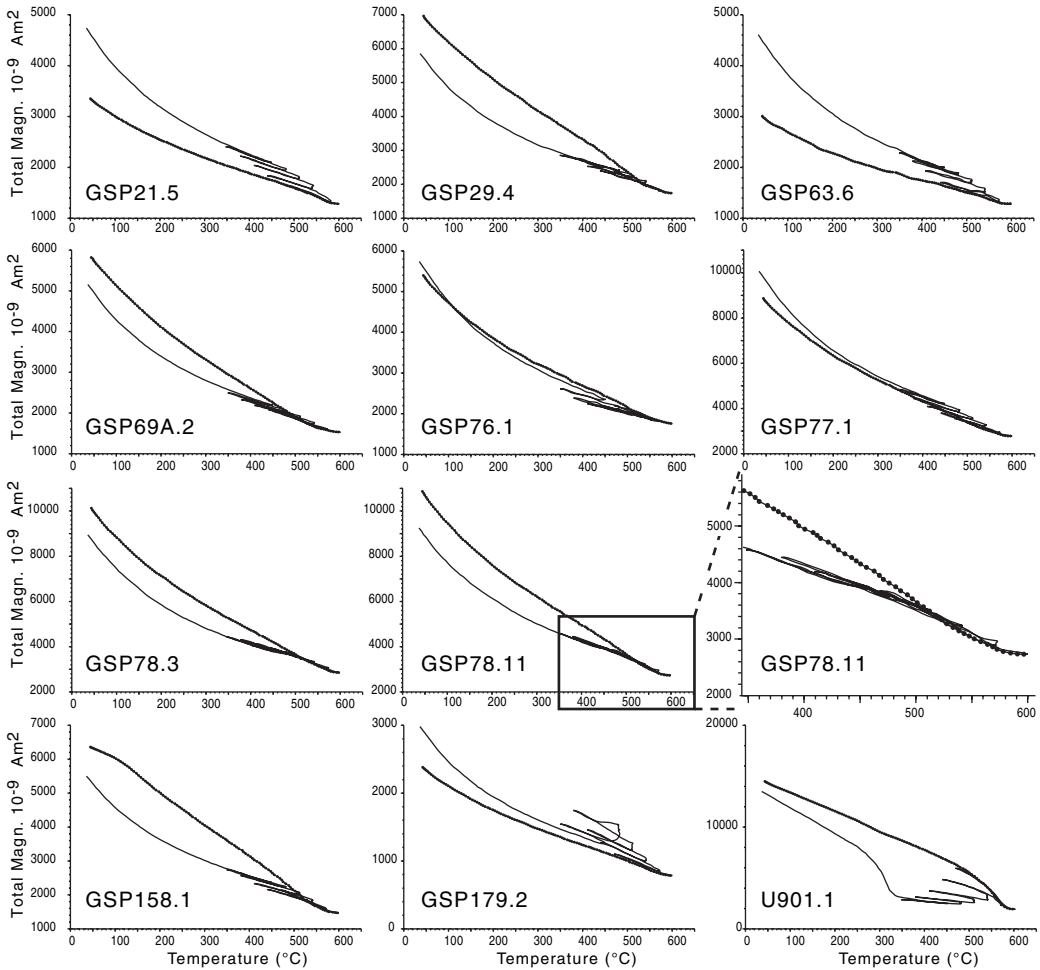
Figure 5.2
Diagrams of total magnetisation *versus* temperature of selected samples measured on the Curie balance. Solid lines represent heating curves and lines with dots are cooling curves. Some samples show little evidence for alteration, e.g. GSP77-79, whereas e.g. GSP21.5, 63.6, 179.2 and U901.1 have clearly altered during the experiment. Notice that alteration progresses when set point temperatures are maintained during 10 minutes.

law. The total paramagnetic moment is calculated by multiplying the specific paramagnetic susceptibility by the applied field. Subsequently, the result is subtracted from the total magnetic moment, which gives the total ferrimagnetic moment.

The plots of the ferrimagnetic moment show that some samples that did not seem to alter much judging from the total magnetic moment plot (e.g. GSP69A.2, Fig. 5.2), have lost up to 50% of ferrimagnetic moment at 510 °C because of alteration (Fig. 5.3). These samples are therefore also not suitable for palaeointensity determination. Sometimes, the paramagnetic moment makes up most of the total magnetic moment, in which case the ferrimagnetic diagram is not useful, as for GSP76.1, which shows considerable noise (Fig.
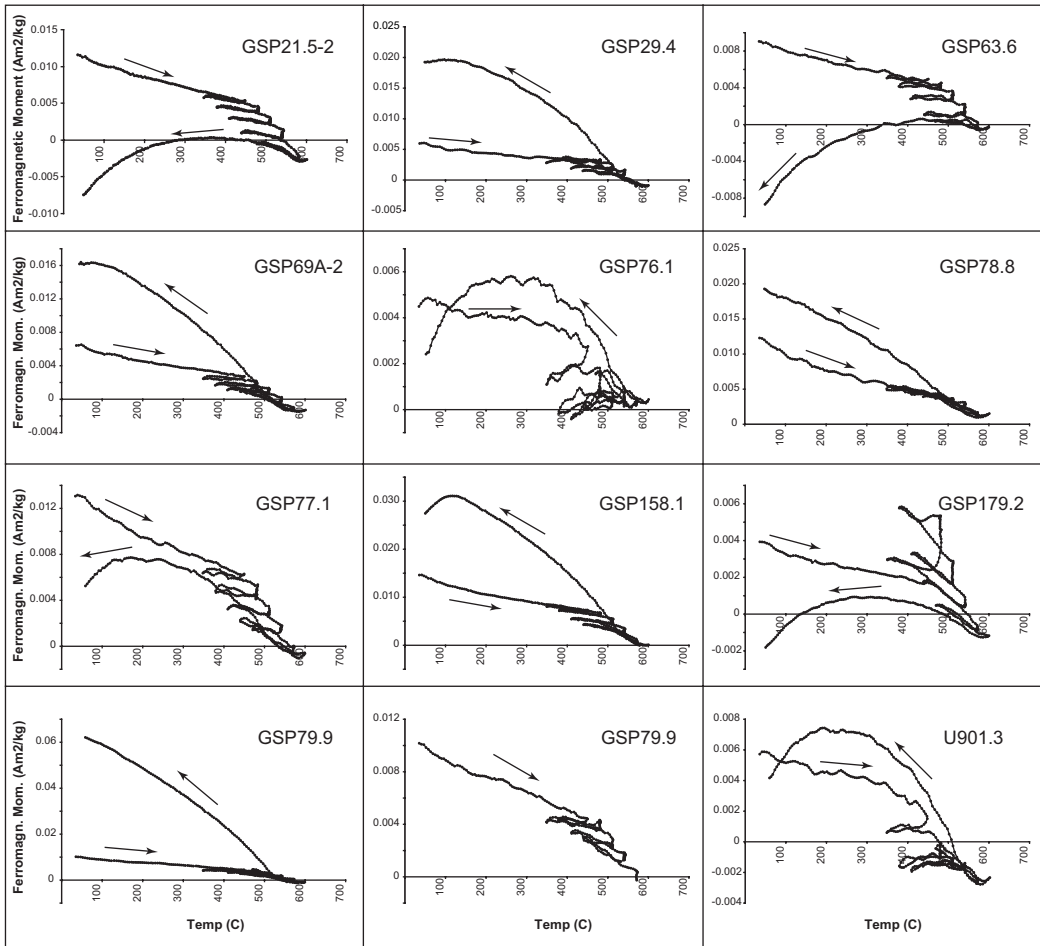
Figure 5.3
Diagrams of the total ferrimagnetic moment *versus* temperature of selected samples calculated from Curie balance measurements. Arrows indicate heating and cooling curves. Many samples show clear alteration, e.g. GSP179.2, U901.3 and GSP77.1. The latter did not show clear alteration from the total magnetisation plot (cf. Fig. 5.2). Sample GSP78.8 shows hardly any alteration and is considered a good target for palaeointensity determination.

5.3). Equally, if there is no clear paramagnetic behaviour (e.g. U901.1, Fig. 5.3), the plot of ferrimagnetic moment is obviously useless.

Based on the outcome of the Curie balance measurements, Package 7 sites GSP77-79 were chosen for palaeointensity determination, as samples from these sites show the least alteration, GSP78 in particular. Samples of Package 1 sites GSP61-63, 65 and 66 sometimes showed alteration starting at 480 °C, but were chosen as the next best target. Package 2 samples from site GSP91 showed clear alteration, but was included to test the preselection method.

Results of the Thellier experiment

The selected samples from Package 1 flood basalts give variable results. Sites GSP 62 and 66 are clearly affected by a secondary component (Fig. 5.4A). Nearly all samples show evidence for alteration from 510 to 520 °C upwards. For samples of which alteration is pronounced (Fig. 5.4B), no reliable palaeointensity estimate can be made. The interpreted fraction of NRM for the best Package 1 samples lies between 250 and 530 °C (Fig. 5.4C). The selected samples from the Package 2 felsic porphyry show a consistent significant alteration with increasing temperature, which is in agreement with the Curie balance results. At 540 °C, the Package 2 samples have unblocked only 10% or less, but alteration at that temperature is pronounced, thus inhibiting reliable interpretations (Fig. 5.4D). For the selected samples of Package 7 flood basalts results are again variable. Sites GSP77 and 79 show clear alteration from 520 °C upward, at which point samples still have less than 10% unblocking (Fig. 5.4E). Site GSP78, however, shows more promising results. Signs of (significant) alteration are apparent only after 540 °C at which point a considerable amount of NRM has been lost, allowing a more reliable interpretation (Fig. 5.4F-H).

To assess the quality of the Thellier-Thellier experiments, we have used six different selection criteria. These are: the fraction of the NRM component used for the slope estimation, parameter f (Coe et al., 1978); the maximum angle of deviation (MAD) of the selected part of the NRM (Kirschvink, 1980); The standard error of the best-fit slope through the selected part of the NRM, also known as "the scatter parameter" β (Coe et al., 1978); the deviation angle (DANG), which is the angle that the best-fit of the selected component makes with the origin (Pick and Tauxe, 1993); the difference ratio sum (DRATS), which is the sum of differences between the original pTRM and the pTRM check, normalised by the pTRM acquired from the highest temperature step used for the best-fit slope of the selected component (Tauxe and Staudigel, 2004); and finally the pTRM tail check (Riisager and Riisager, 2001; Tauxe and Staudigel, 2004), represented by parameter MD, which is the maximum difference (the absolute value of the difference between the original NRMs measured and the second zero field steps), normalised by the vector difference sum of the NRM.

The next step is to determine the values for the quality assessment. Large pTRM tails give high MD values, and often come together with strong zigzagging of the NRM direction (e.g. Fig. 5.4B). Samples with MD values > 5% were discarded, except for GSP61.7 and GSP78.7, for which the higher MD percentage is caused by a single outlier at a higher temperature than the interpreted portion of the NRM. For the other quality criteria, we plotted the cumulative distribution function (CDF) per parameter, to determine the appropriate cut-off as objectively as possible (Fig. 5.5). The following cut-offs were applied: f < 0.2; MAD < 15; β < 0.1; DANG < 15; and DRATS < 50. Samples passing all quality criteria are given a grade A, samples failing one of the quality criteria are graded B, and so forth. For this study, only samples with grade A or B were accepted, except for the above-mentioned samples GSP61.7 and GSP78.7, which were graded C (Tab. 5.1). B_{anc} for Package 1 is determined at 16.0 ± 5.4 μT, which results in a virtual dipole moment (VDM) of 28.1 ± 9.3 ZAm^2 (Z = zeta = 10^{21}) and an average virtual axial dipole moment (VADM) of 25.4 ± 8.5 ZAm^2. B_{anc} for Package 7 is 12.5 ± 1.6 μT, which gives an average VDM of 22.1 ± 4.3 ZAm^2 and a VADM of 19.8 ± 2.5 ZAm^2 (Tab. 5.1).
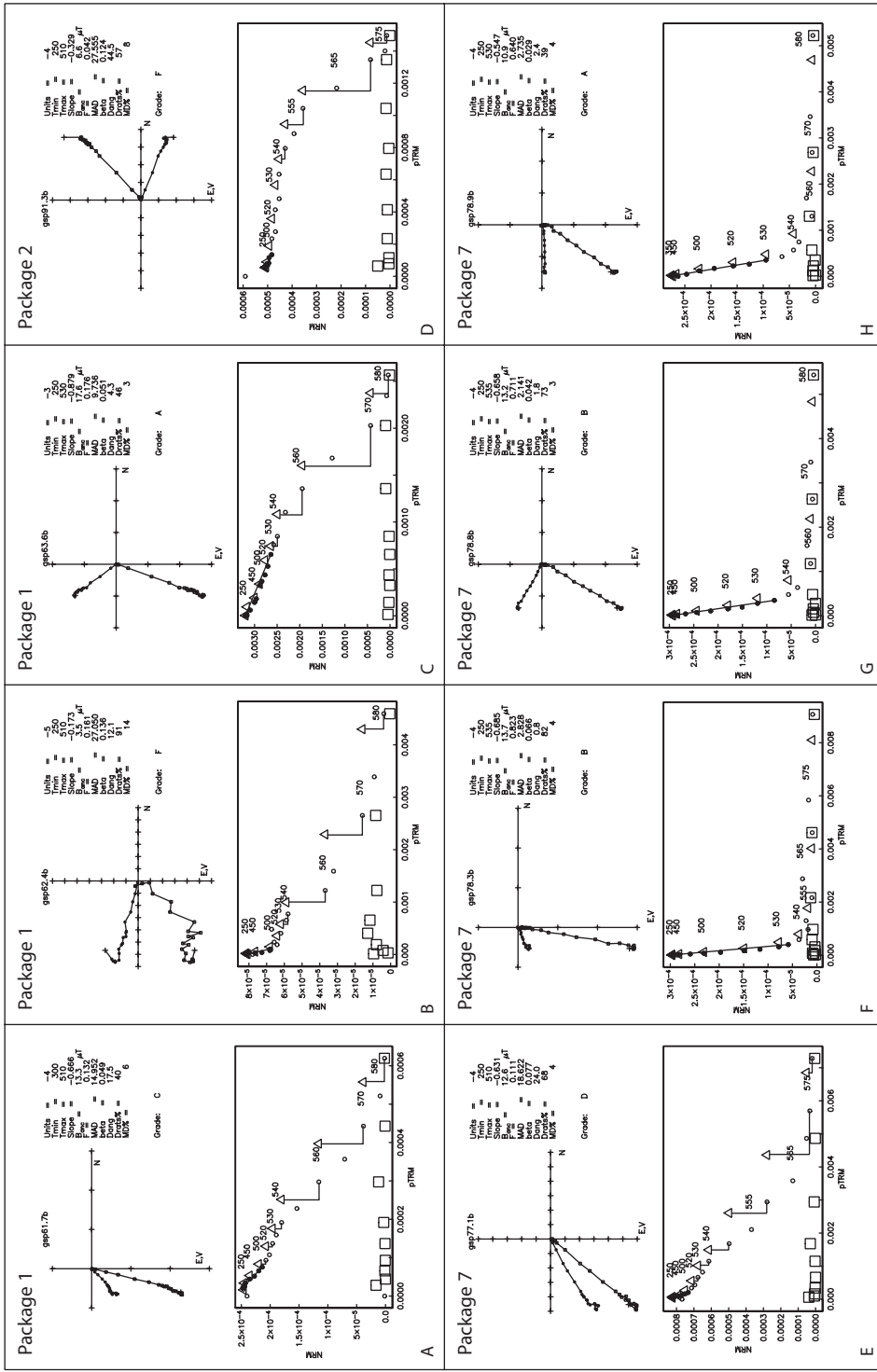
Figure 5.4

A-H: Zijderveld diagrams and NRM *versus* pTRM (Arai) plots of selected samples from Packages 1, 2 and 7. In Zijderveld diagrams, closed symbols represent declination and open symbols the projection of inclination. In Arai plots, squares are pTRM tail checks, triangles are pTRM checks, closed circles with solid line represent the interpreted portion of NRM for which intensity is determined and open symbols are points not included in the intensity estimate.
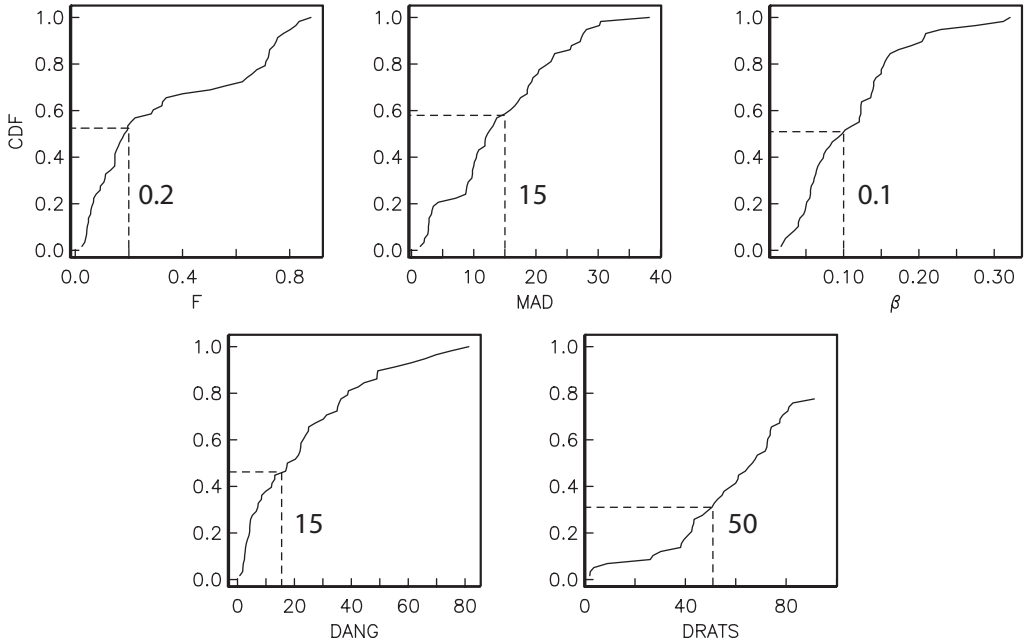
Figure 5.5
Cumulative distribution functions of quality selection parameters for palaeointensity estimates. The cut-off points are indicated with interrupted lines, together with the value.

ASD determination

For a representative estimate of PSV, a significant number of sites is needed per palaeolatitude bin, since the angular standard deviation (ASD) or VGP scatter depends on palaeolatitude (e.g. McElhinny and McFadden, 1997). Our late Archaean data set can be subdivided into a lower group (LG) and an upper group (UG), based on palaeolatitude position. Packages 1 to 7 have palaeolatitudes within error, with an average of 48.6°, for a total of 86 sites. Packages 8 to 11 have palaeolatitudes within error, with an average of 34.4°, for a total of 27 sites (Tab. 5.2). Therefore, 86 and 27 directions were determined in a number of model runs from TK03.GAD, using latitudes of 48.6° S and 34.4° S respectively. Model runs were also done for the respective numbers of directions that determine the averages of Packages 0, 1, 6, 7, 8 and 10. Packages 2 to 5, 9 and 11 were omitted because of the insignificant number of data. Results of the model-runs are summarised in Table 5.2. The ASD values of the model runs and the real data are analysed both with a variable cut-off angle (Vandamme, 1994) and a fixed cut-off angle of 40° (Tab. 5.2). It has been argued that a variable cut-off prevents bias of ASD caused by excursional or transitional data, but for comparison with existing literature (e.g. McElhinny and McFadden, 1997), we have also used a fixed cut-off angle.

A possible error introduced by grouping the data into a lower and an upper sequence is that (block) rotation during the formation of the sequence will affect the VGP scatter. Two rotational events are known. The first rotation affects the lower section, which encompasses three distinct pole positions, namely Package 1, Package 2 and Package 4-7. The Package 2 pole position is reversed with respect to the Packages 1 and 4-7 pole positions,

Package	Sample	Class.	B_{anc}	VDM x 10^{21}	VADM x 10^{21}	inc
1	61.1	A	22.1	38.3		67.2
1	61.3	A	19.9	35.5		69.0
1	61.7	C	13.3	22.8		66.4
1	63.3	A	7.0	13.3		72.2
1	63.6	A	17.6	32.5		70.8
1	63.7	B	16.3	26.1		61.4
mean 1			**16.0 ± 5.4**	**28.1 ± 9.3**	**25.4 ± 8.5**	
7	78.3	B	13.7	23.5		66.7
7	78.7	C	10.8	17.0		59.9
7	78.8	B	13.2	21.7		63.4
7	78.9	A	10.9	19.8		69.9
7	78.10	B	11.7	21.3		70.2
7	78.11	B	14.7	29.6		75.1
mean 7			**12.5 ± 1.6**	**22.1 ± 4.2**	**19.8 ± 2.5**	

Table 5.1
Results of palaeointensity determination for Packages 1 and 7. Capital A means that all quality criteria are met, B means one criterion failed, C means two criteria failed. Abbreviations: class. = classification, VDM = virtual dipole moment, VADM = virtual axial dipole moment.

but has a nearly identical direction as Package 1, so Packages 1 and 2 are grouped together. The mean VGPs of Packages 1-2 and Packages 4-7 were determined and were both rotated onto the pole, so that the two groups have the same mean VGP position, and the VGP scatter can be analysed as a single group without being biased by the rotation of the Pilbara block between Package 1-2 and Package 4-7 times. The second rotational event is that of a significant internal block rotation between the East and West Pilbara Basins at the time that Packages 8 to 10 were extruded. For this reason, the mean Packages 8-10 VGPs of the East and of the West Pilbara Basin were determined separately, and we have applied the same procedure of a common mean VGP. The results are integrated in Table 5.2 (both with and without rotation correction).

It is conceivable that the late Archaean data set includes repeated sampling of the same field vector, because successive basalt flows may have extruded and cooled rapidly after each other (1-2 years) or (near) simultaneously in the case of interfingering flows. We have therefore used two data sets, namely the original set and a set, which is reduced for possible same field sampling (McElhinny and McFadden, 1997). For the latter, the angle θ between successive flows was calculated. We used 6° as the critical value φ, (cf. McElhinny et al., 1996) and if θ is smaller than φ between two (or more) successive flows, they were considered to represent the same field vector, in which case the mean VGP was determined. This reduces, for example, the Packages 1 to 7 data set from 86 to 66 directions (Tab. 5.2). The TK03.GAD model was run again for the new numbers of directions in the reduced data sets (Tab. 5.2) and the ASD was determined again using both a fixed and an optimal cut-off angle (Tab. 5.2).

Fixed cut-off

Series	N	n	cut-off	max. ang.	lon	lat	k	α_{95}	ASD$_{low}$	ASD$_{mean}$	ASD$_{high}$
Upper Group (UG)	27	27	40	38.8	172.7	-60.9	18.5	6.6	16.1	19.0	23.4
UG rotation cor.	27	27	40	31.4	357.4	-90.0	24.2	5.8	14.0	16.6	20.4
Model n27	27	26.3	40	30.7	121.4	86.2	29.7	5.3	12.8	15.1	18.6
Lower Group (LG)	86	82	40	35.5	155.1	-47.0	21.0	3.5	16.1	17.8	19.9
LG rotation cor.	86	85	40	35.0	227.5	-89.5	26.2	3.1	14.4	16.0	17.8
Model n86	86	81.7	40	37.3	138.1	87.3	21.3	3.5	16.0	17.8	19.9
Package 10	10	10	40	23.1	160.4	-62.5	41.7	7.6	9.7	12.6	17.8
Model n10	10	9.9	40	25.7	149.1	85.7	36.2	8.9	11.3	14.7	20.8
Package 8	12	12	40	34.3	186.9	-57.4	15.9	11.2	16.2	20.6	28.2
Model n12	12	11.6	40	28.5	159.0	85.3	27.2	9.0	12.7	16.2	22.3
Package 7	20	19	40	32.8	141.3	-58.7	28.1	6.4	12.6	15.4	19.7
Model n20	20	19.2	40	33.3	302.9	74.6	19.1	8.0	15.6	19.0	24.3
Package 6	14	14	40	31.9	150.0	-56.1	18.3	9.6	15.2	19.1	25.5
Model n14	14	13.7	40	30.6	307.2	76.1	25.7	8.3	13.1	16.4	22.0
Package 1	43	43	40	35.7	160.2	-40.1	32.8	3.9	12.4	14.3	16.8
Model n43	43	42.1	40	35.3	301.3	74.8	22.4	4.9	15.3	17.6	20.6
Package 0	28	25	40	27.4	91.3	-0.2	20.6	6.5	15.1	18.0	22.2
Model n28	28	27.6	40	33.8	297.1	76.5	30.6	5.2	12.9	15.2	18.6

Variable cut-off

Series	N	n	cut-off	max. ang.	lon	lat	k	α_{95}	ASD$_{low}$	ASD$_{mean}$	ASD$_{high}$
Upper Group (UG)	27	27	39.3	38.8	172.7	-60.9	18.5	6.6	16.1	19.0	23.4
UG rotation cor.	27	27	34.9	31.4	357.4	-90.0	24.2	5.8	14.0	16.6	20.4
Model n27	27	25.3	29.5	24.9	144.0	86.4	37.2	4.9	11.4	13.6	16.8
Lower Group (LG)	86	82	37.0	35.5	155.1	-47.0	21.0	3.5	16.1	17.8	19.9
LG rotation cor.	86	80	30.2	27.4	199.6	-88.6	33.9	2.8	12.6	14.0	15.7
Model n86	86	80.9	36.4	35.4	137.7	87.2	22.3	3.4	15.7	17.4	19.6
Package 10	10	10	27.7	23.1	160.4	-62.5	41.7	7.6	9.7	12.6	17.8
Model n10	10	10	32.1	26.6	133.9	85.6	35.7	9.1	11.6	15.0	21.3
Package 8	12	12	42.0	34.3	186.9	-57.4	15.9	11.2	16.2	20.6	28.2
Model n12	12	11.6	33.9	27.8	152.7	84.9	28.5	8.9	12.6	16.1	22.1
Package 7	20	18	29.4	28.8	143.0	-57.2	36.0	5.8	11.1	13.6	17.5
Model n20	20	19.5	40.2	34.6	304.4	75.1	18.9	8.2	16.1	19.5	25.0
Package 6	14	14	39.3	31.9	150.0	-56.1	18.3	9.6	15.2	19.1	25.5
Model n14	14	13.6	33.9	29.1	306.0	76.5	27.9	8.1	12.8	16.1	21.6
Package 1	43	41	27.0	26.4	161.7	-39.1	44.4	3.4	10.6	12.2	14.4
Model n43	43	41.7	36.0	34.3	300.9	74.7	23.7	4.8	15.0	17.2	20.3
Package 0	28	25	37.3	27.4	91.3	-0.2	20.6	6.5	15.1	18.0	22.2
Model n28	28	26.5	29.7	26.5	297.5	75.8	37.2	4.8	11.6	13.7	16.9

Table 5.2
Results of ASD determination for the late Archaean and model data sets. Analysis has been done with fixed and variable cut-off angles, with and without reducing the data set for similar field sampling. For the model data, the average values over 10 runs are given. Abbreviations: Rotation cor. = data corrected for (block) rotation; N = number of directions; n = number of directions after cut-off; max. ang. = maximum accepted angle; lon = longitude; lat = latitude. Cut-off, max. ang., lon, lat, α_{95} and ASD in degrees. Continued on next page.

Fixed cut-off reduced

Series	N	n	cut-off	max. ang.	lon	lat	k	α_{95}	ASD$_{low}$	ASD$_{mean}$	ASD$_{high}$
Upper Group (UG)	22	22	40	38.5	173.3	-60.6	16.0	8.0	17.0	20.5	25.8
UG rotation cor.	22	22	40	30.1	156.2	-90.0	21.4	6.9	14.6	17.6	22.2
Model n22	22	20.6	40	36.0	144.9	86.4	20.6	7.3	14.9	18.1	22.9
Lower Group (LG)	66	63	40	36.1	155.5	-47.7	18.7	4.3	16.8	18.9	21.5
LG rotation cor.	66	65	40	35.4	225.3	-89.3	21.7	3.9	15.7	17.6	20.0
Model n66	66	62.6	40	38.5	154.2	88.1	22.8	3.9	15.3	17.2	19.6
Package 10	7	7	40	25.8	86.7	-85.3	33.1	10.6	10.5	14.2	21.5
Model n7	7	6.8	40	21.8	172.1	83.3	41.8	10.8	10.5	14.1	21.6
Package 8	10	10	40	27.6	252.0	-83.3	23.3	10.2	13.1	16.9	23.9
Model n10	10	9.9	40	25.7	149.1	85.7	36.2	8.9	11.3	14.7	20.8
Package 7	18	18	40	33.2	141.7	-58.4	26.1	6.9	13.0	16.0	20.6
Model n18	18	17.9	40	31.5	122.6	86.0	23.9	7.4	13.9	17.0	22.0
Package 6	11	11	40	29.9	159.3	-55.5	20.2	10.4	14.2	18.2	25.3
Model n11	11	10.4	40	29.1	164.1	84.6	23.2	10.5	13.8	17.7	24.9
Package 1	28	28	40	36.1	160.3	-39.7	22.8	5.8	14.5	17.1	20.9
Model n28	28	27.6	40	33.8	297.1	76.5	30.6	5.2	12.9	15.2	18.6
Package 0	20	18	40	39.1	91.5	-3.3	16.9	8.7	16.2	19.9	25.7
Model n20	20	19.2	40	33.3	302.9	74.6	19.1	8.0	15.6	19.0	24.3

Variable cut-off reduced

Series	N	n	cut-off	max. ang.	lon	lat	k	α_{95}	ASD$_{low}$	ASD$_{mean}$	ASD$_{high}$
Upper Group (UG)	22	22	41.9	38.5	173.3	-60.6	16.0	8.0	17.0	20.5	25.8
UG rotation cor.	22	22	36.7	30.1	156.2	-90.0	21.4	6.9	14.6	17.6	22.2
Model n22	22	20.2	36.1	32.6	136.3	86.5	23.5	7.0	14.2	17.3	21.9
Lower Group (LG)	66	63	39.0	36.1	155.5	-47.7	18.7	4.3	16.8	18.9	21.5
LG rotation cor.	66	65	36.6	35.4	225.3	-89.3	21.7	3.9	15.7	17.6	20.0
Model n66	66	60.8	34.1	31.9	147.0	87.8	26.5	3.7	14.4	16.1	18.4
Package 10	7	7	30.5	25.8	86.7	-85.3	33.1	10.6	10.5	14.2	21.5
Model n7	7	6.8	30.4	21.8	172.1	83.3	41.8	10.8	10.5	14.1	21.6
Package 8	10	10	35.4	27.6	252.0	-83.3	23.3	10.2	13.1	16.9	23.9
Model n10	10	10	32.1	26.6	133.9	85.6	35.7	9.1	11.6	15.0	21.3
Package 7	18	18	33.8	33.2	141.7	-58.4	26.1	6.9	13.0	16.0	20.6
Model n18	18	17.7	34.8	29.3	121.5	85.7	25.5	7.2	13.5	16.6	21.5
Package 6	11	11	37.7	29.9	159.3	-55.5	20.2	10.4	14.2	18.2	25.3
Model n11	11	10.8	41.8	35.1	161.3	84.5	19.3	12.0	15.9	20.4	28.5
Package 1	28	26	31.0	25.1	162.7	-38.0	31.8	5.1	12.2	14.4	17.8
Model n28	28	26.5	29.7	26.5	297.5	75.8	37.2	4.8	11.6	13.7	16.9
Package 0	20	19	44.6	43.8	92.5	-5.4	13.9	9.3	18.1	22.0	28.2
Model n20	20	19.5	40.2	34.6	304.4	75.1	18.9	8.2	16.1	19.5	25.0

Table 5.2 (continued)

Discussion

Effectiveness of Curie balance preselection for palaeointensity studies

This study demonstrates that Curie balance measurements using repeated heating-cooling at consecutively higher temperatures and maintaining set-point temperatures for 10 minutes, provide a quick and reliable method for studying the degree of alteration a specific sample will sustain at different temperatures. Samples that show a high degree of alteration during the successive Curie balance measurements at increasing temperatures also show this during the palaeointensity measurements (Package 2). Further, if alteration occurs only at high temperatures, the strategy of the palaeointensity experiment can be adjusted for this by taking more steps before alteration becomes pronounced. The samples that showed the least evidence for alteration (Package 7, site GSP78) also proved to be most successful in the palaeointensity experiment. Yet, the degree of alteration proved to be more obvious in the palaeointensity experiment than during the Curie balance measurements (e.g. sample GSP78.8, compare Fig. 5.3 with Fig. 5.4G). This can be explained by the longer and more frequent exposure to high temperatures of the IZZI experiment than for the Curie balance measurements.

Field strength in the late Archaean

Out of 56 samples, 12 samples (21 %) appear to be reliable recorders of the palaeofield strength according to our criteria. The applied cut-off values for the quality selection criteria have generated a consistent set of palaeofield strength estimates for Packages 1 and 7. Although we have not been able to meet the criterion of a minimum of 25 estimates to generate a robust estimation of the palaeofield strength (Tauxe and Staudigel, 2004), these
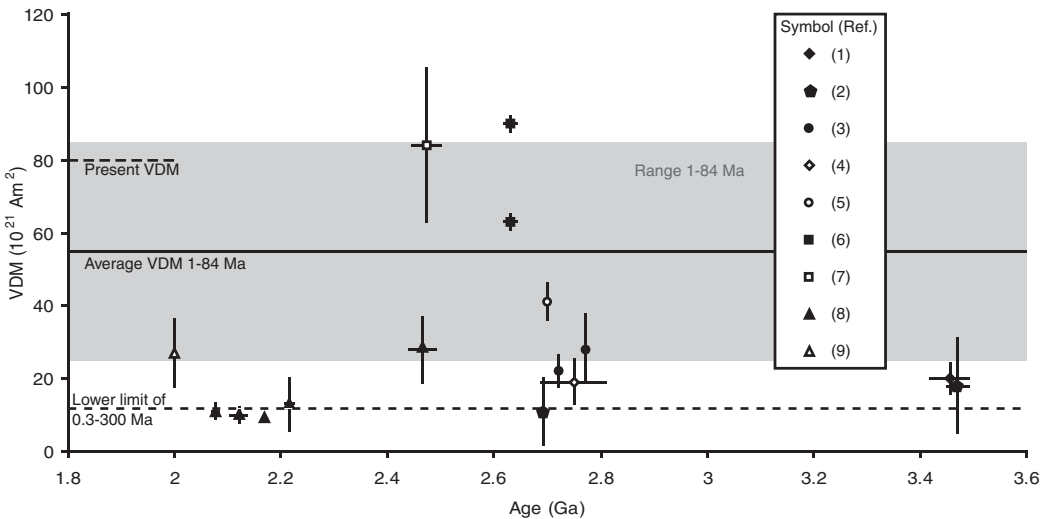
Figure 5.6
Variation of VDM with time for the period between 1.8 and 3.6 Ga. Indicated are the average (solid line) and range (grey box) of VDM in the period between 1 and 84 Ma (Tauxe and Staudigel, 2004), the lower VDM range limit (dashed line) of the period between 0.3 and 300 Ma (Selkin and Tauxe, 2000) and the present VDM value (dashed short line). References to palaeointensity studies: (1) Hale, 1987 (no pTRM checks), (2) Yoshihara and Hamano, 2004, (3) this study, (4) Morimoto et al., 1997, (5) Selkin et al., 2000, (6) Yoshihara and Hamano, 2000, (7) Smirnov et al., 2003, (8) Macouin et al., 2003 and (9) Sumita et al., 2001.
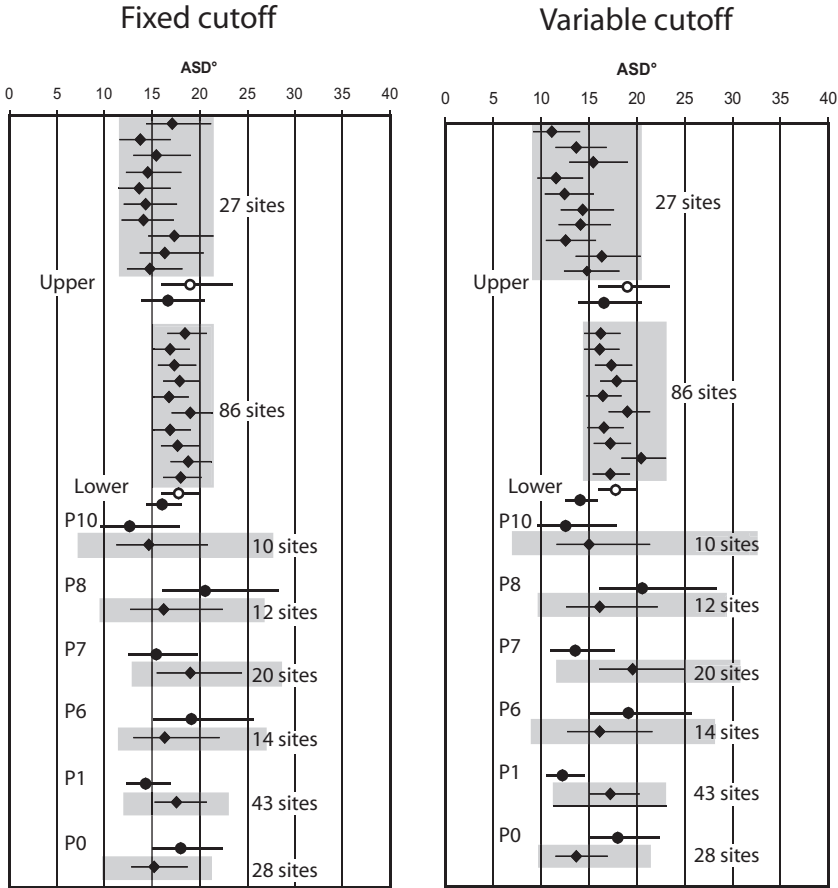
Figure 5.7
Angular standard deviation (ASD) distributions for model (diamonds) and real data (circles), for fixed (40°) and variable cut-off angles, both for the entire and the reduced data sets, with difference between ASD$_{low}$ and ASD$_{high}$ (solid lines). Open circles represent grouped data before (block) rotation correction. Grey boxes represent the total ASD range for 10 model runs. For the upper and lower groups, single model runs are plotted separately, and for the individual packages (P0, P1, P6-P8, P10) the average of 10 model runs is plotted. Generally, the real late Archaean data are in good agreement with the model data for the last 5 Myr. The reduced data sets agree better than the unprocessed sets and fixed cut-off is in slightly better agreement with the model than variable cut-off.

preliminary results indicate a relatively low average VDM of 28.1 ± 9.3 and 22.1 ± 4.2 ZAm^2 in the late Archaean between 2772 ± 2 Ma and 2721 ± 4 Ma. The average field between 84 and 1 Ma is 55 ± 30 ZAm^2 (Tauxe and Staudigel, 2004), which means that the estimates for Packages 1 and 7 are still just within this range, although at the low end (Fig. 5.6). At present, the field strength is ca. 80 ZAm^2.

Few palaeointensity data are available for the Archaean and only a few studies have done pTRM checks (Fig. 5.6). In fact, reliable palaeointensity estimates for the entire Precambrian are sparse. Most studies using recent quality criteria show relatively low palaeointensities, except for the ca. 2.6 Ga diabase dykes of the Slave Province, Canada (Yoshihara and Hamano, 2000) and for single-crystal estimates of the ca. 2.45 Ga Burakovka
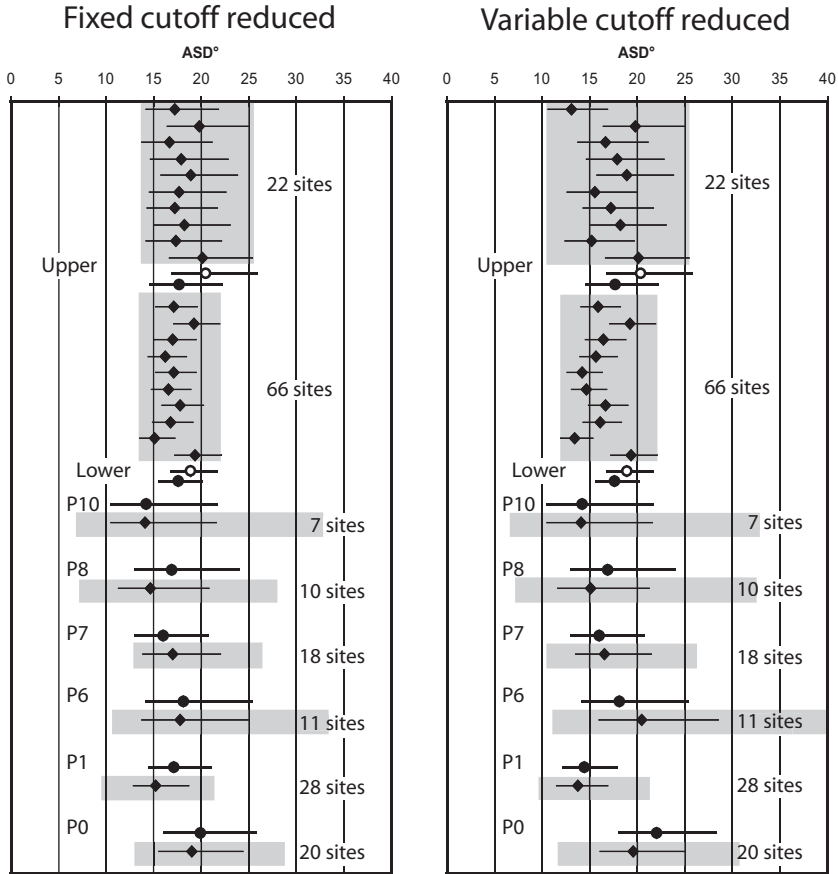
Figure 5.7 (continued)

layered intrusion, Russia (Smirnov et al., 2003), which show intensities similar to the unusually high present day field intensity (Fig. 5.6). So far, the limited number of reliable palaeointensity estimates hinders a robust analysis of the overall intensity of the Precambrian magnetic field, and many estimates are still within error of the palaeointensity range from 84 to 1 Ma, and almost all are within the range of the last 0.3 to 300 Ma (Selkin and Tauxe, 2000), except for some Canadian Mid to Early Proterozoic dykes (Macouin et al., 2003).

Archaean secular variation

We looked at the data with and without correction for (block)rotation. A rotation correction will tend to lower ASD, because the declinational scatter is decreased. The amount and variation of ASD without any corrections on the late Archaean data set lies essentially in the same range as those derived from the TK03.GAD model. There are up to 5 degree differences in the mean ASD values of the Archaean data and the model set (Fig. 5.7). These differences are random, so not consistently higher or lower than the model. Without correction for block rotation, the upper group (P8-11) has ASD_{high} values outside the range

135

of the model set, but after rotation correction the ASD values for the model lie in the same range as the real data (Fig. 5.7). Correcting for rotation between Package 1-2 and Package 4-7 causes a slightly worse fit of the lower group (P1-7) with the model data, especially when variable cut-off is applied (Fig. 5.7). If we neglect the correction for rotation, secular variation will be artificially high, because obviously too much declinational variation is introduced. We therefore regard it justified to correct for rotation.

We also looked at the data with and without a reduction for repeated sampling of the same field in successive lava flows. Introducing this reduction requires the fundamental assumption that secular variation in fact did occur in the late Archaean. The amount of ASD in the uncorrected data seems to justify this assumption. Mean ASD values of the model and the reduced Archaean data agree remarkably well, as well as the mean ASD range (Fig. 5.7), which strengthens our assumption.

It is now interesting to compare our data with the compilation for PSV from lavas of the last 5 Myr (PSVRL) of McElhinny and McFadden (1997). We compare our rotation corrected data before and after reduction, both for variable cut-off (Vandamme, 1994) and a fixed cut-off of 40° (Fig. 5.8). The non-reduced dataset shows a significant deviation from the PSVRL data, which is most pronounced in the case of variable cut-off. The reduced data set, however, shows very good agreement with the TK03.GAD model and the PSVRL data, again with slightly better results for the fixed cut-off angle than for the variable cut-off (Fig. 5.8).

The PSVRL data are in excellent agreement with the reduced lower group, the group that includes the rotation corrected data of Packages 1 to 7, consisting of 66 data points. The average ASD is identical to the 0-5 Ma TK03.GAD model prediction (Fig. 5.8). The ASD ranges of all groups are larger than the range of most of the PSVRL data. Most probably, the limited number of data causes this, because the model predictions for equal numbers of data give similar ASD ranges as the real data (Fig. 5.7). In summary, the observed ASD values of all groups agree with those observed in the last 5 Myr. We must therefore conclude that PSV in the Archaean was the same as it is today.

Implications for the geodynamo and the Earth's core in the late Archaean

The results from this and other studies (e.g. Macouin et al., 2003; Selkin et al., 2000; Smirnov et al., 2003; Yoshihara and Hamano, 2000) indicate that the field strength in the Archaean and Proterozoic did not differ much from the field strength of the last 84 Myr, and in fact covers both high and low extremes. Our study also shows that secular variation did not happen in a fundamentally different way in the late Archaean. The Pilbara data have also documented the oldest known reversals of the geomagnetic field as early as ca. 2770 Myr ago (Strik, 2004; Strik et al., 2003). In addition, these reversals have positive reversal tests, which implies that the field was dipolar. All these observations indicate that the geodynamo at ca. 2.8 Ga operated in a way very similar to today.

The growth of the Earth's solid inner core is thought to strongly influence the operation of the geodynamo (e.g. Buffett and Bloxham, 2002; Labrosse et al., 2001). According to Labrosse and Macouin (2003) and Labrosse et al. (2001), the preferred age of the inner core is 1.0 ± 0.3 Ga, with a maximum age of 2.5 Ga, assuming the absence of radioactive elements in the core. If radioactive elements are present in the core, the maximum age can be extended to 3.0 Ga. A solid inner core growth is not a necessary condition to sustain the geodynamo, because it may also be possible to sustain a dynamo with a rapidly cooling core (e.g. Buffett, 2000; Gubbins et al., 2003; Labrosse and Macouin, 2003; Stevenson, 2003).
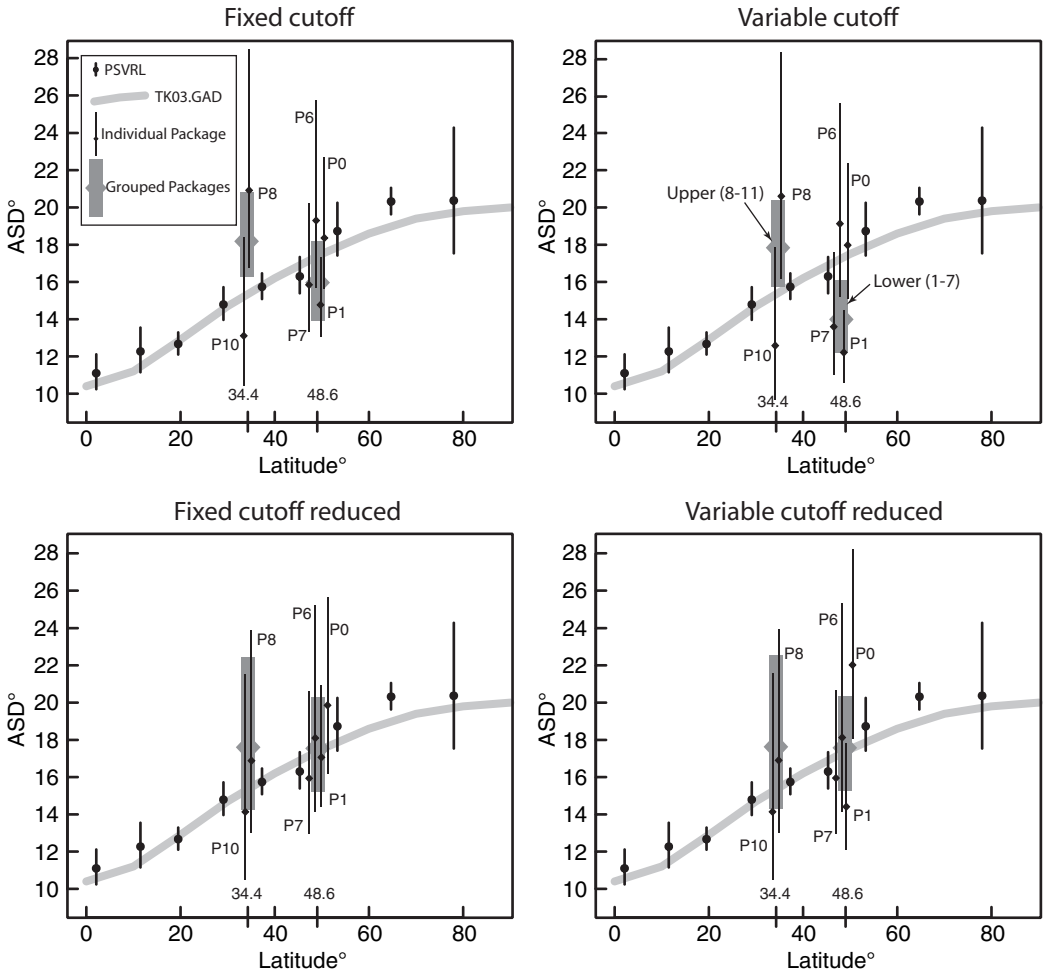
Figure 5.8
ASD of the late Archaean data set (diamonds) *versus* latitude, compared to the PSV database of lavas (PSVRL, circles) from McElhinny and McFadden (1997) and TK03.GAD (shaded line) Tauxe and Kent (2004). Plots are made both for fixed and variable cut-off angles, for both the unprocessed data set and the reduced data set. P0, P1, P6, P7 and the lower set have a palaeolatitude of 48.6° and P8, P10 and the upper set have a palaeolatitude of 34.4°. Reducing the data set for similar field measurements dramatically improves the fit with PSVRL and TK03.GAD.

The absence of an inner core, however, may produce a more 'chaotic' geomagnetic field, because the stabilising effect of the inner core on the geodynamo (Gubbins, 1993; Hollerbach and Jones, 1993) is missing. If a solid inner core is absent at ca. 2.8 Ga, one may therefore expect a field behaviour different from that of the last 1.0 Gyr, although theory has not yet rigorously explored the effects of the absence of an inner core on the geodynamo. So far, we find a low reversal frequency (two confirmed reversed intervals in 60 Myr), no exceptional palaeointensities and secular variation behaviour like the recent field. It is beyond the scope of this paper to speculate on the basis of the available palaeomagnetic data presented here and by others, if inner core growth is a prerequisite for the operation of the geodynamo similar to today. If it were, this would imply that the core has to contain

radioactive elements (Labrosse et al., 2001) and that the inner core must have started its nucleation before ca. 2.8 Ga.

Conclusions

On the basis of palaeointensity measurements of a selection of late Archaean flood basalts and a database of 141 site mean directions we conclude that:

1. Curie balance measurements with repeated heating and cooling cycles provide a useful and quick method to select samples for palaeointensity studies, because they show the degree of alteration of a sample at different temperatures. Selecting samples with little or no alteration increases the probability of successful pTRM checks.

2. The average VDM at 2772 ± 2 Ma is determined at 28.1 ± 9.3 ZAm^2 for Package 1 flood basalts of the Nullagine Supersequence. The average VDM at 2721 ± 4 Ma is determined at 22.1 ± 4.2 ZAm^2 for Package 7 flood basalts of the Mount Jope Supersequence.

3. Analysis of the VGP scatter of 141 sites in an interval between ca. 2775 and 2715 Ma and comparison to the PSVRL data for the last 5 Myr (McElhinny and McFadden, 1997) and to a recent model of the field (TK03.GAD, Tauxe and Kent, 2004) shows that the amount and range of secular variation in the late Archaean was very similar to that of today.

4. Combining the results of conclusions 2 and 3, and including the observation that the geomagnetic field was dipolar and reversing as early as ca. 2770 Myr ago, it seems that the geodynamo operated essentially in the same way as it does in modern times.

5. If solid inner core nucleation is a condition for the operation of the geodynamo, our results imply that it must have started before ca. 2.8 Ga.

Acknowledgments

Epilogue

Epilogue

The research proposal that was written for this PhD project was entitled: Archaean continents: to wander or not to wander? With hindsight, it may not have been the most appropriate question to ask. Published results from various Archaean terrains had already suggested polar wander, although the quality and reliability of pole positions is not always up to modern standards, as is discussed in Chapter 4. A more suitable question would have been: what does Archaean polar wander represent? Are the shifts in pole positions caused by geomagnetic processes, like true polar wander or perhaps the invalidity of the geocentric axial dipole (GAD) hypothesis, or are these shifts caused by the actual horizontal displacement of Archaean lithosphere?

In terms of the character of the geomagnetic field, this thesis presents evidence for a stable dipolar field in the late Archaean. Although normal dipole behaviour may be challenged on the Pilbara Craton by the slightly odd pole position of Package 0 with respect to the other 2.8-2.7 Ga pole positions, there are no constraints on the age of Package 0. Hence, it may be significantly older than Package 1, which allows for a large time window to accommodate the near 180° rotation and thus does not compromise the GAD hypothesis. We demonstrate the occurrence of geomagnetic reversals in the late Archaean, which pass the reversal test and in fact suggest that the GAD hypothesis is valid. Furthermore, the relatively low but not exceptional strength of the late Archaean field as well as the amount of secular variation are additional indications that the geodynamo operated in a similar manner as today. Nevertheless, we must concede that the current database of the Pilbara Craton - which for Archaean times is considerable and at present forms the largest consistent set available for this period - represents a single location on our globe. Clearly, similar and time-equivalent studies of other locations are needed for more robust conclusions. After carefully weighing the evidence, however, I find that the conservative approach is the most appealing and it is now up to advocates of true polar wander and non-dipole fields to further test their hypotheses.

In terms of geodynamics, this thesis shows the occurrence of Archaean apparent polar wander, since the geodynamo appears to be stable and the field seems to be dipolar. This implies that plates have been moving horizontally across the Earth during the late Archaean. Evidently, accurate drift rates cannot be estimated using pole positions that are hundreds of million years apart. To prevent oversimplification, reliable drift rate estimates can only be derived from coherent sequences of accurately dated pole positions, preferably without large time gaps between subsequent poles. This thesis has presented the results of such a sequence from the Pilbara Craton. The shift in palaeolatitude at the Package 7/8 boundary represents considerable horizontal displacement in a relatively short amount of time. The resulting drift rate estimate is higher than the fastest drift rates reported for the Phanerozoic, which could have been caused by higher mantle temperatures in the Archaean.

Whether or not horizontal movement of plates in the Archaean prove that plate tectonics operated in a modern style is a question that still cannot be answered satisfactorily. Most of the evidence for modern-style plate tectonics, if it occurred in the Archaean, will have been destroyed. The continuous recycling of oceanic lithosphere is the main component of plate tectonics, but this oceanic lithosphere is only occasionally preserved e.g. as ophiolites thrusted onto the continental lithosphere. So far, no evidence for Archaean ophiolites has been found. On the other hand, numerous geological data from e.g. the Pilbara Craton point towards processes that can only be explained by modern style plate tectonics, such as

terrain accretion instead of diapirism (cf. Beintema, 2003). Diapirism would inevitably have resulted in dominantly vertical tectonics, which is contradicted by the work presented here in this thesis.

Many of the original research questions could be addressed in this thesis, but inevitably some questions remain and many new and intriguing questions have arisen. Although Archaean flood basalts have proven to be good recorders of the geomagnetic field, why is it that the intensity of NRM is significantly lower than in modern flood basalts, even when taking the low palaeointensities into account? A study of the rock magnetic properties and geochemistry should provide more insight in both the origin of these basalts and the origin and mechanics of NRM acquisition.

Further, it is evident that the Kaapvaal Craton deserves more palaeomagnetic attention, because the need remains to convincingly demonstrate that the original NRM is still preserved in (some of) the rocks. In general, it is desirable in future Archaean palaeomagnetic studies, on any Archaean Craton, to focus on detailing and expanding apparent polar wander paths (APWP's) with discrete sequences that have small time gaps between units. I realise that this will not be an easy task, but this thesis bears evidence that extensive fieldwork does pay off. Such a task evidently goes hand in hand with high precision geochronology, which remains laborious and expensive, but which is an absolute necessity for generating reliable APWP's and, moreover, for studying the geomagnetic behaviour of the ancient field during a time that is argued to have no inner core.

Finally, if the geomagnetic field at 2.8 Ga was similar to today's field, the next question to ask is: when, if ever, was it different? We know virtually nothing about the field older than 2.8 Ga, except for some sporadic pole positions, and a few palaeointensity estimates at ca. 3.5 Ga, for which the magnetic age can only be demonstrated to be older than 2.6 Ga (Hale, 1987; Yoshihara and Hamano, 2004). The Precambrian palaeomagnetic record is far from continuous, and not only are there large gaps in the record of the mid to late Archaean, but also in the Proterozoic, especially in terms of studies of geodynamo behaviour. Concluding, there is plenty of uncharted territory left on early Earth and many real challenges. If anything, this thesis is an example that these challenges can be met successfully.

References

Internet

Global Palaeomagnetic Database (GPMDB) ftp://ftp.ngdc.noaa.gov/Solid_Earth/Paleomag/access/ver4.3

References

Armstrong, N.V., Hunter, D.R. and Wilson, A.H., 1982. Stratigraphy and petrology of the Archaean Nsuze Group, northern Natal and southeastern Transvaal, South Africa. Precambrian Res., 19: 75-107.

Armstrong, R.A., Compston, W., Retief, E.A., Williams, I.S. and Welke, H.J., 1991. Zircon ion microprobe studies bearing on the age and evolution of the Witwatersrand triad. Precambrian Res., 53: 243-266.

Arndt, N.T., Nelson, D.R., Compston, W., Trendall, A.F. and Thorne, A.M., 1991. The age of the Fortescue Group, Hamersley basin, Western Australia, from ion microprobe zircon U-Pb results. Aust. J. Earth Sci., 38: 261-281.

Barley, M.E., Pickard, A.L. and Sylvester, P.J., 1997. Emplacement of a large igneous province as a possible cause of banded iron formation 2.45 billion years ago. Nature, 385: 55-58.

Barton, J.M., Hunter, D.R., Jackson, M.P.A. and Wilson, A.C., 1983. Geochronologic and Sr-isotopic studies of certain units in the Barberton granite-greenstone terrain, Swaziland. Trans. Geol. Soc. S. Afr., 86: 71-80.

Bédard, J.H., Brouillette, P., Madore, L. and Berclaz, A., 2003. Archaean cratonization and deformation in the northern Superior Province, Canada: an evaluation of plate tectonic versus vertical tectonic models. Precamb. Res., 127: 61-87.

Beintema, K.A., 2003. Geodynamics of the Archaean West and Central Pilbara Craton, Australia. Ph. D. thesis Thesis, Utrecht University, Utrecht, 248 pp.

Beukes, N.J. and Cairncross, B., 1991. A lithostratigraphic-sedimentological reference profile for the Late Archaean Mozaan Group, Pongola Sequence: Application to sequence stratigraphy and correlation with the Witwatersrand Supergroup. S. Afr. J. Geol., 94(1): 44-69.

Bickle, M.J. and Eriksson, K.A., 1982. Evolution and subsidence of early Precambrian sedimentary basins. Philos. Trans. Roy. Soc. Lond., Ser. A., 505(1489): 225-244.

Blake, T.S., 1984a. Evidence for stabilization of the Pilbara Block, Australia. Nature, 307: 721-723.

Blake, T.S., 1984b. The lower Fortescue Group of the northern Pilbara Craton: stratigraphy and palaeogeography. In: J.R. Muhling, D.I. Groves and T.S. Blake (Editors), Archaean and Proterozoic Basins of the Pilbara: Evolution and Mineralization Potential. Geol. Dept. and Univ. Extension, Univ. West. Aust., 123-143.

Blake, T.S., 1990. Bedrock geology of the Fortescue Group of the northern Pilbara Craton. Key Centre for Strategic Mineral Deposits, Geol. Dept. and Univ. Extension, Univ. West. Aust.

Blake, T.S., 1993. Late Archaean crustal extension, sedimentary basin formation, flood basalt volcanism and continental rifting: the Nullagine and Mount Jope Supersequences, Western Australia. Precamb. Res., 60: 185-241.

Blake, T.S., 2001. Cyclic continental mafic tuff and flood basalt volcanism in the Late Archaean Nullagine and Mount Jope Supersequences in the eastern Pilbara, Western Australia. Precamb. Res., 107: 139-177.

Blake, T.S., 2004. A new regional stratigraphic framework for the lower succession of the Hamersley Province on the northern Pilbara Craton, Western Australia. in prep.

Blake, T.S. and Barley, M.E., 1992. Tectonic evolution of the late Archean to Early Proterozoic Mount Bruce Megasequence Set, Western Australia. Tectonics, 11(6): 1415-1425.

Blake, T.S., Buick, R., Barley, M.E. and Brown, S.J.A., 2004. High-precision ion microprobe zircon U-Pb geochronology of the Nullagine and Mount Jope Supersequence in the Nullagine Synclinorium, Western Australia. submitted manuscript.

Blake, T.S. and McNaughton, N.J., 1984. A geochronological framework for the Pilbara region. Publ. Univ. West. Aust. Geol. Dept. Ext. Serv., 9: 1-23.

Bloxham, J., 2000. Sensitivity of the geomagnetic axial dipole to thermal core-mantle interactions. Nature, 405: 63-65.

Buchan, K.L., Mortensen, J.K., Card, K.D. and Percival, J.A., 1998. Paleomagnetism and U-Pb geochronology of diabase dyke swarms of Minto block, Superior Province, Quebec, Canada. Can. J. Earth Sci., 35(9): 1054-1069.

Buffett, B.A., 2000. Earth's core and the geodynamo. Science, 288: 2007-2012.

Buffett, B.A. and Bloxham, J., 2002. Energetics of numerical geodynamo models. Geophys. J. Int., 149: 211-224.

Buick, I.S., Maas, R. and Gibson, R., 2001. Precise U–Pb titanite age constraints on the emplacement of the Bushveld Complex, South Africa. J. Geol. Soc. London, 158(1): 3-6.

Burke, K., Kidd, W.S.F. and Kusky, T.M., 1985a. The Pongola structure of southeastern Africa: The world's oldest preserved rift? J. Geodynamics, 2: 35-49.

Button, A., 1981. The Pongola Supergroup. In: D.R. Hunter (Editor), Precambrian of the southern hemisphere. Elsevier, Amsterdam, 501-510.

Cande, S.C. and Kent, D.V., 1995. Revised calibration of the geomagnetic polarity timescale for the Late Cretaceous and Cenozoic. J. Geophys. Res., 100 (B4): 6093-6095.

Cheney, E.S., 1996. Sequence stratigraphy and plate tectonic significance of the Transvaal succession of southern Africa and its equivalent in Western Australia. Precambrian Res., 79: 3-24.

Clendenin, C.W., Charlesworth, E.G. and Maske, S., 1988. Tectonic style and mechanism of Early Proterozoic successor basin development, southern Africa. Tectonophysics, 156: 275-291.

Coe, R.S., Grommé, S. and Mankinen, E.A., 1978. Geomagnetic paleointensities from radiocarbon-dated lava flows on Hawaii and the question of the Pacific nondipole low. J. Geophys. Res., 83: 1740-1756.

Constable, C.G. and Johnson, C.L., 1999. Anisotropic paleosecular variation models: implications for geomagnetic field observables. Phys. Earth Planet Int., 115: 35-51.

Cornell, D.H., 1978. Petrologic studies at T'Kulp: Evidence for metamorphism and alteration of volcanic formations beneath the Transvaal volcanosedimentary pile. Trans. Geol. Soc. S. Afr., 81: 261-270.

Cornell, D.H., Schütte, S.S. and Eglington, B.L., 1996. The Ongeluk basaltic andesite formation in Griqualand West, South Africa: submarine alteration in a 2222 Ma proterozoic sea. Precamb. Res., 79: 101-123.

Courtillot, V. and Besse, J., 1987. Magnetic field reversals, Polar wander, and core-mantle coupling. Science, 237: 1140-1147.

Crow, C. and Condie, K.C., 1988. Geochemistry and origin of late Archaean volcanics from the Ventersdorp Supergroup, South Africa. Precamb. Res., 42: 19-37.

Dankers, P.H.M., 1978. Magnetic properties of dispersed natural iron-oxides of known grain-size. PhD thesis Thesis, Utrecht University, Utrecht, 142 pp.

de Ronde, C.E.J. and de Wit, M.J., 1994. Tectonic history of the Barberton Greenstone Belt, South Africa: 490 million years of Archean evolution. Tectonics, 13(4): 983-1005.

de Wit, M.J., 1998. On Archaean granites, greenstones, cratons and tectonics: does the evidence demand a verdict? Precamb. Res., 91: 181-226.

de Wit, M.J. et al., 1992. Formation of an Archean continent. Nature, 357: 553-562.

Duana, M.J., Roberts, P.J. and Smith, C.B., 1988. Pb and Sr isotopic characteristics of Proterozoic Pb-Zn deposits, Transvaal sequence, South Africa: suggestions for their source areas and genesis. Economic Geology Research Unit, Information circular, 205: 1-15.

Duncan, R.A., Hooper, P.R., Rehacek, J., Marsh, J.S. and Duncan, A.R., 1997. The timing and duration of the Karoo igneous event, southern Gondwana. J. Geophys. Res., 102: 18127-18138.

Eglington, B.M. and Armstrong, R.A., 2004. The Kaapvaal Craton and adjacent orogens, southern Africa: A geochronological database and overview of the geological development of the craton. S. Afr. J. Geol., 107: in press.

Embleton, B.J.J., 1978. The paleomagnetism of 2400 M.Y. old rocks from the Australian Pilbara Craton and its relation to Archean -proterozoic tectonics. Precambrian Res., 6: 275-291.

Encarnacion, J., Fleming, T.H., Elliot, D.H. and Eales, H.V., 1996. Synchronous emplacement of Ferrar and Karoo dolerites and the early breakup of Gondwana. Geology, 24: 535-538.

Eriksson, P.G. et al., 2002. Late Archaean superplume events, a Kaapvaal-Pilbara perspective. J. Geodynamics, 34: 207-247.

Erlank, A.J. (Editor), 1984. Petrogenesis of the volcanic rocks of the Karoo Province. Special Publication, 13. Geol. Soc. S. Africa, 395 pp.

Evans, D.A., Beukes, N.J. and Kirschvink, J.L., 1997. Low-latitude glaciation in the Paleoproterozoic era. Nature, 368: 262-266.

Evans, M.E., 1966. A palaeomagnetic study of the Gaberones Granite of Botswana. Geophys. J. R. Astr. Soc., 12: 491-498.

Evans, M.E. and McElhinny, M.W., 1966. The paleomagnetism of the Modipe Gabbro. J. Geophys. Res., 71(24): 6053-6063.

Fisher, R.A., 1953. Dispersion on a sphere. Proc. R . Soc. Lond., 217: 295-305.

References

Fouch, M.J. et al., 2004. Mantle seismic structure beneath the Kaapvaal and Zimbabwe cratons. S. Afr. J. Geol., 107: in press.

Glatzmaier, G.A., Coe, R.S., Hongre, L. and Roberts, P.H., 1999. The role of the Earth's mantle in controlling the frequency of geomagnetic reversals. Nature, 401: 885-890.

Glatzmaier, G.A. and Roberts, P.H., 1995. A three-dimensional self-consistent computer simulation of a geomagnetic field reversal. Nature, 377: 203-209.

Gold, D.J.C. and von Veh, M.W., 1995. Tectonic evolution of the Late Archaean Pongola-Mozaan basin, South Africa. J. Afr. Earth Sci., 21(2): 203-212.

Graham, K.W.T., 1961. The re-magnetization of a surface outcrop by lightning currents. Gephys. J. London, 6: 85-102.

Grobler, D.F. and Walraven, F., 1993. Geochronology of the Gabarone Granite Complex extensions in the area north of Makifeng, South Africa. Chem. Geol., 105: 319-337.

Gubbins, D., 1993. Geomagnetism; influence of the inner core. Nature, 365: 493.

Gubbins, D., Alfe, D., Masters, G., Price, D.G. and Gillan, J.M., 2003. Can the Earth's dynamo run on heat alone? Geophys. J. Int., 155: 609-622.

Gulson, B.l. and Korsch, M.J., 1983. Isotope studies. Commonwealth Sci. and Ind. Res. Organ. Dev. of Miner. Phys., Sydney, 24-26.

Gutzmer, J., Nhleko, N., Beukes, N.J., Pickard, A. and Barley, M.E., 1999. Geochemistry and ion microprobe (SHRIMP) age of a quartz porphyry sill in the Mozaan Group of the Pongola Supergoup: implications for the Pongola and Witwatersrand Supergroups. S. Afr. J. Geol., 102(2): 139-146.

Hale, C.J., 1987. The intensity of the geomagnetic field at 3.5 Ga: paleointensity results from the Komati Formation, Barberton Mountain Land, South Africa. Earth Planet. Sci. Lett., 86: 354-364.

Hallimond, A.F. and Herroun, E.F., 1933. Laboratory determinations of the magnetic properties of certain igneous rocks. Proc. Roy. Soc., 141: 302-314.

Hamilton, W.B., 1998. Archean magmatism and deformation were not products of plate tectonics. Precambr. Res., 91: 143-181.

Hanson, R.E. et al., 2004. Paleoproterozoic intraplate magmatism and basin development on the Kaapvaal Craton: Age, paleomagnetism and geochemistry of ca. 1.93-1.87 Ga post-Waterberg dolerites. S. Afr. J. Geol., 107: in press.

Hargraves, R.B. and Rehacek, J., 1997. Palaeomahgnetism of the Karoo igneous rocks in Southern Africa. S. Afr. J. Geol., 100(3): 195-212.

Hattingh, P.J., 1986. The paleomagnetism of the Merensky Reef footwall rocks of the Bushveld Complex. Trans. Geol. Soc. S. Afr., 89: 1-8.

Hegner, E., Kröner, A. and Hofmann, A.W., 1984. Age and isotope geochemistry of the Archaean Pongola and Usushwana suites in Swaziland, southern Africa: a case for crustal contamination of mantle-derived magma. Earth Planet. Sci. Lett., 70: 267-279.

Hegner, E., Kröner, A. and Hofmann, A.W., 1993. Trace element and isotopic constraints on the origin of the Archaean Pongola and Usushwana Igneous Suites in Swaziland. In: R. Maphalala and M. Mabuza (Editors). Ext. Abs. 16th Colloquium Afr. Geol., Mbabane, Swaziland, 147-149.

Heslop, D., Dekkers, M.J., Kruiver, P.P. and van Oorschot, I.H.M., 2002. Analysis of isothermal remanent magnetisation acquisition curves using the expectation-maximisation algorithm. Geophys. J. Int., 148: 58-64.

Hickman, A.H., 1997. Dampier, W.A. Sheet 2256: 1: 100 000 Geol. Ser., Geol. Serv. West. Aust., Perth.

Hickman, A.H., Chin, R.J. and Gibson, D.L., 1982. Yarrie, Western Australia 1: 250 000 Geol. Ser., Sheet SF 51-1. Geol. Serv. West. Aust.

Hickman, A.H. and Lipple, S.L., 1978. Marble Bar, Western Australia, 1:250,000. Geol. Ser. Sheet SF50-8, Geol. Serv of W. Aust., Perth.

Hollerbach, R. and Jones, C.A., 1993. Influence of the Earth's inner core on geomagnetic fluctuations and reversals. Nature, 365: 541-543.

Hunter, D.R. and Reid, D.L., 1987. Mafic Dyke swarms in southern Africa. In: H.C. Halls and W.F. Fahrig (Editors), Mafic dyke swarms. Geological Association of Canada Special paper, 445-456.

Idnurm, M. and Giddings, J.W., 1988. Australian precambrian polar wander: a review. Precambrian Res., 40/41: 61-88.

Jones, D.L., Walford, M.E.R. and Gifford, A.C., 1967. A paleomagnetic result from the Ventersdorp Lavas of South Africa. Earth Planet. Sci. Lett., 2: 155-158.

Kent, D.V. and Smethurst, M.A., 1998. Shallow bias of paleomagnetic inclinations in the Paleozoic and Precambrian. Earth Planet. Sci. Lett., 160: 391-402.

Kent, L.E., 1980. Stratigraphy of South Africa, Part 1, Lithostratigraphy of the Republic of South Africa, Southwest Africa, Namibia and the Republics of Bophuthatswana, Transkei and Venda. South African Committee for Stratigraphy, 690 pp.

Kirschvink, J.L., 1980. The least-squares line and plane and the analysis of palaeomagnetic data. Geophys. J. R. Astron. Soc., 62: 699-718.

Kirschvink, J.L., Ripperdan, R.L. and Evans, D.A., 1997. Evidence for a large-scale reorganisation of Early Cambrian continental landmasses by inertial interchange true polar wander. Science, 277: 541-545.

Kröner, A. and Layer, P.W., 1992. Crust formation and plate motion in the Early Archean. Science, 256: 1405-1411.

Kuang, W. and Bloxham, J., 1997. An Earth-like numerical dynamo. Nature, 389: 371-374.

Labrosse, S. and Macouin, M., 2003. The inner core and the geodynamo. C. R. Geoscience, 335: 37-50.

Labrosse, S., Poirier, J.P. and Le Mouël, J.L., 2001. The age of the inner core. Earth Planet. Sci. Lett., 190: 111-123.

Layer, P.W., 1986. Archean paleomagnetism of southern Africa. PhD thesis Thesis, Stanford University, 397 pp.

Layer, P.W., Kröner, A. and McWilliams, M., 1988a. Paleomagntism and the age of the Archean Usushwana Complex, Southern Africa. JGR, 93B1: 449-457.

Layer, P.W., Kröner, A. and McWilliams, M., 1996. An Archean geomagnetic reversal in the Kaap Valley Pluton, South Africa. Science, 273: 943-946.

Layer, P.W., Kröner, A., McWilliams, M. and Clauer, N., 1988b. Regional magnetic overprinting of Witwatersrand Supergroup sediments, South Africa. J. Geophys. Res., 93(B3): 2191-2200.

Layer, P.W., Kröner, A., McWilliams, M. and York, D., 1989. Elements of Archean thermal history and apparant polar wander of the eastern Kaapvaal Craton, Swaziland, from single grain dating and paleomagnetism. Earth Planet. Sci. Lett., 93: 23-34.

Layer, P.W., Lopez-Martinez, M., Kröner, A., York, D. and McWilliams, M., 1998. Thermochronometry and palaeomagnetism of the Archaean Nelshoogte Pluton, South Africa. Geophys.J. Int., 135: 129-145.

Li, Z.X., Guo, W. and Powell, C.M., 2000. Timing and genesis of Hamersley BIF-hosted iron ore deposits: a new palaeomagnetic interpretation. MERIWA 199, Perth, 216 pp.

MacLeod, W.N., de la Hunty, L.E., Jones, W.R. and Halligan, R., 1963. A preliminary report on the Hamersley Iron Province, North-west Division, 44-54.

Macouin, M. et al., 2003. Low paleointensities recorded in 1 to 2.4 Ga Proterozoic dykes, Superior Province, Canada. Earth Planet. Sci. Lett., 213: 79-95.

Marsh, J.S., Hooper, P.R., Rehacek, J., Duncan, R.A. and Duncan, A.R., 1997. Stratigraphy and age of Karoo basalts of Lesotho and implications for correlations with the Karoo Igneous Province. Geophysical Monograph, 100: 247-272.

Matthews, P.E., 1990. A plate tectonic modle for the Late Archean Pongola supergroup in southeastern Africa. In: S.P.H. Sychanthavong (Editor), Crustal evolution and orogeny. Oxford Publisher, New Delhi, 41-73.

McCall, G.J.H., 2003. A critique of the analogy between Archaean and Phanerozoic tectonics based on regional mapping of the Mesozoic-Cenozoic plate convergent zone in the Makran, Iran. Precamb. Res., 127: 5-17.

McElhinny, M.C. and McFadden, P.L., 1997. Palaeosecular variation over the past 5 Myr based on a new generalized database. Geophys. J. Int., 131: 240-252.

McElhinny, M.C., McFadden, P.L. and Merrill, R.T., 1996. The myth of the Pacific dipole window. Earth Planet. Sci. Lett., 143: 13-22.

McElhinny, M.W. and Lock , J., 1996. IAGA paleomagnetic databases with Access. Surveys in Geophysics, 17: 575-591.

McElhinny, M.W. and McFadden, P.L., 2000. Paleomagnetism; continents and oceans. International Geophysics Series, 73. Academic Press, 386 pp.

McFadden, 1990. A new fold test for palaeomagnetic studies. Geophys. J. Int., 103: 163-169.

McFadden, P.L. and McElhinny, M.C., 1995. Combining groups of paeomagnetic directions or poles. Geophys. Res. Lett., 22: 2191-2194.

McFadden, P.L. and McElhinny, M.W., 1990. Classification of the reversal test in palaeomagnetism. Geophys. J. Int., 103: 725-729.

Meert, G.M., 1999. A paleomagnetic analysis of Cambrian true polar wander. Earth Planet. Sci. Lett., 168: 131-144.

References

Meert, G.M., van der Voo, R. and Patel, J., 1994. Paleomagnetism of the late Archean Nyanzian System, western Kenya. Precamb. Res., 69: 113-131.

Meert, G.M. et al., 1993. A plate-tectonic speed limit? Nature, 363: 216-217.

Merrill, R.T., McElhinny, M.C. and McFadden, P.L., 1996. The magnetic field of the Earth: Palaeomagnetism, the core and the deep mantle. Academic Press, San Diego, 531 pp.

Morimoto, C., Otofuji, O., Miki, M., Tanaka, H. and Itaya, T., 1997. Preliminary paleomagnetic results of an Archean dolerite dyke of west Greenland: geomagnetic field intensity at 2.8 Ga. Geophys. J. Int., 128: 585-593.

Moser, D.E., Flowers, R.M. and Hart, R.J., 2001. Birth of the Kaapvaal tectosphere 3.08 billion years ago. Science, 291: 465-468.

Mullender, T.A.T., van Velzen, A.J. and Dekkers, M.J., 1993. Continuous drift correction and separate identification of ferrimagnetic and paramagnetic contribution in thermomagnetic runs. Geophys. J. Int., 114: 663-672.

Nelson, D.R., 1999. Compilation of SHRIMP U-Pb zircon geochronology data, 1998. 1999/2, Geological Survey of Western Australia.

Nelson, D.R., Trendall, A.F., de Laeter, J.R., Grobler, N.J. and Fletcher, I.R., 1992. A comparative study of the geochemical and isotopic systematics of late Archean flood basalts from the Pilbara and Kaapvaal Cratons. Precambrian Res., 54: 231-256.

Onstott, T.C., Hargraves, R.B., Joubert, P. and Reid, D.L., 1986. Constraints on the tectonic evolution of the Namaqua Province; II, Reconnaissance palaeomagnetic and 40Ar/ 39Ar results from the Namaqua Province and Kheis Belt. Trans. Geol. Soc. S. Afr., 89(2): 143-170.

Pick, T. and Tauxe, L., 1993. Holocene paleointensities: Thellier experiments on submarine basaltic glass from the East Pacific Rise. J. Geophys. Res., 98: 17949-17964.

Pidgeon, R.T., 1984. Geochronological constraints on early volcanic evolution of the Pilbara Block, Western Australia. Aust. J. Earth. Sci., 31: 237-242.

Pollack, H.N., 1997. Thermal characteristics of the Archean. In: M.J. de Wit and L.D. Ashwal (Editors), Greenstone Belts. Oxford University Press, Oxford, 223-233.

Porath, H., 1967. Palaeomagnetism and the age of Australian Haematite ore bodies. Earth Planet. Sci. Lett., 2: 409-414.

Poujol, M., Robb, L.J., Anhaeusser, C.R. and Gericke, B., 2003. A review of the geochronological constraints on the evolution of the Kaapvaal Craton, South Africa. Precamb. Res., 127: 181-213.

Reidel, S.P. and Hooper, P.R., 1989. Volcanism and tectonism in the Columbia River flood-basalt province. Spec. Pap., 239. Geol. Soc. Amer., 386 pp.

Reimold, W.U., Leroux, H. and Gibson, R.L., 2002. Shocked and thermally metamorphosed zircon from the Vredefort impact structure, South Africa: a transmission electron microscopic study. Eur. J. Mineral., 14(5): 859-868.

Riisager, P. and Riisager, J., 2001. Detecting multidomain magnetic grains in Thellier palaeointensity experiments. Phys. Earth Planet. Inter., 125: 111-117.

Saunders, A.D., Fitton, J.G., Kerr, A.C., Norry, M.J. and Kent, R.W., 1997. The North Atlantic Igneous Province. Geophysical Monograph, 100: 45-93.

Schmidt, P.W. and Clark, D.A., 1994. Paleomagnetism and magnetic anisotropy of Proterozoic banded iron formations and iron ores of the Hamersley Basin, Western Australia. Precambrian Res., 69: 133-155.

Schmidt, P.W. and Embleton, J.J., 1985. Prefolding and overprint magnetic signatures in Precambrian (~2.9-2.7 Ga) igneous rocks from the Pilbara Craton and Hamersley Basin, NW Australia. J. Geophys. Res., 90B4: 2967-2984.

Schmitz and Bowring, S.A., 2004. Lower crustal granulite formation during Mesoproterozoic Namaqua-Natal collisional orogenesis, southern Africa. S. Afr. J. Geol., 107: in press.

Selkin, P.A., Gee, J.S., Tauxe, L., Meurer, W.P. and Newell, A.J., 2000. The effect of remanence anisotropy on paleointensity estimates: a case study from the Archean Stillwater Complex. Earth Planet. Sci. Lett., 183: 403-416.

Selkin, P.A. and Tauxe, L., 2000. Long-term variations in palaeointensity. Phil. Trans. Roy. Soc. Lond., 358: 1065-1088.

Shipunov, S.V., Muraviev, A.A. and Bazhenov, M.L., 1998. A new conglomerate test in palaeomagnetism. Geophys. J. Int., 133: 721-725.

Smirnov, A.V., Tarduno, J.A. and Pisakin, B.N., 2003. Paleointensity of the early geodynamo (2.45 Ga) as recorded in Karelia: A single-crystal approach. Geology, 31(5): 415-418.

Smith, R.E., Perdrix, J.L. and Parks, T.C., 1982. Burial metamorphism in the Hamersley Basin, Western Australia. J. Petrol., 23: 75-102.

Stankiewicz, J., Chevrot, S., van der Hilst, R.D. and de Wit, M.J., 2002. Crustal thickness, discontinuity depths and uppermantly structure beneath southern Africa: constraints form Body wave inversions. Phys. Earth Planet Inter., 130: 235-251.

Stern, C.R. and de Wit, M.J., 2004. Rocas Verdes ophiolite, southernmost South America: remnants of progressive stages of development of oceanic type crust in a continental back arc basin. Geol. Soc. London(Special Public.): in press.

Stevenson, D.J., 2003. Planetary magnetic fields. Earth Planet. Sci. Lett., 208: 1-11.

Storey, B.C., 1995. The role of mantle plumes in continental break up; case histories from Gondwanaland. Nature, 377: 301-308.

Strik, G., 2004. Palaeomagnetism of late Archaean flood basalt terrains: implications for early Earth geodynamics and geomagnetism. Geologica Ultraiectina, 242. Utrecht University, Utrecht.

Strik, G., Blake, T.S., Zegers, T.E., White, S.H. and Langereis, C.G., 2003. Palaeomagnetism of flood basalts in the Pilbara Craton, Western Australia: Late Archaean continental drift and the oldest known reversal of the geomagnetic field. J. Geophys. Res., 108(B12)(2551): doi:10.1029/2003JB002475.

Sumita, I., Hatakeyama, T., Yoshira, A. and Hamano, Y., 2001. Paleomagnetism of late Archean rocks of Hamersley Basin, Western Australia and the paleointensity at early Proterozoic. Phys. Earth Planet. Inter., 128: 223-241.

Tankard, A.J. et al., 1982. Crustal Evolution of Southern Africa. Sprinter-Verlag, New York, 523 pp.

Tauxe, L., 1998. Paleomagnetic Principles and Practice. Kluwer Academic Publishers, Dordrecht, 299 pp.

Tauxe, L., Constable, C., Johnson, C., Miller, W. and Staudigel, H., 2003. Paleomagnetism of the Southwestern U.S.A. recorded by 0-5 Ma igneous rocks. Geochem. Geophys. Geosyst.: doi: 10.1029/2002GC000343.

Tauxe, L., Genevey, A., Yu, Y., H., R. and Holtezer, A., 2004. A new paleointensity method and application to Israeli copper mining slag deposits. in prep.

Tauxe, L. and Kent, D.V., 2003. A simplified statistical model for the geomagnetic field and the detection of shallow bias in paleomagnetic inclinations: was the ancient magnetic field dipolar?

Tauxe, L. and Staudigel, H., 2004. Strength of the geomagnetic field in the Cretaceous Normal Superchron: new data from submarine basaltic glass of the Troodos Ophiolite. in prep.

Tauxe, L. and Watson, G.S., 1994. The fold test: an eigen analysis approach. Earth Planet. Sci. Lett., 122: 331-341.

Thom, R., Hickman, A.H. and Chin, R.J., 1979. Nullagine, Western Australia 1: 250 000. Geol. Ser. Sheet SF 51-5, Geol. Serv. W. Aust., Perth.

Thorne, A.M. and Hickman, A.H., 2001. Geology of the Fortescue Group, Pilbara Craton, Western Australia, (1: 1,000,000) Perth.

Thorne, A.M. and Trendall, A.F., 2001. Geology of the Fortescue Group, Pilbara Craton, Western Australia. Bulletin (Geological Survey of Western Australia), 144, 249 pp.

Thorne, A.M. and Tyler, I.M., 1996. Roy Hill, Western Australia, 1:250,000. Geol. Ser. Sheet SF50-12, Geol. Serv. W. Aust., Perth.

Tinker, J.H., de Wit, M.J. and Grotzinger, J., 2002. Seismic stratigraphic constraints on Neoarchean-Paleoproterozoic evolution of the western margin of the Kaapvaal Craton, South Africa. S. Afr. J. Geol., 105: 107-134.

Trendall, A.F., 1968. Three great basins of Precambrian banded iron formation deposits- a systematic comparison. Geol. Soc. Am. Bull., 79: 1527-1544.

Trendall, A.F., 1979. A revision of the Mount Bruce Supergroup, Ann. Rep. 1978, 63-71.

Trendall, A.F., 1983. The Hamersley Basin. In: A.F. Trendall and R.C. Morris (Editors), Iron-formation: Facts and Problems. Elsevier, Amsterdam, 69-129.

Tyler, I.M. and Thorne, A.M., 1990. The northern margin of the Capricorn Orogen, Western Australia - an example of an early Proterozoic collision zone. J. Struct. Geol., 12: 685-701.

Tyler, N., 1979. Stratigraphy, origin, and correlation of the Kanye Volcanic Group in west-central Transvaal. Trans. Geol. Soc. S. Afr., 82: 215-226.

Uken, R. and Watkeys, M.K., 1997. An interpretation of dyke swarms of the North-eastern Kaapvaal craton. S. Afr. J. Geol., 100: 341-348.

Valet, J.-P., 2003. Time variations in geomagnetic intensity. Rev. Geophys., 41(1): 1004, doi:10.1029/ 2001RG000104.

van der Voo, R., 1990. Phanerozoic paleomagnetic poles from Europe and North America and comparisons with continental reconstructions. Rev. Geophys., 28: 167-206.

van der Voo, R. and Torsvik, T.H., 2001. Evidence for late Paleozoic and Mesozoic non-dipole fields provides an explanation for the Pangea recontruction problems. Earth Planet. Sci. Lett., 187: 71-81.

van der Westhuizen, W.A., de Bruiyn, H. and Meintjes, P.G., 1991. The Ventersdorp Supergroup: an overview. Jour. African Earth Sci., 13(1): 83-105.

van Velzen, A.J. and Zijderveld, J.D.A., 1995. Effects of weathering on single-domain magnetite in Early Pliocene marine marls. Geophys. J. Int., 121: 267-278.

Vandamme, D., 1994. A new method to determine secular variation. Phys. Earth Planet Int., 85: 131-142.

Vlaar, N.J., van Keken, P.E. and van den Berg, A.P., 1994. Cooling of the Earth in the Archean: consequences of pressure-release melting in a hotter mantle. Earth planet. Sci.Lett, 121: 1-18.

Watson, G.S., 1956. A test for randomness of distributions. Mon. Not. R. Astron. Soc. Geophys. Suppl., 7: 160-161.

Weiss, D. and Wasserberg, G.J., 1987. Rb-Sr and Sm-Nd isotope geochemistry and geochronology of cherts from the Onverwacht Group (3.5 Ga), South Africa. Geochim. Cosmochim. Acta, 51: 973-984.

Westphal, M., Gurevitch, E.L., Samsonov, B.V., Feinberg, H. and Pozzi, J.P., 1998. Magnetostratigraphy of the lower Triassic volcanics from deep drill SG6 in western Siberia: evidence for long-lasting Permo-Trassic volcanic activity. Geophys. J. Int., 134: 254-266.

White, R.S. and McKenzie, D., 1995. Mantle plumes and flood basalts. J. Geophys. Res., 100(9): 17,543-17,585.

Wingate, M.T.D., 1998. A palaeomagnetic test of the Kaapvaal-Pilbara (Vaalbara) connection at 2.78 Ga. S. Afr. J. Geol., 101(4): 257-274.

Wingate, M.T.D., 1999. Ion microprobe baddeleyite and zircon ages for late Archaean mafic dykes of the Pilbara Craton, Western Australia. Aust. J. Earth Sci., 46: 493-500.

Winter, H.d.l.R., 1976. A lithostratigraphic description of the Ventersdorp Succession. Trans. Geol. Soc. S. Afr., 79: 31-48.

Yoshihara, A. and Hamano, Y., 2000. Intensity of the Earth's magnetic field in late Archean obtained from diabase dikes of the Slave Province, Canada. Phys. Earth Planet Int., 117: 295-307.

Yoshihara, A. and Hamano, Y., 2004. Paleomagnetic constraints on the Archean geomagnetic field intensity obtained from komatiites of the Barberton and Belingwe greenstone belts, South Africa and Zimbabwe. Precamb. Res., 131: 111-142.

Yu, Y., Tauxe, L. and Genevey, A., 2004. Towards an optimal geomagnetic field intensity determination technique. submitted manuscript.

Zegers, T.E., 1996. Structural, kinematic and metallogenic evolution of selected domains of the Pilbara granitoid-greenstone terrain; implications for mid Archean tectonic regimes. Ph.D. thesis Thesis, Utrecht University, Utrecht, 208 pp.

Zegers, T.E., de Wit, M.J., Dann, J. and White, S.H., 1998. Vaalbara, Earth's oldest supercontinent: a combined structural, geochronologic, and paleomagnetic test. Terra Nova, 10:5: 250-259.

Zhai, Y.J., Halls, H.C. and Bates, M.P., 1994. Multiple episodes of dike emplacement along the northwestern margin of the Superior Province, Manitoba. J. Geoph. Res., 99(B11): 21717-21732.

Zijderveld, J.D.A., 1967. Demagnetization in rocks: Analysis of results. In: D.C. Collinson, K.M. Creer and S.K. Runcorn (Editors), Methods in palaeomagnetism. Elsevier, New York, 254-286.

Samenvatting (Summary in Dutch)

Samenvatting in het Nederlands

Het onderwerp van het hier beschreven onderzoek is het paleomagnetisme van laat-Archaïsche plateaubasaltterreinen en de implicaties hiervan voor de geodynamische en geomagnetische processen tijdens dit gedeelte van de geschiedenis van de jonge aarde. Het laat-Archaïcum is het 500 miljoen jaar durende geologische tijdperk tussen 3,0 en 2,5 miljard jaar geleden. Het is het jongste deel van de gehele Archaïsche periode van 4,0 tot 2,5 miljard jaar. In die tijd zag de wereld er totaal anders uit dan nu. Men zou het zich kunnen voorstellen als een planeet met uitgestrekte vlakten van kale rotsen en oceanen, met hoge vulkanische activiteit, een zuurstofloze atmosfeer en geen enkel spoor van leven, op misschien enig microbiologisch leven na. De aarde heeft sinds haar geboorte haar warmte willen verliezen aan het om haar heen gelegen universum; hiermee de wetten van de fysica gehoorzamend. Het is zeer waarschijnlijk, dat de aarde in het Archaïcum veel warmer was dan nu en als gevolg hiervan zouden vele geologische en geofysische processen op een andere manier gewerkt kunnen hebben. Of dit zo is en hoe die processen dan werkten zijn een aantal algemene vragen, die ik met dit proefschrift heb willen beantwoorden, tezamen met meer specifieke, plaatsgebonden vraagstukken. Ik zal nu in het kort de achtergrond tot de voornaamste onderzoeksvragen introduceren, de veldwerkgebieden beschrijven en de inhoud van het proefschrift samenvatten. Ik zou dit proefschrift niet hebben kunnen afronden zonder de belangrijke bijdrage van de mensen die co-auteur zijn van de artikelen die de hoofdstukken van dit proefschrift vormen. Als ik het dan ook over 'we' heb, dan bedoel ik de desbetreffende auteurs.

Geodynamica: plaattektoniek in het laat-Archaïcum?

Tegenwoordig verliest de aarde de meeste van haar warmte door de continue cyclus van het aanmaken van lithosfeer bij een oceanische rug, waarbij oudere lithosfeer opzij geschoven wordt, waarna het uiteindelijk subduceerd bij een diepe trog en afsmelt. Dit proces noemen we plaattektoniek, een zeer effectieve manier om warmte te verliezen. De drijvende kracht achter plaattektoniek is de kracht die uitgeoefend wordt op het subducerende deel van een plaat. Omdat dit gedeelte van de plaat behoorlijk is afgekoeld sinds zijn ontstaan, is de dichtheid van de plaat hier veel hoger geworden (en de plaat dus zwaarder), waardoor deze uiteindelijk de lichtere asthenosfeer in wordt getrokken. Het is echter mogelijk dat dit proces niet heeft kunnen plaatsvinden in het Archaïcum, omdat korst- en manteltemperaturen hoger waren (bijv. Hamilton, 1998). In plaats daarvan zou de aarde warmte kunnen verliezen door het opsmelten van diapieren (granitische lichamen die opstijgen door de lithosfeer, vanwege hun lagere dichtheid dan die van de omgeving) als gevolg van plotselinge drukafnames, waardoor een dikke en stabiele grenslaag wordt gevormd met weinig mechanische coherentie, die een moderne vorm van plaattektoniek onmogelijk maakt (bijv. Vlaar c.s., 1994). Zonder plaattektoniek zou de aarde nog steeds efficiënt haar warmte kunnen verliezen, maar verticale in plaats van horizontale tektonische processen zouden dan dominant zijn. De meningen zijn nog steeds verdeeld over het al dan niet voorkomen van plaattektoniek in het Archaïcum. Eén van de belangrijkste doelstellingen van mijn onderzoek is om te kijken of tektonische processen dominant horizontaal of verticaal waren in het (laat-) Archaïcum.

Paleomagnetische studies zijn heel belangrijk voor het maken van tektonische reconstructies, omdat we alleen hiermee (plaat) verplaatsing kunnen kwantificeren. Verder kunnen we aan de hand van nauwkeurige ouderdomsbepalingen schattingen maken van

de bewegingssnelheid van platen. Om nauwkeurige schattingen te kunnen maken is het van uiterst belang, dat de bestudeerde gesteenteopeenvolging de originele, natuurlijke remanente magnetisatie (NRM) heeft behouden, met andere woorden, de magnetisatie moet dezelfde ouderdom hebben als de stenen en de magnetische richting die in de stenen bewaard is moet de positie van het toenmalige magnetische noorden weergeven. Dit is geen triviale voorwaarde, zeker niet voor zulke oude stenen. Remagnetisatie is een zeer bekend fenomeen, dat bijvoorbeeld veroorzaakt wordt door metamorfe processen of hydrothermale activiteit. Voor onze studies moesten we dan ook in eerste instantie terreinen selecteren, die nog steeds de oorspronkelijke NRM behouden zouden kunnen hebben.

Geomagnetisme: de geldigheid van de geocentrische axiale dipool (GAD) hypothese

Als een gesteente nog steeds de originele NRM behouden heeft, verteld ons dat op welke breedtegraad het gesteente is gevormd. De hoek die de magnetische richting maakt met de horizontaal wordt de magnetische inclinatie genoemd. De magnetische inclinatie kan uitgedrukt worden als een (paleo)breedtegraad met behulp van de dipoolformule:

$$\tan I = 2 \tan \lambda$$

waar I staat voor magnetische inclinatie en λ voor paleobreedtegraad. Deze relatie gaat op zolang het aardmagneetveld zich gedraagt als een geocentrische axiale dipool (GAD). Op dit moment is de dipoolbijdrage aan het totale aardmagneetveld ongeveer 90 %. De overige 10 % bestaat uit quadrupool, octupool en hogere-orde-pool bijdragen, die veranderlijk zijn door de tijd en er voor zorgen dat de positie van het magnetische noorden onafhankelijk van plaatbewegingen verandert. Dit noemen we seculaire variatie. We veronderstellen, dat de multipoolbijdragen over voldoende tijd genomen uitmiddelen, waardoor alleen de dipoolbijdrage overblijft. Deze hypothese staat bekend als de GAD hypothese. Voor het maken van Archaïsche tektonische reconstructies met behulp van paleomagnetische metingen is het van fundamenteel belang, dat de aarde ook toen al een GAD had.

Het voorkomen van omkeringen van het aardmagneetveld, waarbij de magnetische noordpool verandert in de magnetische zuidpool en vice versa, kan gebruikt worden om de GAD hypothese te testen. Als het aardmagneetveld gemiddeld genomen inderdaad dipolair is, dan zouden de magnetische richtingen die in een gesteenteopeenvolging bewaard zijn gebleven, voor en na een omkering precies antipodaal zijn. Dit kunnen we testen met de zogenaamde "omkeringstest", welke ook een krachtige test is om de waar-schijnlijkheid te testen of de oorspronkelijke NRM bewaard is gebleven. Om zulk een test te kunnen doen, is het natuurlijk noodzakelijk, dat deze omkeringen ook al in het Archaïcum voorkwamen. Gelukkig hebben we in de bestudeerde secties inderdaad bewijs voor omkeringen aangetroffen.

Het aardmagneetveld wordt opgewekt door convectiestromen in de vloeibare (buiten)kern van de aarde. Ik zet "buiten" expres tussen haakjes, omdat het niet vast staat of de kern van de aarde in het laat-Archaïcum al opgesplitst was in een vaste binnenkern en een vloeibare buitenkern (bijv. Labrosse c.s., 2001; Smirnov c.s., 2003) en de redenaties berusten slechts op modellen. Er wordt gedacht, dat de binnenkern een stabiliserende functie heeft voor het aardmagneetveld (bijv. Gubbins, 1993). Daarom zou het dus kunnen, dat het aardmagneetveld zich zonder die binnenkern veel chaotischer gedraagt en misschien zou de magnetische intensiteit ook lager zijn. Om dit te onderzoeken zijn veel paleomagnetische gegevens nodig, want nu kunnen we nog weinig zeggen over het gedrag van het aardmagneetveld in het Archaïcum. Voor Archaïsche begrippen heeft dit onderzoek veel nieuwe gegevens opgeleverd, die vervolgens gebruikt zijn om de mate van seculaire variatie

in het laat-Archaïcum te analyseren. Daarnaast zijn er ook nog metingen verricht om een schatting te maken van de magnetische veldsterkte van dat tijdperk.

Veldwerkgebieden

Veel Archaïsche terreinen hebben een complexe tektonische en metamorfe geschiedenis en zijn geen ideale gebieden voor paleomagnetische studies, vanwege de hoge kans dat de orginele NRM niet bewaard is gebleven. Het Pilbara Craton in West-Australië en het Kaapvaal Craton in zuidelijk Afrika zijn de twee best bewaard gebleven Archaïsche terreinen ter wereld. Grote delen van deze terreinen bestaan uit laat-Archaïsche opeen-volgingen die onder extensie (oprekking) zijn gevormd en ondere andere bestaan uit grote opeenvolgingen van plateaubasalten, die over het algemeen de magnetische veldrichting goed kunnen opnemen. Deze opeenvolgingen hebben slechts een lichte plooiing en een zeer laaggradige metamorfose ondergaan (nooit hoger dan 350 °C). Deze gebieden zijn daarom uitgekozen voor het onderzoek.

Het Pilbara Craton

Het Pilbara Craton van West-Australië bestaat uit midden- tot laat-Archaïsche graniet-groensteen-terreinen, discordant opgevolgd door laat-Archaïsche plateaubasalt-gedomineerde opeenvolgingen (Fig. 1) die aan het oppervlak zijn uigevloeid. Het veldwerk voor dit onderzoek heeft zich voornamelijk geconcentreerd op de laatstgenoemde opeenvolging, die onderverdeeld is in de Nullagine en Mount Jope Supersequenties, met een ouderdom tussen ongeveer 2775 en 2715 miljoen jaar. De geologie hiervan is uitgebreid bestudeerd (bijv. Blake, 1993; Blake 2001; Thorne en Trendall, 2001) en is nauwkeurig gedateerd (bijv. Arndt, 1991; Blake c.s., 2004; Wingate, 1999).

Het Pilbara Craton ligt zo'n 1300 km ten noorden van Perth, de enige grote stad van West-Australië. In de Pilbara zelf liggen enkel wat kleine dorpjes, waarvan de grootste langs de kust. We hebben veldwerk gedaan in drie verschillende bekkens en afhankelijk daarvan hebben we een basiskamp gekozen in Nullagine, Marble Bar en Karratha. De gebieden zijn enkel per voertuig met vierwielaandrijving te bereiken. Soms duurde het een hele dag om het onderzoeksgebied te bereiken, dus normaal gesproken kampeerden we 4 tot 5 dagen in het veld, of nog langer, afhankelijk van de bereikbaarheid van het gebied. Gedurende mijn onderzoek heb ik in totaal ruim een half jaar in het veld in de Pilbara gezeten. De Pilbara heeft een aride tropisch klimaat en grenst aan de Great Sandy Desert. Veldwerken vonden plaats tussen juni en september, gedurende de Australische winter. Ondanks gemiddelde temperaturen tussen de 25 en 30 °C werd het soms behoorlijk warm en ik heb respect voor diegenen die daar in december nog in het veld zitten, wanneer de temperatuur bijna continu boven de 37 °C ligt. Marble Bar wordt ook wel het heetste dorp van Australië genoemd en staat nog steeds in het Guinness Book of Records, omdat het in de zomer van 1923-24 gedurende 161 dagen (en nachten!) continu warmer was dan 37,8 °C (100 °F).

De plaatsen om monsters te nemen werden over het algemeen uitgekozen met behulp van geologische kaarten op schaal 1:100.000 (Blake, 1990) en luchtfoto's. Paleomag-netische teststudies van Ton van Hoof (1996) toonden aan, dat de beste resultaten kwamen van monsterlocaties in de wat dieper ingesleten valleien en niet van open, onbeschutte gebieden, want deze hebben vaak te maken met blikseminslag, wat een destructief effect op het magnetisch signaal heeft. We gebruikten daarom de luchtfoto's om beschutte plekken te vinden, over het algemeen rivierbeddingen. Een bijkomend voordeel hiervan is, dat het
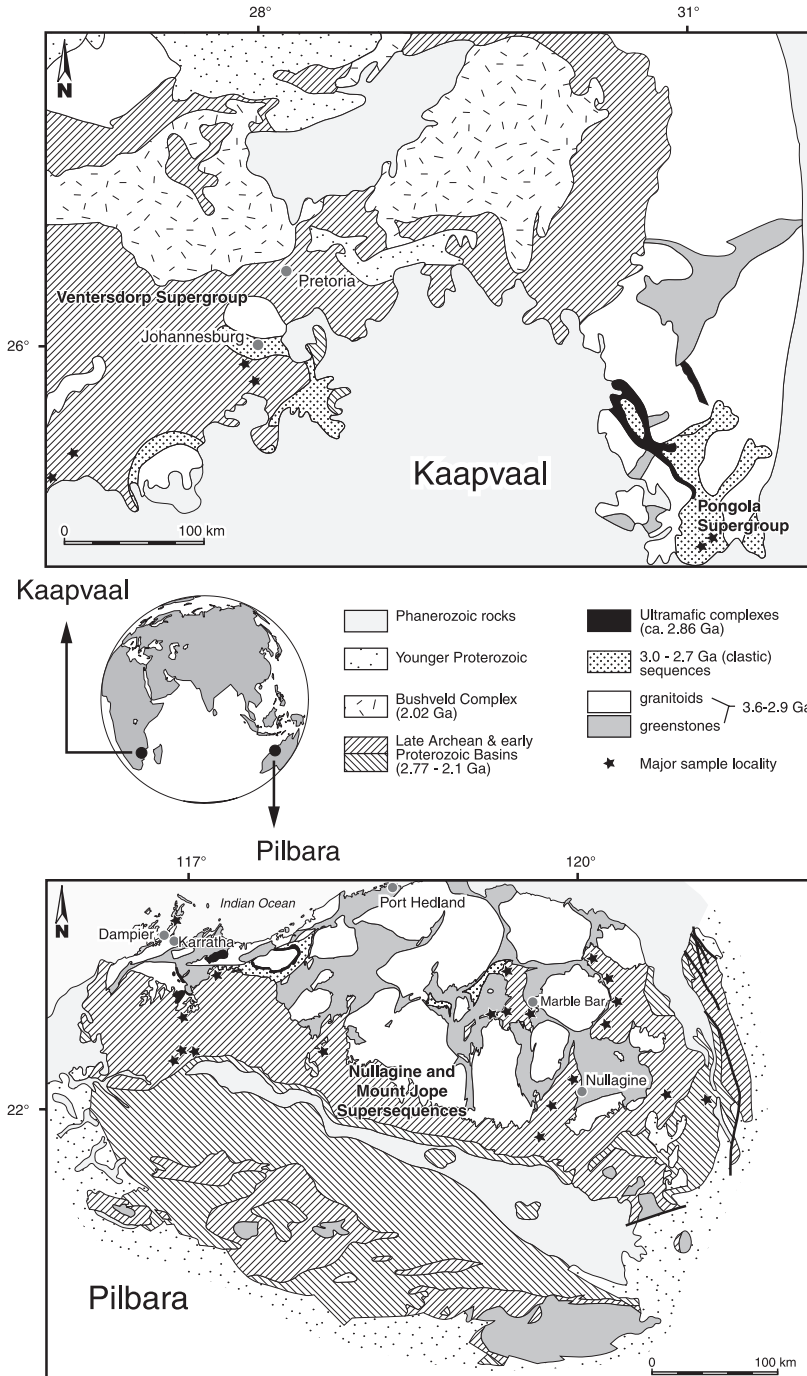
Figuur 1
Vereenvoudigde geologische kaarten van de Kaapvaal en Pilbara Cratons, met daarop de voornaamste monsterlocaties.

gesteente meestal vers ontsloten is en slechts een verweringslaagje van hooguit enkele millimeters heeft. De monsters werden genomen met een draagbare benzineboor. De monsters werden vervolgens georiënteerd, verzameld en naar Nederland verscheept, alwaar ze geprepareerd en geanalyseerd werden in het laboratorium.

Het Kaapvaal Craton.

Het Kaapvaal Craton, gelegen in zuidelijk Afrika, bestaat uit midden- tot laat-Archaïsche graniet-groensteen-terreinen, afgedekt door verschillende sediment-gedomineerde en basalt-gedomineerde pakketten. Het was de bedoeling om dezelfde strategie van monstername toe te passen als in de Pilbara; de nadruk lag dan ook op bemonstering van twee stratigrafische opeenvolgingen die door basaltsequenties gedomineerd worden. De oudste hiervan is de 2,95-2,85 miljard jaar oude Pongola Supergroep. De geologie van de Pongola Supergroep is recentelijk beschreven door bijv. Beukes en Cairncross (1991) en Gold en von Veh (1995). Vervolgens hebben we onze aandacht gericht op de 2,71-2,70 miljard jaar oude Ventersdorp Supergroep. Veel van de type-secties van deze Supergroep zijn gebaseerd op boorkernstudies, want de Ventersdorp Supergroep is over het algemeen slecht ontsloten. De geologie is in detail beschreven door bijv. Winter (1976) en in een recensie door van der Westhuizen c.s. (1991). Gezien er voor datering tot nu toe nog geen geschikte gesteentes gevonden zijn in zowel de Pongola als de Ventersdorp Supergroep, is de geochronologie minder gedetailleerd dan die van de bestudeerde opeenvolging in de Pilbara.

Het veldwerk op het Kaapvaal Craton ging anders in zijn werk dan in Australië. Ontsluitingen zijn relatief eenvoudig te bereiken en de logistiek laat zich makkelijk regelen. In het gebied waar de Pongola Supergroep ontsloten is, is er veel reliëf, waardoor het gemakkelijk is goede ontsluitingen te vinden. De Ventersdorp Supergroep daarentegen, is over het algemeen slecht ontsloten en wordt vaak bedekt door landbouwgrond. Van de Rietgat basalten, bijvoorbeeld, heb ik niet meer gezien dan de tarwevelden die er bovenop liggen. Op een buitengewoon goede ontsluiting langs de Vaal rivier na, waren we vooral afhankelijk van groeves en voor monstername. Het voordeel hiervan was, dat we zeker wisten dat de gesteentes vers waren en niet aan blikseminslag hadden blootgestaan. Het nadeel van ondergrondse mijnen daarentegen is, dat maar op een beperkt aantal plaatsen monsters kunnen worden genomen (namelijk daar, waar de mijngangen nog niet zijn opgespoten met beton) en dat het kompas mogelijk een afwijking heeft vanwege de grote hoeveelheden stalen apparatuur aldaar aanwezig.

Samenvatting

Paleomagnetisme van het Pilbara Craton.

De eerste rapportage van paleomagnetisch onderzoek in de Pilbara dateert uit 1967, waarin resultaten staan van onderzoek van Vroeg-Proterozoïsche (2,5-1,6 miljard jaar) *banded iron* (= dungebande ijzer) formaties te Mount Tom Price en Mount Newman (Porath, 1967). Vanaf die tijd hebben minder dan twee paleomagnetische studies per 10 jaar bijgedragen aan het Precambrische (4,0-0,5 miljard jaar) schijnbare poolpad van de Pilbara, wat resulteerd in een incompleet pad met grote tijdsprongen tussen opeenvolgende poolposities. Hierdoor is het moeilijk om goede tektonische interpretaties te maken. Er is bewijs voor remagnetisaties van verschillende ouderdom (bijv. Li c.s., 2000; Schmidt en Embleton, 1985), maar de oorzaak en de exacte ouderdom hiervan zijn nog onbekend, hoewel men denkt

aan laaggradige metamorfe processen en aan de effecten van gebergtevorming in het Proterozoïcum.

De 2775 tot 2715 miljoen jaar oude Nullagine en Mount Jope Supersequenties zijn bijna niet gemetamorfoseerd, relatief ongedeformeerd en herkenbaar op het gehele Pilbara Craton. Er wordt aangenomen dat de opeenvolging zich gevormd heeft tijdens het opbreken van het continent in het laat-Archaïcum, wat gebeurde in twee fasen (bijv. Blake, 1993; Blake en Barley, 1992). De opeenvolging is daarom ook een ideaal doel voor paleomagnetisch onderzoek, zeker als de vraag is: welk tektonisch mechanisme (dominant verticaal of horizontaal) was van kracht in het laat-Archaïcum?

Hoofdstuk 1 richt zich op het Nullagine Synclinorium, een gebied binnen het Oost-Pilbara Bekken. Hier zijn de Nullagine en Mount Jope Supersequenties onderverdeeld in 12 pakketten (genaamd Package 1 tot Package 12), die gescheiden zijn door discordanties (Blake, 2001). Het belangrijkste doel van dit hoofdstuk voor mijn onderzoek, is overtuigend aan te kunnen tonen, dat de oorspronkelijke NRM nog steeds in deze gesteente-opeenvolging bewaard is gebleven. Zonder bewijs hiervoor zou elke tektonische interpretatie nutteloos zijn. We hebben Package 1 tot en met Package 10 bemonsterd en door middel van een positieve conglomeraat-, plooi- en omkeringstest kunnen bewijzen, dat een hoge-temperatuurcomponent, aanwezig in 7 van de 10 pakketten, inderdaad de oorspronkelijke NRM heeft bewaard. Ook vonden we een middelhoge-temperatuur-component, die een iets andere richting heeft dan eerder beschreven remagnetisatie-richtingen en een aanwijzing is voor een jongere, grootschalige opwarmingsgebeurtenis. De gesteenten van Package 2 hebben een omgekeerde polariteit ten opzichte van de dominante polariteit in de rest van de pakketten. Omdat de omkeringstest positief is, hebben we een goede aanwijzing dat de GAD hypothese ook voor het laat-Archaïcum opgaat. Dit is overigens tot nu toe de oudst waargenomen magnetische omkering met een positieve omkeringstest.

Tussen Package 7 en 8 laten de paleomagnetische gegevens een grote verschuiving in poolpositie zien. We beredeneren dat het niet waarschijnlijk is dat dit veroorzaakt wordt door een geofysisch proces zoals werkelijke poolverschuiving of systematische quadru- en octupool bijdragen. Het ziet er naar uit, dat de verschuiving het resultaat is van daadwer-kelijke horizontale verplaatsing van het Pilbara Craton rond 2,72 miljard jaar geleden, met een snelheid die hoger is dan in enige Phanerozoïsche (ongeveer de laatste 550 miljoen jaar) opeenvolging is waargenomen.

Er lopen vier generaties van mafische gangen in het gebied van het Nullagine Synclinorium die correleren met de plateaubasalten van de Nullagine en Mount Jope Super-sequenties (Blake, 2001). Uit onze paleomagnetische gegevens blijkt deze correlatie ook op te gaan en wij bevestigen, dat de mafische gangen waarschijnlijk de aanvoerkanalen van de plateaubasalten zijn geweest.

Tenslotte hebben we vier nieuwe poolposities aan het Archaïsche poolpad van de Pilbara toe kunnen voegen. Deze nieuwe resultaten hebben we kunnen gebruiken om aan te tonen, dat de argumenten om een mogelijke Archaïsche verbinding van het Pilbara en Kaapvaal Craton af te wijzen (Wingate, 1998), niet langer geldig zijn.

De stratigrafische onderverdeling in 12 pakketten, zoals gedefiniëerd voor het Nullagine Synclinorium, is gemaakt voor de hele noordelijke Pilbara (Blake, 2004). Omdat het aantal monsterlocaties en de grootte van het bestudeerde gebied relatief beperkt is om een goede interpretatie te maken van de stijl van tektoniek en voor het geomagnetisme, wordt in **hoofdstuk 2** het onderzoeksgebied uitgebreid tot het gehele Oost-Pilbara én het

Marble Bar Bekken. Eén van de voornaamste doelen van dit hoofdstuk is om paleomagnetisch de pakketcorrelaties van Blake (2004) te testen. We kunnen de correlaties voor het Oost-Pilbara Bekken inderdaad bevestigen, maar voor het Marble Bar Bekken hebben we wat aanpassingen moeten maken. De paleomagnetische resultaten laten hier namelijk zien, dat het onderste plateaubasaltpakket niet correleerd met Package 1 in het Oost-Pilbara Bekken, waar we in eerste instantie van uitgingen. Het blijkt dat dit onderste plateaubasaltpakket (aanzienlijk) ouder is dan Package 1, want het heeft een totaal andere poolpositie. We hebben dit pakket daarom Package 0 genoemd. Het daaropvolgende plateaubasaltpakket in het Marble Bar Bekken heeft een bijna identieke poolpositie als Package 1 in het Oost-Pilbara Bekken en we gaan er nu van uit, dat deze dezelfde ouderdom hebben. De totaal verschillende poolpositie van Package 0 impliceert, dat ergens tussen de tijd van extrusie van Package 0 en die van Package 1 de Pilbara in zijn geheel bijna 180 graden gedraaid is. Dit is een controversiële (doch niet onmogelijke) oplossing, maar het is de meest conservatieve aanpak en gemakkelijker acceptabel dan het gebruiken van grote werkelijke poolverschuivingen, complexe magnetische excursies of extreem non-dipoolgedrag om de observaties te verklaren.

Een volgend doel van hoofdstuk 2 is om de grootte van paleomagnetische verschuiving tussen Package 7 en 8 beter te bepalen. Als we alle gegevens van het Oost-Pilbara Bekken combineren, dan komen we op een totale verplaatsingssnelheid van onge-veer 50 cm per jaar, wat nog steeds 10 tot 20 cm per jaar sneller is dan de snelste Phanero-zoïsche plaatsnelheden die tot nu toe zijn gerapporteerd (bijv. Meert, 1999; Meert c.s., 1993).

Tenslotte, Package 2 blijkt in het hele Oost-Pilbara Bekken een omgekeerde richting te hebben, net als (tenminste) één basaltstroom van Package 7. De gecombineerde gegevens van hoofdstuk 1 en 2 vormen een goed-bepaald poolpad voor de Pilbara tussen 2772 en 2715 miljoen jaar geleden, zeker voor Archaïsche begrippen.

Hoofdstuk 3 richt zich op het paleomagnetisme van het West-Pilbara Bekken. De correlatie van pakketten zoals die gedefinieerd is voor het Nullagine Synclinorium is hier complexer (Blake, 2004). Sommige pakketten komen niet voor in het West-Pilbara Bekken en andere juist alleen daar, zoals mafische sills (plaatvormige intrusies). De doelstellingen van hoofdstuk 3 zijn om de voorgestelde stratigrafische correlatie met het Nullagine Synclinorium (Blake, 2004) ook hier paleomagnetisch te testen, alsmede om de gehele paleomagnetische gegevensset van de noordelijke Pilbara te gebruiken om een nieuw model voor de tektonische evolutie van de Pilbara tussen 2775 en 2715 miljoen jaar te ontwikkelen, door deze gegevensset te integreren met een bestaand model gebaseerd op geologische gegevens (Blake, 1993; Blake en Barley, 1992). Het aantal bruikbare paleomagnetische gegevens van het West-Pilbara Bekken blijkt veel lager te zijn dan van de Oost-Pilbara en Marble Bar Bekkens, hetgeen een indicatie zou kunnen zijn voor een iets hogere metamorfe graad in het West-Pilbara Bekken. Indicaties uit het Oost-Pilbara Bekken, die wijzen op een geomagnetische omkering van Package 7 ouderdom, worden bevestigd door de omgekeerde polariteit die we vinden in sommige, met Package 7 gecorreleerde, mafische sills van het West-Pilbara Bekken. De omkeringstest voor deze sills is positief, waardoor we opnieuw kunnen aantonen dat de originele NRM bewaard is gebleven. De paleomagnetische gegevens ondersteunen de stratigrafische correlatie, zoals die is voorgesteld door Blake (2004).

De tektonische evolutie van het (noordelijke) Pilbara Craton tussen 2775 en 2715 miljoen jaar geleden kan nu met behulp van de gegevens uit de hoofdstukken 1 tot en met 3, gecombineerd met geologische gegevens, als volgt worden beschreven: tijdens de eerste fase van het opbreken van de Pilbara, wat gebeurde vanaf het uitvloeien van Package 1 tot

aan het uitvloeien van Package 7, onderging het Craton een WNW-OZO extensie met een mogelijke minimum plaatsnelheid van 2,5 cm/jaar. Tevens roteerde het craton ongeveer 30° tegen de klok in gedurende deze periode. Tijdens de tweede fase verplaatste het gehele Pilbara Craton zich rond de 1600 km in equatoriale richting, met een gemiddelde minimum plaatsnelheid van 50 cm/jaar, hetgeen aantoont dat snelle horizontale plaatbewegingen, de essentie van plaattektoniek, plaatsvonden tijdens het laat-Archaïcum.

Paleomagnetisme van het Kaapvaal Craton

Het Kaapvaal Craton kent een vergelijkbaar aantal paleomagnetische studies als het Pilbara Craton, hoewel er weinig recente studies gerapporteerd zijn. De interesse in het paleomagnetisme van de Ventersdorp Supergroep begint in de late zestiger jaren (Jones c.s., 1967), maar sinds die tijd zijn er geen nieuwe gegevens bekend gemaakt. Er zijn nog geen paleomagnetische studies gerapporteerd over de Pongola Supergroep. Het schijnbare poolpad van het Kaapvaal Craton bevat grote tijdsprongen tussen opeenvolgende poolposities, waardoor voorzichigheid is geboden bij het maken van tektonische interpretaties. Desondanks is het poolpad van het Kaapvaal Craton in het verleden gebruikt om tektonische interpretaties te maken (bijv. Kröner en Layer, 1992) die staan of vallen met de kwaliteit van dit poolpad.

Hoofdstuk 4 beschrijft de resultaten van een paleomagnetische studie van basalten van de Pongola en Ventersdorp Supergroepen. Het doel was om het aantal poolposities voor het Kaapvaal Craton uit te breiden en om tektonische interpretaties te vergemak-kelijken. Bijna alle bestudeerde eenheden bevatten een duidelijke, identieke secundaire component, die veroorzaakt is door remagnetisatie rond 180 miljoen jaar geleden, gedurende de vorming van het vulkanische Karoo complex, waar bijna het gehele Kaapvaal Craton mee te maken heeft gehad. Vijf van de bestudeerde eenheden bevatten vervolgens ook een hoge temperatuur component van Archaïsche ouderdom. We hebben verschillende paleomagnetische tests uitgevoerd om de ouderdom van deze hoge temperatuur component preciezer te bepalen, maar we zijn er niet in geslaagd om een Archaïsche ouderdom aan te tonen. We zijn afhankelijk van het reeds bestaande poolpad om de ouderdom van onze gegevens enigszins af te bakenen. Echter, hiervoor is het noodzakelijk om de kwaliteit van de gepubliseerde Archaïsche poolposities te testen. Het blijkt, dat slechts één poolpositie ondersteund wordt met een positieve conglomeraattest (Wingate, 1998), hoewel de spreiding van de richtingen die deze poolpositie bepalen hoger is na tektonische correctie dan ervoor, wat wijst op een negatieve plooitest, hoewel we dit niet hebben kunnen testen aan de hand van de gepubliseerde gegevens. De overige poolposities zijn bepaald zonder veldtesten en in veel gevallen kon de paleohorizontaal niet bepaald worden. We concluderen dan ook, dat de kwaliteit van de paleomagnetische gegevens van het Kaapvaal Craton, inclusief onze nieuwe gegevens, te wensen over laat en dat het schijnbare poolpad hiermee niet goed bepaald kan worden, waardoor het niet geschikt is voor het maken van betrouwbare tektonische interpretaties.

Het aardmagneetveld in het laat-Archaïcum

In **hoofdstuk 5** worden onze paleomagnetische gegevens van het Pilbara Craton gebruikt om het gedrag van het laat-Archaïsche aardmagneetveld te bestuderen. Er worden twee verschillende experimenten beschreven in hoofdstuk 5: ten eerste zijn de gegevens van hoofdstukken 1 tot en met 3 geanalyseerd om een selectie te maken van monsters voor paleointensiteitsbepalingen. Ten tweede zijn de gegevens van de site-gemiddelden uit

hoofdstukken 1 tot en met 3 gebruikt om paleoseculaire variatie te bestuderen. Voor de paleointensiteitexperimenten hebben we monsters gebruikt die alleen de originele NRM laten zien en geen secundaire magnetisaties. Om het slagingspercentage van de experimenten te verhogen hebben we een methode ontwikkeld om de mate van magnetische omzettingen ten opzichte van de temperatuur te bepalen. We hebben hiervoor de Curiebalans gebruikt, waarbij we herhaaldelijk de monsters hebben verhit en afgekoeld, met steeds hoger wordende eindtemperaturen. Alleen de monsters die weinig tot geen omzettingen vertoonden, werden geschikt geacht voor paleointensiteitsbepaling. Het gemiddelde dipoolmoment (VDM) van 2772 ± 2 miljoen jaar geleden is bepaald op 28,1 ± 9,3 ZAm^2 (Z = zeta = 10^{21}) en van 2721 ± 4 miljoen jaar op 22,1 ± 4,2 ZAm^2, wat relatief laag is vergeleken met het huidige dipool moment van ongeveer 80 ZAm^2. Echter, de laat-Archaïsche VDM-waarden liggen binnen de fout van die van de laatste 1 to 84 miljoen jaar geleden, namelijk 55 ± 30 ZAm^2 (Tauxe en Staudigel, 2004).

Het paleoseculaire variatie-experiment omvat de analyse van de gemiddelde spreiding van schijnbare geomagetische polen (VGP) van de Pilbara gegevens. Die zijn vervolgens vergeleken met de VGP spreiding van de laatste 5 miljoen jaar, waarbij gebruik gemaakt is van paleoseculaire variatiegegevens van moderne lava's (PSVRL, McElhinny en McFadden, 1997) en modelvoorspellingen die gebaseerd zijn op PSVRL (TK03.GAD, Tauxe en Kent, 2004). We hebben de Pilbara gegevens geanalyseerd per package en per groep van packages die een gemeenschappelijke paleobreedtegraad hebben. De laatste manier is bruikbaarder, omdat de analyses significanter worden bij een hoger aantal gegevens. Het blijkt dat de voorspellingen van seculaire variatie met het TK03.GAD model overeenkomen met de seculaire variatiegegevens van de Pilbara, zowel voor de individuele packages, als voor de groepen van packages. We kunnen nu voor het eerst concluderen, dat de mate van seculaire variatie in het Archaïcum niet significant verschilt met die van de laatste 5 miljoen jaar.

De conclusie uit de Pilbara gegevens is, dat de GAD hypothese opgaat voor het laat-Archaïcum, dat de intensiteit van het aardmagneetveld lager was dan de huidige intensiteit, maar niet significant lager dan in de periode tussen 1 en 84 miljoen jaar geleden, en dat seculaire variatie vergelijkbaar is met die van de laatste 5 miljoen jaar. Het lijkt er dus op, dat het aardmagneetveld omstreeks 2,8 miljard jaar geleden al stabiel was, wat óf een belangrijke beperking is voor de rol van de vaste binnenkern van de aarde op het aardmagneetveld, óf wat aangeeft dat de vaste binnenkern 2,8 miljard jaar geleden al was gaan groeien. Op dit moment kunnen de theoretische modellen het antwoord hierop nog niet geven.

Acknowledgements

I am grateful to all people who have contributed in one way or the other to the completion of my thesis. In particular, I am thankful to all my past and present colleagues of Fort Hoofddijk, both from a scientific and a personal perspective. Cor, je hebt me enorm veel vrijheid gegeven om mijn eigen weg te zoeken in dit onderzoek, maar je hebt ook op de juiste momenten aangegeven wat er nog moest gebeuren om er een leuk proefschrift van te maken. Je hebt verder altijd achter mijn beslissingen gestaan en bent opgekomen voor mijn belangen, wat ik enorm waardeer. Ik hoop, dat we in de toekomst nog eens samen op veldwerk gaan, want dat was altijd erg productief en gezellig. I thank Stan White, Jan Wijbrans and Wout Nijman for taking me up in the Pilbara-team in 1997. It has been one of those things that changed life for the better. Tim, without you we would still be talking about the Kylena Basalt in the Marble Bar Basin. I am grateful for all the work you have done on the stratigraphy and geochronology, and particularly for explaining it all to me and setting me up for the many fieldworks. I will never forget trips like those to Boodelyerri. Experiences like that have kept me going for most of my PhD time. The project in Nullagine was brilliant and I feel honoured to have been a part of it. I thank you and Kate for all the hospitality you have shown, your house in Chidlow was a second home to me. I wish you all the best in life and hope to see you again sometime. Maarten, ik wil jou graag bedanken voor je gastvrijheid in Kaapstad en je voorbereidingen voor het werk in Zuid-Afrika. Tijdens het veldwerk in de Barberton heb je me ook nog eens laten zien, dat ik in de afgelopen vijf jaar wat geleerd heb. Tom, bedankt voor alle technische ondersteuning, maar zeker ook voor je persoonlijke interesse in mij en mijn onderzoek, en je gewillig oor voor als ik weer eens iets te klagen had. Mark, ondere andere bedankt voor je hulp tijdens de voorbereidingen voor mijn werk in San Diego, de pitchers en limosine-tochtjes in San Francisco en voor het feit, dat je een fotografisch geheugen lijkt te hebben voor alles wat met gesteente- en paleomagnetisme te maken heeft. I thank everybody of the ORLC for the many papers we have discussed and the inspiration I got from that, and Tanja in particular for her interest in my research. Ik wil ook graag Douwe, Gesa, Klaudia en Sjoukje bedanken voor alle informatie en tips omtrent het afronden van een proefschrift. Bernard, bedankt voor al je peptalks in Aliaga. Verder gaat mijn dank uit naar mijn paranimfen Aart-Peter en Marten. Ik wens jullie veel succes met het afronden van jullie proefschriften, het einde is in zicht. Aart-Peter, ik kan me geen betere vriend voorstellen, mede dankzij jou zijn de laatste drie jaar op de faculteit erg gezellig geweest. Pa, ma en Marieke, bedankt dat jullie de weg naar de universiteit voor me geplaveid hebben en dat jullie trots op me zijn, dat is heel wat waard. Pa, bedankt voor de correcties in de samenvatting in het Nederlands. Ik wil ook nog even een woordje richten aan mijn jaargenoten A-P, Frodo, Hubert, Jerfaas, KJ, Martijn, MC en Steven. Sinds 1993 gaan geologie, vriendschap en gezelligheid samen. Dit is voor mij een belangrijke motivatie om te blijven doen wat ik doe. He dejado lo mejor para el final. Carmen, la vida sin ti sería muy distinta y mucho menos interesante. Agradezco el que me hayas acompañado en tantos viajes y que me hayas ayudado en el campo en Australia. Allí me has enseñado que eres una persona muy fuerte, mucho más que yo. Estoy muy orgulloso de ti, tanto como tú de mi, algo que me has dejado sentir claramente. Todo esto me ha inspirado y motivado para acabar esta tesis. Muchas gracias.

Curriculum Vitae

Ik ben geboren op 11 december 1973 in het St. Anna ziekenhuis te Oss. Het grootste deel van mijn kindertijd heb ik doorgebracht in Vorstenbosch. Tussen 1985 en 1992 heb ik middelbaar onderwijs gevolgd op Gymnasium Bernrode te Heeswijk-Dinther. In 1992 ben ik begonnen met mijn studie geologie aan de toenmalige Faculteit Aardwetenschappen van Universiteit Utrecht, waar ik in 1998 mijn bul heb gehaald. Het daaropvolgende jaar heb ik mij in Spanje de Spaanse taal meester gemaakt, onder andere door een cursus aan de Universidad Internacional Menéndez Pelayo te Santander. Tussen 1999 en 2004 ben ik werkzaam geweest als AiO paleomagnetisme aan wat nu de Faculteit Geowetenschappen van Universiteit Utrecht is.